Development of vascularized tumor spheroids mimicking the tumor environment : angiogenesis and hypoxia

Hassan Chaddad

UNIVERSITÉ DE STRASBOURG

ÉCOLE DOCTORALE des Science de la Vie et de la Santé

Faculté de médecine - INSERM U1260 (Regenerative Nanomedecine)

THÈSE

présentée par :

Hassan Chaddad

soutenue le : **18 janvier 2019**

pour obtenir le grade de : **Docteur de l'Université de Strasbourg**

Discipline/ Spécialité : Science pharmaceutique-pharmacologie-pharmacocinétique

Development of vascularized tumor spheroids mimicking the tumor environment: Angiogenesis and Hypoxia

THÈSE dirigée par :

Pr. UBEAUD-SEQUIER Geneviève Professeur - Faculté de pharmacie - Université de Strasbourg

RAPPORTEURS :

Dr. SAVAGNER Pierre Chargé de recherches, INSERM U1186, Institut Gustave Roussy

Dr. BOLOTINE Lina MCU-PH CRAN CNRS UMR 7039 - Université de Lorraine

EXAMINATEUR :

Dr. GAIDDON Christian Directeur de recherches -CNRS- Université de Strasbourg

INVITE :

Dr. IDOUX-GILLET Ysia Maitre de Conférence associée- Université de Strasbourg

ACKNOWLEDGMENTS

After 3 years of continuous hard work, long days, and sleepless nights, I finally made my dream come true and was able to successfully achieve what I came here for. My perseverance has finally paid off.

But all this period, I was never alone. God was always here for me. He has armed me with the strength to tolerate being away from home and enlightened my way and steadied my steps to the intended goal. The awaited day has finally come, and it couldn't have happened without God, whom I'm deeply grateful for and whose mercy and satisfaction I seek all my days.

I thank the jury members who will allocate the time to be present on my thesis day.

I thank Prof Geneviève Ubeaud-Sequier, my thesis' advisor who accepted me to do this project and to complete the research work I have been working on in the domain of cancer. She let me familiar with all the techniques in biology and be confident of myself.

I thank Dr. Nadia Jessel, my supervisor throughout these years who taught me how to be rigid in the hardest times, how to think differently and have new perspectives that could yield very positive results, and how to utilize both knowledge and experience to support my thesis work. She was not only my advisor, she was my support, my guide, and my mother.

I thank Dr Ysia Idoux-Gillet who was always my inspiration. Her smile, her kindness and her positive energy have always given me the motivation and determination to continue what I have started, even when I was at my worst. She helped me in every detail and supported me in all my work by giving advices, doing corrections. With Ysia, nothing is impossible.

I thank Dr Guy Fuhrmann and Dr Laurent Désaubry who have graciously and generously synthesized and gave the molecule Flavagline (FL3) that I used in my second part of my work.

I thank faculty of medicine for making all the required facilities and equipment available and accessible for researchers, helping me excel in my experimental work.

I thank Hadath Baalbeck municipality for funding me during my PhD period.

A special thanks to my family. Words cannot express how grateful I am to my mother, brothers and sisters for all of the sacrifices that they've made on my behalf. Your prayers for me were what sustained me thus far.

I thank everyone whom I missed to mention and who have impacted me positively in my long journey, even in the simplest ways.

Résumé en français

Développement d'un modèle 3D de tumeur vascularisée mimant le microenvironnement tumoral : angiogenèse et hypoxie

➢ Introduction

I. Criblage de molécules thérapeutiques

Le cancer, maladie multifactorielle, est la principale cause de décès chez l'homme dans le monde moderne. Il est responsable de 7,6 millions de décès par an, et les chiffres devraient atteindre 13,1 millions d'ici 2030 (*Singh et al., 2017*). Les systèmes biologiques ont divers mécanismes pour empêcher la propagation du cancer, tels que les gènes suppresseurs de tumeur, les points de contrôle du cycle cellulaire, ou encore les mécanismes de réparation de l'ADN. Une régulation négative ou un dysfonctionnement de ces systèmes lève ces points de contrôle de la cellule pouvant entraîner ainsi l'initiation du cancer.

Le développement de nouvelles molécules thérapeutiques est un processus très long, complexe et coûteux. À ce jour, le temps moyen nécessaire pour développer un nouveau médicament anticancéreux est estimé à 7,3 ans, avec un coût moyen de 648 millions de dollars par nouvelle molécule *(Prasad et al., 2017)*. Au cours de ce processus, le taux d'échec des médicaments anticancéreux atteint 95%, en partie en raison d'une toxicité excessive, du manque de molécules cibles et d'ajustement individuel *(Ledford, 2011 ; Arrowsmith, 2011 ; NIH, About New Therapeutic Uses, https://ncats.nih.gov/ntu/about)*. A l'heure actuelle, la communauté scientifique s'accorde à dire que le problème ne réside pas dans la recherche de molécules pharmacologiquement actives, mais dans les modèles expérimentaux permettant de les sélectionner. Le développement de modèles tumoraux 3D (microtissus, sphéroïdes, organoïdes) a nettement amélioré l'efficacité des tests de sélection et de nombreuses entreprises proposent des lignées cellulaires ou des xénogreffes issues de patients (InSphero, OcellO, Organogenix, Creative Bioarray). Cependant ces modèles *in vitro*, certes humains, n'incluent pas pour autant la vascularisation tumorale. A l'inverse, les tests *in vivo* sur animaux permettent la vascularisation mais n'ont pas les caractéristiques humaines. Ainsi, le développement de nouveaux modèles de criblage de molécules thérapeutiques, comprenant le microenvironnement tumoral (vascularisation, hypoxie, matrice...), est crucial pour améliorer

les effets et la sélection de traitement anticancéreux. La valeur de tout modèle préclinique dépendra en fin de compte de sa capacité à prédire avec précision la réponse clinique.

Les sociétés pharmaceutiques utilisent des approches de criblage à haut débit (HTS) pour évaluer rapidement les entités chimiques nouvelles et/ou existantes afin de déterminer les effets sur les cellules. Actuellement, la majorité des HTS à base de cellules sont effectués sur des cellules cultivées en deux dimensions (2D) sur des surfaces en plastique optimisées pour la culture de tissus. Cependant, des preuves convaincantes suggèrent que les cellules cultivées dans ces conditions non physiologiques ne sont pas représentatives des cellules résidant dans le microenvironnement complexe d'un tissu. Ainsi, les technologies de culture cellulaire tridimensionnelles (3D) mimant mieux les environnements cellulaires *in vivo* sont maintenant utilisées en routine car elles permettent une meilleure précision dans la découverte de médicaments. En effet, il a été montré que ces sphéroïdes avaient une architecture 3D, avec des interactions cellulaires et des dépôts de matrice extracellulaire comparables aux tissus *in vivo (Oloumi et al., 2002)*. De plus, ces sphéroïdes peuvent être cultivés avec plusieurs types cellulaires dans des rapports variés pouvant représenter les conditions physiologiques *in vivo (Fang et al., 2010 ; Lopez et al., 2012)*. Les sphéroïdes ont une limite de diffusion des médicaments, des nutriments ou d'autres facteurs et peuvent développer des régions d'hypoxies qui sont un point critique pour tester des molécules thérapeutiques *(Bredel-Geissler et al., 1992 ; Wartenberg et al., 2001)*. Tous ces arguments placent les sphéroïdes comme le meilleur modèle *in vitro* pour tester la sensibilité et la résistance aux médicaments *(Torisawa et al., 2005 ; Loessner et al., 2010 ; Chwalek et al., 2014).*

La complexité du microenvironnement tumoral nécessite l'incorporation de nombreux facteurs jouant un rôle très important dans la réponse aux médicaments, tels que la matrice extracellulaire, les gradients de concentration ou encore les cellules stromales. Mais le développement d'un modèle de criblage de molécules thérapeutiques se doit également de prendre en compte l'hypoxie et la vascularisation, facteurs clés dans l'efficacité et la sélection des médicaments.

II. Rôle de la vascularisation et de l'hypoxie dans le cancer

La disponibilité de l'oxygène et des nutriments fournis par le système vasculaire est cruciale pour les cellules saines et cancéreuses. Cependant, la nature des vaisseaux intra-tumoraux et leur relation avec les cellules tumorales sont toujours débattues.

L’angiogenèse, ou formation de nouveaux vaisseaux sanguins, est un mécanisme clé dans de nombreux processus physiologiques, tel que le développement ou encore la cicatrisation des plaies, mais est également très largement impliqué dans la progression tumorale et dans l’émergence de métastases. En effet, la découverte de réseaux vasculaires très développés au sein des tumeurs solides a poussé la communauté scientifique à définir de nouvelles cibles thérapeutiques depuis plusieurs années (*Knighton et al., 1977)*. C’est pourquoi, au cours des dernières décennies, des thérapies de plus en plus sélectives ont été développées et actuellement les agents anti-angiogéniques représentent la partie la plus importante des thérapies ciblées *(Alameddine et al., 2014 ; Marçola et al., 2015)*. La grande majorité de ces agents anti-angiogéniques cible le facteur de croissance endothélial vasculaire (VEGF) et son récepteur (VEGFR), qui sont les régulateurs les plus importants de l’angiogenèse. En effet, la signalisation VEGF stimule les voies cellulaires qui conduisent à la formation et à la ramification de nouveaux vaisseaux sanguins tumoraux, favorisant une croissance rapide de la tumeur et facilite le potentiel métastatique *(Zhao et Adjei, 2015)*.
La germination de nouveaux vaisseaux à partir de vaisseaux existants était considérée comme un moyen exclusif de vascularisation de la tumeur, mais au cours des dernières années, plusieurs mécanismes supplémentaires ont été identifiés, tels que l’angiogenèse intussusceptive, le recrutement de cellules souches endothéliales, la co-option vasculaire, la lymphangiogenèse à la croissance tumorale *(Hillen et Griffioen, 2007)*. Ces mécanismes sont maintenant connus pour réguler la vascularisation des tumeurs et déterminer le pronostic du cancer à la suite du traitement. En tant que processus requis pour l'invasion et l’émergence de métastases, l'angiogenèse tumorale constitue un point de contrôle important de la progression du cancer, et est ainsi indispensable dans un modèle de criblage de médicaments.

L'hypoxie, définie comme une diminution du taux d'oxygène dans les tissus, représente une condition physiopathologique fondamentale dans le microenvironnement des tumeurs solides. L’hypoxie tumorale est connue pour être associée à la résistance relative à la chimiothérapie et la radiothérapie, ainsi qu’aux métastases, qui conduisent finalement à la progression du cancer contribuant au mauvais pronostic chez les patients *(Nurwidya et al., 2012)*. La principale cause de l'hypoxie tumorale est la formation de vaisseaux sanguins non fonctionnels dans les tissus néoplasiques, en particulier dans les tumeurs à croissance rapide. L'hypoxie est un facteur clinique important puisqu’elle est associée à des phénotypes tumoraux agressifs, à une résistance au traitement et à un mauvais pronostic pour le patient.

La réponse cellulaire à l'hypoxie est principalement portée par la famille des facteurs de transcription du facteur inductible par l'hypoxie (HIF), qui régule l'expression de multiples gènes impliqués dans les processus entrainant l'adaptation et la progression des cellules cancéreuses, tel que VEGF. Ces voies de signalisation affectent de nombreux marqueurs du cancer, notamment la prolifération cellulaire, l'apoptose, le métabolisme, les réponses immunitaires, l'instabilité génomique, la vascularisation, l'invasion et les métastases. Dans les échantillons de biopsies de patient, l'expression de HIF est associée à un mauvais pronostic et à une rechute lors du traitement. Les HIF semblent être des cibles moléculaires cruciales pouvant être exploitées pour améliorer le traitement du cancer métastatique et résistant au traitement *(Wigerup et al., 2016)*. L'hypoxie est ainsi un critère très important à prendre en considération dans le développement d'un modèle de tests et de sélection de médicaments.

III. Objectifs de la thèse

Dans ce contexte, afin de répondre aux questions et manques soulevés précédemment, ce projet de thèse a pour objectif de développer un modèle 3D plus sélectif et prédictif, prenant compte de la vascularisation et du microenvironnement tumoral. Cette thèse se déclinera ainsi en deux points :

1. **Mimer le microenvironnement vasculaire de la tumeur en utilisant un modèle combiné 2D/3D**
2. **Développer un modèle 2D et 3D d'hypoxie tumorale et tester une molécule pharmacologique d'intérêt: la Flavagline**

Ces deux objectifs s'inscrivent dans un projet plus vaste dont le but final est de développer une plateforme de criblage de molécules thérapeutiques, incluant différents éléments du microenvironnement tumoral (sphéroïdes tumoraux, matrice, hypoxie, vascularisation, immunité) pour être toujours plus proche de l'*in vivo* afin de mieux sélectionner les médicaments.

➢ Résultats

I. Chapitre 1 : Combiner l'angiogenèse et des sphéroïdes tumoraux pour imiter l'environnement tumoral vascularisé

Pour imiter le microenvironnement vascularisé de la tumeur, nous avons cultivé des cellules tumorales d'ostéosarcome (MG-63) en sphéroïdes 3D, que nous avons déposé sur des cellules endothéliales (HUVEC-GFP) cultivées en monocouche 2D. Une fois le sphéroïde tumoral (MT-MG-63) déposé sur le tapis de cellules endothéliales, nous avons pu observer que les cellules tumorales proliféraient rapidement, s'échappant du sphéroïde et formant un front de migration en 7 jours de culture. Après 14 jours de culture, les HUVEC se réorganisaient et commençaient à former des structures tubulaires, s'agençant au sein des cellules tumorales (Figure 1). Au bout de 21 jours de culture du système combiné 2D/3D, les cellules endothéliales formaient un réseau vasculaire organisé et étaient capables d'infiltrer les sphéroïdes tumoraux (Figure 2).

Afin d'expliquer la formation de structures tubulaires par les cellules endothéliales, nous avons étudié l'expression du facteur de croissance endothélial vasculaire (VEGF), par qPCR, dans les cellules MG-63 cultivées en 2D comparées celles cultivées en 3D (MT-MG-63) après 5, 10 et 21 jours de culture. Le taux d'ARNm codant pour le VEGF était significativement plus élevé dans les sphéroïdes (MT) que dans les cellules cultivées en monocouche après 5 jours. Ce niveau d'expression augmentait de manière significative dans les cultures de MT-MG-63 après 10 et 21 jours. Les mêmes analyses ont été effectuées avec les cultures combinées 2D/3D. Nous avons pu observer une augmentation très significative de l'expression de VEGF dans la combinaison MT-MG-63/HUVEC 2D à 10 jours de culture comparée aux HUVEC 2D et MG-63 2D cultivées 10 jours également. Cela signifiait que l'ajout de MT-MG-63 sur une monocouche de cellules HUVEC conduisait à une expression nettement plus élevée de VEGF, après un délai de culture de 10 jours, correspondant au délai nécessaire aux cellules endothéliales pour s'organiser et former des structures tubulaires.

À 21 jours de culture, le réseau vasculaire formé par les cellules endothéliales infiltrait les sphéroïdes tumoraux. Des coupes transversales de ces derniers montrent que les vaisseaux présentaient une lumière dont le diamètre a pu être estimé entre 10 µm et 25 µm, correspondant à la taille des capillaires et artérioles *in vivo* (Figure 2).

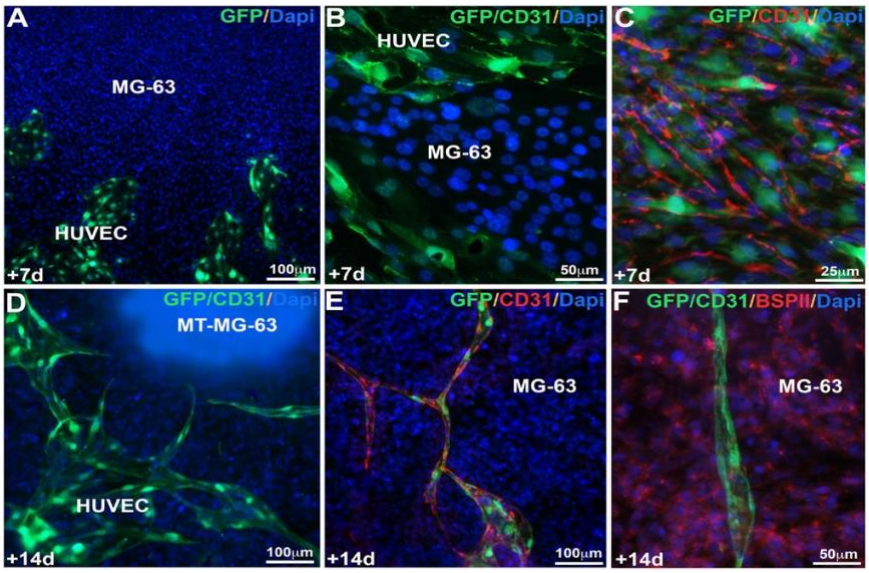

Figure1 *: Immunofluorescence pour GFP, CD31 et BSPII de cultures combinées après 7 jours (A-C) et 14 jours (D-F). Après 7 jours (A-C), les cellules MG-63 ont migré et ont formé un front de migration. Nous pouvons observer une forte expression de CD31 aux jonctions des cellules endothéliales (B, C). Après 14 jours, les HUVEC ont commencé à former des structures tubulaires (D-F). Les cellules MG-63 étaient positives pour BSPII (F), un composant des tissus minéralisés.*

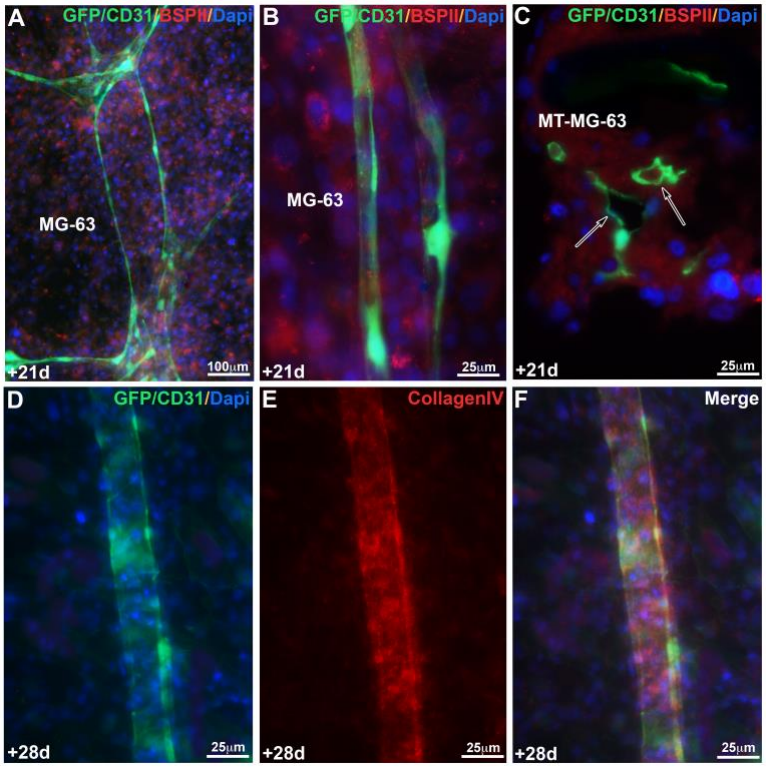

***Figure 2** : Immunofluorescence pour GFP, CD31, BSPII et Collagène IV de cultures combinées après 21 jours (A-C) et 28 jours (D-F). Les cellules d'ostéosarcome MG-63 expriment BSPII (rouge, A-C), et les cellules endothéliales HUVEC forment des structures pseudo-tubulaires (A-B). L'image (C) montre une coupe transversale de tubules (flèches) infiltrant le sphéroïde MT-MG-63. Les structures tubulaires expriment CD31 (vert, D) et collagène IV (E).*

II. Chapitre 2 : Développer un modèle 2D et 3D d'hypoxie tumorale et tester une molécule pharmacologique d'intérêt : la Flavagline

1. Modèle d'hypoxie utilisant l'agent $CoCl_2$ et la culture 3D sur des lignées tumorales

Deux lignées tumorales ont été choisies pour leur agressivité et leur mauvais pronostic lié à l'hypoxie, les cellules d'ostéosarcome (MG-63) et de glioblastome (U87-MG). Afin de reproduire les conditions d'hypoxie, nous avons utilisé deux techniques, l'une par l'ajout de $CoCl_2$, qui mime l'hypoxie en empêchant la dégradation de HIF1α ; l'autre par la culture des cellules en 3D (sphéroïdes ou microtissus) connu pour provoquer l'hypoxie au centre de la structure.

Pour mettre en place ce système, différentes concentrations de $CoCl_2$ ont été testées (50µM, 100µM, 150µM et 200µM) sur les deux types cellulaires MG-63 et U87-MG en 2D. Dans ces conditions nous avons pu observer une augmentation de l'expression de la protéine HIF1α révélée par Western blot, montrant l'efficacité du $CoCl_2$ (Figure 3C). L'analyse par qPCR de l'expression des gènes relatifs à l'hypoxie GLUT1, GLUT3 et VEGF a montré une augmentation suite à l'ajout de $CoCl_2$ comparé au contrôle pour les deux lignées tumorales (Figure 3A). L'expression des gènes de résistance aux médicaments ABCG2 (ATP-binding cassette super-family G member 2) et MRP1 (multidrug resistance-associated protein) n'était pas impactée par le $CoCl_2$, mise à part ABCG2 dans les cellules d'ostéosarcome qui augmentait de manière significative à partir de 150µM de $CoCl_2$ (Figure 3B). Suite à ces résultats, nous avons choisi d'utiliser le $CoCl_2$ à 150µM pendant 24h pour toutes les expériences.

Les mêmes expériences ont été réalisées sur les sphéroïdes 3D (MT) de MG-63 et U87-MG. En comparaison avec le contrôle 2D, il y avait une augmentation de l'expression du gène HIF1α dans les 3D sans effet du $CoCl_2$. Les mêmes résultats ont été observés pour les gènes liés à l'hypoxie, GLUT1, GLUT3 et VEGF, dont l'expression était augmentée dans les MT

avec ou sans $CoCl_2$ (Figure 3D). Cependant, l'ajout du $CoCl_2$ dans les MT conduisait à une augmentation plus élevée pour les gènes de l'hypoxie que dans les MT seuls.

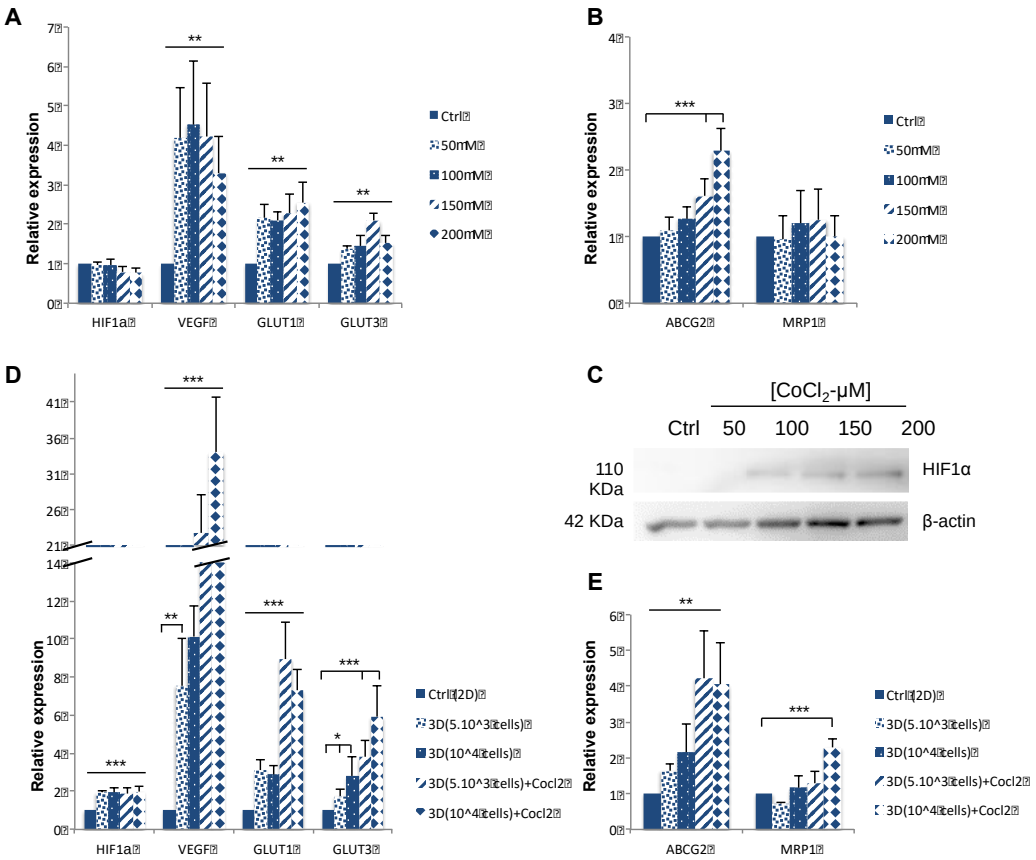

Une augmentation significative était également observée pour les gènes de résistance aux médicaments ABCG2 et MRP1 dans les sphéroïdes traités avec $CoCl_2$ pour les deux lignées tumorales, comparé aux sphéroïdes non traités et au contrôle 2D (Figure 3E). Ainsi, ces résultats ont montré que chaque technique mimant l'hypoxie (2D+$CoCl_2$ ou 3D seul) conduisait à une augmentation relativement équivalente des gènes liés à l'hypoxie, mais surtout que cet effet était significativement amplifié par la combinaison des deux techniques (3D+$CoCl_2$).

Figure 3 *: Développement du modèle 2D et 3D d'hypoxie avec les cellules tumorales d'ostéosarcome. A, Expression relative de gènes liés à l'hypoxie dans les cellules 2D MG-63 traitées avec différentes concentrations de $CoCl_2$. B, Expression relative de gènes résistance aux médicaments dans les cellules 2D MG-63 traitées avec différentes concentrations de $CoCl_2$. C, Analyse en Western Blot du niveau de protéine HIF1α dans les cellules 2D MG-63 traitées avec différentes concentrations de $CoCl_2$. D, Expression relative par analyse en qPCR de gènes liés à l'hypoxie dans les cellules 3D MG-63. E, Expression relative par analyse en qPCR de gènes de résistance aux médicaments dans les cellules 3D MG-63.*

2. Effet de la Flavagline sur les modèles cellulaires

Nous avons ensuite utilisé de la Flavagline synthétisée (FL3), une molécule pharmacologique connue pour avoir des effets anticancéreux, comme un outil pour tester nos modèles d'hypoxie.

Tout d'abord, la viabilité des cellules a été analysée par le test Alamar Blue™, mesurant l'activité métabolique, à différent temps de traitement et différentes concentrations de FL3. Nous avons pu observer une diminution d'environ 60% de viabilité cellulaire pour les deux lignées tumorales à une concentration de 200nM pour un traitement de 48h (Figure 4A). Ces résultats ont été appuyés par les analyses par cytométrie en flux révélant un arrêt du cycle cellulaire en G2 (Figure 4B). Ces données sont corroborées avec la diminution de l'expression protéique de la cycline D1, qui est une protéine importante pour la progression à travers la phase S, ainsi qu'une augmentation de la protéine phospho-p38 MAPK (Mitogen-activated protein kinases) connue pour activer le point de contrôle G2/M pour la réparation de l'ADN et la survie cellulaire (Figure 4C).

L'observation des deux lignées tumorales après traitement à la FL3 indiquait un arrêt de la prolifération et une mort des cellules. Cependant, l'analyse par cytométrie en flux utilisant l'annexine V et l'iodure de propidium n'a pas révélé de mort par apoptose, indiqué également par l'absence d'expression de la caspase-3 clivée dans les cellules traitées.

Puisque nous avons trouvé une diminution de la viabilité cellulaire mais pas d'apoptose dans les cellules 2D traitées avec la FL3, nous avons étudié ses effets sur les cellules en 3D pour le gène de prolifération Ki67 et les gènes liés à l'apoptose Bax et Caspas-3. FL3 dans le modèle 3D seul n'a pas montré d'effet comparé au contrôle, cependant, dans le modèle 3D+$CoCl_2$, il y avait une diminution significative de Ki67. A l'inverse, nous avons pu observer une augmentation des gènes relatifs à l'apoptose, Bax et Caspase-3, dans les modèles 3D et 3D+$CoCl_2$. L'apoptose provoquée par FL3 dans nos modèles 3D était attendue, mais l'absence de marqueur apoptotique en 2D nous a interpellés. Ainsi, nous avons effectué un test de β-Galactosidase pour voir si la Flavagline pouvait induire une sénescence dans nos cellules. Nous avons en effet pu voir quelques cellules MG-63 sénescentes à 6 jours post-traitement, et un grand nombre pour les cellules U87-MG dès 2 jours post-traitement.

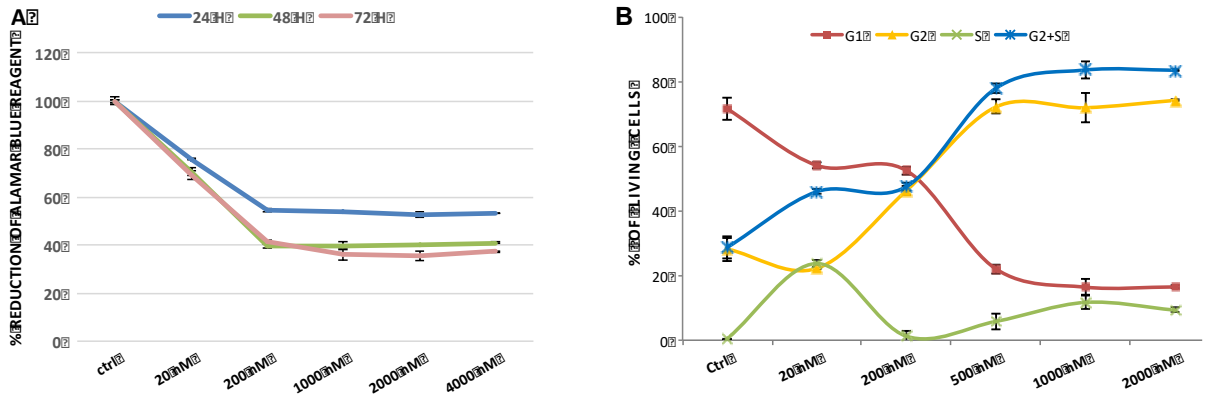

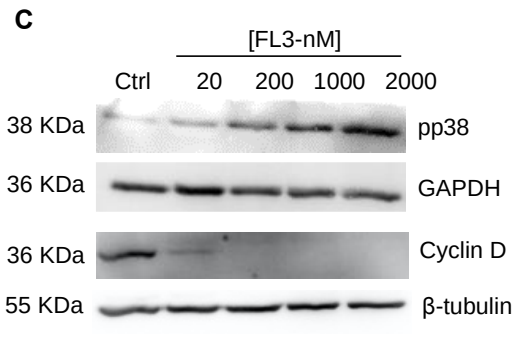

***Figure 4** : Effet de FL3 sur le modèle d'hypoxie 2D et 3D de l'ostéosarcome. A, Analyse de la viabilité des cellules par dosage Alamar Blue™ dans les cellules 2D MG-63 traitées par différentes concentrations de FL3. B, Représentation du pourcentage de cellules dans chaque phase du cycle cellulaire traitées avec différentes concentrations de FL3. C, Analyse en Western Blot du niveau de protéines phospho-p38 et Cycline D dans les cellules 2D MG-63 traitées avec différentes concentrations de FL3.*

➢ Conclusion

Pour la première partie du projet, en utilisant cette stratégie combinée 2D/3D, nous avons montré que les cellules endothéliales pouvaient former un réseau vasculaire en présence de cellules tumorales en sphéroïdes 3D. La combinaison de cellules 2D HUVEC et 3D MT-MG-63 a augmenté l'expression de facteurs angiogéniques, tels que VEGF, ICAM1 et CXCR4, ce qui favorise la prolifération des cellules endothéliales et la formation de structures tubulaires. Ce réseau néo-vasculaire exprime le collagène IV, un marqueur spécifique des vaisseaux, infiltre les sphéroïdes tumoraux et forme des structures tubulaires présentant une lumière. Cette stratégie innovante pourrait être utilisée comme point de départ pour développer l'angiogenèse tumorale *in vitro* en tenant compte non seulement de l'expression des facteurs angiogéniques, mais également de l'environnement cellulaire 3D. Notre stratégie pourrait être une première étape dans l'optimisation d'un environnement 3D tumoral *in vitro* pour être plus proche de l'*in vivo.*

Dans la seconde partie du projet, la culture des spheroïdes 3D a permis l'augmentation de l'expression de HIF1α et de ses gènes associés, augmentation potentialisée par l'ajout de $CoCl_2$. La combinaison 3D+$CoCl_2$ serait un bon modèle pour le criblage des médicaments en termes de résistance aux traitements anticancéreux pour une meilleure sélection des nouvelles molécules thérapeutiques. En effet, dans les deux lignées cellulaires utilisées, le modèle 3D+$CoCl_2$ a montré que c'était un système mimant mieux l'*in vivo*. Le traitement à la Flavagline (FL3) a entraîné une diminution de la viabilité cellulaire dans les deux lignées tumorales et un arrêt du cycle cellulaire en phase G2, corrélé à une augmentation de phospho-p38 et une diminution de la cycline D1. Et surtout, cette étude a montré que la FL3 semblait induire une mort cellulaire différente dans le modèle de cellules en 2D et celui en 3D.

L'angiogenèse et l'hypoxie sont des aspects critiques du développement et de la progression tumorale, de l'émergence de métastases, de l'agressivité du cancer et ainsi du pronostic vital du patient. L'incorporation et la prise en compte de ces deux facteurs au sein d'un modèle *in vitro* permettrait de mieux récapituler le microenvironnement tumoral *in vivo* et ainsi de

perfectionner la création d'une plateforme de criblage de médicaments plus robuste, perspicace et optimisée.

Les perspectives de ce projet portent sur la combinaison de ces deux facteurs dans un système microfluidique. Ce système microfluidique comprend les caractéristiques structurelles des constructions tumorales 3D, des paramètres biomécaniques et cinématiques, tels que la rigidité et l'anisotropie de la matrice, adhérence cellulaire et conditions d'écoulement. De plus, nous utiliserons des cellules non seulement de lignées cellulaires immortalisées, mais également des cellules tumorales obtenues à partir de biopsies de patients, également des cellules stromales, des cellules immunitaires et des cellules endothéliales. Ce système microfluidique 3D permettra de contrôler et d'étudier les milieux de culture cellulaire et le transport des médicaments, l'élimination des déchets, la cytotoxicité et les gradients de concentration des facteurs circulants. Ces paramètres contribuent tous à la création d'un modèle *in vitro* imitant le microenvironnement *in vivo* et permettant d'optimiser le criblage de médicaments, et ouvrant ainsi une voie vers la médecine personnalisée.

List of contents

List of Tables

List of figures

List of abbreviations

Abbreviation	Description
A	
ABC	ATP-binding cassette
ABCG2	ATP Binding Cassette Subfamily G Member 2
ALL	Acute lymphoblastic leukemia
AML	Acute myeloid leukemia
Ang-2	Angiopoetin-2
AKT/PKB	Protein kinase B
B	
BCRP	Breast cancer resistance protein
BM-hMSCs	Bone marrow-derived human mesenchymal stem cells
Bcl-2	B-cell lymphoma 2
BrdU	Bromodeoxyuridine
BSPII	Bone sialoprotein II
C	
CAIX	Carbonic Anhydrase IX
CDK4	Cyclin-dependent kinase 4
CLS	Capillary-like structures
CLL	Chronic lymphocytic leukemia
CML	Chronic myeloid leukemia
$CoCl_2$	Cobalt Chloride
CXCR4	C-X-C chemokine receptor type 4
CXCL8	C-X-C Motif Chemokine Ligand 8
D	
DPC	Dental pulp cells
2D	Two dimensions
3D	Three dimensions
E	
EB	Embryoid body
ECM	Extracellular Matrix
ECs	Endothelial cells
eIF-4E	Eukaryotic translation initiation factor 4E
EMT	Epithelial-Mesenchymal Transition
EPCs	endothelial progenitor cells
EPh-B	Ephrin-B
ERK	Extracellular Signal-Regulated Kinase
ES	Embryonic stem cell

F	
FL3	Flavagline
G	
GBs	Glomeruloid bodies
GFP	Green Fluorescent protein
GLUT 1/3	Glucose transporter type 1/3
H	
HDMEC	Human Dermal Microvascular Endothelial Cells
hEPCs	human endothelial progenitor cells
HIF1α/2α	Hypoxia induced factor 1α/2α
HREs	Hypoxia response elements
HSF1	Heat shock factor 1
Hsp90	Heat shock protein 90
HTS	High Throughouput Screening
HUVEC	Human Embilical vein endothelial cell
I	
IAP-2	Inhibitor Of Apoptosis Protein 2
ICAM-1	InterCellular Adhesion Molecule-1
IGF2	Insulin-like growth factor-2
IMG	Intussusceptive Microvascular Growth
L	
LIF	Leukemia inhibitory factor
LRP	Lung resistance protein
M	
MAPK	Mitogen-activated protein kinases
MCP-1	Monocyte chemoattractant protein 1
Mdm2	Mouse double minute 2 homolog
MDR1	Multidrug-resistance
MMPs	Matrix metalloproteases
MNK	Mitogen-Activated Protein Kinase Interacting Protein Kinase
MRP1	Multidrug-resistance-associated protein 1
mTOR	Mammalian Target of Rapamycin
MTs	Microtissues
N	
NANOG	Nanog homeobox
NT2D1	Teratocarcinomal cancer stem-like
O	
OC	Osteocalcin
OCT4	Octamer-binding transcription factor 4
OPN	Osteopontin

P

PAS	(Per-Arnt-Sim) domain protein
PDGF	Platelet-derived growth factor
PDMS	Polydimethylsiloxane
PECAM-1	Platelet endothelial cell adhesion molecule-1
Pgp	Pglycoprotein
PHB	Prohibitin
PHDs	Propyl hydroxylases
PI3K	Inositol-4,5-bisphosphate-3-kinase
PLGA	Poly lactic-co-glycolic acid
pVHL	von Hippel–Lindau protein
p53	Tumor protein 53
PTEN	Phosphatase and tensin homolog deleted on chromosome 10

R

RAS	Proto-oncogene, GTPase
ROS	Reactive oxygen species

S

SA-βgal	Senescence-associated beta-galactosidase
SDF1	Stromal cell-derived factor 1
SEM	Scanning electron microscopy
Sox2	Sex determining region Y-box2

T

TAMs	Tumor-associated macrophages
TGF-β1	Transforming growth factor beta 1
TNF-α	Tumor necrosis factor-α
TCA	Tricarboxylic acid
TXNIP	Thiredoxin-interacting protein

U

UCB	Urothelial carcinoma of the bladder

V

VCAM1	Vascular cell adhesion protein 1
VEGF	Vascular endothelial growth factor
VEGFR-1	Vascular endothelial growth factor Receptor-1/-2
VPF	Vascular permeability factor
VSMC	Vascular smooth muscle cells

INTRODUCTION

CHAPTER I

Cancer is a genetic disease usually characterized by abnormal cell growth. Normally, human cells grow and divide to form new cells in a constant cycle to repair and replace old cells. However, when cancer develops, this process is disordered, and cells grow in an unrestrained fashion. This may result in tumor formation leading to the spread throughout the body. There are over 100 types of cancer based on the organ or tissue of origin. It is a major cause of morbidity and mortality worldwide, with a disease burden estimated to increase over the coming decades [1].

1. Hallmarks of cancer:

Six hallmarks of cancer constitute an organizing principle for rationalizing the complexities of neoplastic diseases. As normal cells evolve progressively to a neoplastic state, they acquire a succession of these hallmark capabilities [2]. The hallmarks comprise sustaining proliferative signaling, evading growth suppressors, resisting cell death, enabling replicative immortality, inducing angiogenesis, and activating invasion and metastasis (Figure 1). These hallmarks continue to provide a solid foundation for understanding the biology of cancer and they have raised the test of time as being integral components of most forms of cancer [3];[2].

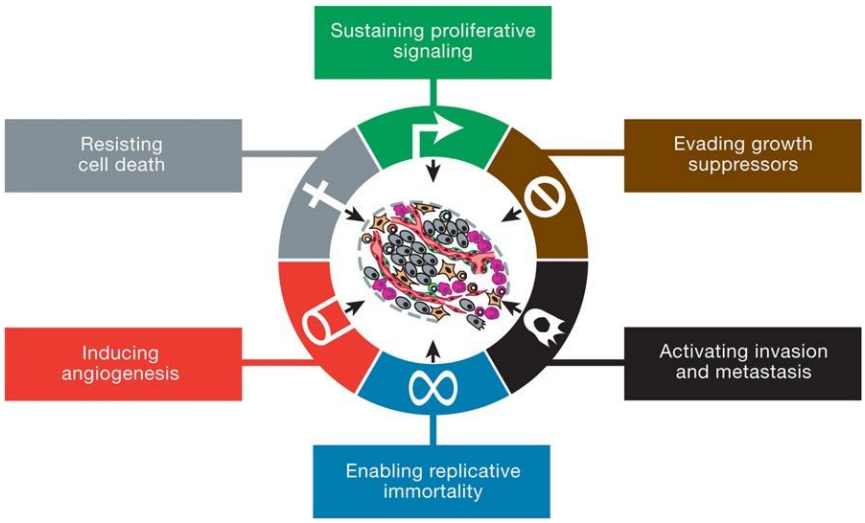

Figure 1: The Hallmarks of Cancer. Schematic illustration showing the six hallmarks of cancer [2].

1.1. Sustaining proliferative signaling

Normally, our normal tissues control the production and release of growth-promoting signals which maintain cell growth and cell division, thereby sustaining the normal tissue architecture and function. However, in cancer cells, dysfunction of these signals will direct them to become chief of their own intentions. They can maintain the proliferative signaling property producing growth factors ligands to act on their own receptors creating an autocrine stimulation, and by sending signals to stimulate normal cells in the tumor's stroma to supply the cancer cells with growth factors [4];[5].

1.2. Evading growth suppressors

This hallmark highlights the capability of cancer cell of surpassing the negative programs that regulate cellular proliferation. Moreover, these programs depend on the activation of tumor suppressor genes which act on limiting the cell growth and proliferation [6].

1.3. Resisting cell death

During the course of tumorigenesis, cancer cells experience a physiologic stress that trigger apoptosis. Among these apoptotic stresses are those arriving from signaling imbalances as a result of elevated levels of oncogene signaling, and DNA damage associated with hyperproliferation. Moreover, the apoptotic process is made of upstream regulators and downstream effector components. The regulators are divided into two major paths, one receiving and processing extracellular death-inducing signals (the extrinsic apoptotic program), and the other sensing and incorporating a variety of signals of intracellular origin (the intrinsic program). The ‘‘apoptotic trigger’’ that transfers signals between the regulators and effectors is controlled by compensating pro- and antiapoptotic members of the Bcl-2 family (apoptosis inhibitor) of regulatory proteins [6];[7].

1.4. Enabling replicative immortality

It has been shown that cancer cells require successive cell growth and division cycles in order to generate macroscopic tumors. However, most normal cell lineage in our body have limitations to pass through these cycles. One of these limitations is the senescence, an

irreversible arrest of cell proliferation; the other is crisis, which is involved in cell death. In general, when cells undergo repeated cycles of cell division, enter in a state of senescence, by contrast, some cells surpass this state and enter in a crisis state in which many cells die. Immortalization emerges when the cells have the ability to proliferate, circumventing both states of senescence and crisis [6].

Induction of senescence is triggered when shortening of telomeres occur, leading to exhaustion of replication potential. Successive divisions lead to cycles of chromosomal fusion and breakage, developing genomic instability and permitting accumulation of alterations [8]. Consequently, cell senescence is emerging theoretically as a protective barrier to neoplastic expansion that can be triggered by various proliferation-associated abnormalities, including high levels of oncogenic signaling and subcritical shortening of telomeres [6].

1.5. Activating invasion and metastasis

The invasion-metastatic cascade is a series of cell-biologic changes. The series begins with local invasion, then intravasation by cancer cells into nearby blood and lymphatic vessels, followed by transport of cancer cells through the lymphatic and hematogenous systems. Next, the outflow of cancer cells from the lumina of such vessels into the parenchyma of distant tissues (extravasation) occurs, followed by the formation of small nodules of cancer cells (micrometastasis), and finally the growth of micrometastatic lesions into macroscopic tumors leading to a process called ‘colonization’ [6].

1.6. Inducing angiogenesis

During embryogenesis, the development of the vascular system is crucial for the cellular and tissue progression. This involves the birth of new endothelial cells and their assembly into tubules (vasculogenesis) and sprouting of new vessels from existing ones (angiogenesis). Like normal cells, cancer cells need to sustain a supply of nutrients and oxygen in order to survive and proliferate, and this process is maintained by the process of angiogenesis [6]. (*This part will be discussed further in details*)**.**

CHAPTER II

1. Screening Technologies

Screening and high-throughput screening aim to create or to produce biologically pertinent assays that are appropriate, reproducible, consistent, and robust. The discovery program encompasses different aspects ranging from developing a pharmaceutical drug to toxicity monitoring assay. In other words, screening is a selective procedure to find few compounds from a large group in order to obtain a specific desired biological activity, whereas HTS relies on the rate, quantity, or automation level of the testing [9].

Drug discovery is a time-consuming process and a costly effort that includes huge financial and human resources. It is estimated that over 12–15 years more than 800 million dollars are invested for the development of a single approved new drug [10]. To overcome these circumstances, it is important to develop new skills to fabricate the next generation of drug-screening platforms at higher throughput in order to reduce time and cost.

2. The requirements for drug screening platforms in cancer

Tumor microenvironment is known to be a major factor of intrinsic resistance to anticancer treatment. In solid tumor types, including breast cancer, lung, and pancreatic cancer, stromal components provide a fibrotic niche, which promotes stemness, Epithelial-Mesenchymale Transition (EMT), chemo and radioresistance of the tumor. However, this microenvironment is not recapitulated in the conventional cell monoculture or xenografts, and thus *in vitro* and *in vivo* preclinical models are unlikely to be predictive of clinical response, which lead to poorly rely on these preclinical drug-screening models [11]. Moreover, in order to predict the clinical activity of an anticancer drug, one should truly summarize this complex disease in terms of tumor microenvironment. One important model system for evaluating candidate anticancer agents is human tumor-derived cell lines. This exhibits different culture growth and survival properties, in comparison to their naturally growing counterparts. However, recent technologies in drug discovery facilitate the parallel analysis of large groups of these

cell lines, together with the genomic technologies to assess the clinical usefulness of new investigational cancer drugs and to discover predictive biomarkers [12].

Predicting the efficacy of anticancer therapy is a standard goal. To achieve this goal, scientists require preclinical models that can consistently screen anticancer agents with strong clinical association. Therefore, tumors contain a heterogeneous architecture of malignant cells, normal and abnormal stroma, immune cells, and dynamic microenvironment containing chemokines, cytokines, and growth factors. Thus, there is an increasing challenge to develop models that can accurately mimic the diversity of the tumor ecosystem, and therefore predict how tumors respond or resist to treatment [13].

Over the past years, there has been a massive increase in drug discovery research for anticancer, ranging from general cytotoxic agents that broadly attack malignancies to the development of more focused compounds such as kinase targeted molecules that directly attack oncogenes [14]. Despite the importance of this discovery achievement and the thousands of developed molecules, only 5% of lead drug candidates reach the clinic state. Indeed, a major limitation to drug development and clinical success is to predict patient outcomes before reaching clinical trial.

To achieve a good preclinical model, it should be amenable to high-throughput screening, and reflecting human-tumor biology as closely as possible. However, this increases a huge barrier in the development of successful preclinical models for cancer drug discovery [13];[15]. There was a revolution over the last decade in drug discovery and development of small molecule cancer drugs moving from a one-size-fits-all approach that underlined cytotoxic chemotherapy to the personalized medicine strategy. The latter is a powerful approach that relies on the discovery and development of molecularly targeted drugs depending on the genetic behavior and characteristics of cancer cells by introducing cancer genome sequencing into screening platforms. In addition, this massive emerging opportunity in functional genomics and proteomics necessitates a start from the linear process of identification, evaluation, and enhancement activities towards a more integrated parallel process [16].

Moreover, predicting drug toxicity is also a major concern in drug discovery platforms in early stages using *in vitro* cell-based assays, which represents an essential aspect of *in vivo* pharmacology and toxicology. Thus, a main challenge in drug candidates screening and in development of new chemicals or biological entities is the accurate determination of their human toxicity [17].

3. Drug screening platforms using 3D models

Numerous efforts aim at finding new and more effective ways to treat cancer. Among these strategies is screening of anticancer drugs [18]. Standard screening has typically been evaluated in animal models. However, some results have shown that animal experiments do not always predict clinical effect in humans, especially with regard to toxicity assessments [19]. Moreover, the use of animals for research is often restricted due to ethical concerns [20]. In light of these issues, an *in vitro* cell-based model is a great alternative, minimizing the need for and number of animal experiments. 2D cell culture was the first procedure established for cell-based screening assays. Although 2D cell culture methods are simple, quick, cost-effective, and have been widely investigated, they present many disadvantages. The primary disadvantage of a 2D system is that it does not mimic an actual 3D tumor and is not biologically relevant [21]. Cells in the *in vivo* environment usually interact with neighboring cells and the ECM; however, 2D cell models cannot recapitulate those characteristics. Thus, a 2D culture model may be totally different from an actual growing tumor with regards to cell morphology, cell proliferation, and gene and protein expression [22]. As a result, only 10% of the drugs passed through *in vitro* testing had a positive effect in the clinic or led to drug approval. The percentage of anticancer drugs which have shown clinical efficacy is even lower, at about 5% [23]. The high rate failure in the clinical testing phase is a waste of time and money. Therefore, it is important to identify promising *in vitro* culture models for evaluating drug efficacy in the early stages of drug discovery and development. Given the advantages of 3D versus 2D cell culture models, 3D cell culture techniques have attracted great attention. The 3D cell culture systems allow cell-based assays to be more physiologically relevant, particularly since cell behavior in 3D culture is much more similar to that of cells in *in vivo* tissues. In 3D models, cell-cell and cell-ECM interactions are maintained, such that cell morphology, proliferation, differentiation, migration, apoptosis, gene expression and protein expression are comparable to those of cells *in vivo* [22].

3D culture of cancer cells forms multicellular tumor spheroids that are tumor cell aggregates grown from one or several cell clones. This *in vitro* model has a three-dimensional structure that mimics micro-tumors or metastases and some of their properties. Multicellular tumor spheroids present, in their center, a necrotic area. The size of necrosis varies according to the spheroid diameter and the cellular type, and due to oxygen gradient, pH, and nutrients [24]. These spheroids will support anchorage-independent growth with functional and mass transport properties similar to those observed in micrometastasis or poorly vascularized regions in solid tumors [25].

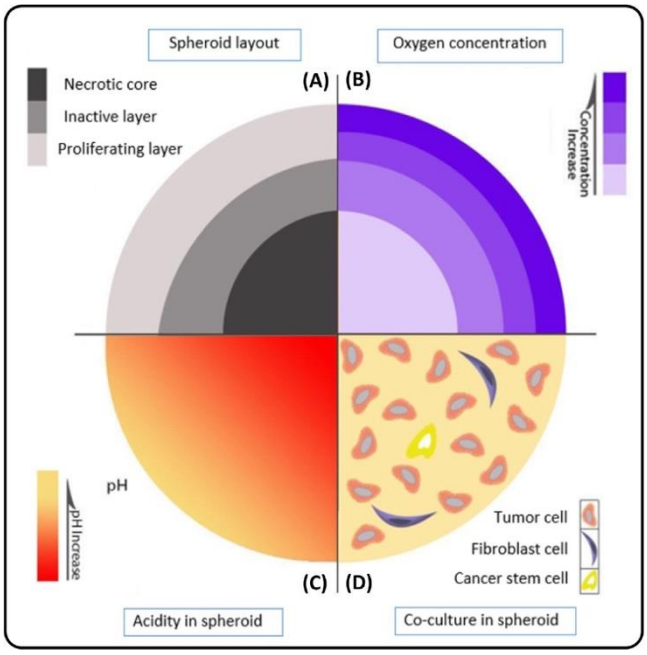

Figure 1: Tumor spheroid characteristics: spheroid layout, acidity, oxygen concentration and cellular content [26].

An ideal 3D model should provide an environment where a combination of factors joined together to create a tissue specific physiological or pathophysiological disease-specific microenvironment where cells can proliferate, aggregate and differentiate. Such model should take into consideration many factors including cell-to-cell and cell-to-ECM interactions, tissue-specific stiffness, oxygen, nutrient and metabolic waste gradients, and a combination of tissue-specific scaffolding cells [27]. Most 3D culture techniques (table 1) are often categorized into non-scaffold, anchorage independent and scaffold-based 3D culture systems as well as hybrid 3D culture models in which formed spheroids are incorporated into a 3D polymeric scaffold. Each of these techniques has strengths and limitations (table 2).

However, many of the newer 3D culture systems permit for microscale 3D cultures and provide a first step toward emerging knowledge for 3D cultures that are compatible with automated high-throughput screening helping in the discovery of new drug candidates or relocating of known drugs in physiologically more relevant cell cultures. Thus, one will need to choose the most appropriate 3D cell culture model for a specific application.

Table 1: Summary of spheroid-based assays including spheroid formation techniques, experimental setups, variables to study and experimental outputs [28].

Spheroid Formation	Experimental Setup	Variables	Outputs
Suspension/Spinner Flasks	Spheroids in Media	Proliferation/ Migration/Invasion	Characterization of spheroid composition, growth and proliferation Protein and gene expression changes Migration and invasion assays
Liquid Overlay Technique Non-adherent Surfaces	Spheroids in Matrix	Drug Screening	Characterization of spheroid composition, growth and proliferation Protein and gene expression changes Survival assays Efficacy, distribution and accumulation of therapeutics
Hanging Drop Technique	Coculture Spheroids	Angiogenesis	Characterization of spheroid composition, growth and proliferation Protein and gene expression changes (i.e. angiogenic factors) Migration and invasion assays Angiogenesis assays
Microfluidic	Cancer cell Endothelial cell Immune cell	Immune Cell Response	Characterization of spheroid composition Protein and gene expression changes Adhesion assays Infiltration of immune cells into spheroids Migration and extravasation assays

Table 2: Advantages and Disadvantages of Different 3D Cell Culture Techniques [33].

Method type	Advantages	Disadvantages
Forced-floating	• Relatively simple • Inexpensive • Suitable for high-throughput testing • Spheroids produced are easily accessible	• Variability in cell size and shape if not as fixed cell no./well • DIY plate-coating is relatively labour intensive
Hanging drop	• Inexpensive if using standard 96-well plate • Homogenous spheroids suitable for high-throughput testing • Spheroids produced are easily accessible	• More expensive if using specialised plates • Labour intensive if preparing plates in-house • Small culture volume makes medium exchange, without disturbing cells, difficult (proposed easier handling with commercially available formats)
Agitation-based approaches	• Simple to culture cells • Large-scale production relatively easily achievable • Motion of culture assists nutrient transport • Spheroids produced are easily accessible	• Specialised equipment required • No control over cell no./size of spheroid (can be overcome by additional culture step; see 'Forced-floating methods') • Time consuming for HTS due to extra step required for homogenous spheroids • Cells possibly exposed to shear force in spinner flasks (may be problematic for sensitive cells)
Matrices and scaffolds	• Provide 3D support that mimics *in vivo* • Some incorporate growth factors	• Can be expensive for large-scale production • Can have difficulty in retrieving cells following 3D culture formation
Microfluidic cell culture platforms	• Described as suitable for high-throughput testing	• Specialised equipment required adding expense • Further analysis of 3D cultures produced may be difficult

4. Microfluidic 3D *in vitro* cancer models

New capabilities to understand cancer and create new roads in cancer research have been emerged currently by the introduction of microfluidic 3D *in vitro* cells models. This is due to the incorporation of tissue engineering into these microfluidic 3D systems that resulted in the evolution of practical *in vivo*-like *in vitro* cancer models.

Microfluidic devices or systems help culturing the cells under perfusion with respect to their supply in oxygen and nutrients as well as mimicking the shear forces that are found *in vivo*. As the result of blood flow, they allow a continuous application of drugs and other soluble molecules like growth factors, understand the effect of the exchange of fluids in different cells compartments and improve the utility of long term tumor cultures [30].

Microfluidic 3D systems provide new insights and results that are not previously obtained because of their reduced volume, which eases the incorporation of this system to invent various microenvironmental components for tumor progression and development. Moreover, it leads to the development of many environmental parameters as well as understanding how these parameters work together to regulate cancer. It has been shown that ECM proteins such as collagen I, fibronectin, and laminin can be measured using these microfluidic systems with significantly low cost [31]. Moreover, co-culture of breast cancer epithelial cells with stromal fibroblasts becomes more responsive to ECM composition, by using a reduced number of

cells from patient's biopsy to study a specific endpoint. This will also allow to study efficiently a large number of endpoints at the same time, and thus studying the characteristics of each patient tumor's with limited time and low cost [32].

Microfluidic 3D *in vitro* models will offer great advances in understanding the biological mechanisms in tumor tissue as well as better orientation in designing the more physiologically compatible with structures [33]. Furthermore, it is crucial to incorporate the biomaterials science in microfluidic tumor and tissue engineering systems because constructing a physiologically relevant 3D tissue *in vitro* necessitates the use of proper materials that have the desired degradation rates, products, as well as good mechanical properties for the desired tissue. An example of these well-designed materials is the signaling molecules like growth factors in 3D *in vitro* models [34];[35]. In addition, another achievement is the use of ECM that can be cleaved only by specific proteases which mimic the signaling mechanisms in the interactions of cell-ECM *in vivo* [36].

The microfluidic 3D systems use biomaterials by modifying their chemical and mechanical characteristics. In order to maximize the efficacy and functionality of the microfluidic models, they need a synchronized collaboration with other disciplines such as tissue engineering and biomaterials science. This will facilitate the translation of these skills into innovative methods for drug development and HTS as well as in clinical research.

Chapter III

1. Vascularization Mechanisms in Cancer

Although cancer cells are not generally controlled by normal regulatory mechanisms, tumor growth is highly dependent on the supply of oxygen, nutrients, and host-derived regulators. It is now established that tumor vasculature is not necessarily derived from endothelial cell sprouting; instead, the cancer tissue can acquire its vasculature by co-option of pre-existing vessels, intussusceptive microvascular growth, postnatal vasculogenesis, glomeruloid angiogenesis, or vasculogenic mimicry (Figure 2). The best known molecular pathway driving tumor vascularization is the hypoxia-adaptation mechanism [37].

1.1. Endothelial Sprouting

The best-known mechanism by which tumors promote their own vascularization is inducing new capillary buds from pre-existing host tissue capillaries.

The basement membrane is locally degraded on the side of the dilated peritumoral postcapillary venule situated closest to the angiogenic stimulus, interendothelial contacts are weakened, and endothelial cells (ECs) emigrate into the connective tissue towards the angiogenic stimuli. Furthermore, there is formation of a solid cord by ECs succeeding one another in a bipolar fashion. Thus, lumen formation occurs by cell-body curving of a single EC or by participation of more ECs in parallel with the synthesis of the new basement membrane and the recruitment of pericytes/mural cells (**perivascular cells** that include vascular smooth muscle cells (VSMCs) and pericytes (cells relating to the wall of the blood vessel)) [38].

During the process of endothelial sprouting, vessels initially dilate and become leaky in response to vascular permeability factor/vascular endothelial growth factor (VPF/VEGF) [39]. This is mediated by the up-regulation of nitric oxide, the development of fenestrations and vesiculo-vacuolar organelles, and by the redistribution of CD31/PECAM-1 and vascular endothelial (VE)-cadherin. The gel-sol transition (gelation) of the basement membrane that is mediated by matrix metalloproteases (MMPs), gelatinases, and the urokinase plasminogen activator system could be partly responsible for the initiation of EC proliferation and migration. Angiopoetin-2 (Ang-2), a mediator of Tie-2 signaling, is involved in the detachment of pericytes and in the relaxing of the matrix. In addition, a large number of molecules stimulate endothelial proliferation and migration, including TGF-β1, tumor necrosis factor (TNF)-α, members of the chemokine system and the VEGF, fibroblast growth factor (FGF), and platelet-derived growth factor (PDGF) families. Furthermore, a wide variety of integrins has been shown to be expressed during sprouting, including $\alpha_1\beta_1$, $\alpha_2\beta_1$, $\alpha_3\beta_1$, $\alpha_5\beta_1$, $\alpha_v\beta_5$, and $\alpha_v\beta_3$. Perhaps the most important among them is $\alpha_v\beta_3$, which mediates the migration of ECs in the fibrin-containing cancer stroma and maintains the unique state or feature of the basement membrane because of its ability to bind to MMP-2. During maturation of nascent vessels, PDGF-BB recruits pericytes and smooth muscle cells, whereas TGF-β1 and Ang-1/Tie-2 stabilize the interaction between endothelial and mural cells. In conclusion, we can say that a tightly regulated balance of pro-angiogenic factors and inhibitors controls sprouting: an angiogenic cytokine promotes EC proliferation, migration or lumen formation, whereas an inhibitor interferes with these steps and modulates the proliferation or migration activity of ECs. However, individual tumor types use various combinations of pro-angiogenic and inhibitory cytokines (figure 3a) [40];[41].

1.2. Vessel co-option

Vessel co-option (or vascular co-option) is a mechanism in which tumors obtain a blood supply by borrowing the existing vasculature and tumor cells migrate along the vessels of the host organ. The co-opted vessels are usually supported by pericytes from outside of the vessels. Pericytes are the supporting cells that stabilize blood vessels by accelerating the metabolism of lysophosphatidic acid [42], while promoting endothelial cell survival via induction of autocrine VEGF-A signaling [43]. Recent evidences suggest that the co-opted vessels can better survive after tumor vasculature normalization, and vessel co-option is an important approach of a solid tumor to evade anti-angiogenic therapy (figure 3b) [44].

1.3. Intussusceptive Microvascular Growth (IMG)

IMG refers to vessel network formation by incorporation of connective tissue columns, called tissue pillars, into the vessel lumen and to subsequent growth of these pillars, resulting in subdividing of the vessel lumen. This type of angiogenesis, which has been observed in a wide variety of normal and malignant tissues, is faster and more economical than sprouting; it occurs within hours or even minutes and does not primarily depend on EC proliferation, basement membrane degradation, and invasion of the connective tissue. Unlike the sprouting, IMG can work only on existing vessel networks. Therefore, the most important feature of IMG seems to be its ability to increase the complexity and density of the tumor microvessel network already built by sprouting, independent of EC proliferation. In addition, IMG can provide more surface area for further sprouting. Furthermore, intussusception is certainly synchronized by several cytokines.

Major candidates are the ones capable of mediating information between ECs or from ECs to mural cells, such as PDGF-BB, angiopoietins and their Tie receptors, TGF, monocyte chemotactic protein-1, and ephrins and Eph-B receptors [45].

After the initial stage of immature capillary network formation by sprouting, additional vascular growth and development of complex vascular beds, including their continuous remodeling and adaptation, may occur by intussusception in cancers. The absence of intense EC proliferation in IMG implies that neovascularization by this mechanism would be resistant to angiosuppressive treatment (figure 3c) [37].

1.4. Glomeruloid Angiogenesis

Glomeruloid bodies (GBs) are best known in high-grade glial malignancies, where they are one of the diagnostic histopathological features of glioblastoma multiforme. However, these complex vascular aggregates have also been described in a wide variety of other malignancies [46]. They are composed of several closely associated microvessels surrounded by a variably thickened basement membrane within which a limited number of pericytes are embedded. The presence of GBs was associated with markers of aggressive tumor behavior and it significantly reduced survival in cancer patients [47]. In the first animal model, GBs developed in mother vessels from recruitment and proliferation of ECs and pericytes (in the absence of tumor cells), and VEGF was essential for their induction and maintenance. In contrast to this model, the GB formation starts immediately after tumor cell extravasation, much earlier than the appearance of necrosis within the metastases. It is found that the proliferating and migrating tumor cells are able to pull the capillaries and the adjacent capillary branching points into the tumor cell nests. This process leads to the appearance of simple coiled vascular structures that later develop into GBs with multiple narrowed afferent and efferent capillaries. Despite the absence of sprouting angiogenesis, necrosis was rare in these lesions, suggesting that the blood supply from the preexistent vascular bed is sufficient to provide the tumor tissue. This type of GB formation cannot be termed as true angiogenesis; it rather represents a remodeling of the existing vasculature of the host lesions, suggesting that the blood supply from the preexistent vascular bed is sufficient to provide the tumor cells with oxygen and nutrients (figure 3f) [37].

1.5. Postnatal Vasculogenesis

Vasculogenesis or the differentiation of vascular ECs from primitive precursor cells, has been thought to appear only in the early stages of vascular development. However, new studies have established that circulating bone marrow-derived endothelial progenitor cells (EPCs) home to sites of physiological and pathological neovascularization and differentiate into ECs. EPCs may be assembled by tumor tissue derived cytokines from the bone marrow [48]. VEGF is the best-characterized cytokine during tumor progression, and the level of circulating VEGF has been shown to rise and to be associated with the number of EPCs in the circulation. After adhesion and insertion of EPCs into the monolayer of surrounding mature vascular ECs, additional local stimuli may stimulate the activation of local endothelium to explicit adhesion molecules to recruit EPCs. In addition to the physical contribution of EPCs to newly formed microvessels, the angiogenic cytokine release of EPCs may be a supportive

mechanism to improve neovascularization [49]. Moreover, VEGFR-1 hematopoietic progenitor cells that multiply in the bone marrow, mobilize to the peripheral blood along with VEGFR-2 EPCs, and integrate into pericapillary connective tissue, thus stabilizing tumor vasculature [50]. These cells seem to home in before the tumor cells arrive, promoting metastatic growth by forming niches where cancer cells can locate and proliferate (figure 3b) [51].

1.6. Vasculogenic mimicry

It is the ability of aggressive cancer cells to express an endothelial cell phenotype and to form vessel-like networks in three-dimensional culture, mimicking the pattern of embryonic vascular networks and recapitulating the patterned networks seen in patients with aggressive tumors correlating with a poor prognosis [52].

The concept of vasculogenic mimicry was developed to incorporate the existence of a fluid-conducting, laminin-containing extracellular matrix network, providing a site for nutritional exchange for aggressive tumors, and probably preventing necrosis (figure 3e) [53]. Vasculogenic mimicry has been confirmed in breast, prostate, ovarian, lung, synovial, rhabdomyo, Ewing sarcomas, and pheochromocytoma [54].

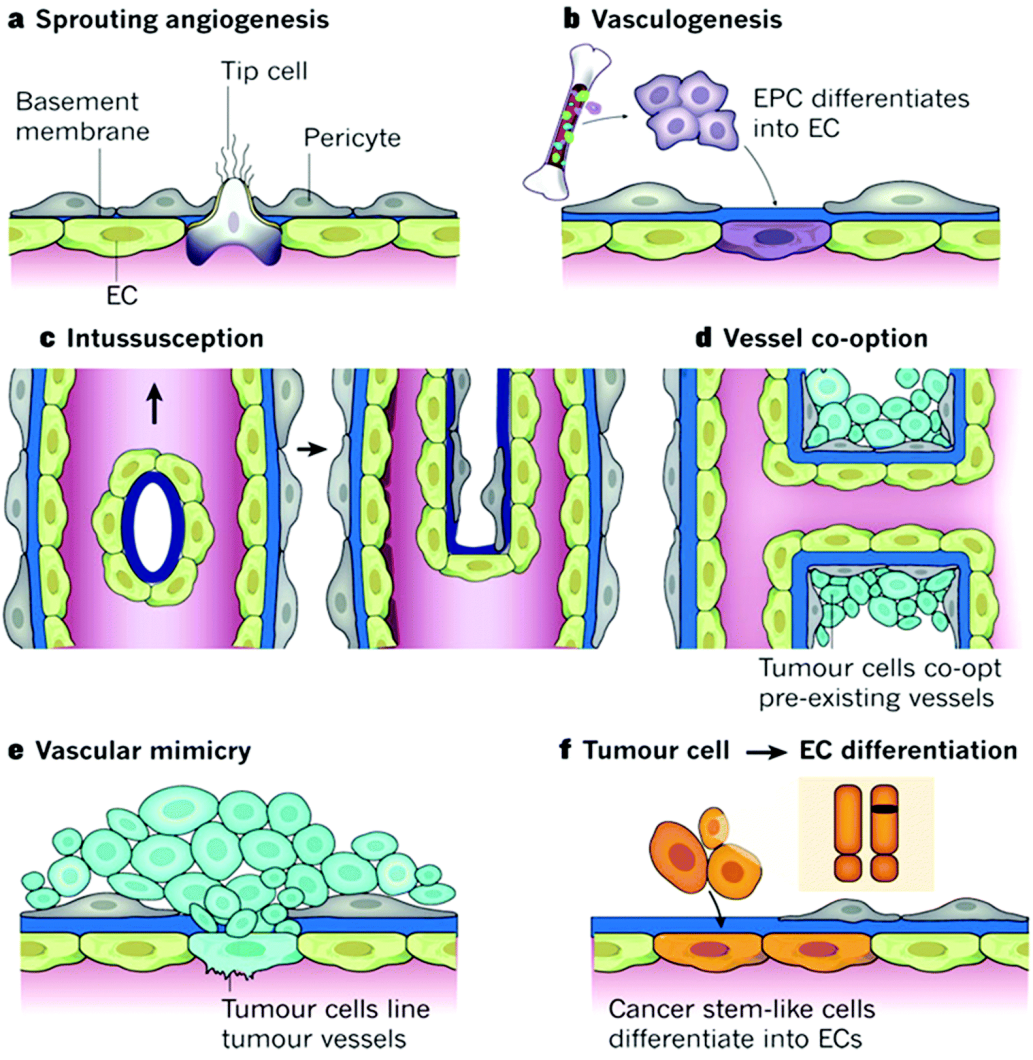

Figure 3: Different mechanisms of tumor vascularization [55].

2. The importance of cancer vascularization and its role in tumor pathogenesis

Cancer cells adapt to new environmental restrictions by increasing the number of receptors or by shifting from paracrine to autocrine production of growth factors. However, to create a clinically significant tumor mass, they mainly need to establish a vascular network to supply their mass transport requirements. Tumor vasculature, in addition to nutrient delivery, regulates tumor hemodynamics, local oxygen tension, and trafficking of immune cells [56].

The role of endothelium in mediating the tumor microenvironment can be enlightened from different features:

First, multiple cell types present within the tumor microenvironment, with endothelial cells being one type of them, consume common resources such as glucose. The competition for

these resources is itself a community modulator. As an example, the glucose uptake measurement has shown doubled amounts of consumption by endothelial cells compared to tumor-associated macrophages (TAMs).

Second, most studies have mostly claimed that the cancer cell genotype dictates the vascular network phenotype. However, strong evidence has shown that microvascular endothelium can also control the behavior of adjacent cancer cells. As an example, endothelial cells orient the stable microvascular zones secreting thrombospondin-1 and keep the metastatic cancer cells in a dormant state. Interestingly, cancer cells are encouraged to proliferate in sprouting neovascular stimuli with a low concentration of thrombospondin-1 and high amounts of periostin and transforming growth factor beta (TGF-β) secreted by endothelial cells [57].

Third, tumor has a crosstalk with homeostatic centers of the body and other tissues, which makes it more like an ecosystem. Vascular and lymphatic networks distributed across the body enable the communications. It was recently declared that the decreased density of lymphatic vessels and lymphocytes are microenvironmental marks of metastasis. Since lymphatic vessels facilitate the tumor antigen presentation for the initiation of immune priming, their absence covers the way for cancer cells to avoid immune cytotoxic mechanisms [58].

3. In vitro vascularization models

Vasculogenesis and angiogenesis are the fundamental processes by which new blood vessels are formed. Vasculogenesis is defined as the differentiation of precursor cells (angioblasts) into endothelial cells and the de novo formation of a primitive vascular network, whereas angiogenesis is defined as the growth of new capillaries from pre-existing blood vessels.

Table 3: The angiogenic molecules, their receptors and their functions [59].

Angiogenic Molecules	Receptors	Functions
VEGF	VEGF-R1 (Flt-1), VEGF-R2 (Kdr)	Initiation of angiogenesis: • Vascular permeability • Detachment of pericytes • Degradation of basement membrane Neovessel formation: • Endothelial cell proliferation and migration • Pericyte proliferation and migration
Angiopoietin-2	Tie-2	Initiation of angiogenesis: • Detachment of pericytes • Degradation of basement Adaptation to tissue needs: • Regression of neovessels due to lack of flow or presence of growth factor
FGFs	FGFRs	Neovessel formation: • Endothelial cell proliferation and migration • Pericyte proliferation and migration
PDGF-B	PDGFR	Neovessel formation: • Endothelial cell proliferation and migration • Pericyte proliferation and migration Maturation: • Attachment of pericytes • Deposition of basement membrane
PLGF	VEGF-R1 (Flt-1)	Neovessel formation: • Endothelial cell proliferation and migration
Thrombospondin-1	CD36, CD47, integrins	Neovessel formation: • Endothelial cell proliferation, migration, adhesion, and motility
Integrins	Extracellular matrix	Neovessel formation: • Endothelial cell proliferation, migration, adhesion, and motility • Endothelial assembly and lumen acquisition
SDF-1	CXCR4	Neovessel formation: • Endothelial cell migration, adhesion, and motility
DLL1-4	Notch	Neovessel formation: • Endothelial cell proliferation, migration, adhesion, and motility
SCF	c-Kit	Neovessel formation: • Endothelial cell proliferation and adhesion
Interleukins	Interleukin receptors	Neovessel formation: • Endothelial cell proliferation and migration
Angiopoietin-1	Tie-2	Maturation: • Endothelial assembly and lumen acquisition • Attachment of pericytes • Deposition of basement membrane • Vessel maintenance
Endothelin-1	Endothelin receptors (Et-A, Et-B)	Maturation: • Vascular permeability, vasoconstriction
Vasohibin-1	Vasohibin receptors	Maturation: • Inhibits endothelial cell proliferation and migration

CXCR4 = CXC chemokine receptor 4; DLL1-4 = delta-like ligands 1-4; FGF = fibroblast growth factor; FGFR = fibroblast growth factor receptor; Flt-1 = fms-related tyrosine kinase 1; Kdr = kinase insert domain containing receptor; PLGF = placenta growth factor; PDGF-B = platelet-derived growth factor beta; PDGF-R = platelet-derived growth factor receptor; SCF = stem cell factor; SDF-1 = stromal-derived growth factor; Tie-2 = TEK tyrosine kinase endothelial; VEGF = vascular endothelial growth factor; VEGF-R = VEGF receptor.

3.1. Vasculogenesis Models

Several *in vitro* systems have been developed for investigating the cellular events of vasculogenesis:

3.1.1. Embryo-derived mesodermal cell culture and embryonic stem cell differentiation assays

These assays enable researchers to virtually investigate vasculogenesis as it occurs in the embryo *in vivo*. Adherent cultures of dissociated cells from quail blastodiscs have been reported to generate both hematopoietic and endothelial cells that aggregate into characteristic blood islands and give rise to vascular structures in long-term culture. Vasculogenesis can also be observed when the same quail blastodisc cells are grown in suspension forming three-dimensional spheres. However, the formation of vascular structures in quail blastodisc cultures is strictly dependent on the presence of fibroblast growth factor-2 (FGF2) [60];[61].

3.1.2. The murine ES cell-derived embryoid body formation assay

This model system, whereby a primitive vascular plexus is formed, provides an attractive tool for dissecting the mechanisms involved in the vasculogenesis process: angioblast differentiation, proliferation, migration, endothelial cell-cell adhesion, and vascular morphogenesis can all be evaluated. ES cells, which are derived from the inner cell mass of mouse blastocysts, are maintained *in vitro* as totipotent stem cells by culture in the presence of the cytokine leukemia inhibitory factor (LIF). When LIF is removed, the cells spontaneously undergo *in vitro* differentiation, resulting in the formation of embryo-like structures called embryoid bodies that have the potential to generate all embryonic cell lineages. Blood island formation and many aspects of normal endothelial differentiation and growth, which lead to the formation of vascular channels, have been reported during ES-derived embryoid body development. Microscopic analysis has revealed that the vascular structures found within the walls of cystic embryoid bodies consist of endothelial cells that form tubular channels with typical endothelial junctions [62].

In addition, endothelial differentiation in ES-derived embryoid bodies was found to be sensitive to both angiogenic and antiangiogenic agents [63]. Thus, the ES/EB model also appears particularly useful for the identification of factors potentially involved in the regulation of angioblast differentiation and further blood vessel formation in a 3D tissue context.

3.2. Angiogenesis Models

In these models, the researchers observed that after long-term culture of capillary endothelial cells, the spontaneous organization of these cells into capillary-like structures (CLS) and the presence of a lumen within these CLS were confirmed by phase contrast microscopy and transmission electron micrography. These provide the basis for the definition of *in vitro* endothelial angiogenesis and the presence of a lumen in the CLS as a criterion for the validation of an *in vitro* model. From a physiological point of view, an ideal *in vitro* model would take into account all the representative steps of *in vivo* angiogenesis, from detachment of endothelial cells from the vascular wall to final tubular morphogenesis, maturation, and connection to a functional vascular network. Furthermore, it should be rapid, easy to use, reproducible, and easily quantifiable [64].

3.2.1. Two-Dimensional Models

They refer to those in which the planar organization of the cells lies parallel to the surface of the culture plate. In such assays, endothelial cells are seeded onto plastic culture dishes that have eventually been coated with adhesive proteins [65]. Alternatively, they can be loaded on top of a gel made of either collagen, fibrin, or Matrigel. Many reports state that CLS formation could be observed spontaneously in long-term planar cultures [66].

It was observed that endothelial cells either proliferate when seeded on Type I or III collagen or differentiate when seeded on Type IV/V collagen. Moreover, the Matrigel, a laminin-rich matrix, promoted the rapid formation of CLS and this could be induced in planar cultures and modulated by variable substrates, such as fibronectin, collagen IV, or gelatin, depending on the density of the coating [67]. It is now recognized that the mechanical signals sensed by cells from the substrate depend on the concentration and biochemical composition of the matrix and regulate the formation of CLS in 2D models [68].

3.2.2. Three-Dimensional Models

These assays are based on the capacity of activated endothelial cells to invade 3D substrates. The matrix may consist of collagen gels, plasma clot, purified fibrin, Matrigel, or a mixture of these proteins with others. The culture medium may be added within the gel before polymerization or on the top of the gel. It is possible to insert and culture vascular explants such as aortic rings in jellified matrices and then to observe endothelial cells sprouting from the intima and forming CL [69]. They closely fulfill the optimal conditions for an *in vitro* model because they allow the preservation of the vessel architecture during the *in vitro* assay, and thus they are close to an "*ex vivo*" model. They can be adapted to quantify angiogenic or angiostatic activities or to study extracellular matrix reorganization during morphogenesis.

Alternatively, one can observe the morphogenic response of isolated endothelial cells that have been seeded on or in gels. When confluent cells cultured on gels are stimulated by cytokines such as basic fibroblast growth factor (bFGF) or by phorbol esters, they invade the underlying gel and form CLS, switching from a planar confluent configuration to a differentiated 3D one [70]. Cells can also be directly overlaid by gels or sandwiched between two gel layers before the polymerization.

In other assays, cells are seeded in gels before polymerization, either dispersed, clustered as spheroids, aggregated, or attached onto microcarrier beads. The 3D models are closer to the *in vivo* environment than to the 2D ones, because they take into account more steps of angiogenesis. In fact, depending on the culture media composition (percentage of serum, addition of cytokines), cells can be induced to sprout, proliferate, migrate, or differentiate in the 3D configuration. Because the biogels are polymers, the concentration and the biochemical conditions of the matrix polymerization must be carefully defined because they may affect the density and the mechanical properties of the substrate, leading to either proliferative, migratory, or tubular endothelial cell phenotypes [71].

3D has provided great advances in the understanding of angiogenesis and appear mainly suitable for studying the effects of cytokines, the role of metalloproteases, and that of the fibrolytic pathway during tubulogenesis. In addition, they allowed the study of apoptosis and

showed the importance of the configuration and composition of the substrate, the role of cell adhesion molecules, and the effect of hypoxia [72].

Another important parameter can be investigated under the three-dimensional configuration is the bioavailability of angiogenic factors. The distance between the cells and the culture medium generates a gradient of diffusion of nutrients, oxygen, and stimulating factors. This is the case when the cells are seeded inside a gel (or sandwiched between two layers of gels) that is subsequently covered by culture medium. This gradient may represent what occurs during angiogenesis *in vivo*. Furthermore, the paracrine VEGF-induced morphogenesis of HUVECs depends on the distance of HUVECs from the edge of the sandwich culture. The cells retain their monolayer configuration at a distance of 0 to 2 mm from the edge of the sandwich, whereas a cell network is fully formed at the most hypoxic inner side of the sandwich (10–12 mm from the edge). This example shows that the three-dimensional configuration most completely models the events occurring during angiogenesis *in vivo*: cell proliferation, migration, and tubulogenesis upon a gradient of nutrients and cytokines [73].

3.2.3. Advanced biomimetic models for angiogenesis

Although the 2D and 3D assays might afford an overall direction for studying the angiogenic capability of a given tissue model, these assays are limited in their capability to predict the angiogenic activities *in vivo* due to their slight anatomical similarity to the native process, including continuous fluid flow that impacts the EC gene expression profile [74]. Thus, recent efforts have combined hydrogel matrices with microfluidic channels to create innate microvessels from which new vessels can arise in a way that allow true 3D observation of angiogenesis from native microvessels with fluid flow that closely mimicking the *in vivo* conditions [75].

The strong method to generate a microfluidic channel within a hydrogel matrix is to locate a cylindrical mold (such as a needle) through the gel as it crosslinks. After the crosslinking of the hydrogel matrix, the needle is gently withdrawn, and the matrix is then left with a cylindrical microfluidic channel that can be used for perfusion. To generate such channels, a 15 mm long stainless steel needle coated with 1% bovine serum albumin to create a microfluidic tube inside their collagen hydrogel, then endothelial cells (either HUVECs or HDMECs) are introduced in a suspension, to form a confluent cell layer along the tube creating a vessel with a viable barrier function and a quick response to inflammatory stimuli [76].

Recently, bio printing has inspired the researches to develop print organs *in vitro* (3D printing). This technique uses bio-ink in either droplets or filaments containing living cells forming layers. Hydrogels have been used in this method because of their capability to encapsulate the cells due to their flexibility and tunable viscosity allowing to obtain a rigid and robust printed tissue's structural integrity. Moreover, after self-assembling of these individual layers into 3D organizations, they create networks similar to that observed during the embryonic development [77].

This bioprinting research aims to create complete functional organs with physiological complexity and sufficient vascularization; however, these efforts exposed several difficulties such as low scalability of the fabrication methods, prolonged time necessary for tissue self-assembly, size of the vascular structure, and the generation of perfusable vascular lumen structures [78];[79].

4. Vascularization in Microfluidic-Based Platforms

Nowadays, in order to reconstruct the blood vessel *in vitro*, there is an incorporation of microfluidic systems that are divided into 4 different categories (Figure 4):

4.1. Cell patterning

In this method, a specific area is marked, and the cells are seeded on this marked pattern, which is the advantage of this method as the flow can be applied and controlled. HUVEC cells are cultured in this method pattern using photolithography [80]. Moreover, endothelial cells (ECs) were placed on the membrane and permeability under flow was measured [81]. Stacked three polydimethylsiloxane (PDMS) layers and two PDMS porous membrane layers were also used by this pattern to mimic metastasis of lung cancer cells [82].

4.2. Sacrificial Molds

This method of microfluidics vascularization targets safe spaces with structures. The temporary molds are removed just before the cell seeding. The sacrificial construct used here is gelatin within a collagen gel [83]. The gelatin is dissolved, then a vasculature within the collagen gel is formed after seeding the HUVECs and an angiogenic sprouting mechanism is observed [84].

4.3. Patterned Microchannel

The patterned microchannel method is a procedure that creates designs using soft lithography in a device and fulfills a hydrogel and cells into the empty channels. The size and direction of the new formed vessel is determined by the designed channels. This method is used to test the effects of drugs on the vascular system by incorporating a 3D lumen structure with a circular cross-section in the extra cellular matrix [85]. In this method, a circular tube in the collagen gel was implanted and there was formation of blood vessel along this tube [86]. Another model was also performed consisting of reproducing tumor angiogenesis and intravasation of circulating tumor cell by co-culturing HUVECs, lung fibroblasts, and cancer cells as well as the interactions between these HUVECs, cancer cells, and macrophages [87]. Furthermore, implantable angiogenic complexes made of poly lactic-co-glycolic acid (PLGA) and human endothelial progenitor cells (hEPCs) were established *in vitro* and later transplanted into *in vivo* mice [88].

4.4. Self-Assembly

In this approach, there is no need to add an extra structure for vascularization, the vascular cells are planted within hydrogels in the device, where the cells reorganize 3D vascular networks or connections by themselves in a way that the vascularization is more physiologically mimicking the *in vivo* in comparing to other methods [89]. In addition, the replication of anastomosis from artery to vein using the engineering artificial vascular networks was done using this model, and this is consisting of a human endothelial colony forming cell-derived ECs and normal human lung fibroblasts in fibrin gel [90]. The effects of pro-angiogenic factors and interstitial flow on the growth and maintenance of vascularization were also investigated [91]. In addition, it was shown that culturing bone marrow-derived human mesenchymal stem cells (BM-hMSCs) and HUVECs together in the microfluidic device lead to functional microvascularization [92].

Figure 4: Schematic representation of fabrication methods using microfluidic device. (**a**) Endothelial cells (ECs) (green) are cultured on the designed pattern or the specified membrane. (**b**) After removal of sacrificial molds, ECs (green) are seeded. (**c**) ECs form monolayer alongside the hydrogel. Immunostaining of vascular endothelial cadherin (VE-cadherin, green) and nuclei (blue) confirm the functionality of the vessel. (**d**) ECs (green) are seeded within the hydrogel, and microvasculature is then formed through vasculogenesis [89].

Chapter IV

1. Hypoxia Overview

Hypoxia is defined as a reduction in the normal level of tissue oxygen, which occurs during acute and chronic vascular disease, pulmonary disease, and cancer. When this process becomes severe and prolonged, this will lead to cell death. Tumors become deprived in O_2 or become hypoxic because new blood vessels they develop are abnormal and have poor blood flow. While hypoxia is toxic to both cancer cells and normal cells, cancer cells endure genetic and adaptive modifications that permit them to survive and proliferate in a hypoxic environment. These processes contribute to the malignant phenotype and to aggressive tumor behavior [93]. One should differentiate between hypoxia and anoxia that is defined as the total absence of oxygen in tissue or organ. Normal ambient air comprises 21% oxygen (partial pressure of oxygen (pO_2) 150 mm Hg) and most of the mammalian tissues exist at 2% to 9% oxygen (on average 40 mm Hg). Hypoxia is defined as ≤ 2% oxygen (10-15 mmHg), and severe hypoxia or anoxia is defined as ≤ 0.02% oxygen (< 10 mmHg) [94].

1.1. Tumor Hypoxia

Hypoxia is a common feature of almost all of the solid tumors and mainly occurs due to a mismatch between tumor growth and angiogenesis [95]. It arises in tumors through the uncontrolled oncogene-driven proliferation of cancer cells in the absence of an efficient vascular bed. Thus, due to the rapid proliferation of cancer cells, the tumor quickly consumes the nutrient and oxygen supply from the normal vasculature, and becomes hypoxic (Figure 5) [96].

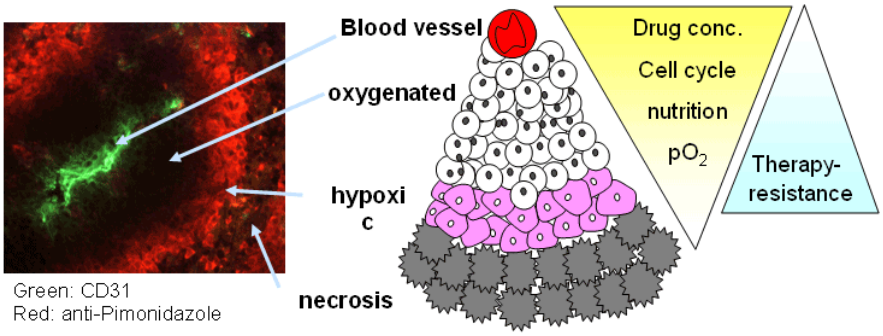

Figure 5: Tumor microenvironment of a solid tumor [97].

The tumor microenvironment is highly dynamic and consists of a heterogeneous population of cancer cells. These subpopulations of cancer cells have highly dynamic gradients of oxygen levels, genomic content, genomic stability, cellular pH and cellular metabolism. Therefore, solid tumors may contain group of cells that have been exposed to varying levels of oxygen for minutes, hours, or even days and re-oxygenated afterwards. This phenomenon is called 'cycling hypoxia' and occurs frequently in solid tumors. Tumor cells in hypoxic microenvironment can be exposed to fluctuating levels of cycling hypoxia at different oxygen gradients for different periods of time [98]. These fluctuations determine tumor cell destiny depending on the severity, duration, and outcome of hypoxia (whether ended by cell death or re-oxygenation). Similarly, in tumors, the abnormal vascular architecture and blood flow that arises, owing to unregulated angiogenesis, is also an important factor in the development of hypoxia [99]. Depending on these two factors (cycling hypoxia and abnormal vasculature), tumor hypoxia can be broadly divided into two types: acute/transient or perfusion-limited hypoxia; and chronic or diffusion-limited hypoxia.

1.1.1. Acute/transient or perfusion-limited hypoxia

In acute hypoxia, tumor cells have been differentially exposed to low intracellular oxygen levels for minutes to hours and then re-oxygenated. It occurs when abnormal/aberrant blood vessels suddenly stop, leading to the development of severe hypoxia at the site connected to these vessels. This can also cause blood flow to be reversed [100]. This shut down is normally transient and closed blood vessels can be reopened, leading to reperfusion of acute hypoxic tissue with oxygenated blood. Reperfusion with oxygenated blood leads to a process known as 're-oxygenation injury' characterized by a sudden and sharp increase in free radicals, tissue damage, and activation of stress-response genes [101]. Free radicals contain oxygen and have unpaired electrons in their outer orbit, which makes them a source of damage to cells and tissues. Free radicals can react with and modify the molecular structures of lipids, carbohydrates, proteins, and DNA [102]. They are produced during the process of cellular metabolism but their rate is significantly increased under acute hypoxia (or ischemia followed

by reperfusion) [103]. Acute hypoxia can also be due to an increase in the surrounding interstitial fluid pressure [104].

1.1.2. Chronic or diffusion-limited hypoxia

In this type of hypoxia, tumor cells (at a distance of >100–200 μm from nearby vessel) are exposed to a more prolonged hypoxia for hours to days and they either undergo cell death or get reoxygenated. These perinecrotic regions of a tumor are located at a median distance of 130 μm from blood vessels, reflecting the limit in oxygen diffusion [105].
In solid tumors, tumor angiogenesis delays behind tumor growth. This uncontrolled proliferation causes tumors to develop their blood vessels, which results in the formation of large hypoxic zones with few or no blood vessels. The diffusion of oxygen and nutrients is limited in these zones and the tumor cells are under continuous severe hypoxia named as chronic hypoxia [106].

2. Hypoxia and the tumor microenvironment

In any cancer, the tumor progression and the initiation of metastasis are directed by the neoplastic angiogenesis process so that this phenomenon of vascularization passes through many linked and sequential steps that leads to the development of neovascular blood supply to the tumors tissue [107];[108]. Many factors as the angiogenic growth factors that are secreted by infiltrating immune cells, adjacent stroma, and tumor cells themselves will attach to specific receptors on endothelial cells provoking endothelial cell proliferation, migration and invasion, finally terminating in capillary formation.
The important homeostatic mechanism that relates vascular oxygen supply to metabolic demand is the angiogenesis that is regulated by hypoxia. Moreover, this is due to molecular representation of angiogenic pathways, establishment of HIFs as their key transcriptional regulators, and the identification of hydroxylases that controls HIF corresponding to the oxygen availability [109].
Moreover, hypoxia conveys resistance to anticancer drugs and radiology. Thus, it plays an important role in drug discovery and development because many chemotherapeutic drugs in

cancer such as alkylating agents melphalan (alkylating agents), bleomycin (cytostatic antibiotic), and etoposide (podophyllotoxin) need optimal oxygenation to have their maximum effectiveness [110].

Hypoxic environment can lead to the resistance of tumors against these drugs by increased production of nucleophilic substances, such as glutathione, competing with the target DNA for alkylation, thus decreasing the drug efficacy [111]. However, there is another class of anticancer agents acting at specific phases of the cell cycle. Examples are antimetabolites (methotrexate) acting against S-phase cells (inhibiting DNA synthesis) and vinca alkaloids that are more M-phase specific (inhibiting spindle formation and alignment of chromosomes), in a way that hypoxia causes the cell cycle to slow down or lead to pre S-phase arrest in extreme conditions [111]. Alternatively, hypoxia can also affect the apoptotic potential of many anticancer drugs by triggering many survival mechanisms and decreasing necrotic cell death, in such a way maintaining the cell viability and reduced drug sensitivity. Hypoxia can enhance cellular adaptation and survival by suppression of protein synthesis and cell growth via mTOR (mammalian target of rapamycin) [112];[113]. Low mTOR activity under hypoxia activates autophagy, which is considered as a survival response to remove damaged or unwanted organelles in order to conserve cell survival and oxygen homeostasis [114].

3. Hypoxia: A key regulatory factor in tumor growth

A solid tumor is a punctured structure with areas of mild-hypoxia leading to severe hypoxia and necrosis as well as areas of fluctuations between acute hypoxia and re-oxygenation [115];[116];[117]. The tumor vasculature architecture can lead to dynamic fluctuations in blood flow, and as a result, fluctuations in oxygen availability leading to phenomena called “Cycling hypoxia”. It was shown that these cycles can vary between seconds to hours even days [117];[98]. It is believed that higher frequency cycling is coming from the changes in blood flow and perfusion, while lower frequency cycling hypoxia that are observed in a matter of days is caused by large-scale transformation of the vascular network and angiogenesis [117]. Moreover, due to the diversity of hypoxic stimuli in tumors, it is difficult to generalize on its effect on tumor biology and metabolism. Moreover, the biology of hypoxic cancer cells is a product of interplay between many factors including hypoxia-induced factors (HIF) and their signaling pathways, oxygen concentration, interacting genetic defects, and cellular damage by reactive oxygen species [96].

3.1. Hypoxia-induced factors (HIFs)

The reductions of oxygen concentration in cancer cells and tissues result in the stabilization and activity of the HIFs through the inactivation of HIF propyl hydroxylases family (PHDs) [118];[119]. The transcription factors of HIF are made of a stable β subunit and one of two oxygen-labile α subunits (HIF1α and HIF2α), so that the stability of the latter is controlled through hydroxylation by PHDs and subsequent binding and ubiquitylation by pVHL (von Hippel–Lindau protein) [120] leading to the rapid degradation of the α subunits in normoxic conditions through proteasomal activity (Figure 6). This alteration results in the inability of HIF1 to transactivate a subdivision of HIF target genes [121].

Both the HIFα and HIFβ subunits exist as a series of isoforms encoded by distinct genetic loci. HIF1β subunits are constitutive nuclear proteins, whereas HIFα subunits are inducible by hypoxia. Among three HIFα isoforms, HIF1α and HIF2α appear to be closely related and each one is able to interact with hypoxia response elements (HREs) to induce transcriptional activity [122];[123]. HIF-3α is involved in negative regulation of the response, through a sequentially spliced transcript termed inhibitory PAS (Per-Arnt-Sim) domain protein [124].

HIFs are transcription factors that bind the hypoxia-responsive elements to the promoter of its specific target genes [125], and thus regulating the expression of a significant number of target genes involved in angiogenesis, metabolic adaptation, survival, and migration [126];[127]. Moreover, the two HIFα subunits have different expression profiles and gene targets, providing a differential response between many tumor types. The expression of HIF1α is ubiquitous whereas HIF2α expression is more restricted and has been described in cell types such as hepatocytes and endothelial cells [128]. The HIF-responsive transcriptome consequently changes between cell types, based on the expression profile of the α subunits in addition to the hypoxia's severity.

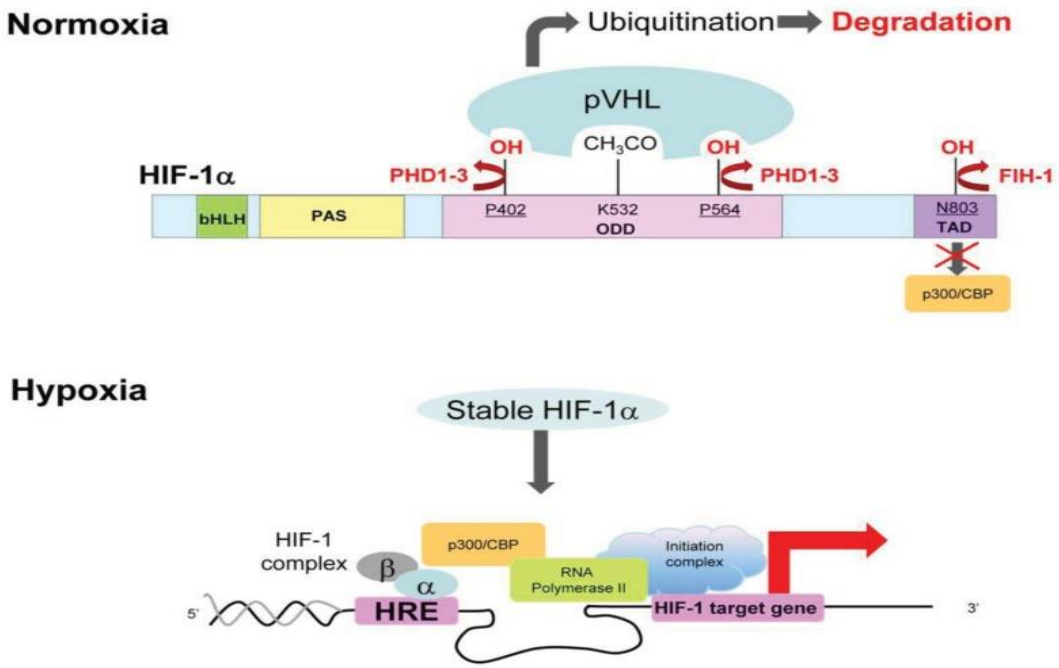

Figure 6: Hypoxia-dependent regulation of HIF1 activity [129].

3.2. The role of HIF1α pathway in cellular adaptation to hypoxic stress

The cells need to maintain a proper oxygen hemostasis in order to achieve their aerobic metabolism and energy generation. This hemostasis is impaired in many conditions such as cancers, heart diseases, or chronic obstructive pulmonary disorders, where the cells become hypoxic [130]. In solid tumors, hypoxic cells proliferate rapidly and form large solid tumor masses, leading to obstruction and compression of the blood vessels that surround these tissues. Moreover, these abnormal blood vessels do not often function appropriately, leading to poor O_2 supply to the center cores of tumor tissues [131]. These hypoxic cells start to adapt to these low oxygen levels by activating several survival pathways. Activation of HIF1 transcription factor is the most known pathway assumed by hypoxic cells in this tough microenvironment. This factor plays a central role in the adaptive responses of the tumor cells to the changes in oxygen through transcriptional activation of over 100 downstream genes that control vital biological procedures needed for tumor survival and progression like the genes involved in glucose metabolism, cell proliferation, migration, and angiogenesis (table 4) [132].

Many studies showed that in rapidly growing tumors, HIF1 helps hypoxic tumor cells to move toward glucose metabolism, from the more effective oxidative phosphorylation to the less efficient glycolytic pathway to maintain their energy production (the Warburg effect) [133]. In addition, in order to meet their energy needs, hypoxic cells tend to consume more glucose so that HIF1 mediates this metabolic process through the induction of enzymes involved in the glycolysis pathway and overexpression of glucose transporters (GLUTs) that increase glucose inflow into tumor cells [134]. Furthermore, another example involving HIF1 transcriptional induction of several pro-angiogenic factors is the vascular endothelial growth factor (VEGF), which plays an important role in angiogenesis to improve tumor cells with oxygen for their growth and surviving [135]. Another important example is that HIF1 helps tumor metastasis into distant and more oxygenated tissues through the transcriptional activation of oncogenic growth factors such as transforming growth factor beta3 (TGF-β3), epidermal growth factor (EGF) and others [136]. Overall, HIF1 activation in tumor cells is one of the key masters coordinating their adaptation mechanisms to the hypoxia environment.

Table 4: Genes induced by hypoxia [137].

Genes induced by hypoxia	
Biological function	**Gene (abbreviation)**
O_2 transport and iron metabolism	Erythropoietin (Epo) Ferritin (FTH1, FTL) Heme oxygenase-1 Transferrin Transferrin receptor (Tfr) Ceruloplasmin
Angiogenesis	Vascular endothelial growth factor (VEGF) VEGF receptor-1 Cyclooxygenase (COX)-2 Leptin (LEP) Endothelin-1, -2 Fibroblast growth factor (FGF)-3 Angiopoietin-4 (Ang-4) Nitric oxide synthase (NOS) Placental growth factor (PlGF) Transforming growth factor (TGF)-α TGF-β1 TGF-β3
Matrix metabolism and coagulation	Metalloproteinases Matrix metalloproteinase (MMP)-13 Plasminogen activator inhibitor-1 Urokinase receptor Collagen prolyl hydroxylase α-Integrin
Glycolysis and glucose metabolism	Adenylate kinase-3 Aldolase-A,C (ALDA,C) Carbonic anhydrase-9 (CA-9) Enolase-1 (ENO1) Glucose transporter-1,3 (GLUT1,3) Glyceraldehyde phosphate dehydrogenase (GAPDH) Hexokinase 1,2 (HK1,2) Lactate dehydrogenase-A (LDHA) Pyruvate kinase M (PKM) Phosphofructokinase L (PFKL) Phosphoglycerate kinase 1 (PGK1) 6-phosphofructo-2-kinase/gructose-2,6-bisphosphate-3 (PFKFB3)
Transcription factors	Hypoxia-inducible factor (HIF)-1α HIF-2α Activator protein (AP-1) Jun Nuclear factor-κB (NF-κB) Insulin-like growth factor (IGF) binding protein-1,-2, -3 Cyclic AMP responsive-element-binding protein (CREB)
Drug resistance **Apoptosis**	Multi-drug resistance (MDR1) Bcl-2/adenovirus E1B 19kD-interacting protein 3 (BNip3) Nip3-like protein X (NIX)
Growth factors and/or cytokines	Insulin-like growth factor-2 (IGF-2) Platelet-derived growth factor (PDGF) Adrenomedullin (ADM) Interleukin-6 (IL-6) Interleukin-8 (IL-8; CXCL8) Tumor Necrosis Factor α (TNFα) Macrophage inflammatory protein 1-α (CCL3; MIP-1α) Macrophage inflammatory protein 2 (MIP-2; CXCL2) Stromal cell-derived factor 1 (SDF-1; CXCL12) Chemokine (C–C motif) ligand (CCL5; RANTES)

3.3. Regulation of HIF1*α* pathway

The activity and accumulation of HIF1*α* protein were found to be controlled at different levels through the life cycle of hypoxic cells. Regardless of the O_2 levels, HIF1*α* is constitutively transcribed and synthesized through a series of signaling events involving several growth factors and other signaling molecules [138]. HIF1*α* endures quick degradation under normoxic conditions and normally has a very short half-life (about 5 min) [139]. However, under hypoxic conditions, several pathways have been shown to control HIF1*α* stability and transcriptional activity *via* post-transnational modifications including hydroxylation, acetylation, ubiquitination, and phosphorylation reactions [138].

3.3.1. Oxygen-dependent regulation of HIF1α pathway "hypoxic regulation"

HIF1α was recognized as the main regulatory subunit for HIF1 activity. Under hypoxic conditions, the expression levels of HIF1α are regulated and mediated by the dioxygenase-dependent and ubiquitin-proteasome pathway-mediated system. Indeed, HIF1α are hydroxylated by dioxygenases, called PHDs in an oxygen-dependent way. However, FIH1 was found to play a key role in the inactivation of HIF1 under normoxic conditions.
Under hypoxia, HIF1α becomes stable, acquires transactivation activity, and induces the transcription initiation of genes by binding to their enhancer element, HRE, which is located in or around the promoter region of each HIF1 regulated gene [140].

3.3.2. Oxygen-independent oncogenic regulation of HIF1α pathway

Although the main role of hydroxylases is in regulating HIF1α activity, there are other pathways involving oncogenic activation to control HIF1α protein level. In non-hypoxic conditions, growth factors, cytokines and other signaling molecules tend to accumulate HIF1α protein in cells.

3.3.2.1. Growth factor signaling pathways

The HIF1α protein translation can be upregulated by the activation of phosphatidyl inositol-4,5-bisphosphate-3-kinase (PI3K) which controls protein synthesis by the activation of Kinase B (AKT) and by the activation of mammalian target of rapamycin (mTOR) [141];[142];[140]. The action of the latter is facilitated by the phosphorylation of eukaryotic translation initiation factor 4E (eIF-4E) binding protein (4E-BP1) leading to HIF1α protein translation. Moreover, mTOR induces protein translation by promoting the ribosomal protein S6 through the phosphorylation of p70 kinase and this pathway can be antagonized by reversing the phosphorylation of PI3K products through the inhibition the tumor suppressor protein (PTEN) [144]. Also, there is other growth factors which can increase the mRNA translation into HIF1α protein like RAS, Extracellular Signal-Regulated Kinase (ERK), and Mitogen-activated protein kinases (MAPK) Interacting Kinases (MNK) (figure 7) [145].

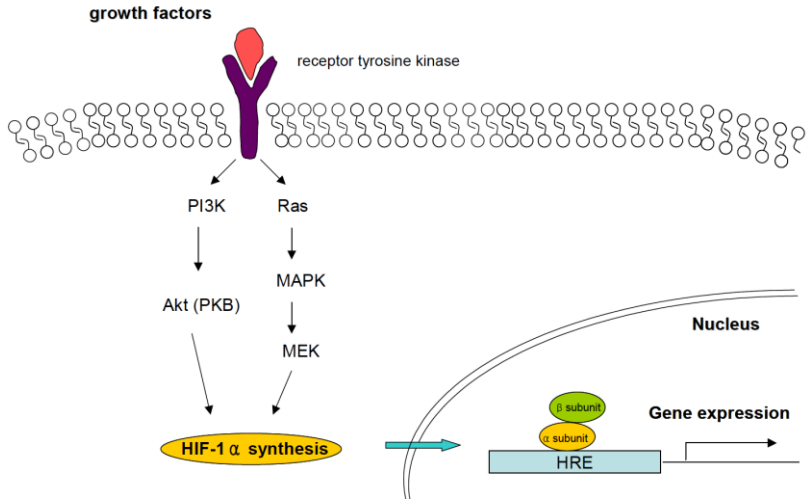

Figure 7: Growth factors (like IGF and TGF) synthesize HIF1α independent of oxygen level via PI3K or MAPK pathways [146].

3.3.2.2. Mdm2 pathway

Mdm2 (mouse double minute 2 homolog), an oncogenic protein, is the principal cellular antagonist of the p53 tumor suppresser gene. It negatively regulates p53 activity through the induction of p53 protein degradation serving as an E3 ubiquitin ligase of p53 which catalyzes polyubiquitination and induces proteasome degradation to downregulate p53 at protein level [147].

It was shown that under normoxic conditions, HIF1α binds to the p53 and induces Mdm2 mediated ubiquitination as well as proteasomal degradation of HIF1α [148]. However, in hypoxic tumors or hypoxic conditions, mutations or variations in tumor suppressor genes will inhibit Mdm2-mediated degradation of HIF1α.

3.3.2.3. Heat shock protein 90 (Hsp90)

It was shown that Hsp90 binds directly to HIF1α inducing some conformational changes in its structure to fit and couple with HIF1β initiating its transactivation, and it can stabilize HIF1α against its non-VHL dependent degradation [149]. To confirm this issue, it was reported that the inhibition of Hsp90 by a drug (geldanamycin) abolishes the HIF1α levels regardless of the oxygen availability [150].

3.4. Hypoxia-regulated pathways

In response to hypoxia, complex mechanisms are triggered to allow cell adaptation to low oxygen conditions, and these are largely mediated by hypoxia-inducible factors (HIFs) and their downstream gene expression networks [151]. Thus, hypoxia can regulate many aspects of tumor hallmarks leading to different cell response (figure 8).

3.4.1. Proliferation

Hypoxia promotes cell proliferation through the induction of various growth factors, and this proliferation is responsible for the initiation of cell migration and regeneration after acute/chronic hypoxia damage. PDGF (platelet-derived growth factor), VEGF (Vascular endothelial growth factor), IGF2 (insulin-like growth factor-2), and TGF-β (transforming growth factor-β) are examples of growth factors shown to be induced by HIF1α [152];[153]. This latter have been shown to be phosphorylated by the p42/p44 mitogen-activated protein kinases that control cell proliferation in response to extracellular growth factors [154]. Other factors are implicated such as phosphatidylinositol 3-OH kinase (PI3K) activity, which is also increased in some cell types under hypoxic conditions and is known to be involved in regulating cell proliferation and suppression of apoptosis [155]. In addition, Ras also plays an important role in proliferation through the subsequent activation of MAPK pathways leading to the synthesis of HIF1α and further cell proliferation.

3.4.2. Angiogenesis

Angiogenesis is the most studied mechanism induced by hypoxia. HIF1α activates the transcription of VEGF and one of its receptors, VEGF-R1, that is primarily expressed in endothelial cells. VEGF is considered as the key regulator of angiogenesis in normal and cancer cells after hypoxia exposure [156]. In addition, HIF1α activation will reduce the expression of antiangiogenic proteins (Thrombospondin-1 and -2) [157].

3.4.3. Glycolysis

When the cells are under hypoxic conditions, the glucose metabolism will switch from oxygen-dependent pathway (tricarboxylic acid :TCA) to oxygen-independent pathway (Glycolysis) in such a way that hypoxic cells use this latter as the primary source of ATP production [158]. This mechanism provides 2 ATP molecules for each glucose molecule, whereas the oxygen-dependent pathway provides 38 ATP molecules. In this case and in order for the cells to acquire their need in ATP, HIF1 interferes to regulate the expression of all the enzymes in the glycolytic pathway leading to the expression of glucose transporters (GLUT1 and GLUT3) [159], which are responsible in cellular glucose uptake [160] and are considered as major physiological facilitators of glucose transport across cell membrane. These glucose transporters belong to a superfamily of membrane transporters called GLUT or SLC2A including 14 facilitators or members, and the GLUTs (1-5) are the most studied [252].
Due to their tissue-wide expression pattern, GLUT1, GLUT3 and GLUT4 (SLC2A4) regulate the majority of glucose uptake [162] and move down its glucose concentration gradient, from relatively high blood levels to relatively low intracellular levels, the high quantity of these proteins increasing the flux of glucose into the hypoxic cell [163]. Once it is taken by the cells, glucose has several metabolic destinies. Intracellularly, glucose is phosphorylated by hexokinases to glucose -6- phosphate and these hexokinases will be induced by HIF1α. It has been shown that Hexokinase 2 has an important role for glucose metabolism in hypoxia [164]. HIF1 can direct glucose into glycolysis by increasing the amounts of the enzymes involved in this process. Almost all the enzymes necessary for glycolysis are regulated or stimulated by the HIF1 [165];[166].

3.4.4. Immortalization and genetic instability

In addition to the other roles of hypoxia in cancer regulation, it has also a role in cellular DNA and chromosomes promoting transformation. So, under hypoxic conditions, telomerase activity of cancer and endothelial cells increases, enhancing cellular immortalization [145]. Moreover, hypoxia stimulates the induction of many genes responsible for amplification and DNA breaks at fragile sites and disrupts repairing of DNA damage [167].

3.4.5. Apoptosis

Severe and prolonged hypoxia can initiate apoptosis, whereas under acute and mild hypoxia, cells resist and survive as an adaptation mechanism to this environmental stress. Furthermore,

HIF1 can initiate hypoxia-mediated apoptosis by increasing the expression of Bcl-2 binding proteins (BNIP3 and NIX), inhibiting the antiapoptotic effect of Bcl-2. HIF1 can stabilize p53 and induce apoptosis. If the cell already has a p53 gene mutation, hypoxia induced apoptosis is blocked. However, hypoxia by itself can also stop apoptosis by inducing the expression of the antiapoptotic protein IAP-2 (apoptosis inhibitory protein 2). In addition, HIF1 may also have an anti-apoptotic function because cells with high amounts of HIF1 are more resistant to hypoxia induced apoptosis [168].

3.4.6. pH regulation

It has been shown that tumors adapt to pH changes. These grow at lower pHs, that take this feature from the glycolysis through the generation of lactic acid. Many proteases are activated under acidic conditions that seem to promote tumor invasion and metastasis. From the enzymes which are involved in pH regulation in tumors, the carbonic anhydrases (especially carbonic anhydrases 9 and 12), which convert carbon dioxide and water to carbonic acid, are strongly induced by hypoxia in a range of tumor cell lines which are regulated by HIF1 [169]. Carbonic anhydrase-9 is found in the perinecrotic areas of many tumors leading to poor prognosis and is activated under hypoxic conditions and is switch off by normoxia [170].

3.4.7. Chemotherapy resistance

It has been shown that areas of hypoxic tumor tissue are more resistant to treatment and are associated with a poor clinical prognosis. Therefore, hypoxia can mediate resistance to anticancer drugs through different pathways such as metabolic alteration, increased drug efflux, inhibition of apoptotic pathways, and hyperactivation of ERK pathway (table 5) [171].

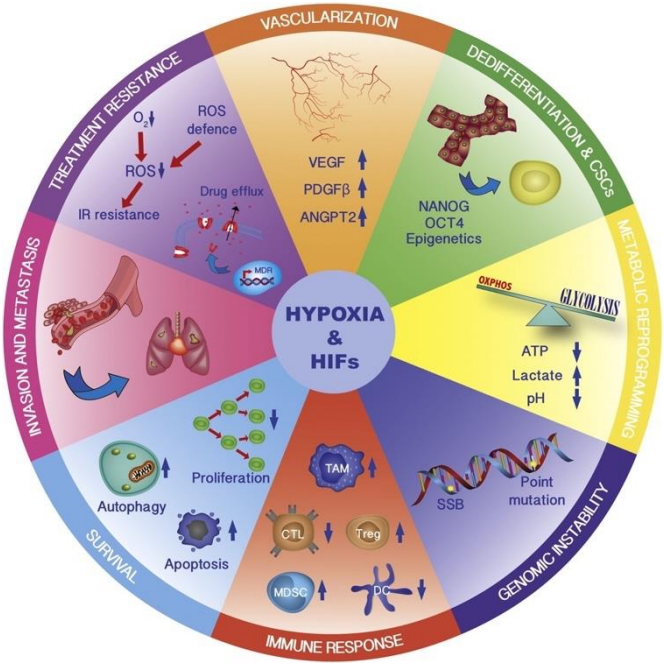

Figure 8: Hallmarks of cancer regulated by hypoxia and HIFs. Hypoxia and HIFs regulate multiple cancer phenotypes. Targeting hypoxia/HIFs will thus inhibit several traits of tumor progression, metastasis, and treatment resistance [172].

4. The role of hypoxia in tumor Angiogenesis

Any tumor at early phase of malignant progression, resides in a dormant avascular state in which the rate of cell proliferation is equal to cell apoptosis. Thereafter, the tumor undergoes a switch from nonangiogenic state to an active angiogenic state [173]. In addition, to show that the angiogenesis is critical for both tumor formation and progression, thrombospondin-1 and -2 were depleted, showing that there is an acceleration in the preclinical model of colorectal cancer and skin carcinogenesis [174]. Tumor vessels have a characteristic of being irregular leaky and poorly functioning, leading to hypoxic areas and HIF1α stabilization regardless to hypoxia such as RAS pathway, P53 mutation, succinate accumulation [175];[176].

There is a strong correlation between HIF system activation and hypoxia revealed as HIF1α and HIF2α which are associated with poor prognosis in many cancers such as breast, head and neck, liver, lung , skin and brain cancers [177]. The resistance in these cancers in hypoxic tumors is due to the lack of O_2 that is required for the cytotoxic effect of ionizing therapy [178] as well as due to inappropriate drug delivery in addition to HIF- mediated expression of ATP dependent efflux pumps [179]. The HIF signaling pathway is considered as an important

stimulus for vascularization in tumors. This is due to the expression of a large pro-angiogenic genes including VEGF, Ang-1, Ang-2, and Tie-2 that are regulated by HIF1α and HIF2α. These genes are implicated in tumor angiogenesis and vascularization. Moreover, VEGF expression is responsible for the angiogenic properties of HIF, while other transcriptional targets are essential for the full effect of HIF on vascular biology. It has been shown that Ang-2 is directly regulated by HIF2α in endothelial cells and indirectly regulated by HIF1α, VEGF that is directly regulated by HIF1α can stimulate the Ang-2 expression [180];[181]. Tie-2 receptor is antagonized by Ang-2, which regulates vascular remodeling in part by destabilizing existing vessels. A Tie-2 receptor agonist, Ang-1, plays a pivotal role in tumor angiogenesis since it is induced by hypoxia in endothelial cells and pericytes [182];[183]. However, hypoxia can regulate other factors enhancing the effect of HIFs. For example, in the endothelium miR-210 that is considered as an HIF1α target, enhances endothelial tube formation and endothelial cells migration [184]. In the endothelium, VEGF and its receptor VEGF-R2 are induced by HIF1α creating a positive feedback leading to endothelial cell proliferation, survival, migration and tube formation [185]. So that , all the studies demonstrate that in the tumor endothelium, HIF1α and HIF2α play harmonizing roles, where HIF1α is crucial for vessel growth, while HIF2α enhances vascular maturation [183].

Hypoxia plays an important role in tumor vasculogenesis. This fact was illustrated by the inhibition of SDF-1/CXCR4 signaling, (SDF1 is a transcriptional target of HIF1α) that is thought to be the primary mechanism for the recruitment of bone derived cells to the areas of vasculogenesis [186]. This inhibition blocks also the vascular growth in glioblastoma [187].

Furthermore, it was shown that HIF1 target genes such as VEGF (vascular endothelium growth factor, FGFs (fibroblast growth factors) and MCP-1(Monocyte chemoattractant protein 1), attract and recruit TAMs to the hypoxic area of the tumors acting as chemoattractive molecules [188]. These TAMs can express HIF1α and HIF2α and the deletion of macrophage-specific HIF2α reduces the progression of inflammation induced by the tumor tissue [189].

Moreover, HIF1α can play an important role in TAM induced angiogenesis through the regulation of glycolytic phenotype promoting migration, invasion and TAMs accumulation in the inflamed hypoxic areas [190, p. 1].

5. Hypoxia and drug resistance

As we discussed before, hypoxia is one of the main features of solid tumors and it is associated with poor outcome in cancer patients [94]. It is harmful for many cells due to lack of oxygen and free radical formation inside, but some cells undergo an adaptation state and confer resistance to chemo and radiotherapy [191] through some regulating processes :

a- Cell cycle arrest (quiescence), a process of reduced cell proliferation that protects cells from external stress [192].
b- Inhibition of apoptosis and senescence of cells
c- Controlling autophagy, p53, and mitochondrial activity [191].
d- Drug delivery and cellular uptake through associated acidity and drug efflux pump expression such as Pgp or MDR1 [193].
e- Lack of oxygen required for the cytotoxicity effect of a number of chemotherapeutics [194].

Hypoxia produces slow proliferating stem cell-like phenotype of cells, decreases senescence, generates hectic and malfunctioning blood vessels, and increases metastasis, altogether provoking therapy resistance [192]. For a better outcome nowadays, the assessment of tumor oxygenation and HIF expression pattern is crucial to determine tumor sensitivity to chemotherapeutics and radiation [195]. HIF expression confers many mechanisms of chemoresistance including HIF1-mediated regulation of drug efflux, alterations in cell proliferation and survival, inhibition of DNA damage, and metabolic reprogramming [191]. However, the most prominent HIF1 mediated resistance is the regulation of drug efflux.

When the cells are under normoxic conditions, radiation leads to generation of ROS that causes irreversible DNA damage and cell death. However, tumoral hypoxia prevents ROS formation, prevents DNA strand breaks, and induces radiation resistance [196]. HIF1α expression can be decreased temporarily after irradiation due to re-oxygenation of the surviving hypoxic tumor cells [197], leading to production of ROS that stabilizes the HIF1α protein and increases the expression of HIF1α and its target genes [98];[198]; thus producing both radiosensitizing effect by promoting proliferation and p53-induced apoptosis as well as radioresistant effects by vascular radioprotection [199]. Cellular responses and resistance to radiation therapy can be regulated by HIF1α mediated alterations in tumor glucose

metabolism [200]. Moreover, inhibition of HIF1α by pharmacological agents will enhance the radiotherapy effect [197]. In addition, blocking HIF2α can increase the radiotherapy effect by activating the p53 pathway and increasing apoptosis [201]. In sum, HIF inhibitors can be used in combination with radiotherapy to target radiotherapy-resistant tumor cells for a better outcome.

Table 5 : Examples of drug resistance phenotype according to each cancer cell model and their involved molecules [202].

(Cancer) Cell model	Drug/molecule	Resistance phenotype	Molecular basis (if known)
Glioma cells	Etoposide, doxorubicin	Drug efflux	MRP1
Glioblastoma cells, colon cancer cells	Adriamycin	Drug efflux	P-gp
Gastric cancer cells	Multiple drugs	Drug efflux	P-gp, MRP1
OSCC cells	5-Fluorouracil, cisplatin	Drug efflux	P-gp
Breast cancer cells	Methotrexate	Drug efflux	P-gp
HCC cells	5-Fluorouracil	Drug efflux	P-gp, MRP1, LRP
HeLa cells	4-HPR	Autophagy induction	Beclin1
Gastric cancer cells	5-Fluorouracil	Apoptosis inhibition	p53, NF-κB
Breast cancer cells	Paclitaxel	Apoptosis inhibition	Caspases 3, 8, 10, Bak, TNFRSF10A, Mcl-1
Prostate cancer cells	Flutamide	Apoptosis inhibition	Bcl-xL
Glioblastoma cells, colon cancer cells	Adriamycin	Apoptosis inhibition	Bcl-2
HCC cells	Etoposide	Apoptosis inhibition	Bak
Fibrosarcoma cells	Cisplatin	Apoptosis inhibition	Bid
Gastric cancer cells	Multiple drugs	Apoptosis inhibition	Bcl-2, Bax
Breast cancer cells	Docetaxel	Apoptosis inhibition	Survivin
Neuroblastoma cells	Etoposide, Vincristine	Apoptosis inhibition	
Pancreatic cancer cells	5-Fluorouracil, doxorubicin, gemcitabine	Apoptosis inhibition	Survivin
Fibrosarcoma cells, colon cancer cells	Etoposide	Apoptosis inhibition	Bid
HNSCC cells	Paclitaxel	Apoptosis inhibition	Bid
Colon cancer cells	Etoposide, oxaliplatin	Apoptosis inhibition	Bid
Gastric cancer cells	5-Fluorouracil	Senescence inhibition	
Breast cancer cells, prostate cancer cells	Etoposide	DNA damage inhibition	Topoisomerase II alpha
Mouse embryonic fibroblasts	Etoposide	DNA damage inhibition	DNA-dependent protein kinase complex
Mouse embryonic fibroblasts	Etoposide, carboplatin	DNA damage inhibition	
OSCC cells	5-Fluorouracil, cisplatin	ROS decrease	HO-1, MnSOD, Ceruplasmin

5.1. HIF1 mediated regulation of drug efflux

In response to hypoxia, HIF1 activates multi-drug resistance gene (MDR) [179]. This gene encodes for the expression of the membrane P-glycoprotein, which belongs to a family of ATP-binding cassette (ABC) transporters. MDR1 is an HIF1 target gene that leads to drug resistance in many tumors such as glioma, gastric, breast, and colon cancers [179];[203];[204];[205]. This acts by pumping out the chemotherapeutic drug by efflux mechanism. Many examples of drugs include vinca-alkaloids, anthracyclines, and paclitaxel.

It has been shown that inhibition of HIF1α expression by antisense oligonucleotides leads to significant suppression of hypoxia-inducible MDR1 expression and a complete loss of basal MDR1 expression in human colon carcinoma tissues. The expression of both HIF1α and Pgp proteins was significantly higher in tissue samples classified as Dukes' stages C or D, involving lymph node metastasis, than in samples classified as Dukes' stages A or B, insisting on the fact that HIF1α is strongly involved in tumor invasion and metastasis. Therefore, HIF1α expression was significantly associated with MDR1/Pgp expression in human colon carcinoma cells (HCT-116, HT-29, LoVo, and SW480) [206].

Another HIF1 related gene that is associated with drug resistance under hypoxia is the multidrug-resistance-associated protein 1 (MRP1) [207] that belongs also to ABC transporter family. This transporter was stated in many brain tumors including glioblastomas [208].

Lung resistance protein (LRP) is also implicated in drug resistance and it is related to HIF1 mediated drug resistance in human hepatocellular carcinoma cells [209]. This protein does not belong to the ABC transporter family; it is a vesicular protein involved in non P-glycoprotein mediated multidrug resistance [210].

In addition, there is another ABC transporter protein, BCRP (Breast cancer resistance protein), that is implicated in drug resistance and drug disposition. This protein is called a "half transporter" ABCG2 and it was first identified as the mediator of acquired resistance in doxorubicin selected breast cancer cell line. It has been shown that hypoxia enhances HIF1α binding to a specific gene sequence in the hypoxia-responsive elements of the ABCG2 promoter, increasing its transcript reformation in pancreatic cancer cells and glioblastomas [211];[316].

6. Hypoxia and 3D culture

Spheroids or microtissues (MTs) are considered as *in vitro* avascular tumor tissues generated by different methods. The diameter of the MTs determines the potential development of hypoxia inside the MTs. A diameter of 400 μm is considered as the starting point where the core of spheroid begins developing hypoxia and activating survival signaling pathways to maintain cell viability, proliferation, cellular metabolism, and DNA damage repair signaling [213];[214];[215].

Hypoxia in the 3D environment of tumors or MTs induces the expression of hypoxia inducible factors (HIF). *In vivo*, the HIF induces the expression of target genes and this expression occurs in tumor regions near to blood vessels and is used to evaluate the hypoxia

[216]. This mechanism is similarly noticed in MTs, but the target genes like Glut1, VEGF, CAIX (Carbonic Anhydrase IX) are found in the inner hypoxic layers and core of the MT [217];[218]. Moreover, as we go away from the MT external surface, there is a formation of different layers leading to the formation of different microenvironments, and as a result, different HIF signaling pathways as a matter of oxygen diffusion into the MT, provoking variable HIF1α stabilization and subsequently tumor cell behavior. However, in the well oxygenated layers which are the outer layers, there are a rapid proliferation and a formation of physical barrier by tight junctions between cells as well as ECM (extracellular matrix) deposition. This leads to different gradients in glucose, catabolites, and variable drug exposure [219];[220].

Chapter V

1. Flavaglines Overview

Nowadays, natural products continue to be an important source of inspiration for the development of new drugs, especially in oncology. Between 2007 and 2013, fourteen natural product derivatives were approved for treatment of cancer [221]. This development added a great achievement in cancer biology, leading to the renew the interest towards exploring the pharmacological effects of Flavaglines in treating cancer [222].

Flavaglines are a class of active molecules found in plants of the genus Aglaia and characterized by a cyclo-penta[*b*]benzofuran complex. These compounds were first discovered in 1982 by KING and his colleagues [223]. Flavaglines are known to have pharmacological effects due to their interactions with prohibitins 1 and 2 and the translation initiation factor eIF4A [224]. These molecules were pharmacologically investigated to treat cancers as well as other diseases like neurological, cardiac, and inflammatory diseases. However, the most prominent effect of such molecules is that they induce death to cancer cells while enhancing the survival of non-cancer cells at very smaller concentrations ranging from subnanomolar to nanomolar [222]. Because of this surprising effect, these molecules attracted the attention of scientists to understand their mechanisms of action in many cancer types. After rocaglamide, a derivative molecule of flavaglines, more than hundred natural flavaglines have been identified as well as other synthetic flavaglines with different pharmacological activities. The most important synthetic molecule is the FL3 that displays a potent anticancer activity and cardioprotective, anti-inflammatory, anti-parkinson, and antiviral activities. In addition, it has a cytoprotective property as it protects the heart and neurons from the undesired effects of many chemotherapies [225]. Moreover, we are interested in our work by FL3, which is a synthetic derivative of flavaglines that showed a good selectivity toward cancer cells and not normal cells [226].

2. Mechanisms of flavaglines as anticancers

2.1. Inhibition of cell cycle progression

Roc-A inhibits the cell cycle progression at G1-S in cancers and reduces the expression of cell cycle proteins like CDK4, cyclin D3, Cdc25A, and Cdc25B [227]. Treatment with Silvestarol and many other FL3 derivatives inhibits the cell cycle at the G0-G1 and G2-M phases in different human cancers like breast cancer cell line BC1, the monocytic leukaemia cell lines 1 and 2, the colon carcinoma cell lines, and prostate cancer cell line LNCaP [228].

2.2. Inhibition of glucose uptake

After investigating many molecules of Flavaglines derivatives, it was shown that Roc-A has a strong inhibition property to HSF1 (heat shock factor 1) activation [229]. Inhibition of this transcription factor to bind to its target genes increases the expression of Thiredoxin - interacting protein (TXNIP) that is a negative regulator of glucose uptake in the cells leading to impairment of malignant cell proliferation *in vitro* and *in vivo* [230].

2.3. Induction of apoptosis

Flavaglines can trigger programmed cell death by two pathways: extrinsic and intrinsic pathways. It was shown that they induce apoptosis in many cancer cell lines isolated from patients (AML, ALL, CLL and CML) by depolarizing the mitochondrial membrane and inducing the caspases -2,-3,-8,-9 [231];[232]. This apoptosis is mediated by the activation of p38 that enhances mitochondrial translocation of the pro-apoptotic Bcl2 family Bax by inducing Bid cleavage (Intrisnic pathway). Some flavaglines (Roc-A and Roc-AB) derivatives activate p38 which is correlated with Bid cleavage [233]. Moreover, silvestrol was shown to induce apoptosis through early reduction of Mcl-1 protein expression in human breast cancer MDA-MB- 231 cells, ALL and CLL [223].

It was shown that Flavaglines can reduce the expression of c-FLIP, an inhibitor of caspase 8, that upregulate the expression of CD95L, sensitizing tumor cell to apoptosis (Extrinsic

pathways) [234]. In addition, they can phosphorylate the tumor suppressor gene p53 and decrease the expression of the oncogene c-Myc that is involved in tumor proliferation and development [235]. Recently, an *in vivo* study has reported that FL3 inhibits the tumor growth of grafted mice with human melanoma cell lines [236].

Furthermore, it has been shown that FL3 induces apoptosis in teratocarcinomal cancer stem-like (NT2D1) cells via caspase-3 dependent activation of p38 MAPK. FL3 exerts cytotoxic activity by decreasing the stemness factors (Oct-4 and Nanog) via a caspase-3-dependent process. Moreover, it activates a p53/p73-independent pro-apoptotic pathway, which gives this drug the advantage to be a promising tool for cancer resistant tumors [237].
In addition, it has been described that FL3 administrated at sub-lethal concentration and for long period downregulate the expression levels of stemness factors such as Oct-4 and Nanog at both transcriptional and translational levels [238].
FL3 also inhibits the proliferation and growth both *in vitro* and *in vivo* of urothelial carcinoma of the bladder (UCB). FL3 has been reported to decrease the interaction of AKT and PHB (Prohibitin), which is essential for many cellular biologic responses like senescence, development, and tumorigenesis and is responsible for poor prognosis in many cancers. Thus, this put into consideration that either FL3 has other effects than apoptosis on some cancer cells or apoptosis maybe tumor type-specific [239].

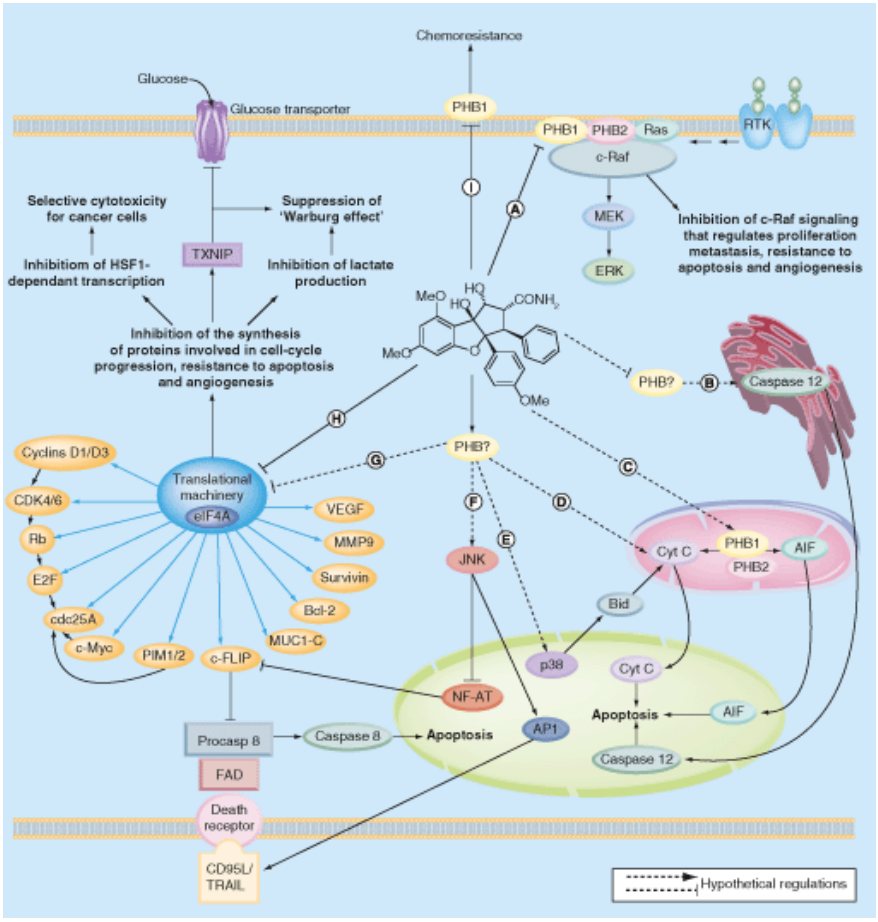

Figure 9: Possible mechanisms of action of flavaglines [222]**.**

OBJECTIVES

The WHO (World Health Organization) estimated that Cancer is the second leading cause of death in the world and is responsible for an estimated 9.6 million deaths in 2018. In general, cancer is causing the death of about 1 in 6 persons. It is thus crucial for effective and better prognosis to improve our understanding of cancer physiopathology, discover new anti-cancer drugs, and acquire novel biomedical technologies. This necessitates a collaboration of multidisciplinary clinicians, biological and materials scientists, and biomedical engineers.

About 95% of new therapeutic molecules are withdrawn at early stages of clinical trials due to their inefficacy. Most of these failures concern trials of anti-cancer drugs, which lead to considerable loss in time and money [240];[241];[242]. These failures are due to lack of efficiency, excessive toxicity, a lack of targeted molecules and of individual adjustment (personalised medicine), because current pre-clinical tests do not reliably identify the best drug candidate in a group of compounds. The scientific community now agrees on the fact that the biggest challenge is not to identify new pharmacologically active molecules, but to have the right experimental model enabling to selectively screen them. In that perspective, drug-screening tests using 3D models of tumors have been developed (called spheroids, organoids, or microtissues), which have been shown to be much more selective than screening tests with 2D cell models. However, none of these drug-screening platforms enables to test molecules on vascularised tumor spheroids. Indeed, although *in vitro* studies on 3D cell culture have shown many advantages compared to 2D cell culture, the 3D human cell spheroid model does not mimic systemic drug administration, rendering such screening tests little predictive and relevant. On the other hand, pre-clinical screening tests are indeed systemic, but unfortunately not human. The missing link between these two models leads to a bias in the selection of therapeutic molecules, creating this considerable failure rate. One of the factors yet lacking is tumor vascularization, a key parameter affecting drug distribution within the tumor and its clearance, directly impacting tumor killing. Indeed, development of 3D tumor models has markedly improved the efficiency of selection tests, and many companies offer these services on the basis of cell lines or xenografts derived from patients (InSphero, OcellO, Organogenix, Eurofins, Creative Bioarray). More recently, 3D tumor spheroid technology has been combined with microfluidic systems as a tool for high throughput screening of cancer drugs (AMS Biotechnology). **However, none of them proposes a 3D tumor with a functional vascularization combined to a 3D microenvironment. They also did not incorporate hypoxia, known to be responsible for**

the resistance of many tumors toward radiotherapy and chemotherapy, which is thus essential for drug selection.

The ultimate goal in selecting an anti-cancer drug is the one that increases the survival rate and improves the quality of life as well as having high efficacy with low side effects on normal cells. To achieve this goal, it is necessary to set up a standardized platform incorporating the tumor microenvironment elements together to mimic *in vivo* tumors. This drug-screening platform is expected to reduce the costs and time of drug testing, minimize the extensive use of animals in preclinical studies, and become accessible and easy-to-use by researchers in drug selecting criteria.

The challenge consists in **the development of a more appropriate *in vitro* model, mimicking tumor vascularization, hypoxia and 3D microenvironment to efficiently select and test anti-cancer drugs.** The ultimate goal is then to create an *in vitro* platform combining different aspect of tumor microenvironment together to achieve a best selection of drugs, and in the longer term, to directly use patients' tumor cells to promote precision medicine.

To this purpose, we first focused on two elements: vascularization and hypoxia. We used 3D tumor spheroids culture, first deposited on endothelial cells to promote vascularization, second with $CoCl_2$ agent to improve hypoxia model.

Thus, the thesis project developed here is composed of two main objectives:

- In order to overcome the lack of vascularization in *in vitro* tests, while using cells and a human environment contrary to *in vivo* tests, the **first** objective was to mimic the tumor vascularization process through the combination of two cellular models, human umbilical endothelial cells (HUVECs) in 2D and tumor osteosarcoma cells (MG-63) cultured in 3D, called spheroid or microtissue. The goal was to observe and analyze the behavior of endothelial cells at the contact of tumor spheroids and characterize the evolution of this combination at different time points to see the reorganization of endothelial cells into vascular structures.

To do this, we characterized the evolution of MG-63 microtissues in term of proliferation and extracellular matrix secretion over the time. We also characterized the combination of

these two cell types, in a 2D/3D system, in terms of vascular formation through the expression of angiogenic markers and immunofluorescence observations.

- The **second** objective was the development of an optimized hypoxia tumoral model in order to better test therapeutic molecules. In this case, we cultured two cell lines, MG-63 and U87-MG (glioblastoma cells), in 3D spheroids with different sizes (5000 and 10000 cells/microtissue) to see the impact of microtissues size on hypoxia. It is well known that 3D cell culture offers many advantages over 2D culture, such as cell-cell interactions, matrix deposition, culture from different cell types, a diffusion limit of drugs, factors and nutrients; i.e, all the criteria that bring us closer to the *in vivo* [243];[244];[245]. But especially the presence of hypoxic nuclei places spheroids as the best model *in vitro* to test sensitivity and drug resistance [246];[247]. To improve this hypoxia model, we added $CoCl_2$ on microtissues and evaluated the induction of hypoxia by measuring its related genes.

Firstly, we tested the effect of $CoCl_2$ on cell lines cultured in monolayer to see the gene expressions according to different concentrations. Then, we cultured the cancer cells in 3D and characterized the effect of this 3D microenvironment with/without $CoCl_2$. For these two culture models, we studied the expression of hypoxia related genes (HIF1α, GLUT1/3, VEGF, ABCG2 and MRP1).

Secondly, we used an original pharmacological molecule, called flavagline (FL3), as a tool to test our 3D tumor hypoxia model. Flavagline is a pharmacologically active molecule known to have anticancer activity and very high selectivity toward tumor cells and not normal cells [233];[248]. This selectivity gave this molecule a great interest in cancer research to discover its activity in many tumor types and aspects (hypoxia, microenvironment, resistance, etc.). Therefore, we investigated the effect of flavagline on these cancer cell lines in our optimized hypoxia model by studying genes involved in hypoxia, proliferation, apoptosis, or resistance.

Finally, the objectives of this project are part of a larger project whose ultimate goal is to develop a platform for drug screening, including different elements of the tumor microenvironment (tumor spheroids, matrix, hypoxia, vascularization, immunity) in order to be always closer to *in vivo* for better drug selection in the preclinical phase. Moreover, in this

big project, we use tumor cells from patient biopsies to promote precision medicine, optimized and personalized.

Given the time and cost of research and development in the field of anticancer molecules, an average of 7.3 years and 648 million USD per new molecule [249], this successful project could have a considerable socio-economic impact, with real impact on the cost of treatment for patients and society. Thereby, the work done, and the results obtained in this thesis are essential for the progress of this larger project.

RESULTS

Manuscript I

Combining 2D angiogenesis and 3D osteosarcoma microtissues to improve vascularization

1. General background and objectives

In general, a solid tumor is a heterogeneous population of many cells. In addition to malignant cells, there is other cells such as macrophages, fibroblast, pericytes, immune and endothelial cells. Moreover, there is a need to optimize a model combining the tumor microenvironment elements in a way that the tumor cells *in vitro* have the same behavior as the tumor *in vivo*. All the researchers' efforts were combined and resulted in a shift from culturing cells in a 2D monolayer which produces a number of downstream effects that differentiate it from cells present in a tumor microenvironment in an *in vivo* setting [250], to a more robust 3D culture model. An essential requirement for the survival and function of this (3D) engineered tissue is the establishment of blood vessels or the creation of *in vitro* vascularization [251]. Despite the substantial advances of current techniques to generate 3D blood vessels, the formation of a functional engineered vascular system with multiscale vessel networks from capillaries to large vessels remained challenging in this field [252]. This is due to the fact that vascularization is crucial in many diseases states for organ transplants (Liver, kidney), many disease states (ischemic heart diseases, diabetes, ulcers), and especially in an *in vitro* drug screening for cancer therapy.

Therefore, our objective is to develop an *in vitro* 3D vascularized tumor model by combining 3D spheroids or microtissues (MTs) of human osteosarcoma cell line and 2D human endothelial cells and reporting their interactions in order to mimic the tumor environment and to be closer to *in vivo* tumor.

2. Results and discussion

2.1. Characterization of 3D MG-63 microtissues

In order to create the 3D MTs from MG-63 cell line, we seeded the cells in GravityPLUS™ plates and cultured them for 5, 10 and 21 days. At each time point, these MTs (MT-MG-63) were characterized by histology and immunofluorescence. For histology, cryostat sections were realized and stained with different tests like Alizarin red for mineralization (revealing

calcium phosphate crystals), and Mallory and BrdU for proliferation. The formation of extracellular matrix was observed after 21 days, detected by its orange color with Mallory. Calcium phosphates crystals revealed an increase in calcium deposits in MTs detected by Alizarin-red by comparing to 5 and 10 days of culture. Moreover, the BrdU test revealed that the number of replicating cells decreased after 21 days (no cells were replicated or stained) in comparison to the experiment periods of 10 days (only the periphery of the spheroids was stained) and 5 days (almost all the cells were replicated) of MTs culture.

On the other hand, immunofluorescence staining with osteocalcin (OC), osteopontin (OPN), and bone sialoprotein II (BSPII) showed that the expression of these 3 proteins increased after 10 days and became more prominent at 21 days of culture time. These results and the results above revealed that as culture time increases, MG-63 cells in 3D structure secrete more extracellular matrix and become mineralized leading to a decrease in proliferation. For our next experiments, we chose the 5 days-cultured MT-MG-63 as with more culture time the cells become quiescent.

2.2. Characterization of combination 2D HUVEC/3D MG-63 and the tubule-like structures

In this section, to record the interaction between these two cellular models, we grew HUVEC on coverslips, then we added the MT-MG-63 cultured in 5 days and let them incubate for different time points.

Many techniques were used to characterize this interaction. Using optical and scanning electron microscopy, we observed that after 7 days of combination, endothelial cells (HUVECs) proliferated to reach the front of cancer cells and organized themselves and began to form tubule-like structures. Then, after 14 days of culture, we observed that these structures were moving considerably towards the MTs of MG-63 cells and formed an organized capillary network at 21 days.

However, in order to characterize this interaction at mRNA level, we used qPCR to study the expression of VEGF (vascular endothelial growth factor), well known to stimulate angiogenesis, in the MG-63 monolayer and MT-MG-63 after 5, 10 ,and 21 days of culture. The level of VEGF was significantly higher in MTs than in cells grown in monolayer after 5 days and it was significantly increased in cultured MT-MG-63 after 10 and 21 days. Moreover, its expression was significant in 2D HUVEC/3D MG-63 combination than each

cellular type cultured alone, and it was prominent in 10 days of culture (combination) in comparison to 5 days.

Finally, we characterized the 2D/3D combination by immunofluorescence, by sing HUVEC-GFP cells and staining for BSPII of MG-63 cells at different time points. We observed that after 7 days of combination, HUVEC-GFP expressed CD31 which is highly concentrated at the intercellular junctions, and after 14 days, they became well organized, forming tubule-like structures directed toward the MTs (cancer cells). Furthermore, at 21 days, the tubule like-structure were formed and well organized on spread MG-63 expressing BSPII. Additionally, it was confirmed by transverse sections that HUVECs entered the MT with the diameter of tubules estimated between 10 µM to 25 µM expressing collagen IV.

In our study, we reported that MG-63 cells in 3D culture (MTs) expressed bone extracellular matrix proteins like osteocalcin (OC), osteopontin (ON) and (bone sialoprotein II) BSPII, and showed a significant expression of VEGF by comparing to 2D monolayer as the tumor *in vivo*. This 3D architecture was responsible for this secretion as the development of hypoxic core inside the MTs over time. Moreover, after a combination 2D HUVEC/3D MG-63 cells and a delay of 10 days of the combined culture, there was a big increase in VEGF expression, meaning that the contact of both types of cells allowed cancer cells to express more VEGF.

It seems that the 3D microenvironment favored the expression of angiogenic markers that led to the formation of tubule like structures that were progressed over time to form vessels.

It was interestingly shown by immunostaining, SEM, and transverse sections that the endothelial cells form a well-organized structure varying between 10 to 25 µm that resembles that of the *in vivo* the capillary diameter varying from 5 to 10 µm, and that arterioles are 10–200 µm [258];[259].

3. Conclusions

This innovative strategy could be used as the starting point to develop tumor angiogenesis *in vitro* considering not only the angiogenic factor expression but also the 3D cell environment. Our strategy could be a first step in the optimization of *in vitro* tumor cell environment closer to the *in vivo*. This strategy should be added to hypoxia as they are the key points in tumor microenvironment in addition to other factors like immune cell, pericytes and neural cells.

4. Perspectives

In the second part of our thesis, we will study the effect of hypoxia because it is a very important element in the tumor microenvironment. Its role has been shown in tumor vascularization and in the induction of angiogenic molecules. Hypoxia and vascularization collaborated together to determine the tumor aspect in terms of drug response/resistance as well as patient prognosis.

Graphical abstract

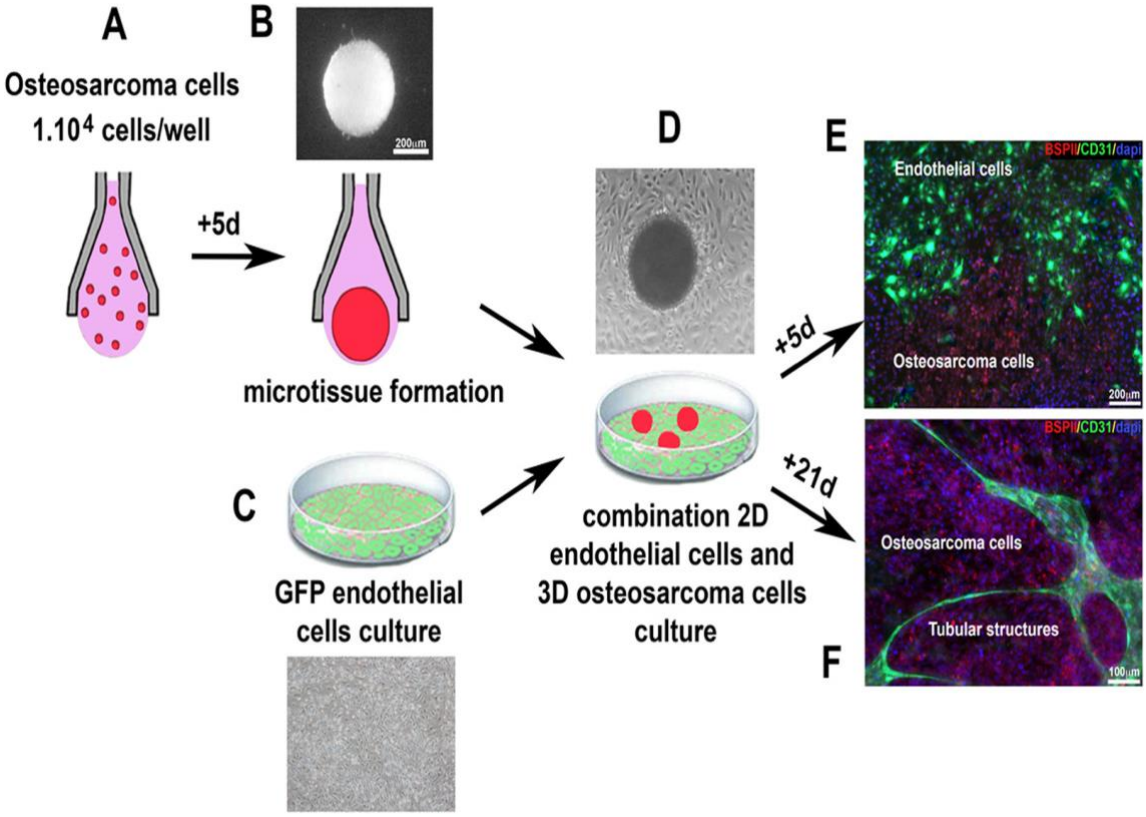

Figure 10: Schematic representation of 2D (HUVEC)/3D (MT-MG-63) combination describing the *in vitro* vascularization process.

Article I

Combining 2D angiogenesis and 3D osteosarcoma microtissues to improve vascularization

Experimental Cell Research 360 (2017) 138–145

Contents lists available at ScienceDirect

Experimental Cell Research

journal homepage: www.elsevier.com/locate/yexcr

Combining 2D angiogenesis and 3D osteosarcoma microtissues to improve vascularization

Hassan Chaddad[a,c,1,2], Sabine Kuchler-Bopp[a,b,1,2], Guy Fuhrmann[a,c,2], Hervé Gegout[a,b,2], Geneviève Ubeaud-Sequier[a,c,2], Pascale Schwinté[a,b,2], Fabien Bornert[a,b,2], Nadia Benkirane-Jessel[a,b,*,2], Ysia Idoux-Gillet[a,b,*,2]

[a] INSERM, UMR 1109, Osteoarticular and Dental Regenerative NanoMedicine Laboratory, FMTS, 11 rue Humann, Strasbourg, France
[b] Université de Strasbourg, Faculté de Chirurgie Dentaire, Hôpitaux Universitaires de Strasbourg (HUS), Strasbourg F-67000, France
[c] Université de Strasbourg, UMR CNRS 7213, EA7293, Faculté de Pharmacie, route du Rhin, 67401 Illkirch-Graffenstaden, France

ARTICLE INFO

Keywords:
Angiogenesis
Spheroids
Osteosarcoma cells
Tubule-like structure
Tumor vascularization

ABSTRACT

Angiogenesis is now well known for being involved in tumor progression, aggressiveness, emergence of metastases, and also resistance to cancer therapies. In this study, to better mimic tumor angiogenesis encountered *in vivo*, we used 3D culture of osteosarcoma cells (MG-63) that we deposited on 2D endothelial cells (HUVEC) grown in monolayer. We report that endothelial cells combined with tumor cells were able to form a well-organized network, and that tubule-like structures corresponding to new vessels infiltrate tumor spheroids. These vessels presented a lumen and expressed specific markers as CD31 and collagen IV. The combination of 2D endothelial cells and 3D microtissues of tumor cells also increased expression of angiogenic factors as VEGF, CXCR4 and ICAM1. The cell environment is the key point to develop tumor vascularization *in vitro* and to be closer to tumor encountered *in vivo*.

1. Introduction

Angiogenesis, or neovascularization, is a key mechanism in many physiological processes, such as wound healing, but is also largely involved in tumor progression and the emergence of metastases. Indeed, the discovery of highly developed vascular networks in solid tumors and the fact that tumors do not grow beyond a few millimeters unless they become vascularized by neoformation or infiltration of adjacent blood vessels, has led the scientific community to identify new therapeutic targets [1–3]. That is why through the decades, increasingly selective therapies have been developed and currently anti-angiogenic agents represent the widest part of targeted therapies [4,5]. However, the tumor vasculature has a structure and abnormal functions leading to a depletion of the oxygen supply, nutrients and growth factors, which makes the tumor even more aggressive and contributes to resistance mechanisms [6,7].

To study the mechanisms of tumor progression, researchers have tried to mimic solid tumors encountered *in vivo*. Now, a lot of different techniques have been implemented to perform 3D culture of tumor cells, called spheroids or microtissues (MTs). The behavior of cells strongly depends on their microenvironment corresponding to the extracellular matrix and surrounding cells, which is provided by 3D suspension culture compared to 2D. This 3D architecture, with cell-cell interactions and deposition of extracellular matrix comparable to *in vivo* tissues, offers many advantages for anti-cancer drug tests, better mimicking *in vivo* tumors [8,9]. However, MTs have diffusional limits to mass transport of drugs, nutrients and other factors and can develop necrotic cores and regions of hypoxia, which is critical for testing anti-cancer therapeutics [10,11]. Despite these points, spheroids remain the best *in vitro* model to test drug sensitivity and resistance [12–15].

About 85% of new therapeutic molecules are withdrawn at early stages of clinical trials due to a lack of efficiency, excessive toxicity, a lack of targeted molecules and of individual adjustment [16,17]. Most of these failures concern trials of anti-cancer drugs, which lead to

Abbreviations: ARS, Alizarin red S; BrdU, 5-bromo-2-deoxy-uridine; BSPII, bone sialoprotein II; CXCR4, C-X-C chemokine receptor type 4; DAPI, 4′, 6-diamidino-2-phenylindole; GFP, green fluorescent protein; HDMS, hexamethyldisilazane; HUVEC, human umbilical vein endothelial cells; ICAM-1, InterCellular Adhesion Molecule; MT, microtissue; OCN, osteocalcin; OPN, osteopontin; PBS, phosphate buffered saline; PFA, paraformaldehyde; SCAP, stem cells from apical papilla; SEM, scanning electron microscopy; VEGF, vascular endothelial growth factor

* Corresponding authors at: Université de Strasbourg, Faculté de Chirurgie Dentaire, Hôpitaux Universitaires de Strasbourg (HUS), Strasbourg F-67000, France.
E-mail addresses: nadia.jessel@inserm.fr (N. Benkirane-Jessel), ysiaidouxgillet@free.fr (Y. Idoux-Gillet).

[1] These authors contributed equally to this work.

[2] http://www.regmed.fr.

http://dx.doi.org/10.1016/j.yexcr.2017.08.035
Received 28 June 2017; Received in revised form 23 August 2017; Accepted 24 August 2017
Available online 01 September 2017
0014-4827/

considerable loss in time and money. The scientific community agrees on the fact that the biggest challenge is not only to identify new pharmacologically active molecules, but also to have the right experimental model enabling to selectively screen them [16]. Over the last 20 years, anticancer drugs have evolved from non-specific cytotoxic agents to specific target-based cancer therapy and immune-related modulators favoring patient's immune system [17]. However, drug developments still have to focus on specific molecules and optimized drugs based on adequate selection processes. These therapeutics molecules should be able to counteract tumor resistance and combined with other anticancer treatment with the least possible side effects. In view of the failure rate of anti-cancer compounds during clinical development, it is imperative that ineffective and toxic molecules are dismissed as soon as possible, preferably before clinical trials and even before animal testing. Thus, the development of an *in vitro* 3D vascularized tumor model is essential. Here we report the combination and the interaction between 3D MTs of human osteosarcoma cell line and 2D human endothelial cells in order to mimic the tumor environment and to be closer to *in vivo* tumor.

2. Materials and methods

2.1. 2D HUVEC culture

Human umbilical vein endothelial cells (HUVEC, PromoCell) and HUVEC-GFP (HUVEC IncuCyte® CytoLight Green Cells, Essen Bioscience, United Kingdom) were grown in a specific endothelial cell growth medium (PromoCell, Germany) with supplement mix. The cells were incubated at 37 °C in a humidified atmosphere of 5% CO_2. When cells reached sub-confluence, they were harvested with trypsin and subcultured.

2.2. Microtissue (MT) culture: 3D MG-63

Osteosarcoma cell line (MG-63, Sigma-Aldrich) were grown in DMEM medium (Lonza, France) with 10 U mL^{-1} penicillin, 100 µg mL^{-1} streptomycin, 250 U mL^{-1} fungizone, 1 mM Na-pyruvate, 2 mM glutamine and 10% FBS. MG-63 cells were seeded in GravityPLUS™ plate (InSphero AG, Zürich, Switzerland) to produce MTs. 1×10^4 cells per MT were seeded in 40 µL of medium and cultured during 5, 10 or 21 days. 7 µl were added to each well every 3–4 days.

2.3. Combination of 2D HUVEC and 3D MG-63

After 5 days in the hanging drop, MTs were cultivated on the HUVEC layer on glass coverslips in the medium constituted of 50% MG-63 medium and 50% HUVEC medium for 5, 7, 10, 14, 21 and 28 days.

2.4. Histology, cell proliferation and mineralization detection

For histology, MTs at different times (5, 10, 21 days) were collected from the hanging drops, fixed for 24 h in Bouin-Hollande and embedded in paraffin. Serial sections (10 µm) were stained with Mallory's stain. Cell proliferation in the MTs was investigated by mapping the distribution of Sphase cells after incorporation of 5-bromo-2-deoxyuridine (BrdU, cell proliferation kit; Amersham Life Science, Amersham Biosciences Europe GmbH, Orsay, France) as previously described [18]. For the detection of the mineralization, MTs were stained for 15 min with 0.01% Alizarin red S (ARS) (Sigma-Aldrich, St. Louis, MO) dissolved in 70% ethanol.

2.5. Indirect immunofluorescence characterization

For the indirect immunofluorescence detection, MTs were fixed with 4% paraformaldehyde (PFA) for 10 min at 4 °C, included in Tissue-Tek® OCT (Optimum Cutting Temperature, Fisher Scientific) and frozen at − 20 °C. Serial sectioning (10 µm) was made using a cryostat (Leica, CM3000). Combination 2D/3D on coverslips were fixed with 4% PFA for 10 min and rinsed three times with PBS. Sections and combination 2D/3D were permeabilized and saturated with 0.1% Triton X-100% and 1% BSA for 1 h, then rinsed three times with PBS. Indirect immunofluorescence was performed after fixation. Primary antibodies were incubated overnight at 4 °C at 1/200, anti-osteopontin (sc-10591, Santa Cruz Biotechnology), anti-osteocalcin (sc-18319, Santa Cruz Biotechnology), anti-BSPII (sc-73497, Santa Cruz Biotechnology), anti-CD31 (ab28364, Abcam), anti-VEGF (ab52917, Abcam) and anti-collagen IV (sc-9301, Santa-Cruz). After three washings with PBS, samples were incubated for 1 h with anti-rabbit conjugated to Alexa Fluor 488, anti-goat conjugated to Alexa Fluor 594, anti-rabbit conjugated to Alexa Fluor 594 or anti-mouse conjugated to Alexa Fluor 594 (Life Technologies) and 5 min with 200 nM 4′,6-diamidino-2-phenylindole (DAPI, Sigma Aldrich). The samples were observed under an epifluorescence microscope (Leica DM4000 B).

2.6. Scanning electron microscopy

For the morphological study by scanning electron microscopy (SEM), glass coverslips were fixed (4% PFA) and dehydrated (successive baths in 25, 50, 75, 90, 100% ethanol) and treated with Hexamethyldisilazane (HDMS). They were stuck on a supporting sample holder using carbon conductive adhesive, then silver-coated and observed with a Philips XL-30 ESEM scanning electron microscope in conventional mode (high vacuum) with a Thornley-Everhart secondary electron detector.

2.7. Analysis of mRNA expression

Total RNAs were isolated from MT-MG-63 obtained after 5, 10 and 21 days in hanging drop culture, HUVEC and MG-63 cultured 10 days in monolayer, combination 2D/3D cultured 5 and 10 days using the High Pure RNA isolation kit (Roche Applied Science, Meylan, France). The total extracted RNA concentration was quantified using NanoDrop 1000 (Fischer Scientific, Illkirch, France). Reverse transcription was performed with the iScript Reverse Transcription Supermix (Bio-Rad Laboratories, Hercules, CA, USA) according to the manufacturer's instructions. To quantify RNA expression, RT-qPCR was performed on the cDNA samples. PCR amplification and analysis were achieved using the CFX Connect™ Real-Time PCR Detection System (Bio-rad, Miltry Mory, France). Amplification reactions have been performed using iTaq Universal SYBR Green Supermix (Bio-rad, Miltry-Mory, France). Actin was used as endogenous RNA control (housekeeping gene) in the samples. The specificity of the reaction was controlled using melting curves analysis. The expression level was calculated using the comparative Ct method ($2^{-\Delta\Delta Ct}$) after normalization to the housekeeping gene. All RT-qPCR assays were performed in triplicate and results were represented by the mean values. Amplified RT-PCR products from MT-MG-63 cultured 5, 10 and 21 days in hanging drop and in monolayer, were separated by electrophoresis on 10% acrylamide gel, which was stained with ethidium bromide and acquired with the Image analyzer (Fusion Fx7, Fisher Bioblock Scientific, Illkirch, France). The RT-PCR reacts were normalized using actin as an internal standard. The molecular weight of PCR products was compared to the DNA molecular weight marker (DNA Ladder, Euromedex, Souffelweyersheim, France).

VEGF for 5′ - CCTGGTGGACATCTTCCAGGAGTACC - 3′ rev 5′ - GAAGCTCATCTCT

CCTATGTGCTGGC - 3′; ICAM-1 for 5′ - GGCCGGCCAGCTTATACAC - 3′ rev 5′ - TAGACACTTGAGCTCGGGCA - 3′; CXCR4 for 5′ - GCCTTATCCTGCCTGGTA

TTGTC - 3′ rev 5′ - GCGAAGAAAGCCAGGATGAGGAT - 3′; actin for 5′ - GATGAGATTGGCATGGCT TT - 3′ rev 5′ - CACCTTCACCGTTC CAGTTT - 3′ (Fisher Scientific S.A.S., Illkirch, France).

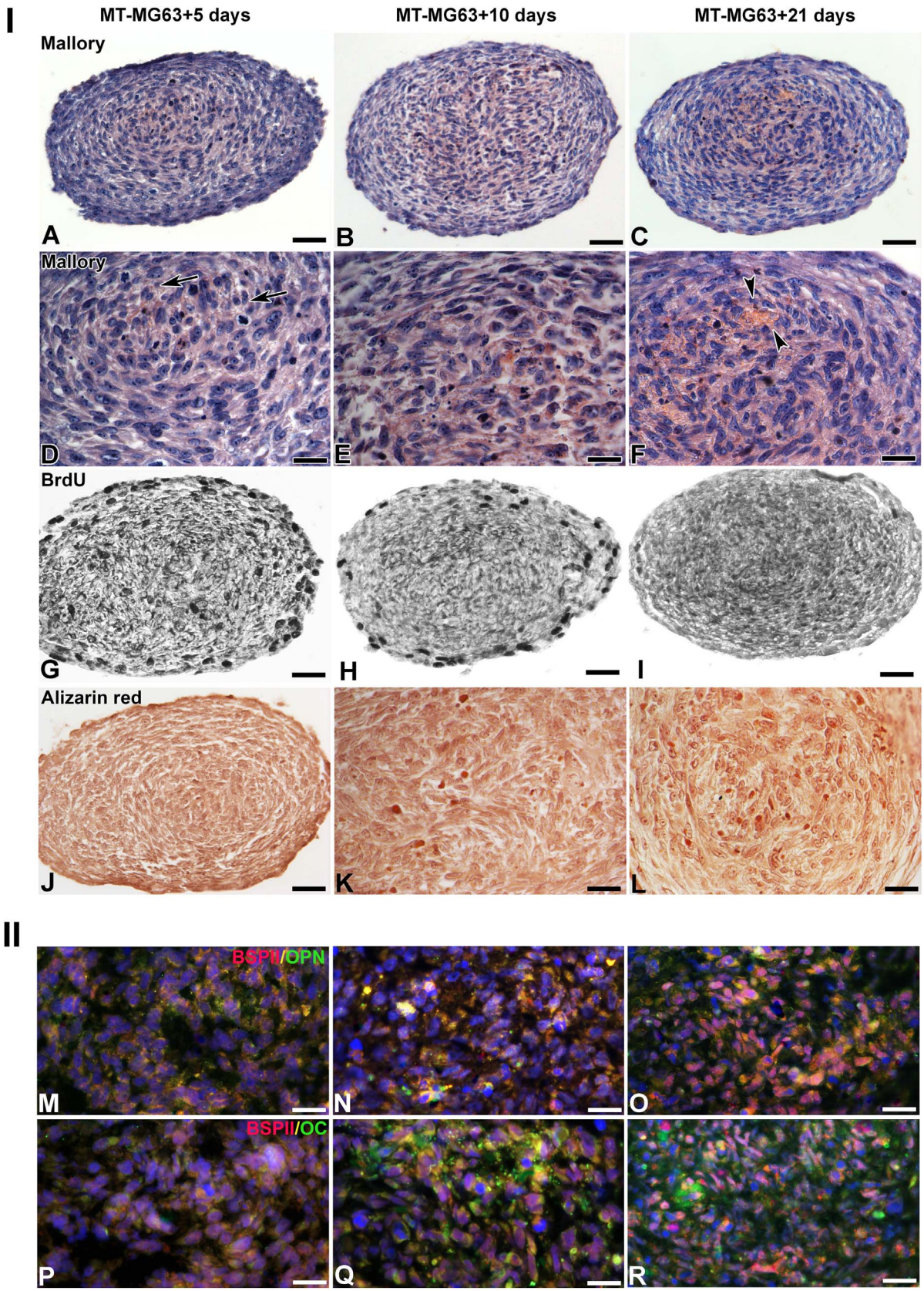

Fig. 1. Histology (A-L) and immunofluorescence (M-R) for BSPII, osteopontin (OPN) and osteocalcin (OC) on MT-MG-63 after 5, 10 and 21 days in hanging drop culture. Histology showed the organization of the MT: Mallory (A-F) and BrdU (G-I) stainings detected proliferative cells and Alizarin red (J-L) mineralization. Arrows in D indicated metaphases, the stage of mitosis in which chromosomes are at their most condensed and coiled stage. Cell proliferation decreased with culture time as mineralization increased. Mineralized nodules were stained positively with Alizarin red (arrowheads in K and L). After 21 days (F), we observed the formation of matrix (arrowheads) detected by its orange color with Mallory. Immunofluorescence showed that MT-MG-63 expressed OPN (M-O) and OC (P-R). The expression of both proteins increased with culture time. MT-MG-63 expressed BSPII after 10 days in culture (N) and its expression increased after 21 days (O).

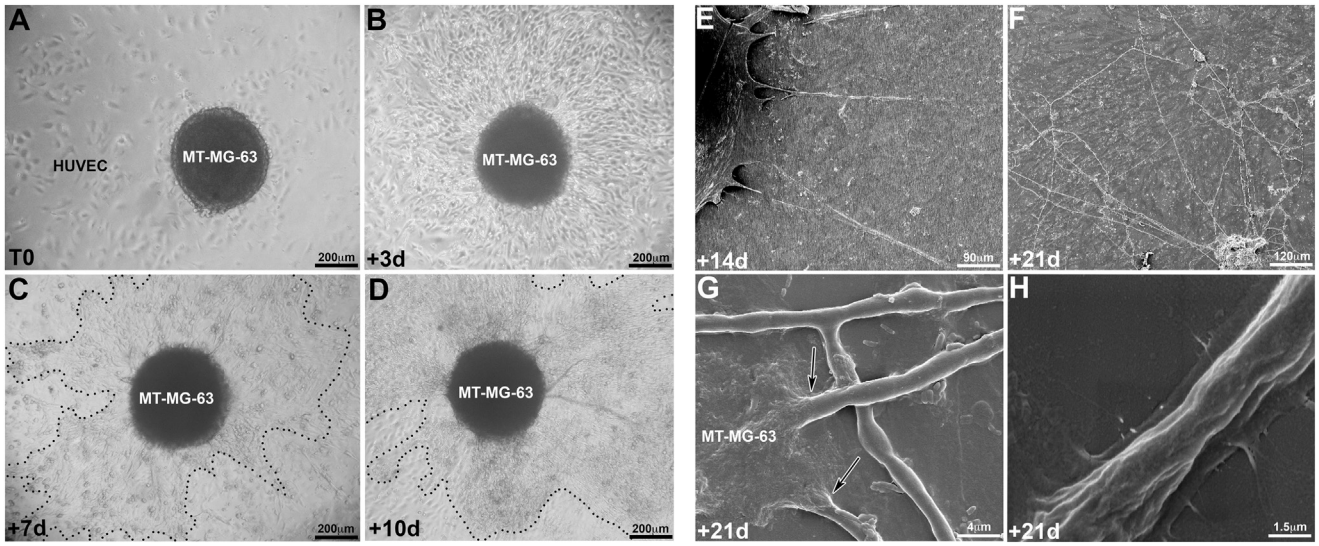

Fig. 2. Optical microscopy (A-D) and scanning electron microscopy (E-H) of combined cultures of MT-MG-63 cultivated for 5 days in hanging drop and deposited on green fluorescent protein-labeled HUVECs on glass coverslips. After 3 days (B), MG-63 cells left the MTs, migrated and after 7 (C) and 10 days (D) formed a migration front indicated by the dotted lines. After 14 and 21 days, HUVECs formed tubule-like structures (E-H). After 21 days, these endothelial cell tubes seemed to enter the MT (G, arrows). The diameter of the tube could be estimated as 1.5 µm (H).

2.8. Statistical analyses

Statistical analyses were performed using GraphPad Prism 5.0 for Windows (GraphPad Software Inc). Statistical significance was evaluated by one-way ANOVA (SigmaStat, Jandel GmbH, Erkrath, Germany). All data were expressed as mean ± SEM. $p < 0.05$ was considered as statistically significant.

3. Results

3.1. Preparation and characterization of 3D MG-63 microtissues

We first prepared MTs of MG-63 cell line using GravityPLUS™ plates (see graphical abstract). MTs of MG-63 cell line (MT-MG-63) were cultured during 5, 10 and 21 days in GravityPLUS™ plates and characterized by histology and immunofluorescence (Fig. 1). This technique of hanging drop plate is the easiest and the best to use because it meets the various challenges of 3D culture, namely be able to form spheroids with a small number of cells, to form and maintain a uniform size, to easily develop spheroids with several cell types, and to collect them readily for characterization and to test the efficacy of drugs. This method allows to obtain spherical, regular and uniform MTs, reaching a diameter of 400 µm (Fig. 1). To characterize the spheroids, we realized cryostat sections before performing immunostaining and paraffin sections for histology. Mallory (Fig. 1A-F) and BrdU (Fig. 1G-I) staining exhibited proliferative cells and Alizarin red (Fig. 1J-L) the mineralization. Mallory staining showed metaphases, which is the step of mitosis in which chromosomes are at their most condensed and coiled stage (Fig. 1D, arrows). After 21 days, we observed the formation of extracellular matrix (Fig. 1F, arrowheads) detected by its orange color with Mallory. Alizarin-red staining, revealing calcium phosphate crystals, showed an increase in calcium deposits in MTs cultured during 21 days compared to 5 and 10 days (Fig. 1L, arrowheads). Conversely, there was more BrdU staining in MTs after 5 days than after 21 days (Fig. 1G-I). Indeed, the number of cells in replication decreased during the time, and their localization changed. At 5 days, we found cells in replication in the whole MTs (Fig. 1G); at 10 days, BrdU staining was localized only in the periphery of the spheroids (Fig. 1H); and at 21 days, almost no cell was marked (Fig. 1I). Cell proliferation decreased with culture time as mineralization increased, as found in bone tissue. Moreover, we saw with Mallory staining that MG-63 cells cultured in MTs secreted extracellular matrix, also showed by immunofluorescence staining revealing osteopontin (OPN) (Fig. 1M-O), osteocalcin (OC) (Fig. 1P-R) and bone sialoprotein II (BSPII) (Fig. 1M-R), which are non-collagen bone matrix proteins [19–21]. The expression of OPN and OCN increased with culture time. After 10 days in culture (Fig. 1N, Q), MT-MG-63 expressed BSPII and its expression increased after 21 days (Fig. 1O, R). These results showed that MT-MG-63 secreted bone matrix proteins from 5 days of culture, and are more active and proliferative at 5 days than later. These experiments also demonstrated that the more MG-63 cells were cultured in MTs for a long time, the more they secreted bone matrix with mineralization in the center of the spheroids, and the more cells seemed to be quiescent. Thus, we chose to use 5 days-cultured MT-MG-63 for all further experiments.

3.2. Characterization of combination 2D HUVEC/3D MG-63

To observe the interactions between osteosarcoma-derived MTs and endothelial cells, we grew HUVEC on coverslips and added MT-MG-63 cultured during 5 days in the hanging drops, that we called combination 2D/3D (graphical abstract). As shown by optical microscopy on Fig. 2A-D, MT-MG-63, deposited on the endothelial cells grew in monolayer, spread and proliferated rapidly compared to HUVEC. They invaded almost the entire surface (Fig. 2B-D). We noted that the deposition of MTs onto endothelial monolayer first led to the death of HUVEC cells in direct contact of MG-63 cells, facilitating the fast spreading and proliferation of cancer cells (Fig. 2B-D). At 7 days of combined 2D/3D culture, endothelial cells proliferated to reach the front of cancer cells (Fig. 2C). At the same time as they proliferated, HUVEC cells organized themselves and began to form tubule-like structures infiltrating MG-63 cells as shown in Fig. 2(E, F). We observed that these tubule-like structures at 14 days of culture were moving considerably towards the MTs of MG-63 cells (Fig. 2E), and formed an organized capillary network at 21 days (Fig. 2F-H). Interestingly, some of the endothelial cell tubules were developed and proliferated on cancer cell monolayer towards the MT, but also penetrated the layer of MG-63 cells, as shown by scanning electron microscopy (SEM) (Fig. 2G, arrows).

To explain the formation of tubule-like structures, we studied by qPCR the expression of VEGF (vascular endothelial growth factor), well known to stimulate angiogenesis, in the MG-63 monolayer and MT-MG-63 after 5, 10 and 21 days culture (Fig. 3). VEGF was expressed in MG-

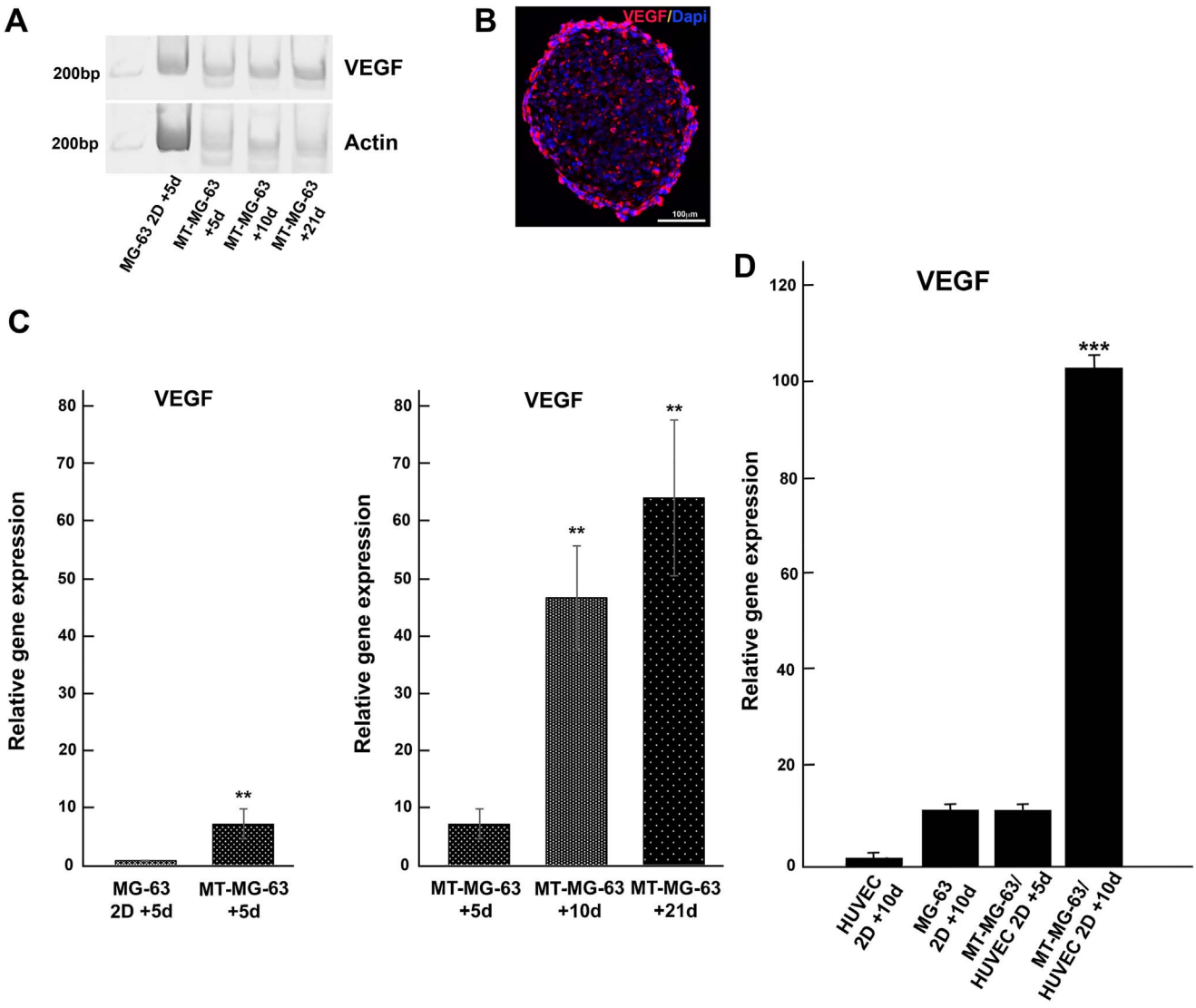

Fig. 3. VEGF expression in MG-63 monolayer cells after 5 days, in MT-MG-63 after 5, 10 and 21 days in culture (A, C), in HUVEC and MG-63 cultured in monolayer during 10 days and in combination 2D HUVEC/3D MG-63 cultured during 5 and 10 days (D) and immunofluorescence for VEGF in MT-MG-63 after 5 days in culture (B). VEGF was expressed in MG-63 monolayer cells and MT-MG-63 culture. An expected band of 196 bp size was visible on the gel (A). The level of mRNA encoding VEGF was significantly higher in MTs than in cells grown in monolayer after 5 days (C). This level increased significantly in cultured MT-MG-63 after 10 and 21 days (C). Immunofluorescence confirmed the localization of the VEGF protein in the cytoplasm of MG-63 cells grown as MTs (B). The angiogenic factor VEGF expression increased significantly in combined cultures of HUVEC and MT-MG-63 compared with each cell type cultured during an equivalent time (D). Statistical significance was evaluated by one-way ANOVA. ** $P < 0.01$***, $P < 0.001$.

63 monolayer cells and MT-MG-63 culture. An expected band of 196 bp size was visible on the gel (Fig. 3A). The expression of VEGF was confirmed at protein level by immunofluorescence staining, showing that most of MG-63 cells in the MTs cultured 5 days expressed VEGF (Fig. 3B). The level of mRNA encoding VEGF was significantly higher in MTs than in cells grown in monolayer after 5 days (Fig. 3C). This level increased significantly in cultured MT-MG-63 after 10 and 21 days (Fig. 3C). We also wanted to see other angiogenic factors expression to observe the impact of combined 2D/3D culture compared to each type of cells cultured in 2D monolayer. Thus we analyzed the expression of VEGF (Fig. 3D), ICAM-1 and CXCR4 (Supplementary Figure) in HUVEC cultured in monolayer during 10 days, in MG-63 cultured in monolayer during 10 days, and in combination 2D HUVEC/3D MG-63 cultured during 5 and 10 days. Interestingly, HUVEC alone did not express VEGF, whereas MG-63 alone in 2D expressed VEGF (Fig. 3D). However, there is a significant increase of VEGF expression in combination 2D/3D at 10 days compared to 5 days, and in each type of cells cultured in monolayer during 10 days. This means that the addition of MT-MG-63 on HUVEC monolayer, after a delay of culture of 10 days, leads to more expression of VEGF. Concerning the marker ICAM1, (Supporting information Fig. SI-1A), HUVEC highly expressed ICAM1 compared to MG-63 cells. The ICAM1 expression analyses showed that 5-days combined 2D/3D cultures expressed ICAM1 at the same level that MG-63 alone, but after 10 days of 2D/3D culture, ICAM1 expression level double. As ICAM1, CXCR4 was highly expressed in HUVEC compared to 2D tumor cells, however there was a more significant increase (20 fold) in combined 2D/3D cultures between 5 days and 10 days (Fig. SI-1B).

3.3. Characterization of the tubule-like structures

To be sure to visualize endothelial cells, we used HUVEC-GFP cells and performed immunostaining for BSPII of MG-63 cells at different times of 2D/3D culture (Figs. 4 and 5). After 7 days of culture, HUVEC-GFP cells reached the front of MG-63 cells (Fig. 4A). HUVEC-GFP expressed CD31, but no endothelial cells organization was noticeable (Fig. 4B, C). As expected, CD31 was highly concentrated at intercellular junctions of endothelial cells (Fig. 4B, C). At 14 days of culture, HUVEC-GFP cells were well organized, forming tubule-like structures directed

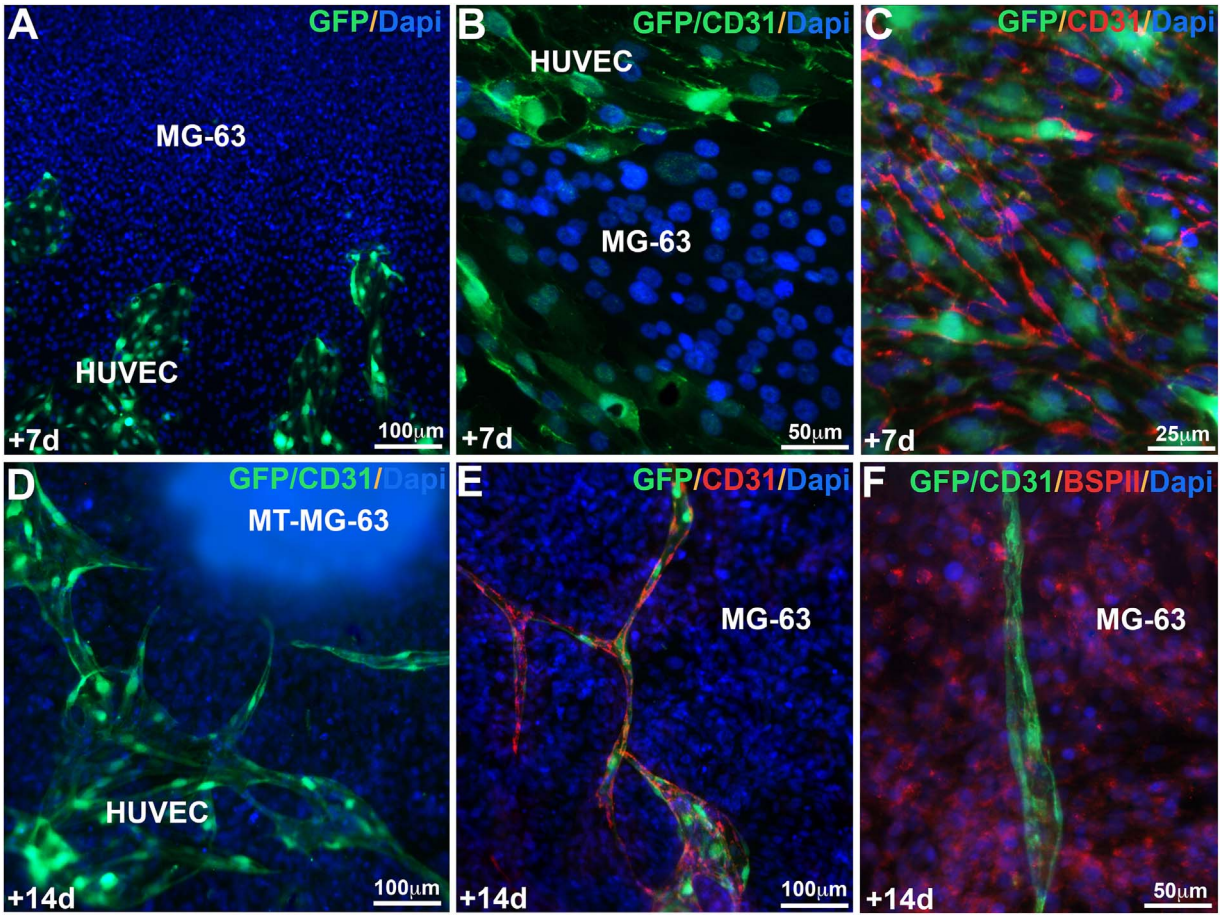

Fig. 4. Immunofluorescence for GFP, CD31 and BSPII of combined cultures after 7 days (A-C) and 14 days (D-F). After 7 days (A-C), MG-63 cells migrated and formed a migration front. CD31 was highly concentrated at inter-endothelial cell contacts (B, C). After 14 days, HUVECs began to form tubule-like structures (D-F). MG-63 cells were positive for BSPII (F), a component of mineralized tissues.

towards the cancer cell MTs (Fig. 4D-F). We also observed, at higher magnification, that endothelial cells proliferated, shaping a tubule on MG-63 cells expressing the extracellular matrix bone protein BSPII (Fig. 4F). At 21 days, HUVEC formed tubule-like structures and showed a well-organized network, on spread MG-63 cells expressing BSPII (Fig. 5A, B). The transverse sections (Fig. 5C) show that endothelial cells penetrated the MT. Some of the endothelial tubules infiltrating the MT-MG-63-secreted matrix seemed to present a lumen (Fig. 5C, arrows). The diameter of the tubules could be estimated as 10 µm to 25 µm. Finally, after 28 days of culture, tubules resembled blood vessels with the formation of a basal membrane positive to collagen IV (Fig. 5D-F).

4. Discussion

The combination of 3D MG-63 and 2D HUVEC has never been used. Some authors have grown HUVEC and MG-63 in direct co-culture or on titanium surfaces. Under these conditions of co-culture, MG-63 released VEGF which induced HUVEC proliferation and expression of angiogenesis associated genes [22]. Others have mixed MG-63 cells with HUVEC (ratio 2:1) that have been grown in multiwell dishes or separately in transwell dishes [23]. These authors showed that mineralization nodus numbers were increased in this MG-63 co-culture system. To obtain formation of three-dimensional vessel-like structures *in vitro*, stem cells from apical papilla (SCAP) and human umbilical vein endothelial cells under hypoxia were co-cultured [24]. In these conditions, VEGF secreted by SCAP might be used by HUVEC to accelerate the formation of vessel-like structures. It has also been shown previously that MG-63 cells seeded into 3D porous hydroxyapatite ceramics under vacuum expressed a matrix-bound variant of vascular endothelial growth factor-A (VEGF-A) [25].

In the present study, we reported for the first time the combination between 2D HUVEC and 3D MG-63 cell microtissues. In this innovative strategy of 2D/3D culture, MG-63 tumor cells cultured as 3D spheroids (microtissues: MTs) allowed expression of extracellular matrix proteins as osteocalcin, osteopontin and BSPII (Fig. 1II), and lead to the establishment of an organized architecture within the MT closer to tumor encountered *in vivo* [26]. Moreover, MG-63 cells cultured in 3D spheroids lead to more expression of bone proteins and VEGF than in monolayer (Fig. 3C). The architecture of MTs, with a cellular activity at the periphery and quiescent cells embedded in matrix at the center of the spheroid (Fig. 1I), could lead to hypoxic core favoring the secretion of VEGF, also explaining the increase in VEGF expression in MTs over time. VEGF secreted by the MT-MG-63 helps to attract endothelial cells to the spheroid tumor, to form vessel-like structures and to organize a vascular network. The secretion of VEGF in the microenvironment could explain the resurgence of endothelial cells after their first deadly contact with MG-63 cells. This was also supported by the significant increase of VEGF expression between 5-day and 10-day combined cultures (Fig. 3D). These results showed that the addition of MT-MG-63 on HUVEC monolayer, after a delay of 10 days culture, lead to more expression of VEGF. Thus, the contact of both types of cells first lead to the death of HUVEC cells in direct contact to tumor cells MTs, then cancer cells expressed VEGF favoring endothelial cells proliferation and morphogenesis. This was only after a delay of 10 days of combined culture that there was a big increase of VEGF expression, meaning that

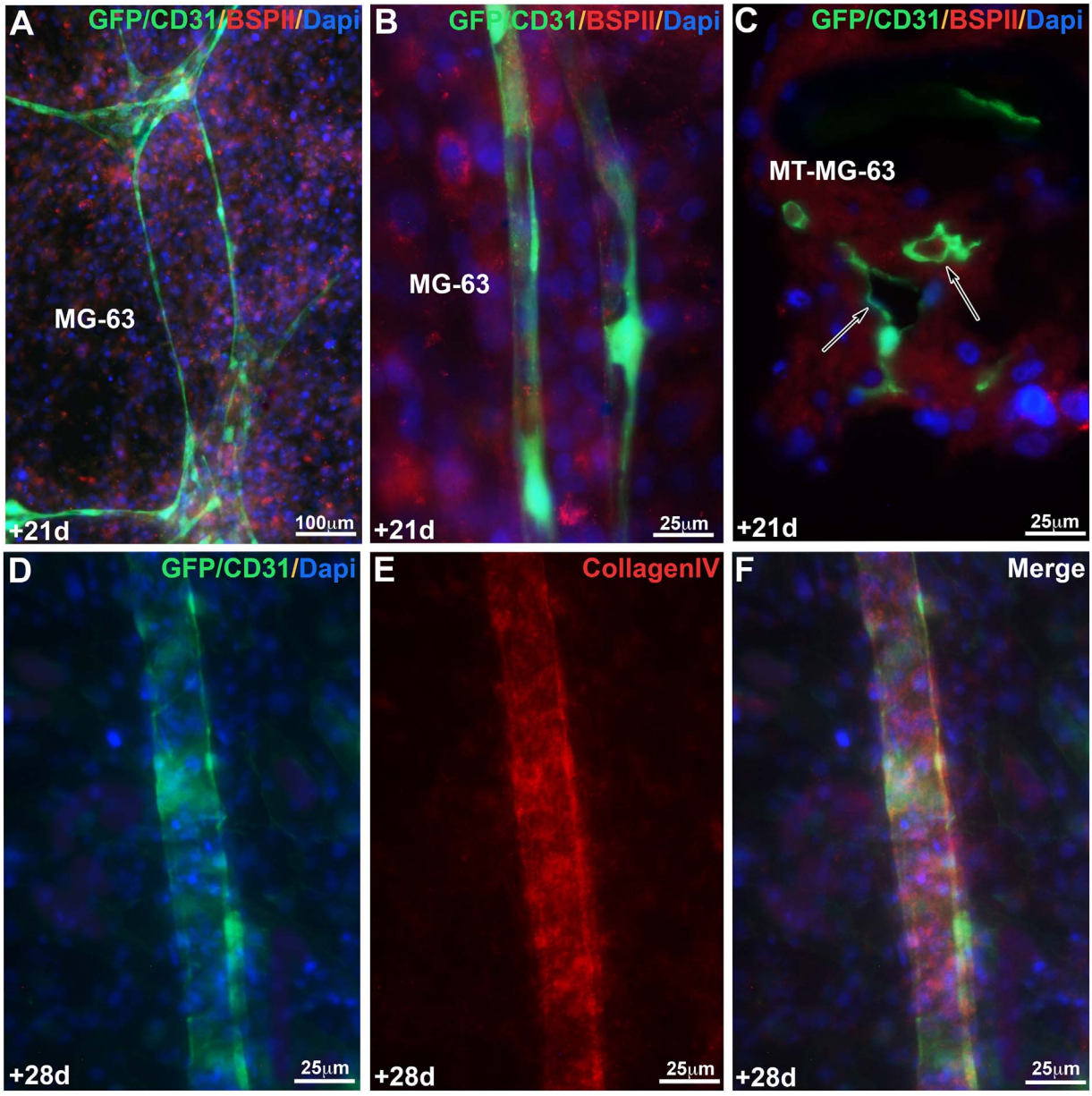

Fig. 5. Immunofluorescence for GFP, CD31, BSPII and Collagen IV of combined cultures after 21 days (A-C) and 28 days (D-F). MG-63 cells were positive for BSPII (A-C). HUVECs formed tubule-like structures (A, B). The image (C) showed the transversely cut tubules (arrows) entering the MT-MG-63. The tubule-like structure was stained with anti-CD31 (D) and Collagen IV (E). The presence of Collagen IV was in favor of the formation of a basal membrane surrounding the blood vessels *in vivo*.

the contact of both types of cells allowed cancer cells to express more VEGF. The combination of HUVEC and MT-MG-63 promoted the expression of this angiogenic factor. Concerning the marker ICAM1 (Fig. SI-1A), localized in the membrane of a wide variety of cells, as endothelial and cancer cells [27], it is well reported that this marker is induced by VEGF with angiogenic activity [28–31]. Indeed, we have shown an increase of this marker over the time. We have also followed the expression of CXCR4 (Fig. SI-1B), a chemokine receptor expressed in membrane cells and involved in endothelial cells morphogenesis leading to angiogenesis [32], and found more relevant increase than ICAM1.

It is well reported that the endothelial cells need not only angiogenic factors, but also 3D environment to form vessels. By combining the endothelial cells and our 3D system, the MT-MG63-secreted matrix favors the creation of tubule-like structure and lumen. Interestingly, endothelial vessels proliferated on and under tumor cells as shown by immunofluorescence, and also infiltrated the tumor spheroid as observed by SEM and by the transverse sections of MTs (Figs. 2, 4, 5). These observations mean that endothelial cells form a well-organized network able to interpenetrate and to tangle around the tumor cells. In the literature, it has been described that *in vivo* the capillary diameter varies from 5 to 10 µm, and that arterioles are 10–200 µm [33,34]. We have also observed that tubule-like structures of HUVEC cells seemed to grow over the time and varied from 10 to 25 µm (Figs. 4 and 5), which corresponds to the values found in *in vitro* assays [35,36]. Furthermore, after 28 days of combined 2D/3D strategy, endothelial cells organized in tubules, secreted collagen IV, a specific marker of the vessels' basal membrane (Fig. 5). It was reported that CD31 could also be involved in endothelial cell migration to form the tubular networks [37]. By using our combined 2D/3D strategy, we have shown that CD31 detected in the endothelial cell junctions was co-localized with collagen IV in some areas of the vessel-like structures.

By using this combined 2D/3D strategy, we have shown that endothelial cells were able to form a vascular-like network in the presence

of 3D MT-MG-63 tumor cells. The combination of 3D MT-MG-63 and 2D HUVEC cells increased the expression of angiogenic factors, as VEGF, ICAM1 and CXCR4, which promotes endothelial cells proliferation and tubule-like formation. This neo-vascular network express collagen IV, a specific marker, infiltrates tumor spheroids, and forms tubules structures presenting lumen. This innovative strategy could be used as the starting point to develop tumor angiogenesis *in vitro* taking into account not only the angiogenic factor expression but also the 3D cell environment. Our strategy could be a first step in the optimization of *in vitro* tumor cell environment closer to the *in vivo*.

Author contributions

Y.I-G, P.S. and N.B-J were responsible for project conception and direction. S.K-B, H.C., G.F. and H.G. performed experimental work and analyzed the data. G. U-S. and F. B. helped to write and correct the manuscript. All authors read and approved the final version of the manuscript.

Conflict of interests

The authors declare that they have no conflict of interest.

Funding

This work has been supported by the project Angiomatrix from the “Agence Nationale de la Recherche, ANR”. N.B-J and P.S. are indebted to “Société d'Accélération de Transfert de Technologies Conectus”Conectus” for the financial support. Y.I-G and H.G. are indebted to “Faculté de Chirurgie Dentaire de Strasbourg” for the financial support.

Acknowledgments

We are indebted to Arielle Ferrandon for their technical support.

Appendix A. Supporting information

Supplementary data associated with this article can be found in the online version at http://dx.doi.org/10.1016/j.yexcr.2017.08.035.

References

[1] D. Knighton, D. Ausprunk, D. Tapper, J. Folkman, Avascular and vascular phases of tumour growth in the chick embryo, Br. J. Cancer 35 (1977) 347–356.
[2] N. Ferrara, K.J. Hillan, H.P. Gerber, W. Novotny, Discovery and development of bevacizumab, an anti-VEGF antibody for treating cancer, Nat. Rev. Drug Discov. 3 (2004) 391–400.
[3] J. Folkman, Role of angiogenesis in tumor growth and metastasis, Semin. Oncol. 29 (2002) 15–18.
[4] R.S. Alameddine, L. Hamieh, A. Shamseddine, From sprouting angiogenesis to erythrocytes generation by cancer stem cells: evolving concepts in tumor microcirculation, Biomed. Res. Int. 2014 (2014) 986768.
[5] M. Marçola, C.E. Rodrigues, Endothelial progenitor cells in tumor angiogenesis: another brick in the wall, Stem Cells Int. 2015 (2015) 832649.
[6] M. Potente, H. Gerhardt, P. Carmeliet, Basic and therapeutic aspects of angiogenesis, Cell 146 (2011) 873–887.
[7] R.N. Gacche, Compensatory angiogenesis and tumor refractoriness, Oncogenesis 4 (2015) e153.
[8] A. Oloumi, W. Lam, J.P. Banáth, P.L. Olive, Identification of genes differentially expressed in V79 cells grown as multicell spheroids, Int. J. Radiat. Biol. 78 (2002) 483–492.
[9] G. Mehta, A.Y. Hsiao, M. Ingram, G.D. Luker, S. Takayama, Opportunities and challenges for use of tumor spheroids as models to test drug delivery and efficacy, J. Control Release 164 (2012) 192–204.
[10] A. Bredel-Geissler, U. Karbach, S. Walenta, L. Vollrath, W. Mueller-Klieser, Proliferation-associated oxygen consumption and morphology of tumor cells in monolayer and spheroid culture, J. Cell Physiol. 153 (1992) 44–52.
[11] M. Wartenberg, F. Dönmez, F.C. Ling, H. Acker, J. Hescheler, H. Sauer, Tumor-induced angiogenesis studied in confrontation cultures of multicellular tumor spheroids and embryoid bodies grown from pluripotent embryonic stem cells, FASEB J. 15 (2001) 995–1005.
[12] Y.S. Torisawa, A. Takagi, H. Shiku, T. Yasukawa, T. Matsue, A multicellular spheroid-based drug sensitivity test by scanning electrochemical microscopy, Oncol. Rep. 13 (2005) 1107–1112.
[13] D. Loessner, K.S. Stok, M.P. Lutolf, D.W. Hutmacher, J.A. Clements, S.C. Rizzi, Bioengineered 3D platform to explore cell-ECM interactions and drug resistance of epithelial ovarian cancer cells, Biomaterials 31 (2010) 8494–8506.
[14] Y.C. Tung, A.Y. Hsiao, S.G. Allen, Y.S. Torisawa, M. Ho, S. Takayama, High-throughput 3D spheroid culture and drug testing using a 384 hanging drop array, Analyst 136 (2011) 473–478.
[15] K. Chwalek, L.J. Bray, C. Werner, Tissue-engineered 3D tumor angiogenesis models: potential technologies for anti-cancer drug discovery, Adv. Drug Deliv. Rev. 79–80 (2014) 30–39.
[16] J.J. Xu, W.W. Mao, Overview of research and development for anticancer drugs, J. Cancer Ther. 7 (2016) 762–772.
[17] Z. Liu, B. Delavan, R. Roberts, W. Tong, Lessons learned from two decades of anticancer drugs, Trends Pharmacol. Sci. (2017).
[18] B. Hu, A. Nadiri, S. Bopp-Küchler, F. Perrin-Schmitt, Dental epithelial histomorphogenesis in vitro, J. Dent. Res. 8 (2005) 521–525.
[19] A.I. Alford, K.M. Kozloff, K.D. Hankenson, Extracellular matrix networks in bone remodeling, Int. J. Biochem. Cell Biol. 65 (2015) 20–31.
[20] T. Alliston, Biological regulation of bone quality, Curr. Osteoporos. Rep. 12 (2014) 366–375.
[21] M.D. McKee, A. Nanci, Osteopontin at mineralized tissue interfaces in bone, teeth, and osseointegrated implants: ultrastructural distribution and implications for mineralized tissue formation, turnover, and repair, Microsc. Res. Tech. 33 (1996) 141–164.
[22] B. Shi, O. Andrukhov, S. Berner, A. Schedle, X. Rausch-Fan, The angiogenic behaviors of human umbilical vein endothelial cells (HUVEC) in co-culture with osteoblast-like cells (MG-63) on different titanium surfaces, Dent. Mater. 30 (2014) 839–847.
[23] Y. Bo, L. Yan, Z. Gang, L. Tao, T. Yinghui, Effect of calcitonin gene-related peptide on osteoblast differentiation in an osteoblast and endothelial cell co-culture system, Cell Biol. Int. 36 (2012) 909–915.
[24] C. Yuan, P. Wang, L. Zhu, W.L. Dissanayaka, D.W. Green, E.H. Tong, L. Jin, C. Zhang, Coculture of stem cells from apical papilla and human umbilical vein endothelial cell under hypoxia increases the formation of three-dimensional vessel-like structures in vitro, Tissue Eng. Part A 21 (2015) 1163–1172.
[25] V. Dumas, A. Perrier, L. Malaval, N. Laroche, A. Guignandon, L. Vico, A. Rattner, The effect of dual frequency cyclic compression on matrix deposition by osteoblast-like cells grown in 3D scaffolds and on modulation of VEGF variant expression, Biomaterials 30 (2009) 3279–3288.
[26] S. Yazdani, A. Kasajima, K. Tamaki, Y. Nakamura, F. Fujishima, H. Ohtsuka, F. Motoi, M. Unno, M. Watanabe, Y. Sato, H. Sasano, Angiogenesis and vascular maturation in neuroendocrine tumors, Hum. Pathol. 45 (2014) 866–874.
[27] Y. Usami, K. Ishida, S. Sato, M. Kishino, M. Kiryu, Y. Ogawa, M. Okura, Y. Fukuda, S. Toyosawa, Intercellular adhesion molecule-1 (ICAM-1) expression correlates with oral cancer progression and induces macrophage/cancer cell adhesion, Int. J. Cancer 133 (2013) 568–578.
[28] Z. Radisavljevic, H. Avraham, S. Avraham, Vascular endothelial growth factor up-regulates ICAM-1 expression via the phosphatidylinositol 3 OH-kinase/AKT/Nitric oxide pathway and modulates migration of brain microvascular endothelial cells, J. Biol. Chem. 275 (2000) 20770–20774.
[29] I. Kim, S.O. Moon, S.K. Park, S.W. Chae, G.Y. Koh, Angiopoietin-1 reduces VEGF-stimulated leukocyte adhesion to endothelial cells by reducing ICAM-1, VCAM-1, and E-selectin expression, Circ. Res. 89 (2001) 477–479.
[30] A.M. Edelman, D.K. Blumenthal, E.G. Krebs, Protein serine/threonine kinases, Annu. Rev. Biochem. 56 (1987) 567–613.
[31] Y.S. Gho, H.K. Kleinman, G. Sosne, Angiogenic activity of human soluble intercellular adhesion molecule-1, Cancer Res. 59 (1999) 5128–5132.
[32] O. Salvucci, M. Basik, L. Yao, R. Bianchi, G. Tosato, Evidence for the involvement of SDF-1 and CXCR4 in the disruption of endothelial cell-branching morphogenesis and angiogenesis by TNF-alpha and IFN-gamma, J. Leukoc. Biol. 76 (2004) 217–226.
[33] R.F. Potter, A.C. Groom, Capillary diameter and geometry in cardiac and skeletal muscle studied by means of corrosion casts, Microvasc. Res. 25 (1983) 68–84.
[34] P. Datta, B. Ayan, I.T. Ozbolat, Bioprinting for vascular and vascularized tissues biofabrication, Acta Biomater. 51 (2017) 1–20.
[35] M.N. Nakatsu, R.C. Sainson, S. Pérez-del-Pulgar, J.N. Aoto, M. Aitkenhead, K.L. Taylor, P.M. Carpenter, C.C. Hughes, VEGF(121) and VEGF(165) regulate blood vessel diameter through vascular endothelial growth factor receptor 2 in an in vitro angiogenesis model, Lab. Investig. 83 (2003) 1873–1885.
[36] L.B. Wood, R. Ge, R.D. Kamm, H.H. Asada, Nascent vessel elongation rate is inversely related to diameter in in vitro angiogenesis, Integr. Biol. 4 (2012) 1081–1089.
[37] G. Cao, C.D. O'Brien, Z. Zhou, S.M. Sanders, J.N. Greenbaum, A. Makrigiannakis, H.M. DeLisser, Involvement of human PECAM-1 in angiogenesis and in vitro endothelial cell migration, Am. J. Physiol. Cell Physiol. 282 (2002) C1181–C1190.

Manuscript II

(in preparation)

Comparison of two cancer cells lines in hypoxia 2D and 3D models: effect of a flavagline derivative

1. General Background and objectives

Tumor progression and emergence of metastases are due to many parameters and combinations of a lot of factors. One of these factors favoring tumor progression and its aggressiveness is hypoxia. Hypoxia is commonly found in human solid tumor increasing hypoxia-inducible factors (HIFs) activity, which contribute to angiogenesis, extracellular matrix remodeling, cancer stem cell maintenance, tumor growth, metastasis, and treatment resistance. It is well known that solid tumors superior to a few millimeters need vasculature for oxygen supply and continue to growth (Knighton *et al.*, 1977; Horsman and Vaupel, 2016).

Conventional therapies, as radiations and chemotherapy, kill proliferating and well-oxygenated cells that are not therefore the most dangerous cancer cells, unlike hypoxic cells. Indeed, HIF1 is able to upregulate resistance genes as breast cancer resistance protein (BRCP or ABCG2) and multidrug resistance-associated protein (MRP1 or ABCC1), which are membrane glycoproteins pumping foreign molecules out of cells (Liu L *et al.*, 2008; Ding Z *et al.*, 2010; Chen J *et al.*, 2014; Sun Y *et al.*, 2016). These mechanisms explain cancer cells resistance by drug efflux out of these cells, contributing to growth and survival of tumor cells.

Knowing this, it is essential to take into account hypoxia in cell model to select new drugs.

In a first part of this study, we compared the effect of hypoxia on the two tumor cell lines, osteosarcoma cells (MG-63) and glioblastoma cells (U87-MG), based on *in vitro* model mimicking hypoxia in 2D and 3D. These two cell lines are known to be aggressive tumors and to express HIF1, which correlates with a poor prognosis and advanced stage of tumors (K. L. Søndergaard *et al.*, 2002; Ren H.Y., *et al.*, 2016). In a second part, we studied on these models the impact of the flavagline derivative, FL3 synthetic molecule, known to their anticancer effects without being toxic to healthy cells (Polier G *et al.*, 2012; Qureshi R *et al.*, 2015), and observed its effect on cell proliferation and viability, and drug resistance genes.

2. Results and discussion

2.1. Development of 3D hypoxia model

To reproduce hypoxia conditions, we used two techniques, one by adding CoCl2, agent that mimics hypoxia by preventing HIF1-α protein degradation, the other by culturing cells in 3D (spheroids or microtissues), known to provoke hypoxia in the center of the structure. We performed three conditions: 2D+$CoCl_2$, 3D alone and the combination 3D+$CoCl_2$. We found that for the two cell types MG-63 and U87-MG, there was a significantly increase of hypoxia related genes (VEGF, GLUT1 et GLUT3) in the three conditions. However, the hypoxia 3D+$CoCl_2$ model showed the highest increase in each case. Concerning drug resistance genes, both osteosarcoma MG-63 cells and gliobalstoma U87-MG cells overexpressed ABCG2 and MRP1 in the 3D+$CoCl_2$ model. These results showed that the combination of the two hypoxia techniques, 3D+$CoCl_2$, allowed to obtained highest expressions of hypoxia and drug resistance genes, and thus that was the best model.

2.2. Effect of FL3 on hypoxia models

We used synthetized Flavagline (FL3), a pharmacological molecule known to have anticancer effect, as a tool to test our hypoxia model. First, on cancer cells in 2D, we found that FL3 decreased cell metabolic activity and viability by provoking cell cycle arrest at G2 phase for the two cell lines. It has been described that some FL3 derivatives could lead to cell cycle arrest at G0/G1 or G2/M in different cancer cell lines as breast, colon and prostate cancer cells (Hausott B *et al.*, 2004; Cencic R *et al.*, 2009), causing apoptosis (Hausott B *et al.*, 2004; Thuaud F *et al.*, 2009). In our study, flow cytometry analysis showed that FL3 did not lead to apoptosis in 2D cells, what was also found by Yuan et al. in bladder cancer cells, supporting the fact that FL3 induced apoptosis might be tumor type dependent (Yuan et al., 2018). In contrast to what we found in 2D, in 3D model with or without $CoCl_2$, FL3 lead to apoptosis with the increase of Bax and Caspase-3 genes, and induced significant decrease of proliferation in hypoxia 3D model. These results highlight the impact of 3D culture on cell behavior, which differs from that of 2D. Concerning ABC transporters genes, we showed that they are increased by FL3 treatment in 2D and 3D, with or without $CoCl_2$. Moreover, we could observe a cumulative effect of $CoCl_2$ and FL3 for ABCG2 gene in MG-63 cells and for MRP1 gene in U87-MG.

These results are supported by the publication of Thuaud *et al.* in 2009, which reported that some flavaglines derivatives were sensitive to multidrug resistance, and expressed efflux pumps in some cancer cell lines. Thus FL3 induced cell resistance with the overexpression of efflux pumps, but also cell death. We hypothesize that FL3 provokes cell cycle arrest, which triggers of survival signaling, sustained by the increase of phospho-p38 protein level, which fails and leads to cell death.

2.3. FL3 induced senescence in 2D cells

The apoptosis caused by FL3 in our 3D models was expected, however the absence of apoptotic marker in 2D challenged us. Thus we performed β-Galactosidase assay to see if Flavagline could induce senescence in our cells. Only few osteosarcoma MG-63 cells were stained at 6 days post-treatment of FL3, supporting the idea that they might take another cell death pathway. Conversely, we found that 48h after FL3 treatment, glioblastoma U87-MG cells were marked in blue and that the number of cells involved in senescence significantly increased with time. It is the first time that FL3 is described to induce senescence.

3. Conclusion

The 3D hypoxia model was very similar to solid tumor conditions *in vivo*, with a strong increase in hypoxia and drug resistance genes. The important point of this study was that cancer cells reacted differently when they were in 2D or 3D, for the expression of drug resistance genes and for the borrowed cell death pathway. Thus the 3D system, combined with $CoCl_2$ to better mimic hypoxia condition, is essential to better understand cancer mechanisms and to better select and screen new drugs.

4. Perspectives

This manuscript is being prepared and we wish to add some experiments, which are in progress, in order to complete it. These experiments primarily concern: western blot in osteosarcoma MG-63 cells for cyclin D; qPCR analyzes targeting senescence genes (p16, p19, p21) in 2D and 3D models; deeper characterization of 3D+$CoCl_2$+FL3 and 3D+FL3 models for apoptosis, with cleaved-caspase 3 RNA and protein level analysis, but also cryostat sections for immunofluorescence staining, and live/death kit.

Article II

Comparison of two cancer cells lines in hypoxia 2D and 3D models: effect of a flavagline derivative

Title

Comparison of two cancer cells lines in hypoxia 2D and 3D models: effect of a flavagline derivative.

Abstract

Most of new therapeutic molecules fail before reaching the final stages of clinical trials, and the vast majority involves anti-cancer molecules. The scientific community agrees to say that the problem lies not in finding pharmacologically active new molecules, but in the experimental models for selecting them. To achieve this objective, we must create a model that takes into account the maximum of parameters in order to best mimic *in vivo* solid tumors. One of the factors favoring tumor progression and its aggressiveness is hypoxia. In the first part of this study we performed a 2D and 3D hypoxia model to compare its effect on the two tumor cell lines, osteosarcoma cells (MG-63) and glioblastoma cells (U87-MG). In a second part, we studied on these models the impact of the FL3 synthetic molecule, a flavagline derivative, and observed the effect on cell proliferation and viability, and drug resistance genes. We showed that 3D+$CoCl_2$ model lead to an increase of hypoxia related genes and drug resistance genes higher than simple models as 2D+$CoCl_2$ and 3D alone. We also found that FL3 had a different effect on cell behavior depending of their spatial arrangement, namely 2D or 3D. These results demonstrate that our hypoxia 3D+$CoCl_2$ model could be useful in *in vitro* drug assays, and that the 3D structure is essential to better understand cancer mechanisms and to better select and screen new drugs.

Introduction

Tumor progression and emergence of metastases are due to many parameters and combinations of a lot of factors. One of these factors favoring tumor progression and its aggressiveness is hypoxia. Hypoxia is commonly found in human solid tumor increasing hypoxia-inducible factors (HIFs) activity, which contribute to angiogenesis, extracellular matrix remodeling, cancer stem cell maintenance, tumor growth, metastasis, and treatment resistance. It is well known that solid tumors superior to a few millimeters need vasculature for oxygen supply and continue to growth (Knighton *et al.*, 1977; Horsman and Vaupel, 2016). Hypoxia contributes to this growth by promoting angiogenesis, via HIFs transcription factors regulated genes, as vascular endothelial growth factor (VEGF), attracting endothelial cells and so increasing blood vessels formations, tumor growth and tumor cells dissemination (Dvorak *et al.*, 1999; Lee *et al.*, 2009; Saharinen *et al.*, 2011).

Osteosarcoma and glioblastoma cancer both have rapid pretreatment growth and are aggressive tumors with 20% of patients presenting metastases leading to a 5-year survival rate of 30% for osteosarcoma (Lee J.A. *et al.*, 2016; Liapis V *et al.*, 2017; Xugui Li *et al.*, 2018), and on survival average of 14 months for patient with glioblastoma (Rønning PA *et al.*, 2012; Kore R.A. *et al.*, 2018). It has been shown that osteosarcoma expressed HIF1, correlating with poor prognosis and metastasis (Ren H.Y. *et al.*, 2016). HIF1 was also shown to be highly expressed in high-grade glioblastoma (Søndergaard K. L. *et al.*, 2002).

Conventional therapies, as radiations and chemotherapy, kill proliferating and well-oxygenated cells that are not therefore the most dangerous cancer cells, unlike hypoxic cells. Indeed, HIF1 is able to upregulate resistance genes as breast cancer resistance protein (BRCP or ABCG2) and multidrug resistance-associated protein (MRP1 or ABCC1), which are membrane glycoproteins pumping foreign molecules out of cells (Mo W and Zhang J.T., 2012; Taylor N.M.I. *et al.*, 2017; Cole S.P., 2014). These mechanisms explain cancer cells resistance by drug efflux out of these cells. It is also known, that depending of the cell type, hypoxia can induce apoptosis or contribute to drug resistance by inhibiting apoptotic pathways (Erler J.T. *et al.*, 2004; Piret J.P. *et al.*, 2005). For example, it has been noted that HIF2α knockdown increased apoptosis in osteosarcoma cells, and that U87 cell under hypoxic conditions showed an increase in cell survival and a decrease in apoptosis (Wang *et al.*, 2017; Zeng F *et al.*, 2018). Concerning radiotherapy, cytotoxic effects are due to intracellular ROS production requiring oxygen (Gupta S.C. *et al.*, 2012). Then, hypoxic cells have limited access to oxygen and therefore are resistant to radiotherapy.

Knowing this, it is essential to take into account hypoxia in cell model to select new drugs. To date, the average time to develop a new cancer drug is estimated at 7.3 years, with an average cost of $ 648 million per new molecule, and more than 95% failed during this clinical process (Arrowsmith, 2011; Ledford, 2011; Prasad V *et al.*, 2017; NIH website, About New Therapeutic Uses, 2018). The scientific community agrees that the most difficulty is not to find pharmacologically active molecules, but to get the more predictive experimental model to select these molecules. In this context, we have to develop a better model mimicking the tumor and its microenvironment.

We focused in this study on the effect of a synthetic derivative of Flavagline (FL3), known to their anticancer effects without being toxic to healthy cells (Polier G *et al.*, 2012; Qureshi R *et al.*, 2015). The first agent of this family of flavaglines, rocaglamide, was shown to have a strong anti-leukemic potential (King M. *et al.*, 1982). Compared to its parent compound (racemic rocaglaol), FL3 decreased cell proliferation and viability at lower doses with an IC_{50} near to 1nM (Thuaud *et al.*, 2009). Cytotoxicity effect of flavaglines has been reported in a lot of cancer cell lines, such as lung, breast and colon cancer (Kim S *et al.*, 2006), leading to the inhibition of proliferation inducing cell cycle arrest or apoptosis in tumor cells (Emhemmed F *et al.*, 2014; Yuan G *et al.*, 2018).

Here, in a first part, we compared the effect of hypoxia on the two tumor cell lines, osteosarcoma cells (MG-63) and glioblastoma cells (U87-MG), based on *in vitro* model mimicking hypoxia in 2D and 3D. In a second part, we studied on these models the impact of the flavagline derivative, FL3 synthetic molecule, and observed the effect on cell proliferation and viability, and drug resistance genes.

Materials and Methods

1. Cell lines and culture conditions

Osteosarcoma cell line (MG-63, Sigma-Aldrich) growth in DMEM medium (biowest, France) with 10 $U.mL^{-1}$ penicillin, 100 µg mL^{-1} streptomycin, 250 $U.mL^{-1}$ fungizone, and 10% FBS. U87-MG cell line is purchased from IGBMC (Institut de Génétique et de Biologie Moléculaire et Cellulaire, Strasbourg, France) and growth in MEM medium (Dominique Dutsher) with

10 $U.mL^{-1}$ penicillin, 100 $\mu g.mL^{-1}$ streptomycin, 250 $U.mL^{-1}$ fungizone, 1 mM Na-pyruvate, 2 mM glutamine and 10% FBS. These cells are incubated at 37 °C in a humidified atmosphere of 5% CO2. When cells reached sub-confluence (70–80%), they are harvested with trypsin and subcultured in 6 well plates for treatment.

2. Spheroid culture: 3D MG-63 and U87

MG-63 and U87-MG cells were seeded in GravityPLUS™ plate (InSphero AG, Zürich, Switzerland) to produce spheroids. 10^4 cells and $0{,}5.10^4$ per spheroids were seeded in 40µL of DMEM or MEM medium and cultured during 5 days, 10µl of medium were added to each well every 2 days, and PBS was also added to keep the environment humidified.

3. Cells treatment

$CoCl_2$ treatment in 2D monolayer: After seeding 20.10^4 cells in 6 well plates and keeping them adhere (16 to 24 hours), a mother solution of $CoCl_2$ (10mM) is prepared by dissolving 23,8mg of $CoCl_2$ in $6H_2O$ (Sigma-Aldrich) in 10ml of sterile distilled water, then the solution is filtered after making sure that the powder is totally dissolved. After calculating the desired volume for each concentration, the cells are treated with different concentrations of $CoCl_2$ ranging from 50µM to 300µM, and incubated at 37°C in a humidified atmosphere of 5% CO2 for 24 hours.

$CoCl_2$ treatment in 3D spheroids: After 5 days of spheroids formation, the cells were transferred to ultra-low adherent plates (Corning® Ultra-Low Attachment Surface Products) and treated with 150µM of $CoCl_2$ for 24 hours.

FL3 treatment: A solution of FL3 in DMSO (10mM) was graciously given to us by Dr. Laurent Désaubry (Laboratoire d'Innovation Thérapeutique, UMR 7200). For our purpose, cell lines (MG-63 and U87-MG) were incubated with and without different concentrations of FL3 (20nM to 4000nM) in culture medium. The highest concentration of DMSO (for treated and untreated cells) never exceeded 0.02% (v/v) to avoid side effects, like cell toxicity or induction of differentiation.

Fl3 treatment with $CoCl_2$ (2D): After seeding the cells in 6 well plates until adherence, 150µM of $CoCl_2$ were added to these cells during 24 hours, and then washed with PBS and treated with 200nM of FL3 for additional 48 hours.

Fl3 treatment with $CoCl_2$ (3D): After spheroids formation, they were collected and treated with 150µM of $CoCl_2$ for 24 hours, and then they were washed with PBS and treated with 200nM of FL3 for additional 48 hours.

4. Cell viability and proliferation:

To analyze the metabolic activity of cells as a response to FL3 treatment, 5.10^4 cells per well were seeded for each cell line (MG-63 and U87-MG) in 24 well plates during 24 hours. Then these cells were treated with different FL3 concentrations (0, 20, 200, 1000, 2000 and 4000nM) for 24, 48, and 72 hours. AlamarBlue® (Invitrogen, Thermo Fisher Scientific,

Waltham, MA, USA) was used to assess cell proliferation over time. The AlamarBlue® test is a nontoxic, water-soluble, colorimetric redox indicator that changes color in response to cell metabolism. After each timing set point, the cells were washed with PBS then incubated with the solution of 10% AlamarBlue® diluted with phenol free medium and kept incubated at 37 °C in a humidified atmosphere of 5% CO_2 for 4 hours. Each condition was prepared as triplicate. After 4 hours incubation, 150µl of incubation medium from each well is transferred to 96-well plate and the resulting absorbance was measured with excitation at 570mM and emission at 595mM respectively in a spectrophotometer. The results are expressed as a percentage of reduction of AlamarBlue® test and the percentage of living cell was calculated as a ratio of the OD value of each FL3-treated cell sample to the OD value of the control blank.

5. Cell cycle analysis

Both cell lines (MG-63 and U87-MG) were seeded in 6 well plates at 20.10^4 and growth for 24 hours and then treated with FL3 during 48 hours. After 48 hours FL3 treatment, cells and their supernatant were collected and centrifuged to have a unique pellet. Pellet was redispersed, washed with PBS and fixed with ethanol 70% for 30 min at 4°C, then washed two times with PBS, spinned at 850 g and treated with 100 µg/ml of ribonuclease (Sigma Aldrich), to finally be stained with 200 µl of Propidium Iodide (PI) (*life* technologies, Sigma-Aldrich) at a concentration of 50 µg/ml (prepared from 5mg/ml stock solution). After 30 min incubation in dark at room temperature, cells were examined by flow cytometer (MACS Quant de Miltenyi Biotec GmbH/Bergisch Gladbach R. F. A). A minimum of 20,000 cells was acquired per sample and the data were analyzed using ModFit LT version 3.3 software. The percentage of cells in G0/G1, S and G2/M was determined from DNA content histograms.

6. Apoptosis rate analysis by annexin V assay

Apoptosis was evaluated by the externalization of phosphatidylserine and nucleus labeling of propidium iodide (PI). For that purpose, cells were cultured, treated with FL3 and collected as described above (see section cells treatment). Apoptosis rates were assessed by flow cytometry (LSR 2 de Becton Dickinson Biosciences/San Jose California U. S. A.) using the Annexin V-FITC/PI Apoptosis Assay (Miltenyi biotec), according to the manufacturer's recommendations. The data were analyzed using DiVa 6.2 software (également de BD).

7. Analysis of mRNA expression

Total RNAs were isolated from both cell lines (MG-63 and U87) in monolayer (2D) and spheroids (3D) with 3D-MG-63 and 3D-U87-MG obtained after 5 days in hanging drop culture, treated with and without either $CoCl_2$, either FL3, or either the mixture FL3 + $CoCl_2$. The total extracted RNA concentration was quantified using NanoDrop 1000 (Fischer Scientific, Illkirch, France). 1µg of RNA was transcripted using the iScript Reverse Transcription Supermix (Bio-Rad Laboratories, Hercules, CA, USA) according to the manufacturer's instructions. To quantify RNA expression, RT-qPCR was performed on the cDNA samples. PCR amplification and analysis were achieved using the CFX Connect™ Real-Time PCR Detection System (Bio-rad, Miltry Mory, France). Amplification reactions have been performed using iTaq Universal SYBR Green Supermix (Bio-rad, Miltry-Mory, France).

Actin was used as endogenous RNA control (housekeeping gene) in the samples. The specificity of the reaction was controlled using melting curves analysis. The expression level was calculated using the comparative Ct method ($2^{-\Delta\Delta Ct}$) after normalization to the housekeeping gene. All RT-qPCR assays were performed in triplicate and results were represented by the mean values.

Gene	Forward	Reverse
Actin	5'- GATGAGATTGGCATGGCTTT- 3'	5'- CACCTTCACCGTTCCAGTTT- 3'
ABCG2	5'- GCCGTGGAACTCTTTGTGGTAG - 3'	5'- ACAGCCAAGATGCAATGGTTGT -3'
Bax	5'- CCTTTTCTACTTTGCCAGCAAAC - 3'	5'- GAGGCCGTCCCAACCAC - 3'
Caspase 3	5'- AGAACTGGACTGTGGCATTGAG - 3'	5'- GCTTGTCGGCATACTGTTTCAG - 3'
GLUT1	5'- CTGAAGTCGCACAGTGAATA - 3'	5'- TGGGTGGAGTTAATGGAGTA - 3'
GLUT3	5'- GACCCAGAGATGCTGTAATGGT - 3'	5'- TGGCAAATATCAGAGCTGGGG - 3'
HIF1α	5'- CTGCCACCACTGATGAATTA - 3'	5'- GTATGTGGGTAGGAGATGGA - 3'
MRP1	5'- TCTACCTCCTGTGGCTGAATCTG - 3'	5'- CCGATTGTCTTTGCTCTTCATG - 3'
VEGF	5'- CCTGGTGGACATCTTCCAGGAGTACC -3'	5'- GAAGCTCATCTCTCCTATGTGCTGGC- 3'

Table 1: The primers nucleotides sequences (Fisher Scientific S.A.S., Illkirch, France).

8. Western blot analysis

Cells were treated either with FL3 at different concentrations or with the vehicle and incubated for 48 hours. Cells were then lysed in RIPA buffer (50 mM Tris pH 7.5, 150 mM NaCl, 0,5% sodium deoxycholate, 0.1% SDS, 1% Triton) supplemented with protease inhibitors cocktail (Sigma-Aldrich). Proteins from cell lysates were then extracted, separated on 10–15% SDS–polyacrylamide gels and transferred to membranes using the iBlot transfer (Invitrogen). Immunoblotting was performed by using a Rabbit monoclonal anti-HIF1α antibody (Abcam, Ab17983), a mouse monoclonal anti-cyclin D1 antibody (Santa Cruz, sc-8396), a rabbit monoclonal phospho-p38 MAPK antibody (9215-S), mouse monoclonal anti-beta-actin antibody (Proteintech, 66009-1-Ig), mouse monoclonal anti-GAPDH antibody (Proteintech, 60004-1-Ig), and rabbit monoclonal beta-tubulin (Proteintech, 10094-1-AP) according to the manufacturer's instructions. Membranes were then incubated with the appropriate horseradish peroxidase-conjugated secondary antibody, for secondary mouse (Bethyl Laboratories, A90-147P) and secondary rabbit (Santa Cruz, sc-2004). Immunoreactive bands were detected using ECL chemiluminescence substrate solution (SuperSignal™ West Pico Plus, Thermo Scientific, USA). Autoradiographic signals were captured on iBright™ Imaging System (Invitrogen) and analyzed by the NIH's Image J software.

9. Senescence detection

5.10^4 cells/well for each cell line (MG-63 and U87-MG) were seeded in 24 well plates, during 24 hours, then treated with FL3 for additional 48 hours. After these 48 hours, the treatment was stopped, the plates were washed with PBS, replaced with new fresh medium and cells were incubated during 8 days. Medium was changed every two days. At each set point (2,

4,6 and 8 days), the cells were fixed with a fixation solution and stained for senescence using the senescence β-galactosidase staining kit (Cell Signalling, Ozyme). After staining, the plates were incubated at 37°C for overnight in a dry incubator (no CO_2) because its presence will cause changes in the pH which may affect staining results, then the plates were checked under microscope (Nikon Eclipse TS100) for the development of blue color and photographies were taken.

Results

Development of 3D hypoxia model

To reproduce hypoxia conditions, we used two techniques, one by adding $CoCl_2$, agent that mimics hypoxia by preventing HIF1α protein degradation, the other by culturing cells in 3D (spheroids or microtissues), known to provoke hypoxia in the center of the structure. First, we added $CoCl_2$ at several concentrations on MG-63 cells to see the effect on hypoxia related genes and multidrug resistance genes to be compared to 3D spheroids (Figure 1). $CoCl_2$ agent had the expected effect on MG-63 cells since the results showed an increase in HIF1α protein level and no modification in its RNA expression regarding the different concentrations of $CoCl_2$ and the control (Figure 1A and C). We also saw a significant increase of glucose transporter 1 (GLUT1) and 3 (GLUT3), which are recognized to be hypoxia-sensitive in many cells, for all concentrations of $CoCl_2$. But no effect was found for multidrug resistance genes, the multidrug resistance 1 (MDR1) and the multidrug resistance associated proteins 1 (MRP1), except for the breast cancer resistance protein (ABCG2), that showed a significant increase for concentrations of 150µM and 200µM $CoCl_2$ (Figure 1B). Moreover, vascular endothelial growth factor (VEGF) gene expression was increased with $CoCl_2$ since VEGF is a major transcriptional target for HIF1α (Figure 1A).
By comparison, we performed 3D culture with MG-63 cells to obtain spheroids of 5.10^3 and 10^4 cells, with or without $CoCl_2$ (Figure 1D and E). mRNA expression of HIF1α was significantly increased in spheroids compared to 2D control, but no difference was observed between the conditions of spheroids, 5.10^3 and 10^4 cells, with or without $CoCl_2$. Concerning VEGF expression gene, results have shown an increase of its expression in spheroids, which is largely accentuated in spheroids with $CoCl_2$. The same trend of results was observed for GLUT1 and GLUT3 genes expression, with a big increase in spheroids treated with $CoCl_2$. Interestingly, multidrug resistance genes showed different profile depending of the gene. ABCG2 and MRP1 gene expression showed high increases for spheroids with $CoCl_2$, compared to 2D control and spheroids without $CoCl_2$. So these results showed that each technique (2D+$CoCl_2$ and 3D alone) lead to a relatively equivalent increase for each hypoxia related gene, but especially that this effect is significantly improved by the combination of the two techniques (3D+ $CoCl_2$).

We did the same experiments with glioblastoma cells (U87-MG) and obtained quite similar effect of $CoCl_2$ on 2D cells (Figure 2). First, we controlled the impact of $CoCl_2$ treatment by HIF1α protein level. As expected, there was no effect on HIF1α mRNA expression, but an increase in protein expression (Figure 2A and C). We saw, as previously, a significant increase of VEGF, GLUT1 and GLUT3 genes for all $CoCl_2$ concentrations. MRP1 multidrug resistance gene expression has not shown significant difference compared to control, but unlike for MG-63 cells, here $CoCl_2$ had no effect on ABCG2.

To follow, the same experiments done with osteosarcoma cells, we also performed two sizes of spheroids with or without $CoCl_2$ with U87-MG cells. As expected, HIF1α gene expression was increased in all spheroids without being affected by $CoCl_2$. Expression of VEGF, GLUT1 and GLUT3 genes is increased in spheroids without $CoCl_2$, which is amplified with adding of $CoCl_2$, as in MG-63 cells (Figure 2D). Concerning multidrug resistance genes, the same profile was observed with a significant augmentation in spheroids treated with $CoCl_2$, for the two genes observed ABCG2 and MRP1 (Figure 2E).
These results showed that the model 2D+$CoCl_2$, as 3D model, lead to an increase of hypoxia related genes (VEGF, GLUT1 and GLUT3) in the two cell types, glioblastoma and osteosarcoma cancer cells. However, the combination of the two models, 3D+$CoCl_2$, was the best to recreate the hypoxic situation. We thus have used this 3D+$CoCl_2$ model for the rest of experiments using 150mM $CoCl_2$ concentration according to the results.

Effect of FL3 on hypoxia models

Next, we used synthetized Flavagline (FL3), a pharmacological molecule known to have anticancer effect, as a tool to test our hypoxia model (Figure 3 and 4). First, cell viability has been analyzed by Alamar Blue assay at different times of treatment, using different concentrations of Flavagline (FL3) on 2D MG-63 cells. We wanted to evaluate the concentration of FL3 we will use later, and simply observe the effect of FL3 on our cells as we did with $CoCl_2$. These results showed a significant decrease of Alamar Blue reduction percentage from 20nM of FL3, corresponding to 25% loss of cell viability after 24h treatment, up to 50% loss of viability to 200nM of FL3. We observed saturation beyond this concentration (Figure 3A). After 48h treatment there was a loss of 30% of cell viability at 20nM FL3, up to 60% for 200nM. Beyond 200nM, we saw the same phenomenon of saturation. The effect of FL3 is more relevant after 48h treatment, compared to 24h, and 72h treatment followed the same curve than 48h. In view of these results, we chose to perform all experiments with 200nM of FL3 during 48h treatment. We could also notice the effect of FL3 on the cell viability by simple observation of the treated cells, which did not proliferate or less and of which a part floated compared to the control cells (Figure 5A). We have seen a decrease in metabolic activity and cell viability, FL3 can cause cell death or cell cycle arrest or simply a decrease in cell metabolism.

We thus performed cell cycle analysis revealing a cell cycle arrest in S/G2 phase, cells accumulating in G2 phase with FL3 concentrations (Figures 3B and S2). These results were supported by the increase of phospho-p38 MAPK (Mitogen-activated protein kinases) known to activate G2/M checkpoint for DNA repair and cell survival. Interestingly, we analyzed FL3 treated cells by flow cytometer with annexin V and propidium iodide, and did not find apoptosis (Figure S1). Then, we wanted to observe the effect of FL3 on our hypoxia model in 2D and 3D. qPCR analysis in Figure 3D showed an augmentation of the two multidrug resistance genes in 2D MG-63 cells treated with FL3, which was amplified in $CoCl_2$ models. The same effect of FL3 was observed in the 3D hypoxia model with a high increase of these expression drug resistance genes in spheroids (Figure 3E). Since we found a decrease in cell viability but no apoptosis in 2D cells treated with FL3, we studied its effect in 3D cells of Ki67 for proliferation, Bax and Caspase-3 for apoptosis. FL3 in 3D alone did not show difference compared to control for Ki67, but in 3D+$CoCl_2$ model, there was a relevant decrease of this

proliferative gene. Interestingly, we observed an increase of apoptosis related genes Bax and Caspase-3 in 3D and 3D+$CoCl_2$ model (Figure 3F).

Same experiments to test FL3 were performed with U87-MG cells (Figure 4). Alamar Blue assay showed a drastic decrease of cell viability for treatment 72h, but for the comparison, we chose to use the same time and the same concentration of FL3 as for MG63, whose curve at 48h (Figure 4A). Cell cycle analysis, as in MG-63, revealed an arrest in G2 phase, and correlating with the cyclin D protein decrease in Western Blot analysis, important for progression of cells through S phase (Figure 4B, C and S2). These results were also supported by the increase of phospho-p38 at protein level. As in osteosarcoma cells, no apoptosis was found in treated 2D U87-MG cells treated with FL3 (Figure S1). The effect of FL3 in 2D and 3D hypoxia model showed a significantly increase of ABCG2 and MRP1 mRNA expression significantly (Figure 4D and E). Here again, results showed a decrease of proliferative Ki67 gene and an increase of apoptosis related genes, Bax and Caspase-3, in hypoxia 3D model (Figure 4F).

FL3 induced senescence in 2D cells

The apoptosis caused by FL3 in our 3D models was expected, however the absence of apoptotic marker in 2D challenged us. Thus we performed β-Galactosidase assay to see if Flavagline could induce senescence in our cells. MG-63 and U87-MG were treated with 200nM of FL3 during 48h, then medium were changed every two days, during 8 days (Figure 5). For osteosarcoma MG-63 cells, we observed only few cells staining in blue from 6 days post-treatment (Figure 5A). Conversely, for glioblastoma U87-MG cells, some cells already had a blue mark on the second day, and the number of cells involved in senescence significantly increased with time (Figure 5B).

Discussion

This study allowed comparing the effect of hypoxia on two cancer cell lines, osteosarcoma (MG-63) and glioblastoma (U87-MG), using two techniques to obtain hypoxia, one with $CoCl_2$ agent, the other with 3D culture. The results showed that the combination of $CoCl_2$ and 3D was the best model to mimic hypoxia. The cobalt of $CoCl_2$ agent can replace the iron core of the HIF1α enzyme degradation preventing its degradation. $CoCl_2$ can also inhibit the interaction between HIF1α and von Hippel Lindau (VHL) protein, which is implicated too in the degradation of HIF1α (Epstein *et al.*, 2001; Lee H.R. *et al.*, 2018). That is why after $CoCl_2$ treatment, we could see an accumulation of HIF1α at protein level, but not in RNA expression (Figure 1A, C and Figure 2A, C). However, we observed an increase of HIF1α at RNA level in the 3D model, which remained stable after the addition of $CoCl_2$, since it has no effect on RNA level (Figure 1D and 2D). Indeed, the 3D structure induces hypoxia core when tumor spheroids reach a greater than 500µm in size, due to the diffusion distance of oxygen to cells in the center (Brown *et al.*, 1998; Wartenberg *et al.*, 2001). Thus, the increase of HIF1α due to a lack of oxygen or an inhibition of protein degradation lead to expression of its target genes, such as VEGF, GLUT1 and GLUT3 (Masoud G.N. and Li W., 2015). We observed a significant increase for these three target genes in 2D+$CoCl_2$ and in 3D model, but the combination of the two conditions, inhibition of protein degradation and lack of oxygen resulted in an amplification of the effect (3D+$CoCl_2$, Figure 1D and 2D), due to the increase

and accumulation of HIF1α in cytoplasm, translocating with HIF1β in the nucleus to trigger the transcription of target genes.
The overexpression of breast cancer resistance protein (BRCP or ABCG2) and multidrug resistance associated protein 1 (MRP1 or ABCC1) is one of the major mechanisms supporting the Multi Drug Resistance process. These plasma membrane efflux pumps constitute a large family (48 transporters in human) and are ubiquitously expressed in human tissue (Mo W and Zhang J.T., 2012; Cole S.P., 2014). In our study, $CoCl_2$ on 2D MG-63 cells had only effect on ABCG2 expression but not on MRP1 (Figure 1B). It has been shown that $CoCl_2$ agent induced the increase ABCG2 in pancreatic cancer cells and colon cancer cells (He X. *et al.*, 2015; Pinzón-Daza M.L. *et al.*, 2017). MRP1 has been also increased in colon cancer cells following $CoCl_2$ treatment (Lv Y. *et al.*, 2015). So these results simply shown that, following $CoCl_2$ treatment, ATP-binding cassette transporters are expressed differently depending of cancer cell types. Concerning glioblastoma cancer cells, they also express ABCG2 and MRP1 (Shen H. *et al.*, 2015; Emery I.F. *et al.*, 2017), which did not change by $CoCl_2$ agent in our study (Figure 2B). The hypothesis is that other efflux transporters should be overexpressed in 2D U87-MG cells treated with $CoCl_2$.
Different studies have reported that ABC transporters were increased in 3D culture compared to 2D culture (Martins-Neves *et al.*, 2012; Bai C. *et al.*, 2015; Breslin S. *et al.*, 2016), what we observed for ABCG2 for the two cell types in Figure 1E and 2E. However, there was a significant increase for the two drug resistance genes in each cell line in the 3D+$CoCl_2$ model. This highlights the importance of 3D culture on cell behavior against a foreign molecule. In 3D spheroids, closer to *in vivo*, cells expressed efflux transporters that they did not in 2D.

Synthetic flavagline FL3 is known to have anticancer effects and has been study in a lot of cancer cells but no studies were done yet in MG-63 osteosarcoma cells or U87-MG glioblastoma cells. Here, we showed that FL3 decreased cell metabolic activity and viability by provoking cell cycle arrest at G2 phase for the two cell lines (Figure 3A, B and 4A, B). It has been described that some FL3 derivatives could lead to cell cycle arrest at G0/G1 or G2/M in different cancer cell lines as breast, colon and prostate cancer cells (Hausott B. *et al.*, 2004; Cencic R. *et al.*, 2009). Moreover, in the literature, these molecules caused apoptosis in cancer cells cultured in 2D (Hausott B. *et al.*, 2004; Thuaud F. *et al.*, 2009). In our study, FL3 did not lead to apoptosis in 2D cells (Figure S1), what was also found by Yuan *et al.* in bladder cancer cells, supporting the fact that FL3 induced apoptosis might be tumor type dependent (Yuan G. *et al.*, 2018). We showed that the cell death type caused by FL3 was senescence in glioblastoma cells (Figure 5B). MG-63 osteosarcoma cells might be taking another cell death pathway. For example, in melanoma cells, it has been reported that a flavagline derivative, silvestrol, induced early autophagy (Chen W.L. *et al.*, 2016). In contrast to what we found in 2D, in 3D model with or without $CoCl_2$, FL3 seemed to lead to apoptosis with the increase of Bax and Caspase-3 genes, and induced significant decrease of proliferation in hypoxia 3D model (Figure 1F and 2F). But more characterization should be done concerning apoptosis, for exemple with the study of cleaved-caspase 3 at RNA and protein level. Again, these results highlight the impact of 3D culture on cell behavior, which differs from that of 2D. Concerning ABC transporters genes, we showed that they are increased by FL3 treatment in 2D and 3D, with or without $CoCl_2$ (Figure 3D, E and 4D, E). Moreover, we could observe a cumulative effect of $CoCl_2$ and FL3 for ABCG2 gene in MG-63 cells and for MRP1 gene in U87-MG. These results are supported by the publication of

Thuaud *et al.* in 2009, which reported that some flavaglines derivatives were sensitive to multidrug resistance, and expressed efflux pumps in some cancer cell lines. Thus FL3 induced cell resistance with the overexpression of efflux pumps, but also cell death. We hypothesize that FL3 provokes cell cycle arrest, which triggers of survival signaling, sustained by the increase of phospho-p38 protein level, which fails and leads to cell death.

In conclusion, the 3D hypoxia model was very similar to solid tumor conditions in vivo, with a strong increase in hypoxia and drug resistance genes. The important point of this study was that cancer cells reacted differently when they were in 2D or 3D, for the expression of drug resistance genes and for the borrowed cell death pathway. Thus the 3D system, combined with CoCl2 to better mimic hypoxia condition, is essential to better understand cancer mechanisms and to better select and screen new drugs.

References

1. Arrowsmith, J., Trial watch: phase III and submission failures: 2007-2010. *Nat Rev Drug Discov* **2011,** *10* (2), 87.
2. Bai, C.; Yang, M.; Fan, Z.; Li, S.; Gao, T.; Fang, Z., Associations of chemo- and radio-resistant phenotypes with the gap junction, adhesion and extracellular matrix in a three-dimensional culture model of soft sarcoma. *J Exp Clin Cancer Res* **2015,** *34*, 58.
3. Breslin, S.; O'Driscoll, L., The relevance of using 3D cell cultures, in addition to 2D monolayer cultures, when evaluating breast cancer drug sensitivity and resistance. *Oncotarget* **2016,** *7* (29), 45745-45756.
4. Brown, J. M.; Giaccia, A. J., The unique physiology of solid tumors: opportunities (and problems) for cancer therapy. *Cancer Res* **1998,** *58* (7), 1408-16.
5. Cencic, R.; Carrier, M.; Galicia-Vázquez, G.; Bordeleau, M. E.; Sukarieh, R.; Bourdeau, A.; Brem, B.; Teodoro, J. G.; Greger, H.; Tremblay, M. L.; Porco, J. A.; Pelletier, J., Antitumor activity and mechanism of action of the cyclopenta[b]benzofuran, silvestrol. *PLoS One* **2009,** *4* (4), e5223.
6. Chen, W. L.; Pan, L.; Kinghorn, A. D.; Swanson, S. M.; Burdette, J. E., Silvestrol induces early autophagy and apoptosis in human melanoma cells. *BMC Cancer* **2016,** *16*, 17.
7. Cole, S. P., Multidrug resistance protein 1 (MRP1, ABCC1), a "multitasking" ATP-binding cassette (ABC) transporter. *J Biol Chem* **2014,** *289* (45), 30880-8.
8. Dvorak, H. F.; Nagy, J. A.; Feng, D.; Brown, L. F.; Dvorak, A. M., Vascular permeability factor/vascular endothelial growth factor and the significance of microvascular hyperpermeability in angiogenesis. *Curr Top Microbiol Immunol* **1999,** *237*, 97-132.
9. Emery, I. F.; Gopalan, A.; Wood, S.; Chow, K. H.; Battelli, C.; George, J.; Blaszyk, H.; Florman, J.; Yun, K., Expression and function of ABCG2 and XIAP in glioblastomas. *J Neurooncol* **2017,** *133* (1), 47-57.
10. Emhemmed, F.; Ali Azouaou, S.; Thuaud, F.; Schini-Kerth, V.; Désaubry, L.; Muller, C. D.; Fuhrmann, G., Selective anticancer effects of a synthetic flavagline on human Oct4-expressing cancer stem-like cells via a p38 MAPK-dependent caspase-3-dependent pathway. *Biochem Pharmacol* **2014,** *89* (2), 185-96.
11. Epstein, A. C.; Gleadle, J. M.; McNeill, L. A.; Hewitson, K. S.; O'Rourke, J.; Mole, D. R.; Mukherji, M.; Metzen, E.; Wilson, M. I.; Dhanda, A.; Tian, Y. M.; Masson, N.; Hamilton, D. L.; Jaakkola, P.; Barstead, R.; Hodgkin, J.; Maxwell, P. H.; Pugh, C. W.; Schofield, C. J.; Ratcliffe, P. J., C. elegans EGL-9 and mammalian homologs define a family of dioxygenases that regulate HIF by prolyl hydroxylation. *Cell* **2001,** *107* (1), 43-54.
12. Erler, J. T.; Cawthorne, C. J.; Williams, K. J.; Koritzinsky, M.; Wouters, B. G.; Wilson, C.; Miller, C.; Demonacos, C.; Stratford, I. J.; Dive, C., Hypoxia-mediated down-regulation of Bid and Bax in tumors occurs via hypoxia-inducible factor 1-dependent and -independent mechanisms and contributes to drug resistance. *Mol Cell Biol* **2004,** *24* (7), 2875-89.
13. Gupta, S. C.; Hevia, D.; Patchva, S.; Park, B.; Koh, W.; Aggarwal, B. B., Upsides and downsides of reactive oxygen species for cancer: the roles of reactive oxygen species in tumorigenesis, prevention, and therapy. *Antioxid Redox Signal* **2012,** *16* (11), 1295-322.
14. Hausott, B.; Greger, H.; Marian, B., Flavaglines: a group of efficient growth inhibitors block cell cycle progression and induce apoptosis in colorectal cancer cells. *Int J Cancer* **2004,** *109* (6), 933-40.

15. He, X.; Wang, J.; Wei, W.; Shi, M.; Xin, B.; Zhang, T.; Shen, X., Hypoxia regulates ABCG2 activity through the activivation of ERK1/2/HIF-1α and contributes to chemoresistance in pancreatic cancer cells. *Cancer Biol Ther* **2016,** *17* (2), 188-98.
16. Horsman, M. R.; Vaupel, P., Pathophysiological Basis for the Formation of the Tumor Microenvironment. *Front Oncol* **2016,** *6*, 66.
17. Kim, S.; Salim, A. A.; Swanson, S. M.; Kinghorn, A. D., Potential of cyclopenta[b]benzofurans from Aglaia species in cancer chemotherapy. *Anticancer Agents Med Chem* **2006,** *6* (4), 319-45.
18. King, M.L.; Chiang, C.C.; Ling, H.C. ; Fujita, E.; Ochiai, M.; McPhail, A.T., X-Ray crystal structure of rocaglamide, a novel antileulemic 1H-cyclopenta[b]benzofuran from Aglaia elliptifolia. *J. Chem. Soc., Chem. Commun.*, **1982,** 0**,** 1150-1151.
19. Knighton, D.; Ausprunk, D.; Tapper, D.; Folkman, J., Avascular and vascular phases of tumour growth in the chick embryo. *Br J Cancer* **1977,** *35* (3), 347-56.
20. Kore, R. A.; Edmondson, J. L.; Jenkins, S. V.; Jamshidi-Parsian, A.; Dings, R. P. M.; Reyna, N. S.; Griffin, R. J., Hypoxia-derived exosomes induce putative altered pathways in biosynthesis and ion regulatory channels in glioblastoma cells. *Biochem Biophys Rep* **2018,** *14*, 104-113.
21. Ledford, H., Translational research: 4 ways to fix the clinical trial. *Nature* **2011,** *477* (7366), 526-8.
22. Lee, H. R.; Leslie, F.; Azarin, S. M., A facile in vitro platform to study cancer cell dormancy under hypoxic microenvironments using CoCl. *J Biol Eng* **2018,** *12*, 12.
23. Lee, J. A.; Paik, E. K.; Seo, J.; Kim, D. H.; Lim, J. S.; Yoo, J. Y.; Kim, M. S., Radiotherapy and gemcitabine-docetaxel chemotherapy in children and adolescents with unresectable recurrent or refractory osteosarcoma. *Jpn J Clin Oncol* **2016,** *46* (2), 138-43.
24. Li, X.; Lu, Q.; Xie, W.; Wang, Y.; Wang, G., Anti-tumor effects of triptolide on angiogenesis and cell apoptosis in osteosarcoma cells by inducing autophagy via repressing Wnt/β-Catenin signaling. *Biochem Biophys Res Commun* **2018,** *496* (2), 443-449.
25. Liapis, V.; Zysk, A.; DeNichilo, M.; Zinonos, I.; Hay, S.; Panagopoulos, V.; Shoubridge, A.; Difelice, C.; Ponomarev, V.; Ingman, W.; Atkins, G. J.; Findlay, D. M.; Zannettino, A. C. W.; Evdokiou, A., Anticancer efficacy of the hypoxia-activated prodrug evofosfamide is enhanced in combination with proapoptotic receptor agonists against osteosarcoma. *Cancer Med* **2017,** *6* (9), 2164-2176.
26. Lv, Y.; Zhao, S.; Han, J.; Zheng, L.; Yang, Z.; Zhao, L., Hypoxia-inducible factor-1α induces multidrug resistance protein in colon cancer. *Onco Targets Ther* **2015,** *8*, 1941-8.
27. Martins-Neves, S. R.; Lopes, Á.; do Carmo, A.; Paiva, A. A.; Simões, P. C.; Abrunhosa, A. J.; Gomes, C. M., Therapeutic implications of an enriched cancer stem-like cell population in a human osteosarcoma cell line. *BMC Cancer* **2012,** *12*, 139.
28. Masoud, G. N.; Li, W., HIF-1α pathway: role, regulation and intervention for cancer therapy. *Acta Pharm Sin B* **2015,** *5* (5), 378-89.
29. Mo, W.; Zhang, J. T., Human ABCG2: structure, function, and its role in multidrug resistance. *Int J Biochem Mol Biol* **2012,** *3* (1), 1-27.
30. Pinzón-Daza, M. L.; Cuellar-Saenz, Y.; Nualart, F.; Ondo-Mendez, A.; Del Riesgo, L.; Castillo-Rivera, F.; Garzón, R., Oxidative Stress Promotes Doxorubicin-Induced Pgp and BCRP Expression in Colon Cancer Cells Under Hypoxic Conditions. *J Cell Biochem* **2017,** *118* (7), 1868-1878.
31. Piret, J. P.; Minet, E.; Cosse, J. P.; Ninane, N.; Debacq, C.; Raes, M.; Michiels, C., Hypoxia-inducible factor-1-dependent overexpression of myeloid cell factor-1 protects hypoxic cells against tert-butyl hydroperoxide-induced apoptosis. *J Biol Chem* **2005,** *280* (10), 9336-44.
32. Polier, G.; Neumann, J.; Thuaud, F.; Ribeiro, N.; Gelhaus, C.; Schmidt, H.; Giaisi, M.; Köhler, R.; Müller, W. W.; Proksch, P.; Leippe, M.; Janssen, O.; Désaubry, L.; Krammer, P. H.; Li-Weber, M., The natural anticancer compounds rocaglamides inhibit the Raf-MEK-ERK pathway by targeting prohibitin 1 and 2. *Chem Biol* **2012,** *19* (9), 1093-104.
33. Prasad, V.; Mailankody, S., Research and Development Spending to Bring a Single Cancer Drug to Market and Revenues After Approval. *JAMA Intern Med* **2017,** *177* (11), 1569-1575.
34. Qureshi, R.; Yildirim, O.; Gasser, A.; Basmadjian, C.; Zhao, Q.; Wilmet, J. P.; Désaubry, L.; Nebigil, C. G., FL3, a Synthetic Flavagline and Ligand of Prohibitins, Protects Cardiomyocytes via STAT3 from Doxorubicin Toxicity. *PLoS One* **2015,** *10* (11), e0141826.
35. Ren, H. Y.; Zhang, Y. H.; Li, H. Y.; Xie, T.; Sun, L. L.; Zhu, T.; Wang, S. D.; Ye, Z. M., Prognostic role of hypoxia-inducible factor-1 alpha expression in osteosarcoma: a meta-analysis. *Onco Targets Ther* **2016,** *9*, 1477-87.
36. Rønning, P. A.; Helseth, E.; Meling, T. R.; Johannesen, T. B., A population-based study on the effect of temozolomide in the treatment of glioblastoma multiforme. *Neuro Oncol* **2012,** *14* (9), 1178-84.

37. Saharinen, P.; Eklund, L.; Pulkki, K.; Bono, P.; Alitalo, K., VEGF and angiopoietin signaling in tumor angiogenesis and metastasis. *Trends Mol Med* **2011,** *17* (7), 347-62.
38. Shen, H.; Hau, E.; Joshi, S.; Dilda, P. J.; McDonald, K. L., Sensitization of Glioblastoma Cells to Irradiation by Modulating the Glucose Metabolism. *Mol Cancer Ther* **2015,** *14* (8), 1794-804.
39. Søndergaard, K. L.; Hilton, D. A.; Penney, M.; Ollerenshaw, M.; Demaine, A. G., Expression of hypoxia-inducible factor 1alpha in tumours of patients with glioblastoma. *Neuropathol Appl Neurobiol* **2002,** *28* (3), 210-7.
40. Taylor, N. M. I.; Manolaridis, I.; Jackson, S. M.; Kowal, J.; Stahlberg, H.; Locher, K. P., Structure of the human multidrug transporter ABCG2. *Nature* **2017,** *546* (7659), 504-509.
41. Thuaud, F.; Bernard, Y.; Türkeri, G.; Dirr, R.; Aubert, G.; Cresteil, T.; Baguet, A.; Tomasetto, C.; Svitkin, Y.; Sonenberg, N.; Nebigil, C. G.; Désaubry, L., Synthetic analogue of rocaglaol displays a potent and selective cytotoxicity in cancer cells: involvement of apoptosis inducing factor and caspase-12. *J Med Chem* **2009,** *52* (16), 5176-87.
42. Wang, Y.; Wang, X.; Su, X.; Liu, T., HIF-2α affects proliferation and apoptosis of MG-63 osteosarcoma cells through MAPK signaling. *Mol Med Rep* **2017,** *15* (4), 2174-2178.
43. Wartenberg, M.; Dönmez, F.; Ling, F. C.; Acker, H.; Hescheler, J.; Sauer, H., Tumor-induced angiogenesis studied in confrontation cultures of multicellular tumor spheroids and embryoid bodies grown from pluripotent embryonic stem cells. *FASEB J* **2001,** *15* (6), 995-1005.
44. Yuan, G.; Chen, X.; Liu, Z.; Wei, W.; Shu, Q.; Abou-Hamdan, H.; Jiang, L.; Li, X.; Chen, R.; Désaubry, L.; Zhou, F.; Xie, D., Flavagline analog FL3 induces cell cycle arrest in urothelial carcinoma cell of the bladder by inhibiting the Akt/PHB interaction to activate the GADD45α pathway. *J Exp Clin Cancer Res* **2018,** *37* (1), 21.
45. Zeng, F.; Chen, H.; Zhang, Z.; Yao, T.; Wang, G.; Zeng, Q.; Duan, S.; Zhan, Y., Regulating glioma stem cells by hypoxia through the Notch1 and Oct3/4 signaling pathway. *Oncol Lett* **2018,** *16* (5), 6315-6322.
46. National Institute of Health, About New Therapeutic Uses, https://ncats.nih.gov/ntu/about.

Legends of figures

Figure 1: Development of 3D hypoxia model of osteosarcoma. A, Relative expression of hypoxia related genes in 2D MG-63 cells treated with different concentrations of $CoCl_2$. B, Relative expression of multidrug resistance genes in 2D MG-63 cells treated with different concentrations of $CoCl_2$. C, Western Blot analysis of HIF1α protein level in 2D MG-63 cells treated with different concentrations of $CoCl_2$. D, Relative expression by qPCR analysis of hypoxia related genes in 3D MG-63 cells. E, Relative expression by qPCR analysis of multidrug resistance genes in 3D MG-63 cells.

Figure 2: Development of 3D hypoxia model of glioblastoma. A, Relative expression of hypoxia related genes in 2D U87-MG cells treated with different concentrations of $CoCl_2$. B, Relative expression of multidrug resistance genes in 2D U87-MG cells treated with different concentrations of $CoCl_2$. C, Western Blot analysis of HIF1α protein level in 2D U87-MG cells treated with different concentrations of $CoCl_2$. D, Relative expression by qPCR analysis of hypoxia related genes in 3D U87-MG cells. E, Relative expression by qPCR analysis of multidrug resistance genes in 3D U87-MG cells.

Figure 3: Effect of FL3 on 2D and 3D hypoxia model of osteosarcoma. A, Analysis of cells viability by Alamar Blue assay in 2D MG-63 cells treated by different concentrations of FL3. B, Representation of percentage of cells in each cell cycle phase treated with different concentrations of FL3. C, Western Blot analysis of phospho-p38 protein level in 2D MG-63 cells treated with different concentrations of FL3. D, Relative expression of multidrug resistance genes in 2D hypoxia model. E, Relative expression of multidrug resistance genes in

3D hypoxia model. F, Relative expression of proliferation and apoptosis related genes in 3D hypoxia model.

Figure 4: Effect of FL3 on 2D and 3D hypoxia model of glioblastoma. A, Analysis of cells viability by Alamar Blue assay in 2D U87-MG cells treated by different concentrations of FL3. B, Representation of percentage of cells in each cell cycle phase treated with different concentrations of FL3. C, Western Blot analysis of phospho-p38 and Cyclin D protein level in 2D U87-MG cells treated with different concentrations of FL3. D, Relative expression of multidrug resistance genes in 2D hypoxia model. E, Relative expression of multidrug resistance genes in 3D hypoxia model. F, Relative expression of proliferation and apoptosis related genes in 3D hypoxia model.

Figure 5: FL3 induced senescence in 2D cells. A, 2D MG-63 cells treated by FL3 during 48h, pictures taken every two days during 8 days. B, 2D U87-MG cells treated by FL3 during 48h, pictures taken every two days during 8 days.

Figure S1: Apoptosis analysis by flow cytometer. A, 2D MG-63 cells treated with FL3. B, 2D U87-MG cells treated with FL3.

Figure S2: Cell cycle analysis. A, 2D MG-63 cells treated with different concentrations of FL3. B, 2D U87-MG cells treated with different concentrations of FL3.

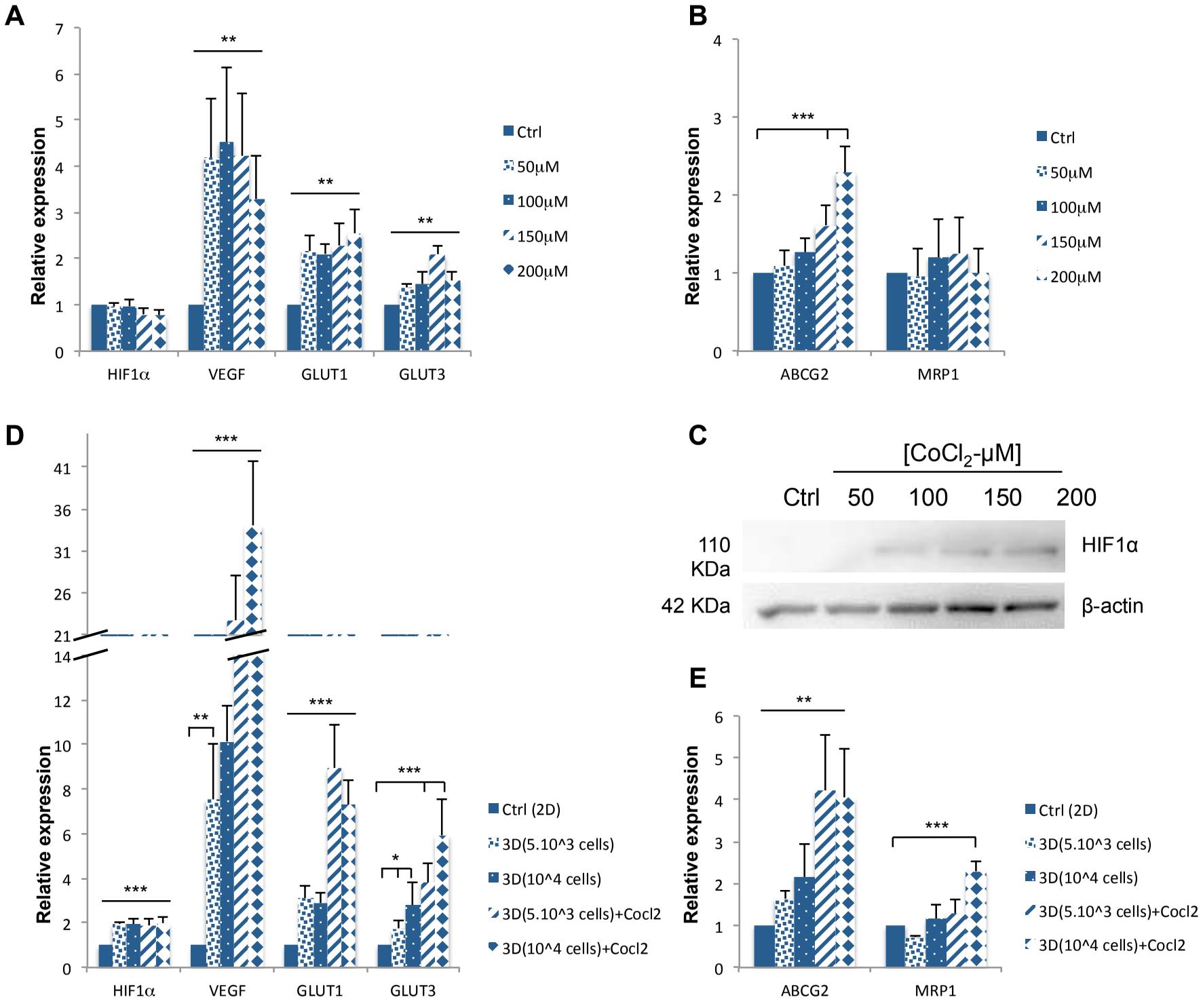
A
Relative expression
HIF1α
VEGF
GLUT1
GLUT3
Ctrl
50μM
100μM
150μM
200μM
B
Relative expression
ABCG2
MRP1
C
[CoCl2-μM]
Ctrl
50
100
150
200
110 KDa
HIF1α
42 KDa
β-actin
D
Relative expression
Ctrl (2D)
3D(5.10^3 cells)
3D(10^4 cells)
3D(5.10^3 cells)+Cocl2
3D(10^4 cells)+Cocl2
E
Relative expression
ABCG2
MRP1

Figure 1

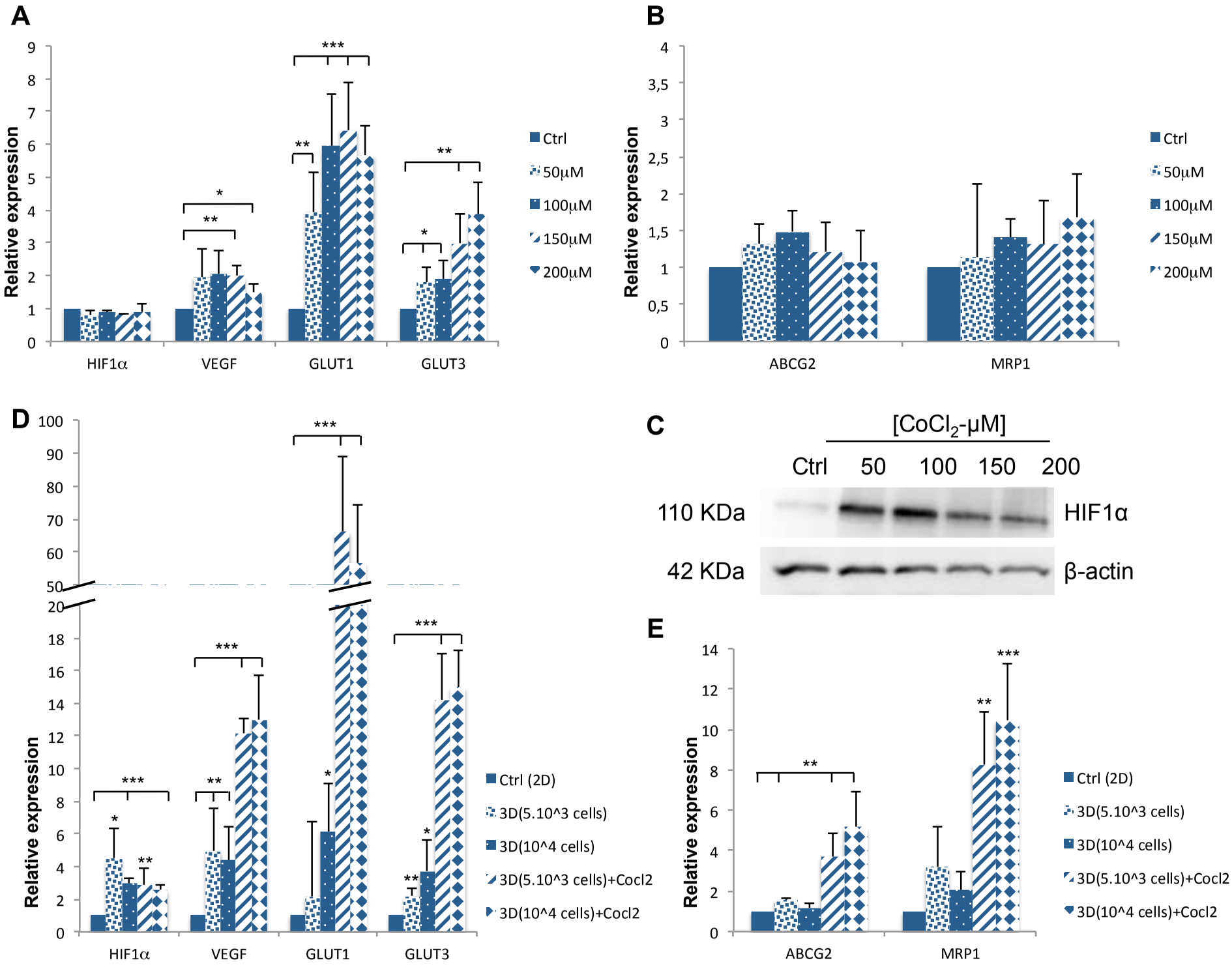
A
Relative expression
HIF1α
VEGF
GLUT1
GLUT3
Ctrl
50µM
100µM
150µM
200µM
B
Relative expression
ABCG2
MRP1
Ctrl
50µM
100µM
150µM
200µM
C
[CoCl2-µM]
Ctrl
50
100
150
200
110 KDa
HIF1α
42 KDa
β-actin
D
Relative expression
HIF1α
VEGF
GLUT1
GLUT3
Ctrl (2D)
3D(5.10^3 cells)
3D(10^4 cells)
3D(5.10^3 cells)+Cocl2
3D(10^4 cells)+Cocl2
E
Relative expression
ABCG2
MRP1
Ctrl (2D)
3D(5.10^3 cells)
3D(10^4 cells)
3D(5.10^3 cells)+Cocl2
3D(10^4 cells)+Cocl2

Figure 2

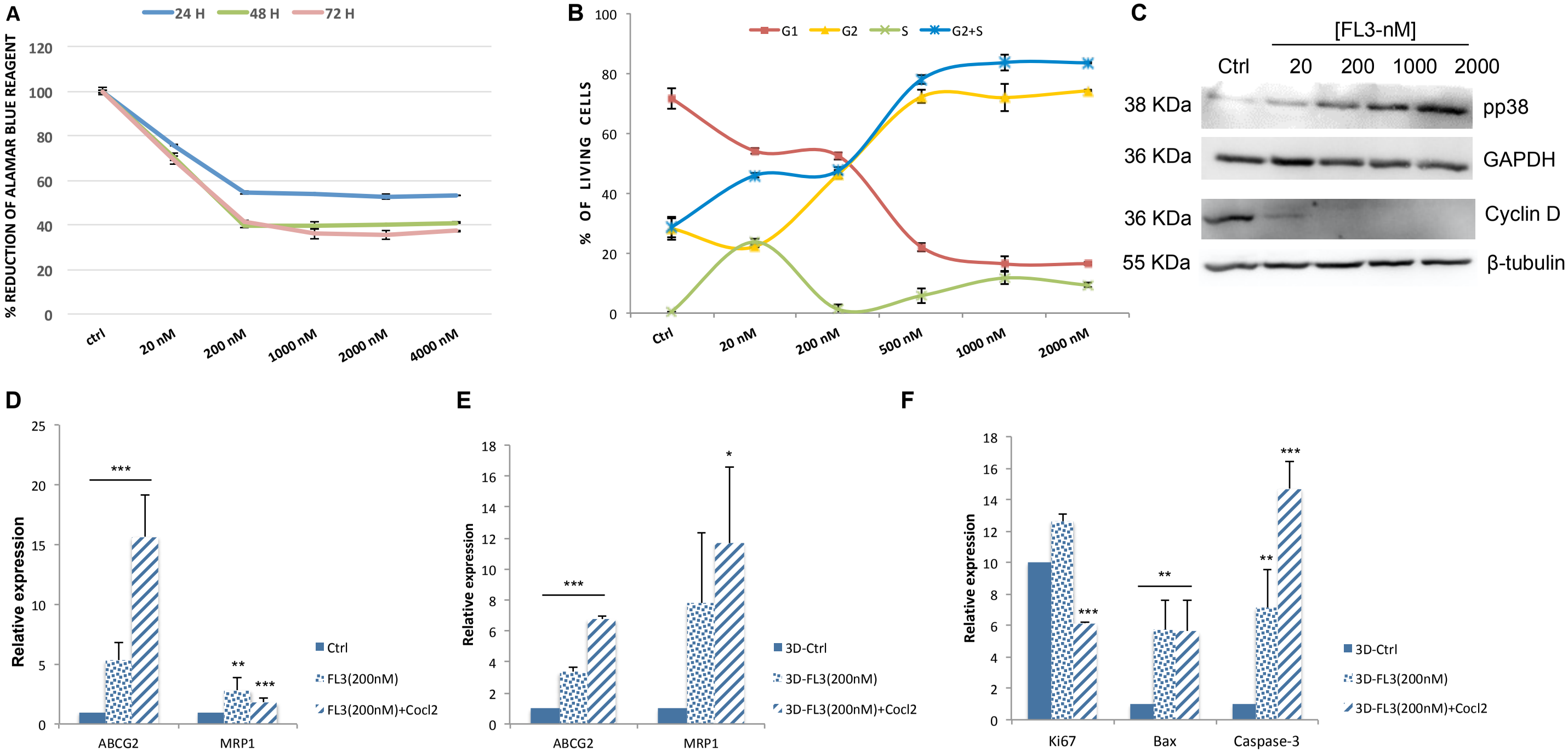
A
24 H
48 H
72 H
% REDUCTION OF ALAMAR BLUE REAGENT
120
100
80
60
40
20
0
ctrl
20 nM
200 nM
1000 nM
2000 nM
4000 nM
B
G1
G2
S
G2+S
% OF LIVING CELLS
100
80
60
40
20
0
Ctrl
20 nM
200 nM
500 nM
1000 nM
2000 nM
C
[FL3-nM]
Ctrl
20
200
1000
2000
38 KDa
pp38
36 KDa
GAPDH
36 KDa
Cyclin D
55 KDa
β-tubulin
D
Relative expression
25
20
15
10
5
0
***
**
***
ABCG2
MRP1
Ctrl
FL3(200nM)
FL3(200nM)+Cocl2
E
Relative expression
18
16
14
12
10
8
6
4
2
0
***
*
ABCG2
MRP1
3D-Ctrl
3D-FL3(200nM)
3D-FL3(200nM)+Cocl2
F
Relative expression
18
16
14
12
10
8
6
4
2
0
***
**
**
***
Ki67
Bax
Caspase-3
3D-Ctrl
3D-FL3(200nM)
3D-FL3(200nM)+Cocl2

Figure 3

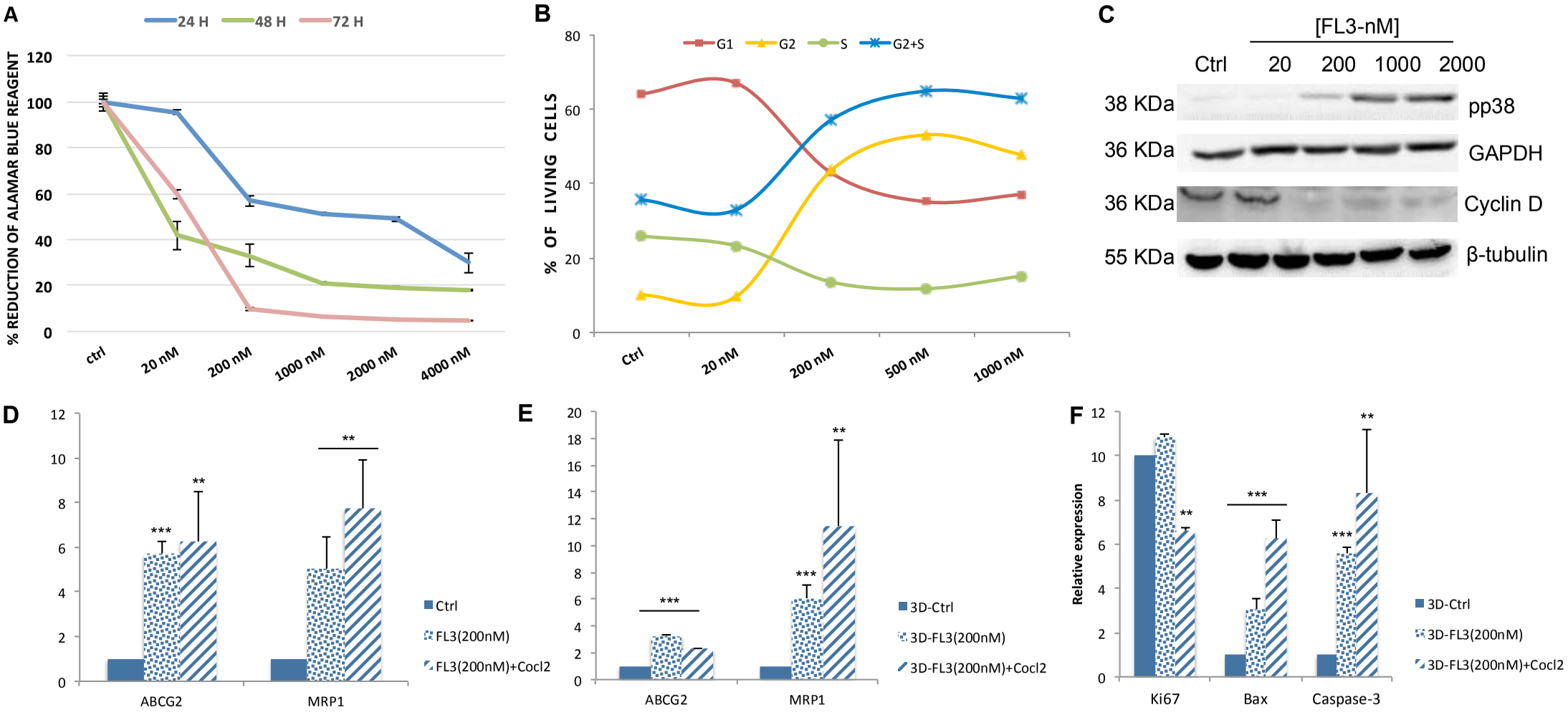
A
24 H
48 H
72 H
% REDUCTION OF ALAMAR BLUE REAGENT
120
100
80
60
40
20
0
ctrl
20 nM
200 nM
1000 nM
2000 nM
4000 nM
B
G1
G2
S
G2+S
% OF LIVING CELLS
80
60
40
20
0
Ctrl
20 nM
200 nM
500 nM
1000 nM
C
[FL3-nM]
Ctrl
20
200
1000
2000
38 KDa
pp38
36 KDa
GAPDH
36 KDa
Cyclin D
55 KDa
β-tubulin
D
12
10
8
6
4
2
0
***
**
**
ABCG2
MRP1
Ctrl
FL3(200nM)
FL3(200nM)+Cocl2
E
20
18
16
14
12
10
8
6
4
2
0
***
***
**
ABCG2
MRP1
3D-Ctrl
3D-FL3(200nM)
3D-FL3(200nM)+Cocl2
F
Relative expression
12
10
8
6
4
2
0
**
***
***
**
Ki67
Bax
Caspase-3
3D-Ctrl
3D-FL3(200nM)
3D-FL3(200nM)+Cocl2

Figure 4

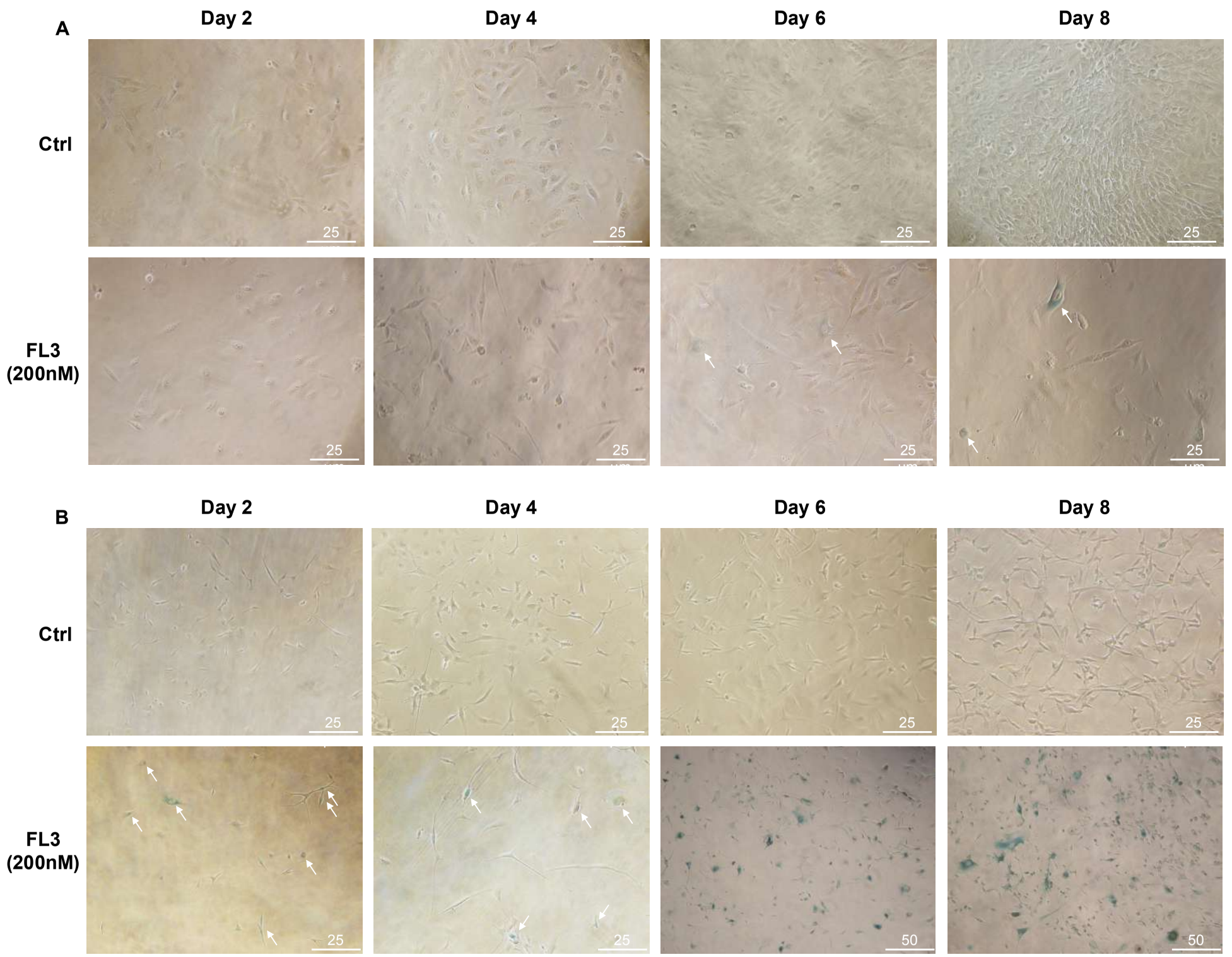
A
Day 2
Day 4
Day 6
Day 8
Ctrl
FL3
(200nM)
25
B
Day 2
Day 4
Day 6
Day 8
Ctrl
FL3
(200nM)
25
50

Figure 5

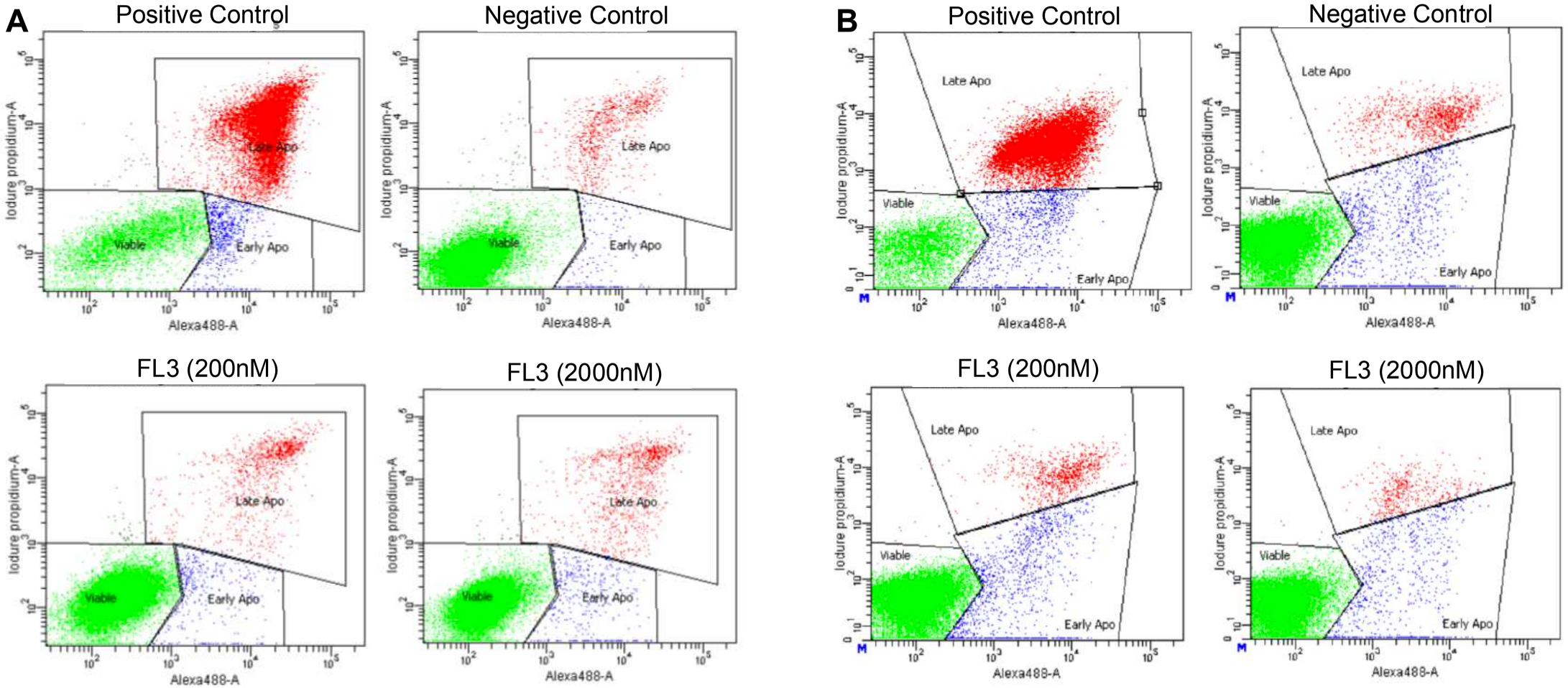
A
Positive Control
Negative Control
FL3 (200nM)
FL3 (2000nM)
B
Positive Control
Negative Control
FL3 (200nM)
FL3 (2000nM)
Late Apo
Early Apo
Viable
Iodure propidium-A
Alexa488-A

Figure S1

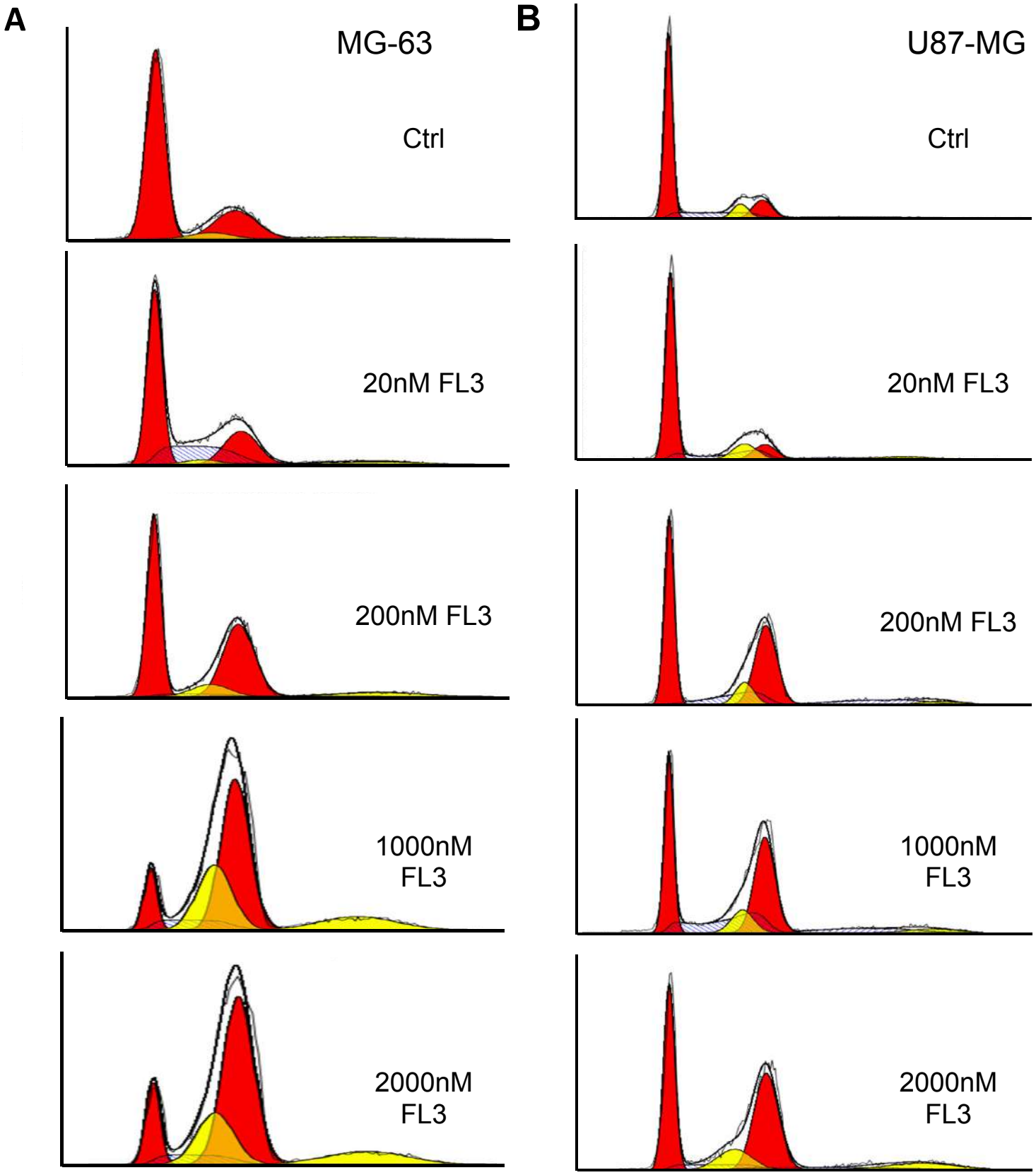
A
MG-63
Ctrl
20nM FL3
200nM FL3
1000nM
FL3
2000nM
FL3
B
U87-MG
Ctrl
20nM FL3
200nM FL3
1000nM
FL3
2000nM
FL3

Figure S2

GENERAL DISCUSSION

Although the great success of pre-clinical studies in drug discovery, 85% of early clinical trials for novel drugs fail, and only 50% pass all the required approvals for clinical use from those that continue to phase III. Between all drug trials, oncology drug trials experience the highest rate of failures. The enhanced advances in tissue engineering and microfabrication techniques, have noticeably improved the ability to raise and maintain cell cultures, tissue fragments and organoids *ex vivo*. 3D cell models, which can simulate the tumor microenvironment, could substantially improve the rationality of the assays, and better predict drugs' success [260].

Indeed, the hanging drop technique used in our experiments to generate the 3D microtissues (MTs), is a well-established cell culture method to generate MTs from cell lines as well as other primary cells [261]. Unlike the other liquid overlay technologies, tissue engineered models and microfluidic devices; the hanging drop model permits the precise control over the initial cell population in each microtissue and allows the addition of new cells, drugs and media at any time to reach a long-term cultivation. Additionally, it enables the generation of high numbers of reproducible microtissues and hence makes it possible to test drugs in a standardized manner. Scaffold free microtissues generated by hanging drop technique are more relevant than those generated from scaffolds because they better mimic the essential functions of the natural ECM and the have many signals interaction properties regulating the communication between cells like the *in vivo* 3D microenvironment [262].

Angiogenesis has received considerable attention during the past few decades hoping that using regulators of angiogenesis may afford biological therapies against disease processes that involve insufficient or vigorous vascularization in their pathogenesis. Moreover, it is difficult to have results in animal studies that are similar to the results of two dimensional (2D) *in vitro* experiments. Thus, there is a growing consensus that three dimensional (3D*) in vitro* angiogenesis assays offer a model which is much closer to the actual environment *in vivo* than the one achieved using 2D cultures [263]. Therefore, 3D system is reproducible and able to mimic several of the major steps in angiogenesis.

It has been shown that during the study of 3D tumor models for *in vitro* evaluation of anticancer drugs, researchers found the anti-proliferative effect of a drug in 3D model is significantly lower than in a 2D monolayer, which was distinct from the 12 to 23-fold differences in their IC50 values. In addition, it was shown that during culturing cells in 3D model, the collagen content was 2-fold greater than that of the cells grown in 2D, recommending greater synthesis of extracellular matrix in the 3D model, which acted as a

barrier to drug diffusion through the tissues and entering the cells to induce its effect [264]. Importantly, 3D cultures will answer many critical questions before having to switch to whole-animal research.

In the first part of our work, we reported the combination of 3D MG-63 cells and 2D HUVECs, in which it was a novel combination since the 3D cultures models recently become the mostly used models in drug screening platforms. This combination allowed the reorganization of endothelial cells and expression of angiogenic factors (VEGF, Collagen IV, and CD31) and the formation of 3D tubules like-structures inside the tumor tissues. In our study, we determined an *in vitro* tumor angiogenesis based on the hypothesis that paracrine signaling is responsible for inducing the angiogenic response without adding pro-angiogenic growth factors when tumor microtissues (MT-MG-63) co-cultured with endothelial cells (HUVECs).

It was reported in a study that direct cell to cell interactions (endothelial cells and tumor cells) is crucial for the formation of vessel but the most important is to find co-culture conditions with specific amounts of each cellular type, allowing this proper interaction during the experiment. One cell type can influence the proliferation of another cell type while they are in direct contact. Thus, the proportion of MG-63 and HUVECs was of 1:5 and this allowed continuous interaction of these two cellular types all over the experiment or the observation time [267].

In contrast to our model, there is no need to manipulate the proportion of each cell type as it can influence the results of these experiments and need less optimization studies. Culturing tumor cells in 3D allowed to minimize the need for a specific ratio for each cell line as well as become more relevant to the *in vivo* vascularization.

Moreover, we noticed in our model of tumor angiogenesis that there was an increase in the expression of VEGF revealed by qPCR and immunofluorescence; hence this angiogenic phenotype is believed to rely on a paracrine manner or due to the co-culturing of tumor cells and endothelial cells. In this case, we can say that our model exploits multicellular interactions in generating *in vitro* angiogenesis without using an exogenous stimulus and provides more relevant and realistic results to the *in vivo* tumor vascularization. Thus, the latter is a positive point in comparison to the other models of *in vitro* vascularization protocols that need pro-angiogenic factors to be added to the cells.

In addition, concerning the HUVECs, it was shown in a study that when co-culturing with DPCs (dental pulp cells) in a microtissue environment, HUVECs not only survived but also, organized into a tubular network. This result might be due to several aspects; it might be caused in part because DPCs secrete proangiogenic factors promoting the survival and function of HUVECs in microtissue spheroids. Furthermore, immunohistochemical analysis of the endothelial cell–specific surface marker CD31 in co-cultured macrotissues (agglomeration of many microtissues) identified a dense network of endothelial cells arranged into vascular structures even after assembling into a macrotissue and culturing over a period of 4 week [268]. These results were consistent with our results showing that when we combined 2D (HUVECs) with 3D (MT MG-63), the endothelial cells arrange themselves into tubule-like structures, and the expression of mRNA VEGF was significantly higher in this combination compared to the HUVECs alone and CD31 positive cells were seen after 7 days of combination.

Consistent with our results that showed a significant expression of the pro-angiogenic factors VEGF, ICAM1, CXCR4, it has been shown that the interaction or the combination of HUVECs with human lung adenocarcinoma CL1-5 cells in a Matrigel increases the expression of survival, migration, and angiogenesis-related genes such as CXCL8, VCAM-1 and ICAM-1 were increased by comparison to HUVECs alone. In addition, there was also upregulation of PI3K/Akt pathway and thus induction of VEGF expression in cancer cells [269].

For future work, our system can include primary cells derived from patients instead of cell lines that we used for both cancer cells (MG-63) and the endothelial cells (HUVECs) in order to have a more physiological relevant system. HUVEC vessels, which are known to be derived from large vessels exhibiting lot-specific variability, were sufficient to produce angiogenic signals in the MT-MG-63. However, it is more likely that organotypic endothelial cells will be needed to recognize therapies that will be clinically efficacious and to accurately design the osteosarcomas microenvironment for mechanistic studies. Furthermore, we used only two cellular types (tumor and vascular endothelial cells), this will deny the true cellular complexity of the tumor microenvironment. There is a need to incorporate another cellular component like stromal cells, perivascular endothelial cells and immune cells into the MTs.

Moreover, there is need for a functional vascularization for nutrients and oxygen transport to the tumor to be more predictive to the *in vivo* model, and the corporation of these factors may

control many metabolic and mechanical factors and functions inside the 3D tumor. So, nowadays, the integration of the microfluidics and its pivotal role in tissue engineering platforms has led to the recapitulation of the tumor microenvironment *in vitro*. Using a microfluidic perfusable platform for *in vitro* vascularization allows a better kinetic examination of cancer progression stages and predicts the efficacy/toxicity of pharmacologically molecules in preclinicals phases [270]. Indeed, combining tissue-engineering principles of vascularization with microfluidic technologies has a great potential to fill the gaps of *in vitro* vascularization as in the case of our model that showed its robustness in *in vitro* assays. The combination of microfluidic with 3D helps in the fabrication of 3D structures with controlled and manipulated spatial relations between different cells, favors the presence of flow-induced signaling and transduction that communicates the different cells compartments together mimicking the *in vivo* tumoral tissues. Moreover, it has the ability to initiate the chemical gradients necessary to reproduce the architecture of the *in vivo* microenvironment, and obtain quantitative measurements on circulating tumor cells, extravasation and micrometastasis. Furthermore, as the angiogenesis is crucial in cancer models and drug discovery platforms and plays an essential role in tumor growth, invasion, progression and metastasis, microfluidics can offer potentials of drug delivery and extraction to control the biochemistry of the tumor microenvironment and quality of vascular network. This could also help delivering of circulating cells and controlling tension and shearing stress during angiogenesis, tumor growth and drug delivery [271].
Moreover, our model would be a promising tool in *in vitro* vascularization platforms and it can be a physiologically vascularized tumor by introducing in addition to cancer cells and endothelial cells, stromal and immune cells, together to achieve a standard vascularized tumor.

In general, it is well known that the monolayer culture of tumor cell lines is simple, convenient and flexible to use in high-throughput drug screening studies and it was used by all the researches since many years in drug screening platforms and research. However, due to the complexity of tumor and its arrangement *in vivo*, the 2D monolayer failed to capture the complication involved of the tumor, such as the variability in chemical and physical parameters that enhance the generation of hypoxic/necrotic areas and cancer cells phenotypic heterogeneity. Thus, the incorporation of 3D culture models was crucial to minimize the limits of 2D-cultures and to be reliably mirror physiologically and architecturally to the solid tumors. Therefore, they gained a great attention in the development of *in vitro* assays leading

to more relevant clinical outcomes as they showed many realistic characteristics such as the resistance to chemotherapy, radiotherapy and apoptosis [272]. The field of drug discovery might benefit from incorporating hypoxia in platform design. Indeed, it is well argued that hypoxia and accumulation of hypoxia-inducible factors (HIFs) in solid tumors have been associated with resistance to treatment and poor prognosis by promoting survival of cancer cells, enhancing the maintenance of cancer stem cells and the cellular adaptation to low oxygen level as well as genetic instability in hypoxic tumors.

It was established that *in vivo* tumor cell proliferation in avascular nodules, micrometastasis or intercapillary regions of solid tumors, might generate gradients of concentration nutrients, oxygen and catabolites [98]. In addition to these factors, cell-to-cell and cell-to-matrix interactions that are found in 3D structures have an impact on protein expression profiles as well as distribution and penetration of soluble factors including drugs which result in poor drug response [272]. Moreover, it was established that the size of microtissues determines the development of hypoxia in a way that if the size of the microtissue grows beyond the threshold for oxygen diffusion, the cells in the core of the microtissue become hypoxic or necrotic and the outer remain proliferating. In this case, hypoxia can manifest itself in the form of gene and protein expression perturbations leading also to variability in drug response.

In this work, we tried to develop an *in vitro* hypoxic model close to *in vivo*. We created a hypoxia model with 3D tumor spheroids (MT) of the two cell lines U87-MG (Glioblastoma) and MG-63 (Osteosarcoma), with or without adding $CoCl_2$, and we showed the effect of this model on the development of hypoxia. Our results showed that when the tumors cells of these cell lines were in 3D structures, they developed hypoxia revealed by the gene expression of HIF1α and its relative genes expressions (VEGF, GLUT1/3). We reported in the first part of our work, that the 3D environment increases the expression of VEGF in comparison to monolayer (2D). These results are consistent with published works, insisting that HIF target genes (GLUT1, VEGF-A) are expressed in the inner hypoxic cell layers [273]. Moreover, the expression of HIF in 3D microtissues and tumors has been related to cell survival through the suppression of proapoptotic signaling, suppression of proliferation, and the regulation of metabolic reprograming [217]. Accordingly, regionalization of microtissues cell layers and the formation of microenvironments as a function of cell distance from the microtissue surface is made by HIF.

Furthermore, to mimic a hypoxic environment *in vitro* and to create a reliable easy-to-operate hypoxic model, a hypoxia mimetic agent ($CoCl_2$) was added on the 3D microtissue to see its effect on hypoxia inducing genes in both cell lines as the final goal was to generate a hypoxic 3D model physiologically relevant to test anticancer drugs. This agent was known as HIF1α stabilizing agent by inhibiting prolyl hydroxylase enzymes then induces hypoxia genes in 2D cell lines. It was shown in many studies that $CoCl_2$ induced the expression of HIF1α in many cancer cell lines at protein levels and hypoxia inducing genes (VEGF, GLUT1, MRP, and others) are markedly increased following treatment with $CoCl_2$ in a dose-dependent manner and that the level of hypoxia coincided with the expression of HIF1α [274];[275].

$CoCl_2$ in combination with 3D tumor structure significantly induced the expression of HIF1α and hypoxia related genes like GLUT1/3, VEGF, and genes implicated in drug resistance genes (ABCG2 and MRP), showing that this combination is more physiologic and more mimicking the *in vivo* model. It was shown in a study that $CoCl_2$ treatment showed similar effects to those of a hypoxia chamber in limiting proliferation of MCF-7 breast cancer cells and OVCAR-3 ovarian cancer. This reduced the expression of cell cycling marker Ki67 in conjunction with upregulation of hypoxia markers HIF1α and GLUT1 and reversible cell cycle arrest in G0/G1 phase, and they showed also that the effect of $CoCl_2$ on these cells were HIF1α dependent. Furthermore, the characters of the dormant state were also found in 3D-cultured MCF-7 cells under true hypoxic conditions (0.1% O_2), suggesting that the 3D $CoCl_2$-based platform can also recapitulate cellular responses to hypoxia. Moreover, MCF-7 cells cultured in 2D and 3D systems under $CoCl_2$ treatment exhibited similar key signaling features of dormant cells [276]. These results corroborated our results that 3D environment can be more physiologically relevant to 2D culture systems and the addition of $CoCl_2$ accelerated the development of hypoxia in these 3D structures, giving a true mirror of the *in vivo* tumor.

Our model is robust and simple due to many factors, the 3D microenvironment (mimicking *in vivo* tumors), the stabilizing potency of $CoCl_2$ in maintaining the half-life of HIF1α and its hypoxia induced genes. In addition, it allows for real-time description of cancer cells that has not been practical with hypoxic chambers due to the extremely short half-life of HIF1α ($t_{1/2}$ < 5 min) upon reoxygenation [277]. It also involves affordable $CoCl_2$ with a simplicity of preparation and handling in contrast to hypoxic chambers that need specific handling procedures and materials. Therefore, they need precise control over gas concentrations in a way that the CO_2 incubator should be equipped with another nitrogen gas flow which controls

the oxygen concentration within the incubator, but the oxygen concentration inside still different than that on the cells and tissues.

So far, our model has two limitations: first, it doesn't reflect all the aspects of *in vivo* tumor microenvironment and it lacks geometrical complexity because there is absence of cellular components such as immune cells, stromal cells, stem cells and endothelial cells. All these factors can play an important role in developing hypoxia and maintaining biological processes involved in cell cycle and apoptosis, which might have a direct consequence on treatment effectiveness. Second, it should be considered that a microtissue is composed of the three layers, the outer proliferating layer, the middle inactive layer, and the inner layer which is the hypoxic/necrotic layer [26], and that the challenging point is the repartition of oxygen, nutrients, and catabolites between these layers. Thus, considering that we performed the RNA extraction of the whole microtissue, we didn't evaluate the repartition of these factors between the different layers that drive the expression of genes involved in different biological processes. This can mask some measures occurring at specific areas of microtissues, which can be detectable at protein level using western blot or immunohistochemistry.

Furthermore, the effect of the established 3D hypoxic model was evaluated using a pharmacologically active molecule called Flavagline FL3, known to have anticancer effects. Many studies were done to evaluate the anticancer mechanism of action of this molecule. It was shown that this molecule induces cell cycle arrest in the G2/M phase in urothelial carcinoma cell of the bladder but no apoptosis was detected in this cell line [239]. Moreover, it inhibited the growth of teratocarcinomal cells by promoting cell cycle arrest at G1 phase followed by apoptosis in human embryonal teratocarcinoma stem cells NT2D1 [236]. These results are consistent with our results showing that FL3 induces cell cycle arrest in our cell lines (MG-63 and U87-MG) with no apoptosis. This apoptosis feature is specific to some cell lines, suggesting that FL3 might have another mechanism of cellular death other than apoptosis like senescence. Cellular senescence is a permanent or irreversible state of cell cycle arrest that occurs when cells experience potentially oncogenic stress. The permanence of the senescence growth arrest imposes the idea that the senescence response changed partly to suppress the development of cancer. Therefore, it is considered irreversible because no known physiological stimuli can enhance senescent cells to reenter the cell cycle. The

possible causes of senescence comport telomere shortening, genomic damage, mitogens and proliferation-associated signals, epigenomic damage, and activation of tumor suppressors [8].

We investigated the presence of senescence by detecting the positive staining of SA-βgal in treated MG-63 and U87-MG cells, and the absence of apoptosis in the latter treated cancer cell lines. Thus, we explored the innovative senescence effect of FL3 on our two cell lines giving insights towards the newly effect of this pharmacologically active molecule in the future treatments of cancer.

CONCLUSIONS AND PERSPECTIVES

The three-dimensional culture systems or spheroids are largely used today in drug screening platforms of cancer to enhance the spatial repartition of cancer cells as well as *in vivo* tumors. In the first study, we created a vascularized model that gives innovative strategy to develop angiogenesis *in vitro* system, taking into account different aspects of tumor microenvironment like the 3D microenvironment and the behavior of cancer cells in terms of angiogenic factors and gene expressions.

In the second study, we insisted on the role of 3D environment in the development of hypoxia, thus creating a $CoCl_2$-based *in vitro* model mimicking hypoxic regulation of cancer resistance and recapitulating different responses to hypoxia. This $CoCl_2$-based model gives advantage over conventional systems in its ability to stably induce and maintain hypoxia of *in vitro*, even in the presence of oxygen.

Taken together, angiogenesis and hypoxia are critical aspects in tumor progression. Angiogenesis is vital for the process of solid tumor formation and progression when the supply of oxygen and nutrients is inadequate in tumor cell. Thus, incorporation of these two factors together can better recapitulate the *in vivo* microenvironment and give insights toward creating a robust drug screening platform.

Our perspectives focus on the combination of these two factors together in a microfluidic system. This microfluidic system includes structural features of 3D tumor constructs, biomechanical and kinematic parameters (branch of classical mechanics that describes the motion of points, objects and systems of groups of objects, without reference to the causes of motion) such as matrix stiffness and anisotropy, cell adhesion and flow conditions. Moreover, we will use cells not only from immortalized cell lines, but also cells derived from patients' biopsies including stromal cells, stem cells, immune cells, and endothelial cells. This 3D microfluidic system will allow to control and study cell culture media and drug transport, waste removal and cytotoxicity and concentration gradients of circulating factors. These parameters altogether help in inventing an in vitro platform mimicking that of in vivo microenvironment suitable for drug screening, and thus open an avenue towards the personalized medicine.

REFERENCES

[1] W. B. Miller and J. S. Torday, “A systematic approach to cancer: evolution beyond selection,” *Clin. Transl. Med.*, vol. 6, no. 1, p. 2, 2017.

[2] D. Hanahan and R. A. Weinberg, “The hallmarks of cancer,” *Cell*, vol. 100, no. 1, pp. 57–70, 2000.

[3] Y. A. Fouad and C. Aanei, “Revisiting the hallmarks of cancer,” *Am. J. Cancer Res.*, vol. 7, no. 5, pp. 1016–1036, 2017.

[4] N. Cheng, A. Chytil, Y. Shyr, A. Joly, and H. L. Moses, “Transforming growth factor-beta signaling-deficient fibroblasts enhance hepatocyte growth factor signaling in mammary carcinoma cells to promote scattering and invasion,” *Mol. Cancer Res. MCR*, vol. 6, no. 10, pp. 1521–1533, 2008.

[5] N. A. Bhowmick, E. G. Neilson, and H. L. Moses, “Stromal fibroblasts in cancer initiation and progression,” *Nature*, vol. 432, no. 7015, pp. 332–337, 2004.

[6] D. Hanahan and R. A. Weinberg, “Hallmarks of cancer: the next generation,” *Cell*, vol. 144, no. 5, pp. 646–674, 2011.

[7] J. Adams and S. Cory, “The Bcl-2 apoptotic switch in cancer development and therapy,” *Oncogene*, vol. 26, no. 9, pp. 1324–1337, 2007.

[8] J. Campisi, “Aging, Cellular Senescence, and Cancer,” *Annu. Rev. Physiol.*, vol. 75, no. 1, pp. 685–705, 2013.

[9] W. P. Janzen, “Screening Technologies for Small Molecule Discovery: The State of the Art,” *Chem. Biol.*, vol. 21, no. 9, pp. 1162–1170, 2014.

[10] J. A. DiMasi, R. W. Hansen, and H. G. Grabowski, “The price of innovation: new estimates of drug development costs,” *J. Health Econ.*, vol. 22, no. 2, pp. 151–185, 2003.

[11] R. Xu and F. M. Richards, “Development of In Vitro Co-Culture Model in Anti-Cancer Drug Development Cascade,” *Comb. Chem. High Throughput Screen.*, vol. 20, no. 5, pp. 451–457, 2017.

[12] S. V. Sharma, D. A. Haber, and J. Settleman, “Cell line-based platforms to evaluate the therapeutic efficacy of candidate anticancer agents,” *Nat. Rev. Cancer*, vol. 10, no. 4, pp. 241–253, 2010.

[13] M. Dhandapani and A. Goldman, “Preclinical Cancer Models and Biomarkers for Drug Development: New Technologies and Emerging Tools,” *J. Mol. Biomark. Diagn.*, vol. 08, no. 05, 2017.

[14] S. Hoelder, P. A. Clarke, and P. Workman, “Discovery of small molecule cancer drugs: Successes, challenges and opportunities,” *Mol. Oncol.*, vol. 6, no. 2, pp. 155–176, 2012.

[15] M. Dean, T. Fojo, and S. Bates, “Tumour stem cells and drug resistance,” *Nat. Rev. Cancer*, vol. 5, no. 4, pp. 275–284, 2005.

[16] K. H. Bleicher, H.-J. Böhm, K. Müller, and A. I. Alanine, “Hit and lead generation: beyond high-throughput screening: A guide to drug discovery,” *Nat. Rev. Drug Discov.*, vol. 2, no. 5, pp. 369–378, 2003.

[17] T. J. Giezen, A. K. Mantel-Teeuwisse, S. M. J. M. Straus, H. Schellekens, H. G. M. Leufkens, and A. C. G. Egberts, “Safety-related regulatory actions for biologicals approved in the United States and the European Union,” *JAMA*, vol. 300, no. 16, pp. 1887–1896, 2008.

[18] B. K. Sekhon, R. H. Roubin, A. Tan, W. K. Chan, and D. M.-Y. Sze, “High-throughput screening platform for anticancer therapeutic drug cytotoxicity,” *Assay Drug Dev. Technol.*, vol. 6, no. 5, pp. 711–721, 2008.

[19] A. Knight, “Systematic reviews of animal experiments demonstrate poor contributions toward human healthcare,” *Rev. Recent Clin. Trials*, vol. 3, no. 2, pp. 89–96, 2008.

[20] S. Festing and R. Wilkinson, “The ethics of animal research. Talking Point on the use of animals in scientific research,” *EMBO Rep.*, vol. 8, no. 6, pp. 526–530, 2007.

[21] C. J. Lovitt, T. B. Shelper, and V. M. Avery, “Advanced cell culture techniques for cancer drug discovery,” *Biology*, vol. 3, no. 2, pp. 345–367, 2014.

[22] R. Edmondson, J. J. Broglie, A. F. Adcock, and L. Yang, “Three-dimensional cell culture systems and their applications in drug discovery and cell-based biosensors,” *Assay Drug Dev. Technol.*, vol. 12, no. 4, pp. 207–218, 2014.

[23] R. A. Westhouse, “Safety assessment considerations and strategies for targeted small molecule cancer therapeutics in drug discovery,” *Toxicol. Pathol.*, vol. 38, no. 1, pp. 165–168, 2010.

[24] C. Dubessy, J. M. Merlin, C. Marchal, and F. Guillemin, “Spheroids in radiobiology and photodynamic therapy,” *Crit. Rev. Oncol. Hematol.*, vol. 36, no. 2–3, pp. 179–192, Dec. 2000.

[25] F. Hirschhaeuser, H. Menne, C. Dittfeld, J. West, W. Mueller-Klieser, and L. A. Kunz-Schughart, “Multicellular tumor spheroids: An underestimated tool is catching up again,” *J. Biotechnol.*, vol. 148, no. 1, pp. 3–15, 2010.

[26] K. Moshksayan *et al.*, “Spheroids-on-a-chip: Recent advances and design considerations in microfluidic platforms for spheroid formation and culture,” *Sens. Actuators B Chem.*, vol. 263, pp. 151–176, 2018.

[27] L. G. Griffith and M. A. Swartz, “Capturing complex 3D tissue physiology in vitro,” *Nat. Rev. Mol. Cell Biol.*, vol. 7, no. 3, pp. 211–224, 2006.

[28] M. E. Katt, A. L. Placone, A. D. Wong, Z. S. Xu, and P. C. Searson, “In Vitro Tumor Models: Advantages, Disadvantages, Variables, and Selecting the Right Platform,” *Front. Bioeng. Biotechnol.*, vol. 4, 2016.

[29] S. Breslin and L. O'Driscoll, "Three-dimensional cell culture: the missing link in drug discovery," *Drug Discov. Today*, vol. 18, no. 5–6, pp. 240–249, 2013.

[30] K. M. A. Yong, Z. Li, S. D. Merajver, and J. Fu, "Tracking the tumor invasion front using long-term fluidic tumoroid culture," *Sci. Rep.*, vol. 7, no. 1, p. 10784, 2017.

[31] S. I. Montanez-Sauri, K. E. Sung, E. Berthier, and D. J. Beebe, "Enabling screening in 3D microenvironments: probing matrix and stromal effects on the morphology and proliferation of T47D breast carcinoma cells," *Integr. Biol. Quant. Biosci. Nano Macro*, vol. 5, no. 3, pp. 631–640, 2013.

[32] G. Su, K. E. Sung, D. J. Beebe, and A. Friedl, "Functional screen of paracrine signals in breast carcinoma fibroblasts," *PloS One*, vol. 7, no. 10, p. e46685, 2012.

[33] A. Khademhosseini, R. Langer, J. Borenstein, and J. P. Vacanti, "Microscale technologies for tissue engineering and biology," *Proc. Natl. Acad. Sci.*, vol. 103, no. 8, pp. 2480–2487, 2006.

[34] T. P. Richardson, M. C. Peters, A. B. Ennett, and D. J. Mooney, "Polymeric system for dual growth factor delivery," *Nat. Biotechnol.*, vol. 19, no. 11, pp. 1029–1034, 2001.

[35] C. Wiegand and U.-C. Hipler, "A superabsorbent polymer-containing wound dressing efficiently sequesters MMPs and inhibits collagenase activity in vitro," *J. Mater. Sci. Mater. Med.*, vol. 24, no. 10, pp. 2473–2478, 2013.

[36] M. P. Schwartz *et al.*, "A Quantitative Comparison of Human HT-1080 Fibrosarcoma Cells and Primary Human Dermal Fibroblasts Identifies a 3D Migration Mechanism with Properties Unique to the Transformed Phenotype," *PLOS ONE*, vol. 8, no. 12, p. e81689, 2013.

[37] B. Döme, M. J. C. Hendrix, S. Paku, J. Tóvári, and J. Tímár, "Alternative Vascularization Mechanisms in Cancer," *Am. J. Pathol.*, vol. 170, no. 1, pp. 1–15, 2007.

[38] D. H. Ausprunk and J. Folkman, "Migration and proliferation of endothelial cells in preformed and newly formed blood vessels during tumor angiogenesis," *Microvasc. Res.*, vol. 14, no. 1, pp. 53–65, 1977.

[39] H. F. Dvorak, L. F. Brown, M. Detmar, and A. M. Dvorak, "Vascular permeability factor/vascular endothelial growth factor, microvascular hyperpermeability, and angiogenesis.," *Am. J. Pathol.*, vol. 146, no. 5, pp. 1029–1039, 1995.

[40] P. Carmeliet, "Angiogenesis in life, disease and medicine," *Nature*, vol. 438, no. 7070, pp. 932–936, 2005.

[41] G. Serini, D. Valdembri, and F. Bussolino, "Integrins and angiogenesis: a sticky business," *Exp. Cell Res.*, vol. 312, no. 5, pp. 651–658, 2006.

[42] C. Schrimpf *et al.*, "Pericyte TIMP3 and ADAMTS1 modulate vascular stability after kidney injury," *J. Am. Soc. Nephrol. JASN*, vol. 23, no. 5, pp. 868–883, 2012.

[43] M. Franco, P. Roswall, E. Cortez, D. Hanahan, and K. Pietras, "Pericytes promote endothelial cell survival through induction of autocrine VEGF-A signaling and Bcl-w expression," *Blood*, vol. 118, no. 10, pp. 2906–2917, 2011.

[44] G. Bergers and D. Hanahan, "Modes of resistance to anti-angiogenic therapy," *Nat. Rev. Cancer*, vol. 8, no. 8, pp. 592–603, 2008.

[45] H. Kurz, P. H. Burri, and V. G. Djonov, "Angiogenesis and vascular remodeling by intussusception: from form to function," *News Physiol. Sci. Int. J. Physiol. Prod. Jointly Int. Union Physiol. Sci. Am. Physiol. Soc.*, vol. 18, pp. 65–70, 2003.

[46] D. J. Brat and E. G. Van Meir, "Glomeruloid Microvascular Proliferation Orchestrated by VPF/VEGF," *Am. J. Pathol.*, vol. 158, no. 3, pp. 789–796, 2001.

[47] O. Straume *et al.*, "Prognostic importance of glomeruloid microvascular proliferation indicates an aggressive angiogenic phenotype in human cancers," *Cancer Res.*, vol. 62, no. 23, pp. 6808–6811, 2002.

[48] T. Asahara and A. Kawamoto, "Endothelial progenitor cells for postnatal vasculogenesis," *Am. J. Physiol. Cell Physiol.*, vol. 287, no. 3, pp. C572-579, 2004.

[49] C. Urbich *et al.*, "Soluble factors released by endothelial progenitor cells promote migration of endothelial cells and cardiac resident progenitor cells," *J. Mol. Cell. Cardiol.*, vol. 39, no. 5, pp. 733–742, 2005.

[50] D. Lyden *et al.*, "Impaired recruitment of bone-marrow-derived endothelial and hematopoietic precursor cells blocks tumor angiogenesis and growth," *Nat. Med.*, vol. 7, no. 11, pp. 1194–1201, 2001.

[51] R. N. Kaplan *et al.*, "VEGFR1-positive haematopoietic bone marrow progenitors initiate the pre-metastatic niche," *Nature*, vol. 438, no. 7069, pp. 820–827, 2005.

[52] A. J. Maniotis *et al.*, "Vascular channel formation by human melanoma cells in vivo and in vitro: vasculogenic mimicry," *Am. J. Pathol.*, vol. 155, no. 3, pp. 739–752, 1999.

[53] A. J. Maniotis *et al.*, "Control of melanoma morphogenesis, endothelial survival, and perfusion by extracellular matrix," *Lab. Investig. J. Tech. Methods Pathol.*, vol. 82, no. 8, pp. 1031–1043, 2002.

[54] M. J. C. Hendrix, E. A. Seftor, A. R. Hess, and R. E. B. Seftor, "Vasculogenic mimicry and tumour-cell plasticity: lessons from melanoma," *Nat. Rev. Cancer*, vol. 3, no. 6, pp. 411–421, 2003.

[55] S. Mukherjee and C. R. Patra, "Therapeutic application of anti-angiogenic nanomaterials in cancers," *Nanoscale*, vol. 8, no. 25, pp. 12444–12470, 2016.

[56] C. Holohan, S. Van Schaeybroeck, D. B. Longley, and P. G. Johnston, "Cancer drug resistance: an evolving paradigm," *Nat. Rev. Cancer*, vol. 13, no. 10, pp. 714–726, 2013.

[57] Y. Huang, S. Goel, D. G. Duda, D. Fukumura, and R. K. Jain, "Vascular normalization as an emerging strategy to enhance cancer immunotherapy," *Cancer Res.*, vol. 73, no. 10, pp. 2943–2948, 2013.

[58] B. Mlecnik *et al.*, "The tumor microenvironment and Immunoscore are critical determinants of dissemination to distant metastasis," *Sci. Transl. Med.*, vol. 8, no. 327, p. 327ra26, 2016.

[59] B. L. Krock, N. Skuli, and M. C. Simon, "Hypoxia-Induced Angiogenesis: Good and Evil," *Genes Cancer*, vol. 2, no. 12, pp. 1117–1133, 2011.

[60] I. Flamme and W. Risau, "Induction of vasculogenesis and hematopoiesis in vitro," *Development*, vol. 116, no. 2, pp. 435–439, 1992.

[61] K. Krah, V. Mironov, W. Risau, and I. Flamme, "Induction of Vasculogenesis in Quail Blastodisc-Derived Embryoid Bodies," *Dev. Biol.*, vol. 164, no. 1, pp. 123–132, J 1994.

[62] R. Wang, R. Clark, and V. L. Bautch, "Embryonic stem cell-derived cystic embryoid bodies form vascular channels: an in vitro model of blood vessel development," *Dev. Camb. Engl.*, vol. 114, no. 2, pp. 303–316, 1992.

[63] H. Sauer, J. Günther, J. Hescheler, and M. Wartenberg, "Thalidomide inhibits angiogenesis in embryoid bodies by the generation of hydroxyl radicals," *Am. J. Pathol.*, vol. 156, no. 1, pp. 151–158, 2000.

[64] B. Vailhé, D. Vittet, and J.-J. Feige, "*In Vitro* Models of Vasculogenesis and Angiogenesis," *Lab. Invest.*, vol. 81, no. 4, pp. 439–452, 2001.

[65] L. Pelletier, J. Regnard, D. Fellmann, and P. Charbord, "An in vitro model for the study of human bone marrow angiogenesis: role of hematopoietic cytokines," *Lab. Investig. J. Tech. Methods Pathol.*, vol. 80, no. 4, pp. 501–511, 2000.

[66] J. Feder, J. C. Marasa, and J. V. Olander, "The formation of capillary-like tubes by calf aortic endothelial cells grown in vitro," *J. Cell. Physiol.*, vol. 116, no. 1, pp. 1–6, 1983.

[67] D. E. Ingber and J. Folkman, "Mechanochemical switching between growth and differentiation during fibroblast growth factor-stimulated angiogenesis in vitro: role of extracellular matrix," *J. Cell Biol.*, vol. 109, no. 1, pp. 317–330, 1989.

[68] B. Vailhé, X. Ronot, P. Tracqui, Y. Usson, and L. Tranqui, "In vitro angiogenesis is modulated by the mechanical properties of fibrin gels and is related to alpha(v)beta3 integrin localization," *In Vitro Cell. Dev. Biol. Anim.*, vol. 33, no. 10, pp. 763–773, 1997.

[69] W. H. Zhu, X. Guo, S. Villaschi, and R. Francesco Nicosia, "Regulation of vascular growth and regression by matrix metalloproteinases in the rat aorta model of

angiogenesis," *Lab. Investig. J. Tech. Methods Pathol.*, vol. 80, no. 4, pp. 545–555, 2000.

[70] R. Montesano, J. D. Vassalli, A. Baird, R. Guillemin, and L. Orci, "Basic fibroblast growth factor induces angiogenesis in vitro," *Proc. Natl. Acad. Sci. U. S. A.*, vol. 83, no. 19, pp. 7297–7301, 1986.

[71] I. Ferrenq, L. Tranqui, B. Vailhé, P. Y. Gumery, and P. Tracqui, "Modelling biological gel contraction by cells: mechanocellular formulation and cell traction force quantification," *Acta Biotheor.*, vol. 45, no. 3–4, pp. 267–293, 1997.

[72] P. G. Phillips, L. M. Birnby, and A. Narendran, "Hypoxia induces capillary network formation in cultured bovine pulmonary microvessel endothelial cells," *Am. J. Physiol.*, vol. 268, no. 5 Pt 1, pp. L789-800, 1995.

[73] G. Helmlinger, M. Endo, N. Ferrara, L. Hlatky, and R. K. Jain, "Formation of endothelial cell networks," *Nature*, vol. 405, no. 6783, pp. 139–141, 2000.

[74] C. A. Staton, M. W. R. Reed, and N. J. Brown, "A critical analysis of current in vitro and in vivo angiogenesis assays," *Int. J. Exp. Pathol.*, vol. 90, no. 3, pp. 195–221, 2009.

[75] H.-H. G. Song, K. M. Park, and S. Gerecht, "Hydrogels to model 3D in vitro microenvironment of tumor vascularization," *Adv. Drug Deliv. Rev.*, vol. 79–80, pp. 19–29, 2014.

[76] K. M. Chrobak, D. R. Potter, and J. Tien, "Formation of perfused, functional microvascular tubes in vitro," *Microvasc. Res.*, vol. 71, no. 3, pp. 185–196, 2006.

[77] V. Mironov, R. P. Visconti, V. Kasyanov, G. Forgacs, C. J. Drake, and R. R. Markwald, "Organ printing: tissue spheroids as building blocks," *Biomaterials*, vol. 30, no. 12, pp. 2164–2174, 2009.

[78] A. Skardal, J. Zhang, and G. D. Prestwich, "Bioprinting vessel-like constructs using hyaluronan hydrogels crosslinked with tetrahedral polyethylene glycol tetracrylates," *Biomaterials*, vol. 31, no. 24, pp. 6173–6181, 2010.

[79] R. P. Visconti, V. Kasyanov, C. Gentile, J. Zhang, R. R. Markwald, and V. Mironov, "Towards organ printing: engineering an intra-organ branched vascular tree," *Expert Opin. Biol. Ther.*, vol. 10, no. 3, pp. 409–420, 2010.

[80] L. Wang, Z.-L. Zhang, J. Wdzieczak-Bakala, D.-W. Pang, J. Liu, and Y. Chen, "Patterning cells and shear flow conditions: convenient observation of endothelial cell remoulding, enhanced production of angiogenesis factors and drug response," *Lab. Chip*, vol. 11, no. 24, pp. 4235–4240, 2011.

[81] E. W. K. Young, M. W. L. Watson, S. Srigunapalan, A. R. Wheeler, and C. A. Simmons, "Technique for real-time measurements of endothelial permeability in a microfluidic membrane chip using laser-induced fluorescence detection," *Anal. Chem.*, vol. 82, no. 3, pp. 808–816, 2010.

[82] Z. Xu *et al.*, "Design and Construction of a Multi-Organ Microfluidic Chip Mimicking the in vivo Microenvironment of Lung Cancer Metastasis," *ACS Appl. Mater. Interfaces*, vol. 8, no. 39, pp. 25840–25847, 2016.

[83] B. M. Baker, B. Trappmann, S. C. Stapleton, E. Toro, and C. S. Chen, "Microfluidics embedded within extracellular matrix to define vascular architectures and pattern diffusive gradients," *Lab. Chip*, vol. 13, no. 16, pp. 3246–3252, 2013.

[84] D.-H. T. Nguyen *et al.*, "Biomimetic model to reconstitute angiogenic sprouting morphogenesis in vitro," *Proc. Natl. Acad. Sci. U. S. A.*, vol. 110, no. 17, pp. 6712–6717, 2013.

[85] A. D. van der Meer, V. V. Orlova, P. ten Dijke, A. van den Berg, and C. L. Mummery, "Three-dimensional co-cultures of human endothelial cells and embryonic stem cell-derived pericytes inside a microfluidic device," *Lab. Chip*, vol. 13, no. 18, pp. 3562–3568, 2013.

[86] X.-Y. Wang *et al.*, "An artificial blood vessel implanted three-dimensional microsystem for modeling transvascular migration of tumor cells," *Lab. Chip*, vol. 15, no. 4, pp. 1178–1187, 2015.

[87] H. Lee, W. Park, H. Ryu, and N. L. Jeon, "A microfluidic platform for quantitative analysis of cancer angiogenesis and intravasation," *Biomicrofluidics*, vol. 8, no. 5, p. 054102, 2014.

[88] Z. Z. Wang *et al.*, "Endothelial cells derived from human embryonic stem cells form durable blood vessels in vivo," *Nat. Biotechnol.*, vol. 25, no. 3, pp. 317–318, 2007.

[89] S. Kim, W. Kim, S. Lim, and J. S. Jeon, "Vasculature-On-A-Chip for In Vitro Disease Models," *Bioeng. Basel Switz.*, vol. 4, no. 1, 2017.

[90] X. Wang, D. T. T. Phan, A. Sobrino, S. C. George, C. C. W. Hughes, and A. P. Lee, "Engineering anastomosis between living capillary networks and endothelial cell-lined microfluidic channels," *Lab. Chip*, vol. 16, no. 2, pp. 282–290, 2016.

[91] S. Kim, M. Chung, J. Ahn, S. Lee, and N. L. Jeon, "Interstitial flow regulates the angiogenic response and phenotype of endothelial cells in a 3D culture model," *Lab. Chip*, vol. 16, no. 21, pp. 4189–4199, 2016.

[92] J. S. Jeon *et al.*, "Generation of 3D functional microvascular networks with human mesenchymal stem cells in microfluidic systems," *Integr. Biol. Quant. Biosci. Nano Macro*, vol. 6, no. 5, pp. 555–563, 2014.

[93] A. L. Harris, "Hypoxia — a key regulatory factor in tumour growth," *Nat. Rev. Cancer*, vol. 2, no. 1, pp. 38–47, 2002.

[94] G. L. Semenza, "Defining the Role of Hypoxia-Inducible Factor 1 in Cancer Biology and Therapeutics," *Oncogene*, vol. 29, no. 5, pp. 625–634, 2010.

[95] A. L. Harris, “Hypoxia--a key regulatory factor in tumour growth,” *Nat. Rev. Cancer*, vol. 2, no. 1, pp. 38–47, 2002.

[96] K. L. Eales, K. E. R. Hollinshead, and D. A. Tennant, “Hypoxia and metabolic adaptation of cancer cells,” *Oncogenesis*, vol. 5, no. 1, p. e190, 2016.

[97] S. Kizaka-Kondoh, M. Inoue, H. Harada, and M. Hiraoka, “Tumor hypoxia: a target for selective cancer therapy,” *Cancer Sci.*, vol. 94, no. 12, pp. 1021–1028, 2003.

[98] M. W. Dewhirst, Y. Cao, and B. Moeller, “Cycling hypoxia and free radicals regulate angiogenesis and radiotherapy response,” *Nat. Rev. Cancer*, vol. 8, no. 6, pp. 425–437, 2008.

[99] P. Carmeliet and R. K. Jain, “Angiogenesis in cancer and other diseases,” *Nature*, vol. 407, no. 6801, pp. 249–257, 2000.

[100] J. L. Tatum *et al.*, “Hypoxia: importance in tumor biology, noninvasive measurement by imaging, and value of its measurement in the management of cancer therapy,” *Int. J. Radiat. Biol.*, vol. 82, no. 10, pp. 699–757, 2006.

[101] D. M. Brizel *et al.*, “Tumor oxygenation predicts for the likelihood of distant metastases in human soft tissue sarcoma,” *Cancer Res.*, vol. 56, no. 5, pp. 941–943, 1996.

[102] S. W. Tuttle *et al.*, “Detection of reactive oxygen species via endogenous oxidative pentose phosphate cycle activity in response to oxygen concentration: implications for the mechanism of HIF-1alpha stabilization under moderate hypoxia,” *J. Biol. Chem.*, vol. 282, no. 51, pp. 36790–36796, 2007.

[103] G. L. Semenza, “Oxygen-dependent regulation of mitochondrial respiration by hypoxia-inducible factor 1,” *Biochem. J.*, vol. 405, no. 1, pp. 1–9, 2007.

[104] L. E. Huang, R. S. Bindra, P. M. Glazer, and A. L. Harris, “Hypoxia-induced genetic instability--a calculated mechanism underlying tumor progression,” *J. Mol. Med. Berl. Ger.*, vol. 85, no. 2, pp. 139–148, 2007.

[105] N. J. Beasley *et al.*, “Carbonic anhydrase IX, an endogenous hypoxia marker, expression in head and neck squamous cell carcinoma and its relationship to hypoxia, necrosis, and microvessel density,” *Cancer Res.*, vol. 61, no. 13, pp. 5262–5267, 2001.

[106] R. G. Bristow and R. P. Hill, “Hypoxia and metabolism. Hypoxia, DNA repair and genetic instability,” *Nat. Rev. Cancer*, vol. 8, no. 3, pp. 180–192, 2008.

[107] R. S. Kerbel, “Antiangiogenic therapy: a universal chemosensitization strategy for cancer?,” *Science*, vol. 312, no. 5777, pp. 1171–1175, 2006.

[108] P. Khosravi Shahi, “Angiogénesis y neoplasias,” *An. Med. Interna*, vol. 23, no. 8, pp. 355–356, 2006.

[109] C. W. Pugh and P. J. Ratcliffe, “Regulation of angiogenesis by hypoxia: role of the HIF system,” *Nat. Med.*, vol. 9, no. 6, pp. 677–684, 2003.

[110] A. M. Shannon, D. J. Bouchier-Hayes, C. M. Condron, and D. Toomey, “Tumour hypoxia, chemotherapeutic resistance and hypoxia-related therapies,” *Cancer Treat. Rev.*, vol. 29, no. 4, pp. 297–307, 2003.

[111] T. Danielsen, M. Hvidsten, T. Stokke, K. Solberg, and E. K. Rofstad, “Hypoxia induces p53 accumulation in the S-phase and accumulation of hypophosphorylated retinoblastoma protein in all cell cycle phases of human melanoma cells.,” *Br. J. Cancer*, vol. 78, no. 12, pp. 1547–1558, 1998.

[112] A. M. Arsham, J. J. Howell, and M. C. Simon, “A novel hypoxia-inducible factor-independent hypoxic response regulating mammalian target of rapamycin and its targets,” *J. Biol. Chem.*, vol. 278, no. 32, pp. 29655–29660, 2003.

[113] J. Pouysségur, F. Dayan, and N. M. Mazure, “Hypoxia signalling in cancer and approaches to enforce tumour regression,” *Nature*, vol. 441, no. 7092, pp. 437–443, 2006.

[114] H. Zhang *et al.*, “Mitochondrial autophagy is an HIF-1-dependent adaptive metabolic response to hypoxia,” *J. Biol. Chem.*, vol. 283, no. 16, pp. 10892–10903, 2008.

[115] G. L. Semenza, “Hypoxia-inducible factors: mediators of cancer progression and targets for cancer therapy,” *Trends Pharmacol. Sci.*, vol. 33, no. 4, pp. 207–214, 2012.

[116] C. V. Dang, M. Hamaker, P. Sun, A. Le, and P. Gao, “Therapeutic targeting of cancer cell metabolism,” *J. Mol. Med. Berl. Ger.*, vol. 89, no. 3, pp. 205–212, 2011.

[117] M. W. Dewhirst, “Relationships between Cycling Hypoxia, HIF-1, Angiogenesis and Oxidative Stress,” *Radiat. Res.*, vol. 172, no. 6, pp. 653–665, 2009.

[118] A. C. Epstein *et al.*, “C. elegans EGL-9 and mammalian homologs define a family of dioxygenases that regulate HIF by prolyl hydroxylation,” *Cell*, vol. 107, no. 1, pp. 43–54, 2001.

[119] E. Berra, A. Ginouvès, and J. Pouysségur, “The hypoxia-inducible-factor hydroxylases bring fresh air into hypoxia signalling,” *EMBO Rep.*, vol. 7, no. 1, pp. 41–45, 2006.

[120] E. Berra, D. Roux, D. E. Richard, and J. Pouysségur, “Hypoxia-inducible factor-1 alpha (HIF-1 alpha) escapes O(2)-driven proteasomal degradation irrespective of its subcellular localization: nucleus or cytoplasm,” *EMBO Rep.*, vol. 2, no. 7, pp. 615–620, 2001.

[121] F. Dayan, D. Roux, M. C. Brahimi-Horn, J. Pouyssegur, and N. M. Mazure, “The oxygen sensor factor-inhibiting hypoxia-inducible factor-1 controls expression of distinct genes through the bifunctional transcriptional character of hypoxia-inducible factor-1alpha,” *Cancer Res.*, vol. 66, no. 7, pp. 3688–3698, 2006.

[122] H. Tian, S. L. McKnight, and D. W. Russell, “Endothelial PAS domain protein 1 (EPAS1), a transcription factor selectively expressed in endothelial cells,” *Genes Dev.*, vol. 11, no. 1, pp. 72–82, 1997.

[123] M. S. Wiesener *et al.*, “Induction of Endothelial PAS Domain Protein-1 by Hypoxia: Characterization and Comparison With Hypoxia-Inducible Factor-1α,” *Blood*, vol. 92, no. 7, pp. 2260–2268, 1998.

[124] Y. Makino *et al.*, “Inhibitory PAS domain protein is a negative regulator of hypoxia-inducible gene expression,” *Nature*, vol. 414, no. 6863, pp. 550–554, 2001.

[125] J. Schödel, S. Oikonomopoulos, J. Ragoussis, C. W. Pugh, P. J. Ratcliffe, and D. R. Mole, “High-resolution genome-wide mapping of HIF-binding sites by ChIP-seq,” *Blood*, vol. 117, no. 23, pp. e207-217, 2011.

[126] D. Liao and R. S. Johnson, “Hypoxia: a key regulator of angiogenesis in cancer,” *Cancer Metastasis Rev.*, vol. 26, no. 2, pp. 281–290, Jun. 2007.

[127] T. Shah *et al.*, “HIF isoforms have divergent effects on invasion, metastasis, metabolism and formation of lipid droplets,” *Oncotarget*, vol. 6, no. 29, pp. 28104–28119, 2015.

[128] M. S. Wiesener *et al.*, “Widespread hypoxia-inducible expression of HIF-2alpha in distinct cell populations of different organs,” *FASEB J. Off. Publ. Fed. Am. Soc. Exp. Biol.*, vol. 17, no. 2, pp. 271–273, 2003.

[129] C. J. Yeom, L. Zeng, Y. Zhu, M. Hiraoka, and H. Harada, “Strategies To Assess Hypoxic/HIF-1-Active Cancer Cells for the Development of Innovative Radiation Therapy,” *Cancers*, vol. 3, no. 3, pp. 3610–3631, 2011.

[130] G. L. Semenza, “HIF-1 and human disease: one highly involved factor,” *Genes Dev.*, vol. 14, no. 16, pp. 1983–1991, 2000.

[131] G. Powis and L. Kirkpatrick, “Hypoxia inducible factor-1alpha as a cancer drug target,” *Mol. Cancer Ther.*, vol. 3, no. 5, pp. 647–654, 2004.

[132] G. L. Semenza, “HIF-1 and mechanisms of hypoxia sensing,” *Curr. Opin. Cell Biol.*, vol. 13, no. 2, pp. 167–171, 2001.

[133] M. V. Liberti and J. W. Locasale, “The Warburg Effect: How Does it Benefit Cancer Cells?,” *Trends Biochem. Sci.*, vol. 41, no. 3, pp. 211–218, 2016.

[134] N. C. Denko, “Hypoxia, HIF1 and glucose metabolism in the solid tumour,” *Nat. Rev. Cancer*, vol. 8, no. 9, pp. 705–713, 2008.

[135] P. Carmeliet and R. K. Jain, “Molecular mechanisms and clinical applications of angiogenesis,” *Nature*, vol. 473, no. 7347, pp. 298–307, 2011.

[136] K. R. Laderoute *et al.*, “The Response of c-Jun/AP-1 to Chronic Hypoxia Is Hypoxia-Inducible Factor 1α Dependent,” *Mol. Cell. Biol.*, vol. 22, no. 8, pp. 2515–2523, 2002.

[137] A. Asthana and W. S. Kisaalita, “Microtissue size and hypoxia in HTS with 3D cultures,” *Drug Discov. Today*, vol. 17, no. 15, pp. 810–817, 2012.

[138] P. J. Kallio, I. Pongratz, K. Gradin, J. McGuire, and L. Poellinger, “Activation of hypoxia-inducible factor 1alpha: posttranscriptional regulation and conformational change by recruitment of the Arnt transcription factor,” *Proc. Natl. Acad. Sci. U. S. A.*, vol. 94, no. 11, pp. 5667–5672, 1997.

[139] S. Salceda and J. Caro, “Hypoxia-inducible factor 1alpha (HIF-1alpha) protein is rapidly degraded by the ubiquitin-proteasome system under normoxic conditions. Its stabilization by hypoxia depends on redox-induced changes,” *J. Biol. Chem.*, vol. 272, no. 36, pp. 22642–22647, 1997.

[140] S. Koyasu, M. Kobayashi, Y. Goto, M. Hiraoka, and H. Harada, “Regulatory mechanisms of hypoxia-inducible factor 1 activity: Two decades of knowledge,” *Cancer Sci.*, vol. 109, no. 3, pp. 560–571, 2018.

[141] B. H. Jiang, G. Jiang, J. Z. Zheng, Z. Lu, T. Hunter, and P. K. Vogt, “Phosphatidylinositol 3-kinase signaling controls levels of hypoxia-inducible factor 1,” *Cell Growth Differ. Mol. Biol. J. Am. Assoc. Cancer Res.*, vol. 12, no. 7, pp. 363–369, 2001.

[142] G. Semenza, “Signal transduction to hypoxia-inducible factor 1,” *Biochem. Pharmacol.*, vol. 64, no. 5–6, pp. 993–998, 2002.

[143] P. W. Conrad, T. L. Freeman, D. Beitner-Johnson, and D. E. Millhorn, “EPAS1 trans-Activation during Hypoxia Requires p42/p44 MAPK,” *J. Biol. Chem.*, vol. 274, no. 47, pp. 33709–33713, 1999.

[144] A. C. Gingras, B. Raught, and N. Sonenberg, “Regulation of translation initiation by FRAP/mTOR,” *Genes Dev.*, vol. 15, no. 7, pp. 807–826, 2001.

[145] N. Sang, D. P. Stiehl, J. Bohensky, I. Leshchinsky, V. Srinivas, and J. Caro, “MAPK signaling up-regulates the activity of hypoxia-inducible factors by its effects on p300,” *J. Biol. Chem.*, vol. 278, no. 16, pp. 14013–14019, 2003.

[146] J.-W. Lee, S.-H. Bae, J.-W. Jeong, S.-H. Kim, and K.-W. Kim, “Hypoxia-inducible factor (HIF-1)α: its protein stability and biological functions,” *Exp. Mol. Med.*, vol. 36, no. 1, pp. 1–12, 2004.

[147] D. Shi and W. Gu, “Dual Roles of MDM2 in the Regulation of p53,” *Genes Cancer*, vol. 3, no. 3–4, pp. 240–248, 2012.

[148] R. Ravi *et al.*, “Regulation of tumor angiogenesis by p53-induced degradation of hypoxia-inducible factor 1α,” *Genes Dev.*, vol. 14, no. 1, pp. 34–44, 2000.

[149] K. Gradin *et al.*, “Functional interference between hypoxia and dioxin signal transduction pathways: competition for recruitment of the Arnt transcription factor,” *Mol. Cell. Biol.*, vol. 16, no. 10, pp. 5221–5231, 1996.

[150] J. S. Isaacs, Y.-J. Jung, E. G. Mimnaugh, A. Martinez, F. Cuttitta, and L. M. Neckers, "Hsp90 regulates a von Hippel Lindau-independent hypoxia-inducible factor-1 alpha-degradative pathway," *J. Biol. Chem.*, vol. 277, no. 33, pp. 29936–29944, 2002.

[151] G.-Z. Qiu, M.-Z. Jin, J.-X. Dai, W. Sun, J.-H. Feng, and W.-L. Jin, "Reprogramming of the Tumor in the Hypoxic Niche: The Emerging Concept and Associated Therapeutic Strategies," *Trends Pharmacol. Sci.*, vol. 38, no. 8, pp. 669–686,. 2017.

[152] N. Denko, C. Schindler, A. Koong, K. Laderoute, C. Green, and A. Giaccia, "Epigenetic regulation of gene expression in cervical cancer cells by the tumor microenvironment," *Clin. Cancer Res. Off. J. Am. Assoc. Cancer Res.*, vol. 6, no. 2, pp. 480–487, 2000.

[153] A. Lal *et al.*, "Transcriptional Response to Hypoxia in Human Tumors," *JNCI J. Natl. Cancer Inst.*, vol. 93, no. 17, pp. 1337–1343, 2001.

[154] E. Berra *et al.*, "Signaling angiogenesis via p42/p44 MAP kinase and hypoxia.," *Biochem. Pharmacol.*, vol. 60, no. 8, pp. 1171–1178, 2000.

[155] E. Y. Chen, N. M. Mazure, J. A. Cooper, and A. J. Giaccia, "Hypoxia activates a platelet-derived growth factor receptor/phosphatidylinositol 3-kinase/Akt pathway that results in glycogen synthase kinase-3 inactivation," *Cancer Res.*, vol. 61, no. 6, pp. 2429–2433,. 2001.

[156] L. A. Palmer, G. L. Semenza, M. H. Stoler, and R. A. Johns, "Hypoxia induces type II NOS gene expression in pulmonary artery endothelial cells via HIF-1," *Am. J. Physiol.*, vol. 274, no. 2 Pt 1, pp. L212-219, 1998.

[157] A. L. Kung, S. Wang, J. M. Klco, W. G. Kaelin, and D. M. Livingston, "Suppression of tumor growth through disruption of hypoxia-inducible transcription," *Nat. Med.*, vol. 6, no. 12, pp. 1335–1340, 2000.

[158] C. V. Dang and G. L. Semenza, "Oncogenic alterations of metabolism," *Trends Biochem. Sci.*, vol. 24, no. 2, pp. 68–72, 1999.

[159] C. Chen, N. Pore, A. Behrooz, F. Ismail-Beigi, and A. Maity, "Regulation of glut1 mRNA by hypoxia-inducible factor-1. Interaction between H-ras and hypoxia," *J. Biol. Chem.*, vol. 276, no. 12, pp. 9519–9525, 2001.

[160] P. H. Maxwell *et al.*, "Hypoxia-inducible factor-1 modulates gene expression in solid tumors and influences both angiogenesis and tumor growth," *Proc. Natl. Acad. Sci. U. S. A.*, vol. 94, no. 15, pp. 8104–8109, 1997.

[161] M. Mueckler and B. Thorens, "The SLC2 (GLUT) Family of Membrane Transporters," *Mol. Aspects Med.*, vol. 34, no. 0, pp. 121–138, 2013.

[162] G. K. Brown, "Glucose transporters: Structure, function and consequences of deficiency," *J. Inherit. Metab. Dis.*, vol. 23, no. 3, pp. 237–246, 2000.

[163] I. H. Ozbudak, S. Karaveli, T. Simsek, G. Erdogan, and E. Pestereli, “Neoangiogenesis and expression of hypoxia-inducible factor 1alpha, vascular endothelial growth factor, and glucose transporter-1 in endometrioid type endometrium adenocarcinomas,” *Gynecol. Oncol.*, vol. 108, no. 3, pp. 603–608, 2008.

[164] S. P. Mathupala, A. Rempel, and P. L. Pedersen, “Glucose catabolism in cancer cells: identification and characterization of a marked activation response of the type II hexokinase gene to hypoxic conditions,” *J. Biol. Chem.*, vol. 276, no. 46, pp. 43407–43412, 2001.

[165] N. V. Iyer *et al.*, “Cellular and developmental control of O2 homeostasis by hypoxia-inducible factor 1 alpha,” *Genes Dev.*, vol. 12, no. 2, pp. 149–162, 1998.

[166] T. N. Seagroves *et al.*, “Transcription factor HIF-1 is a necessary mediator of the pasteur effect in mammalian cells,” *Mol. Cell. Biol.*, vol. 21, no. 10, pp. 3436–3444, 2001.

[167] A. Coquelle, F. Toledo, S. Stern, A. Bieth, and M. Debatisse, “A new role for hypoxia in tumor progression: induction of fragile site triggering genomic rearrangements and formation of complex DMs and HSRs,” *Mol. Cell*, vol. 2, no. 2, pp. 259–265, 1998.

[168] A. E. Greijer and E. van der Wall, “The role of hypoxia inducible factor 1 (HIF-1) in hypoxia induced apoptosis,” *J. Clin. Pathol.*, vol. 57, no. 10, pp. 1009–1014, 2004.

[169] C. C. Wykoff *et al.*, “Hypoxia-inducible expression of tumor-associated carbonic anhydrases,” *Cancer Res.*, vol. 60, no. 24, pp. 7075–7083, 2000.

[170] J. A. Loncaster *et al.*, “Carbonic anhydrase (CA IX) expression, a potential new intrinsic marker of hypoxia: correlations with tumor oxygen measurements and prognosis in locally advanced carcinoma of the cervix,” *Cancer Res.*, vol. 61, no. 17, pp. 6394–6399, 2001.

[171] S.-C. Lin, W.-L. Liao, J.-C. Lee, and S.-J. Tsai, “Hypoxia-regulated gene network in drug resistance and cancer progression,” *Exp. Biol. Med.*, vol. 239, no. 7, pp. 779–792, 2014.

[172] C. Wigerup, S. Påhlman, and D. Bexell, “Therapeutic targeting of hypoxia and hypoxia-inducible factors in cancer,” *Pharmacol. Ther.*, vol. 164, pp. 152–169, 2016.

[173] J. Folkman, “Angiogenesis in cancer, vascular, rheumatoid and other disease,” *Nat. Med.*, vol. 1, no. 1, pp. 27–31, Jan. 1995.

[174] L. S. Gutierrez, M. Suckow, J. Lawler, V. A. Ploplis, and F. J. Castellino, “Thrombospondin 1—a regulator of adenoma growth and carcinoma progression in the APC Min/+ mouse model,” *Carcinogenesis*, vol. 24, no. 2, pp. 199–207, 2003.

[175] M. A. Selak *et al.*, “Succinate links TCA cycle dysfunction to oncogenesis by inhibiting HIF-alpha prolyl hydroxylase,” *Cancer Cell*, vol. 7, no. 1, pp. 77–85, 2005.

[176] H. Kikuchi, M. S. Pino, M. Zeng, S. Shirasawa, and D. C. Chung, "Oncogenic KRAS and BRAF Differentially Regulate Hypoxia-Inducible Factor-1α and -2α in Colon Cancer," *Cancer Res.*, vol. 69, no. 21, pp. 8499–8506, 2009.

[177] J. A. Bertout, S. A. Patel, and M. C. Simon, "The impact of O2 availability on human cancer," *Nat. Rev. Cancer*, vol. 8, no. 12, pp. 967–975, 2008.

[178] null Höckel, null Schlenger, null Mitze, null Schäffer, and null Vaupel, "Hypoxia and Radiation Response in Human Tumors," *Semin. Radiat. Oncol.*, vol. 6, no. 1, pp. 3–9, 1996.

[179] K. M. Comerford, T. J. Wallace, J. Karhausen, N. A. Louis, M. C. Montalto, and S. P. Colgan, "Hypoxia-inducible factor-1-dependent regulation of the multidrug resistance (MDR1) gene," *Cancer Res.*, vol. 62, no. 12, pp. 3387–3394, 2002.

[180] J. Gu *et al.*, "Hypoxia-induced up-regulation of angiopoietin-2 in colorectal cancer," *Oncol. Rep.*, vol. 15, no. 4, pp. 779–783, 2006.

[181] L. Zhang *et al.*, "Tumor-derived vascular endothelial growth factor up-regulates angiopoietin-2 in host endothelium and destabilizes host vasculature, supporting angiogenesis in ovarian cancer," *Cancer Res.*, vol. 63, no. 12, pp. 3403–3412, 2003.

[182] C. Suri *et al.*, "Requisite role of angiopoietin-1, a ligand for the TIE2 receptor, during embryonic angiogenesis," *Cell*, vol. 87, no. 7, pp. 1171–1180, 1996.

[183] N. Skuli *et al.*, "Endothelial deletion of hypoxia-inducible factor-2alpha (HIF-2alpha) alters vascular function and tumor angiogenesis," *Blood*, vol. 114, no. 2, pp. 469–477, 2009.

[184] P. Fasanaro *et al.*, "MicroRNA-210 modulates endothelial cell response to hypoxia and inhibits the receptor tyrosine kinase ligand Ephrin-A3," *J. Biol. Chem.*, vol. 283, no. 23, pp. 15878–15883, 2008.

[185] N. Tang *et al.*, "Loss of HIF-1alpha in endothelial cells disrupts a hypoxia-driven VEGF autocrine loop necessary for tumorigenesis," *Cancer Cell*, vol. 6, no. 5, pp. 485–495, 2004.

[186] D. J. Ceradini *et al.*, "Progenitor cell trafficking is regulated by hypoxic gradients through HIF-1 induction of SDF-1," *Nat. Med.*, vol. 10, no. 8, pp. 858–864, 2004.

[187] M. Kioi, H. Vogel, G. Schultz, R. M. Hoffman, G. R. Harsh, and J. M. Brown, "Inhibition of vasculogenesis, but not angiogenesis, prevents the recurrence of glioblastoma after irradiation in mice," *J. Clin. Invest.*, vol. 120, no. 3, pp. 694–705, 2010.

[188] T. Kawanaka, A. Kubo, H. Ikushima, T. Sano, Y. Takegawa, and H. Nishitani, "Prognostic significance of HIF-2alpha expression on tumor infiltrating macrophages in patients with uterine cervical cancer undergoing radiotherapy," *J. Med. Investig. JMI*, vol. 55, no. 1–2, pp. 78–86, 2008.

[189] H. Z. Imtiyaz *et al.*, "Hypoxia-inducible factor 2alpha regulates macrophage function in mouse models of acute and tumor inflammation," *J. Clin. Invest.*, vol. 120, no. 8, pp. 2699–2714, 2010.

[190] T. Cramer *et al.*, "HIF-1alpha is essential for myeloid cell-mediated inflammation," *Cell*, vol. 112, no. 5, pp. 645–657, 2003.

[191] N. Rohwer and T. Cramer, "Hypoxia-mediated drug resistance: novel insights on the functional interaction of HIFs and cell death pathways," *Drug Resist. Updat. Rev. Comment. Antimicrob. Anticancer Chemother.*, vol. 14, no. 3, pp. 191–201, J 2011.

[192] P. Vaupel, D. K. Kelleher, and M. Höckel, "Oxygen status of malignant tumors: pathogenesis of hypoxia and significance for tumor therapy," *Semin. Oncol.*, vol. 28, no. 2 Suppl 8, pp. 29–35, 2001.

[193] J. Abraham, N. N. Salama, and A. K. Azab, "The role of P-glycoprotein in drug resistance in multiple myeloma," *Leuk. Lymphoma*, vol. 56, no. 1, pp. 26–33, 2015.

[194] J.-P. Cosse and C. Michiels, "Tumour hypoxia affects the responsiveness of cancer cells to chemotherapy and promotes cancer progression," *Anticancer Agents Med. Chem.*, vol. 8, no. 7, pp. 790–797, 2008.

[195] D. M. Aebersold *et al.*, "Expression of hypoxia-inducible factor-1alpha: a novel predictive and prognostic parameter in the radiotherapy of oropharyngeal cancer," *Cancer Res.*, vol. 61, no. 7, pp. 2911–2916, 2001.

[196] J. M. Brown and W. R. Wilson, "Exploiting tumour hypoxia in cancer treatment," *Nat. Rev. Cancer*, vol. 4, no. 6, pp. 437–447, 2004.

[197] H. Harada *et al.*, "Cancer cells that survive radiation therapy acquire HIF-1 activity and translocate towards tumour blood vessels," *Nat. Commun.*, vol. 3, p. 783, 2012.

[198] B. J. Moeller, Y. Cao, C. Y. Li, and M. W. Dewhirst, "Radiation activates HIF-1 to regulate vascular radiosensitivity in tumors: role of reoxygenation, free radicals, and stress granules," *Cancer Cell*, vol. 5, no. 5, pp. 429–441, 2004.

[199] B. J. Moeller *et al.*, "Pleiotropic effects of HIF-1 blockade on tumor radiosensitivity," *Cancer Cell*, vol. 8, no. 2, pp. 99–110, 2005.

[200] T. W. H. Meijer, J. H. A. M. Kaanders, P. N. Span, and J. Bussink, "Targeting hypoxia, HIF-1, and tumor glucose metabolism to improve radiotherapy efficacy," *Clin. Cancer Res. Off. J. Am. Assoc. Cancer Res.*, vol. 18, no. 20, pp. 5585–5594, 2012.

[201] J. A. Bertout *et al.*, "HIF2alpha inhibition promotes p53 pathway activity, tumor cell death, and radiation responses," *Proc. Natl. Acad. Sci. U. S. A.*, vol. 106, no. 34, pp. 14391–14396, 2009.

[202] N. Rohwer and T. Cramer, "Hypoxia-mediated drug resistance: Novel insights on the functional interaction of HIFs and cell death pathways," *Drug Resist. Updat.*, vol. 14, no. 3, pp. 191–201, 2011.

[203] J. Li *et al.*, "Knockdown of hypoxia-inducible factor-1alpha in breast carcinoma MCF-7 cells results in reduced tumor growth and increased sensitivity to methotrexate," *Biochem. Biophys. Res. Commun.*, vol. 342, no. 4, pp. 1341–1351, 2006.

[204] L. Liu *et al.*, "Hypoxia-inducible factor-1 alpha contributes to hypoxia-induced chemoresistance in gastric cancer," *Cancer Sci.*, vol. 99, no. 1, pp. 121–128, 2008.

[205] L. Nardinocchi, R. Puca, A. Sacchi, and G. D'Orazi, "Inhibition of HIF-1alpha activity by homeodomain-interacting protein kinase-2 correlates with sensitization of chemoresistant cells to undergo apoptosis," *Mol. Cancer*, vol. 8, p. 1, 2009.

[206] Z. Ding *et al.*, "Expression and significance of hypoxia-inducible factor-1 alpha and MDR1/P-glycoprotein in human colon carcinoma tissue and cells," *J. Cancer Res. Clin. Oncol.*, vol. 136, no. 11, pp. 1697–1707, 2010.

[207] L. Chen *et al.*, "Effect of hypoxia-inducible factor-1alpha silencing on the sensitivity of human brain glioma cells to doxorubicin and etoposide," *Neurochem. Res.*, vol. 34, no. 5, pp. 984–990, 2009.

[208] C.-W. Chou *et al.*, "Tumor cycling hypoxia induces chemoresistance in glioblastoma multiforme by upregulating the expression and function of ABCB1," *Neuro-Oncol.*, vol. 14, no. 10, pp. 1227–1238, 2012.

[209] H. Zhu, X. P. Chen, S. F. Luo, J. Guan, W. G. Zhang, and B. X. Zhang, "Involvement of hypoxia-inducible factor-1-alpha in multidrug resistance induced by hypoxia in HepG2 cells," *J. Exp. Clin. Cancer Res. CR*, vol. 24, no. 4, pp. 565–574, 2005.

[210] H. J. Broxterman *et al.*, "Do P-glycoprotein and major vault protein (MVP/LRP) expression correlate with in vitro daunorubicin resistance in acute myeloid leukemia?," *Leukemia*, vol. 13, no. 2, pp. 258–265, Feb. 1999.

[211] X. He *et al.*, "Hypoxia regulates ABCG2 activity through the activivation of ERK1/2/HIF-1α and contributes to chemoresistance in pancreatic cancer cells," *Cancer Biol. Ther.*, vol. 17, no. 2, pp. 188–198, 2016.

[212] A.-M. Bleau, J. T. Huse, and E. C. Holland, "The ABCG2 resistance network of glioblastoma," *Cell Cycle*, vol. 8, no. 18, pp. 2937–2945, 2009.

[213] K. E. A. LaRue, M. Khalil, and J. P. Freyer, "Microenvironmental regulation of proliferation in multicellular spheroids is mediated through differential expression of cyclin-dependent kinase inhibitors," *Cancer Res.*, vol. 64, no. 5, pp. 1621–1631, 2004.

[214] H. R. Kumar *et al.*, "Three-dimensional neuroblastoma cell culture: proteomic analysis between monolayer and multicellular tumor spheroids," *Pediatr. Surg. Int.*, vol. 24, no. 11, pp. 1229–1234, 2008.

[215] S. L. Collins, R. Hervé, C. W. Keevil, J. P. Blaydes, and J. S. Webb, "Down-Regulation of DNA Mismatch Repair Enhances Initiation and Growth of

Neuroblastoma and Brain Tumour Multicellular Spheroids," *PLOS ONE*, vol. 6, no. 12, p. e28123, 2011.

[216] E. M. Hammond, M.-C. Asselin, D. Forster, J. P. B. O'Connor, J. M. Senra, and K. J. Williams, "The meaning, measurement and modification of hypoxia in the laboratory and the clinic," *Clin. Oncol. R. Coll. Radiol. G. B.*, vol. 26, no. 5, pp. 277–288, 2014.

[217] H. Menrad *et al.*, "Roles of hypoxia-inducible factor-1alpha (HIF-1alpha) versus HIF-2alpha in the survival of hepatocellular tumor spheroids," *Hepatol. Baltim. Md*, vol. 51, no. 6, pp. 2183–2192, 2010.

[218] D. Shweiki, M. Neeman, A. Itin, and E. Keshet, "Induction of vascular endothelial growth factor expression by hypoxia and by glucose deficiency in multicell spheroids: implications for tumor angiogenesis," *Proc. Natl. Acad. Sci. U. S. A.*, vol. 92, no. 3, pp. 768–772, 1995.

[219] B. M. Baker and C. S. Chen, "Deconstructing the third dimension: how 3D culture microenvironments alter cellular cues," *J. Cell Sci.*, vol. 125, no. Pt 13, pp. 3015–3024, 2012.

[220] R. H. Grantab and I. F. Tannock, "Penetration of anticancer drugs through tumour tissue as a function of cellular packing density and interstitial fluid pressure and its modification by bortezomib," *BMC Cancer*, vol. 12, p. 214, 2012.

[221] C. Basmadjian *et al.*, "Cancer wars: natural products strike back," *Front. Chem.*, vol. 2, 2014.

[222] "Publications | Medicinal chemistry of prohibitin ligands and anticancer agents."

[223] D. M. Lucas *et al.*, "The novel plant-derived agent silvestrol has B-cell selective activity in chronic lymphocytic leukemia and acute lymphoblastic leukemia in vitro and in vivo," *Blood*, vol. 113, no. 19, pp. 4656–4666, 2009.

[224] H. Sadlish *et al.*, "Evidence for a functionally relevant rocaglamide binding site on the eIF4A:RNA complex," *ACS Chem. Biol.*, vol. 8, no. 7, pp. 1519–1527, 2013.

[225] Q. Zhao, H. Abou-Hamdan, and L. Désaubry, "Recent Advances in the Synthesis of Flavaglines, a Family of Potent Bioactive Natural Compounds Originating from Traditional Chinese Medicine," *Eur. J. Org. Chem.*, vol. 2016, no. 36, pp. 5908–5916, 2016.

[226] Q. Zhao, H. Abou-Hamdan, and L. Désaubry, "Recent Advances in the Synthesis of Flavaglines, a Family of Potent Bioactive Natural Compounds Originating from Traditional Chinese Medicine," *Eur. J. Org. Chem.*, vol. 2016, no. 36, pp. 5908–5916, 2016.

[227] G. Polier *et al.*, "The natural anticancer compounds rocaglamides inhibit the Raf-MEK-ERK pathway by targeting prohibitin 1 and 2," *Chem. Biol.*, vol. 19, no. 9, pp. 1093–1104, 2012.

[228] S. K. Lee, B. Cui, R. R. Mehta, A. D. Kinghorn, and J. M. Pezzuto, "Cytostatic mechanism and antitumor potential of novel 1H-cyclopenta[b]benzofuran lignans isolated from Aglaia elliptica.," *Chem. Biol. Interact.*, vol. 115, no. 3, pp. 215–228, 1998.

[229] S. Santagata *et al.*, "Tight coordination of protein translation and HSF1 activation supports the anabolic malignant state," *Science*, vol. 341, no. 6143, p. 1238303, J 2013.

[230] H. Parikh *et al.*, "TXNIP Regulates Peripheral Glucose Metabolism in Humans," *PLoS Med.*, vol. 4, no. 5, 2007.

[231] J. Y. Zhu *et al.*, "The traditional Chinese herbal compound rocaglamide preferentially induces apoptosis in leukemia cells by modulation of mitogen-activated protein kinase activities," *Int. J. Cancer*, vol. 121, no. 8, pp. 1839–1846, 2007.

[232] S. KIM *et al.*, "Silvestrol, a Potential Anticancer Rocaglate Derivative from Aglaia foveolata, Induces Apoptosis in LNCaP Cells through the Mitochondrial/Apoptosome Pathway without Activation of Executioner Caspase-3 or -7," *Anticancer Res.*, vol. 27, no. 4B, pp. 2175–2183, 2007.

[233] M. Li-Weber, "Molecular mechanisms and anti-cancer aspects of the medicinal phytochemicals rocaglamides (=flavaglines)," *Int. J. Cancer*, vol. 137, no. 8, pp. 1791–1799, 2015.

[234] J. Y. Zhu *et al.*, "Rocaglamide sensitizes leukemic T cells to activation-induced cell death by differential regulation of CD95L and c-FLIP expression," *Cell Death Differ.*, vol. 16, no. 9, pp. 1289–1299, 2009.

[235] K. P. Callahan *et al.*, "Flavaglines target primitive leukemia cells and enhance anti-leukemia drug activity," *Leukemia*, vol. 28, no. 10, pp. 1960–1968, 2014.

[236] L. Boussemart *et al.*, "eIF4F is a nexus of resistance to anti-BRAF and anti-MEK cancer therapies," *Nature*, vol. 513, no. 7516, pp. 105–109, 2014.

[237] F. Emhemmed *et al.*, "Selective anticancer effects of a synthetic flavagline on human Oct4-expressing cancer stem-like cells via a p38 MAPK-dependent caspase-3-dependent pathway," *Biochem. Pharmacol.*, vol. 89, no. 2, pp. 185–196, 2014.

[238] F. Emhemmed *et al.*, "Pro-differentiating effects of a synthetic flavagline on human teratocarcinomal cancer stem-like cells," *Cell Biol. Toxicol.*, vol. 33, no. 3, pp. 295–306, 2017.

[239] G. Yuan *et al.*, "Flavagline analog FL3 induces cell cycle arrest in urothelial carcinoma cell of the bladder by inhibiting the Akt/PHB interaction to activate the GADD45α pathway," *J. Exp. Clin. Cancer Res.*, vol. 37, no. 1, p. 21, 2018.

[240] H. Ledford, "Cancer theory faces doubts," *Nature*, vol. 472, no. 7343, pp. 273–273, 2011.

[241] J. Arrowsmith, “Trial watch: Phase III and submission failures: 2007–2010,” *Nat. Rev. Drug Discov.*, vol. 10, p. 87, 2011.

[242] “About New Therapeutic Uses,” *National Center for Advancing Translational Sciences*, 18-Mar-2015.

[243] A. Oloumi, W. Lam, J. P. Banáth, and P. L. Olive, “Identification of genes differentially expressed in V79 cells grown as multicell spheroids,” *Int. J. Radiat. Biol.*, vol. 78, no. 6, pp. 483–492, 2002.

[244] D. D. Fang *et al.*, “Expansion of CD133(+) colon cancer cultures retaining stem cell properties to enable cancer stem cell target discovery,” *Br. J. Cancer*, vol. 102, no. 8, pp. 1265–1275, 2010.

[245] M. Wartenberg, F. Dönmez, F. C. Ling, H. Acker, J. Hescheler, and H. Sauer, “Tumor-induced angiogenesis studied in confrontation cultures of multicellular tumor spheroids and embryoid bodies grown from pluripotent embryonic stem cells,” *FASEB J. Off. Publ. Fed. Am. Soc. Exp. Biol.*, vol. 15, no. 6, pp. 995–1005, 2001.

[246] M. Mehta *et al.*, “Retinoblastoma,” *Singapore Med. J.*, vol. 53, no. 2, pp. 128–135; quiz 136, 2012.

[247] K. Chwalek, L. J. Bray, and C. Werner, “Tissue-engineered 3D tumor angiogenesis models: Potential technologies for anti-cancer drug discovery,” *Adv. Drug Deliv. Rev.*, vol. 79–80, pp. 30–39, 2014.

[248] N. Ribeiro *et al.*, “Flavaglines as Potent Anticancer and Cytoprotective Agents,” *J. Med. Chem.*, vol. 55, no. 22, pp. 10064–10073, 2012.

[249] V. Prasad and S. Mailankody, “Research and Development Spending to Bring a Single Cancer Drug to Market and Revenues After Approval,” *JAMA Intern. Med.*, vol. 177, no. 11, pp. 1569–1575, 2017.

[250] K. M. Tevis, Y. L. Colson, and M. W. Grinstaff, “Embedded Spheroids as Models of the Cancer Microenvironment,” *Adv. Biosyst.*, vol. 1, no. 10, p. 1700083, 2017.

[251] A. K. Miri, A. Khalilpour, B. Cecen, S. Maharjan, S. R. Shin, and A. Khademhosseini, “Multiscale bioprinting of vascularized models,” *Biomaterials*, 2018.

[252] S. J. Paulsen and J. S. Miller, “Tissue vascularization through 3D printing: Will technology bring us flow?,” *Dev. Dyn. Off. Publ. Am. Assoc. Anat.*, vol. 244, no. 5, pp. 629–640, 2015.

[253] B. Shi, O. Andrukhov, S. Berner, A. Schedle, and X. Rausch-Fan, “The angiogenic behaviors of human umbilical vein endothelial cells (HUVEC) in co-culture with osteoblast-like cells (MG-63) on different titanium surfaces,” *Dent. Mater.*, vol. 30, no. 8, pp. 839–847, 2014.

[254] Y. Bo, L. Yan, Z. Gang, L. Tao, and T. Yinghui, “Effect of calcitonin gene-related peptide on osteoblast differentiation in an osteoblast and endothelial cell co-culture system,” *Cell Biol. Int.*, vol. 36, no. 10, pp. 909–915, 2012.

[255] C. Yuan *et al.*, "Coculture of Stem Cells from Apical Papilla and Human Umbilical Vein Endothelial Cell Under Hypoxia Increases the Formation of Three-Dimensional Vessel-Like Structures in Vitro," *Tissue Eng. Part A*, vol. 21, no. 5–6, pp. 1163–1172, 2014.

[256] Y. S. Gho, H. K. Kleinman, and G. Sosne, "Angiogenic activity of human soluble intercellular adhesion molecule-1," *Cancer Res.*, vol. 59, no. 20, pp. 5128–5132, 1999.

[257] O. Salvucci, M. Basik, L. Yao, R. Bianchi, and G. Tosato, "Evidence for the involvement of SDF-1 and CXCR4 in the disruption of endothelial cell-branching morphogenesis and angiogenesis by TNF-α and IFN-γ," *J. Leukoc. Biol.*, vol. 76, no. 1, pp. 217–226, 2004.

[258] R. F. Potter and A. C. Groom, "Capillary diameter and geometry in cardiac and skeletal muscle studied by means of corrosion casts," *Microvasc. Res.*, vol. 25, no. 1, pp. 68–84, 1983.

[259] P. Datta, B. Ayan, and I. T. Ozbolat, "Bioprinting for vascular and vascularized tissue biofabrication," *Acta Biomater.*, vol. 51, pp. 1–20, 2017.

[260] H. Shoval *et al.*, "Tumor cells and their crosstalk with endothelial cells in 3D spheroids," *Sci. Rep.*, vol. 7, no. 1, p. 10428, 2017.

[261] S. Koeck *et al.*, "Infiltration of lymphocyte subpopulations into cancer microtissues as a tool for the exploration of immunomodulatory agents and biomarkers," *Immunobiology*, vol. 221, no. 5, pp. 604–617, 2016.

[262] J. M. Kelm *et al.*, "Design of Custom-Shaped Vascularized Tissues Using Microtissue Spheroids as Minimal Building Units," *Tissue Eng.*, vol. 12, no. 8, pp. 2151–2160, 2006.

[263] A. Wenger *et al.*, "Development and characterization of a spheroidal coculture model of endothelial cells and fibroblasts for improving angiogenesis in tissue engineering.," *Cells Tissues Organs*, vol. 181, no. 2, pp. 80–88, 2005.

[264] J. L. Horning *et al.*, "3-D tumor model for in vitro evaluation of anticancer drugs," *Mol. Pharm.*, vol. 5, no. 5, pp. 849–862, 2008.

[265] N. An, A. Schedle, M. Wieland, O. Andrukhov, M. Matejka, and X. Rausch-Fan, "Proliferation, behavior, and cytokine gene expression of human umbilical vascular endothelial cells in response to different titanium surfaces," *J. Biomed. Mater. Res. A*, vol. 93, no. 1, pp. 364–372, 2010.

[266] M. Grellier, N. Ferreira-Tojais, C. Bourget, R. Bareille, F. Guillemot, and J. Amédée, "Role of vascular endothelial growth factor in the communication between human osteoprogenitors and endothelial cells," *J. Cell. Biochem.*, vol. 106, no. 3, pp. 390–398, 2009.

[267] Y. Zhang *et al.*, "Osteogenic properties of hydrophilic and hydrophobic titanium surfaces evaluated with osteoblast-like cells (MG63) in coculture with human umbilical vein endothelial cells (HUVEC)," *Dent. Mater. Off. Publ. Acad. Dent. Mater.*, vol. 26, no. 11, pp. 1043–1051, 2010.

[268] W. L. Dissanayaka, L. Zhu, K. M. Hargreaves, L. Jin, and C. Zhang, "In vitro analysis of scaffold-free prevascularized microtissue spheroids containing human dental pulp cells and endothelial cells," *J. Endod.*, vol. 41, no. 5, pp. 663–670, 2015.

[269] H.-W. Cheng *et al.*, "Cancer cells increase endothelial cell tube formation and survival by activating the PI3K/Akt signalling pathway," *J. Exp. Clin. Cancer Res.*, vol. 36, no. 1, p. 27, 2017.

[270] H.-F. Tsai, A. Trubelja, A. Q. Shen, and G. Bao, "Tumour-on-a-chip: microfluidic models of tumour morphology, growth and microenvironment," *J. R. Soc. Interface*, vol. 14, no. 131, 2017.

[271] M. R. Carvalho, D. Lima, R. L. Reis, V. M. Correlo, and J. M. Oliveira, "Evaluating Biomaterial- and Microfluidic-Based 3D Tumor Models," *Trends Biotechnol.*, vol. 33, no. 11, pp. 667–678, 2015.

[272] S. Däster *et al.*, "Induction of hypoxia and necrosis in multicellular tumor spheroids is associated with resistance to chemotherapy treatment," *Oncotarget*, vol. 8, no. 1, pp. 1725–1736, 2017.

[273] R. Leek, D. R. Grimes, A. L. Harris, and A. McIntyre, "Methods: Using Three-Dimensional Culture (Spheroids) as an In Vitro Model of Tumour Hypoxia," *Adv. Exp. Med. Biol.*, vol. 899, pp. 167–196, 2016.

[274] Q. Li, R. Ma, and M. Zhang, "CoCl2 increases the expression of hypoxic markers HIF-1α, VEGF and CXCR4 in breast cancer MCF-7 cells," *Oncol. Lett.*, vol. 15, no. 1, pp. 1119–1124, 2018.

[275] G. Yang, S. Xu, L. Peng, H. Li, Y. Zhao, and Y. Hu, "The hypoxia-mimetic agent $CoCl_2$ induces chemotherapy resistance in LOVO colorectal cancer cells," *Mol. Med. Rep.*, vol. 13, no. 3, pp. 2583–2589, 2016.

[276] H. R. Lee, F. Leslie, and S. M. Azarin, "A facile in vitro platform to study cancer cell dormancy under hypoxic microenvironments using CoCl2," *J. Biol. Eng.*, vol. 12, p. 12, 2018.

[277] L. E. Huang, Z. Arany, D. M. Livingston, and H. F. Bunn, "Activation of hypoxia-inducible transcription factor depends primarily upon redox-sensitive stabilization of its alpha subunit," *J. Biol. Chem.*, vol. 271, no. 50, pp. 32253–32259, 1996.

ANNEX

Lung Tumor Patient Derived Organoids including Vasculature and Mesenchymal Stem Cells as a New Tool for Personalized Medicine

J. Seitlinger[1,3]*, H. Chaddad[1]*, V. Lindner[1,4], R. Akasov[5], E. Markvicheva[5], MP. Chenard[4], A. Olland[1,3], PE. Falcoz[1,3], G. Massard[1,3], N. Benkirane-Jessel[1,2], Y. Idoux-Gillet[1,2]

[1] INSERM (French National Institute of Health and Medical Research), UMR 1260, Regenerative Nanomedicine (RNM), FMTS, 67000 Strasbourg, France.

[2] Université de Strasbourg, Faculté de chirurgie dentaire, Hôpitaux Universitaires de Strasbourg, Strasbourg, France.

[3] Hôpitaux Universitaires de Strasbourg (CHRU), Service de Chirurgie Thoracique, Faculté de Médecine de Strasbourg, France.

[4] Hôpitaux Universitaires de Strasbourg (CHRU), Service d'Anatomopathologie, Faculté de Médecine de Strasbourg, France.

[5] Department of Biomaterials and Biotechnologies, Shemyakin-Ovchinnikov Institute of Bioorganic Chemistry, Russian Academy of Sciences, Moscow 117997, Russia

Abstract

In order to enable the advent of personalized medicine, we need solid *in vitro* models, taking into account the 3D microenvironment of the tumor, the human component, and the vasculature, to test both the toxicity and efficacy of new molecules. Today, the drug screenings are performed on 3D cell lines models and Patient-Derived Xenografts models. These models are not able to recapitulate the whole tumor microenvironment and vasculature, with hopeless return to the patient. Here, we propose our *in vitro* model, based on Patient-Derived Organoids, in a vascularized 3D environment, including mesenchymal stem cells. We believe that this will greatly contribute to the development of personalized medicine, since we are working on both healthy tissue (toxicity) and tumor tissue (efficacy). The second step of this model will be the integration of immune cells based on recent discoveries.

Introduction

Nowadays, non-small lung cancer (NSCLC) remains the first cause of cancer-related deaths worldwide (1). Surgery is the cornerstone of treatment in located stages. Depending on stages, patients need a chemotherapy that is still probabilistic. Indeed, the chemotherapy is not previously tested on the patient for evident reasons. During the last decade, some new treatment has proved their efficacy in advanced stages, whereas for long years, new treatment was hardly lacking. Targeted therapies have proved their efficacy in selected patient, with specific mutation. More recently, the discovery of immune checkpoints has changed the hallmarks of cancer (2). For the first time in cancer history, target was not the tumor cells but tumor microenvironment. Indeed, the focus of therapeutic targets has switched from cancer cells to tumor cells since it has been recognized that immune cells in cancer has a key role in tumor immune-surveillance (3). Now therapies seek to target immune cells to modulate their interaction with tumor cells. The recent studies testing immunotherapy had spectacularly results and increase the modality to treat NSCLC (4), even in first line for selected patients (5).

With these highlights, the need of *in vitro* testing model is deep and a solid platform with human cells is lacking. The aim of a perfect *in vitro* model would be human tumor of patient, vascularized in 3D, with cells of microenvironment embedded in extracellular matrix, allowing to help the therapeutic decision in order to develop personalized medicine.

It is well known that 3D cell culture offers many advantages compared to 2D culture, such as cell-cell interactions, matrix deposition, culture from different cell types, hypoxic nuclei, a diffusion limit of drugs, factors and nutrients, all criteria that bring us closer to the *in vivo*, helping tissue regeneration, and placing spheroids as the best model *in vitro* to test sensitivity and drug resistance (6) (7) (8). Actually, the testing *in vitro* models are as following: use of organoids from line cells, both not vascularized and not in extracellular matrix, or use of Patient Derived Xenograft (PDX). The first model lacks cells heterogeneity; indeed, a tumor is more complicated that tumor cells in aggregates and is surrounded by human microenvironment including immune cells. The second one uses patient tumor xenografts in mice, and presents the advantage of vascularization and microenvironment, but those are provided by the mice and could not be considered as predicting model for human therapeutics. More, the engraftment latency of PDX last some months, when it works (depending of each histology), and do not allow the back to patients.

Our objective was therefore to provide an *in vitro* model allowing the switch from PDX to vascularized organoid embedded in gel allowing to predict response to therapeutics including the new one (targeted therapy and immunotherapy).

Results

To analyze and form patient derived organoids (PDO), we started a collaboration with "Centre de Ressources Biologique des Hôpitaux Universitaires de Strasbourg" (CRB) and the Department of Pathology. We started a protocol concerning 100 biopsies of fresh tumor and healthy tissues from patient who underwent an anatomic lung resection (i.e. segmentectomy, lobectomy, pneumonectomy) for lung cancer. We exclude Small Cell Lung cancer (SCLC), pregnant women, patient under 18 years old, and patient with viral pathology known previously (hepatitis, VIH).

The sampling was carried out by the pathologist and consisted in fragment of about $5mm^3$ for each sample (healthy and tumor tissues).

In one month, we obtained samples from 5 patients, corresponding to 4 adenocarcinoma and 1 composite neuroendocrine carcinoma. We managed to form 4 organoids from tumor samples (80%) and 3 organoids from healthy samples (60%). We used 24 wells "Ultra Low Adherent" (ULA) plate for both samples, allowing us to form organoids after 3-4 culture days (Figure 1).

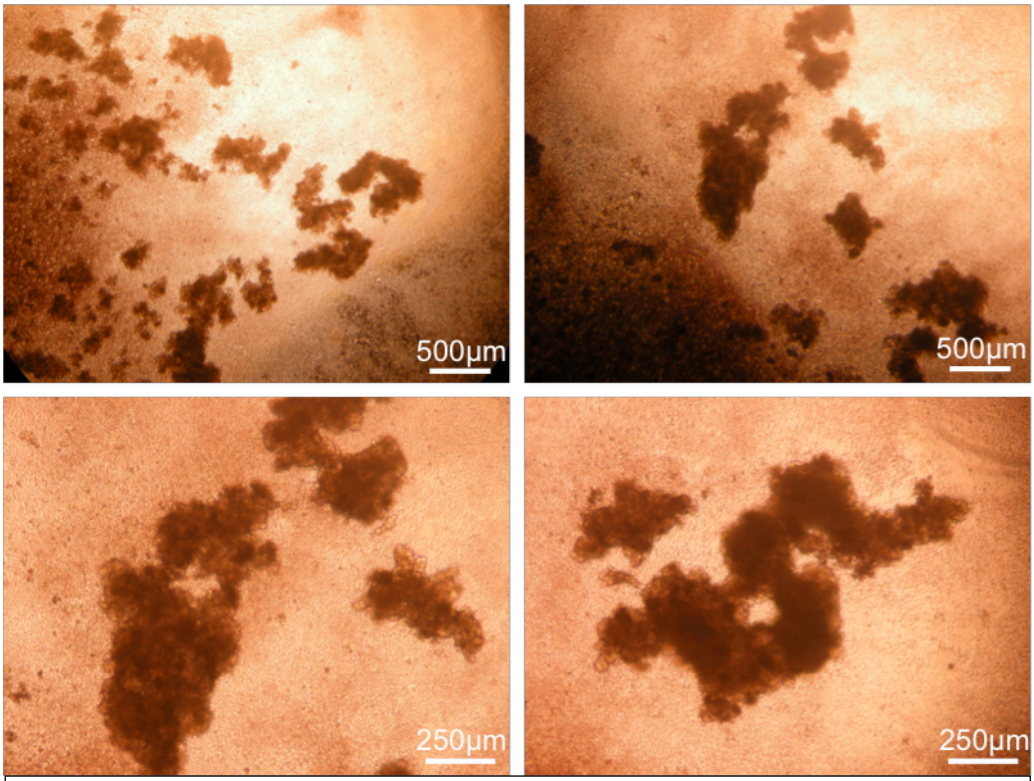

Figure 1: Optic microscopy observation of lung tumor organoids derived from patient (adenocarcinoma stage IV) after 7 days of culture in ULA plate.

The analysis of tumor organoids included in paraffin and examined with haematoxylin and eosin staining were anarchic structures, spontaneously forming large aggregates. The histological type was easily distinguished, with dark homogenous organoid for adenocarcinoma and heterogeneous for neuroendocrine composite carcinoma. However, the compared morphology of organoid from the first patient and his original tumor didn't allow to identify a glandular architecture in organoid, presents in tumor tissue.

After immunohistochemistry analysis, the panel of antibodies used as CD45 (leucocyte common antigen, 2B11 + PD7/26), Cytokeratin (AE1-AE3), Ki67 (Mib1), respectively as leucocyte, epithelial and proliferation markers, highlights presence of tumor cells, inflammatory cells, with some peripheral spindle cells (fibroblast or endothelial cells) (figure 2).

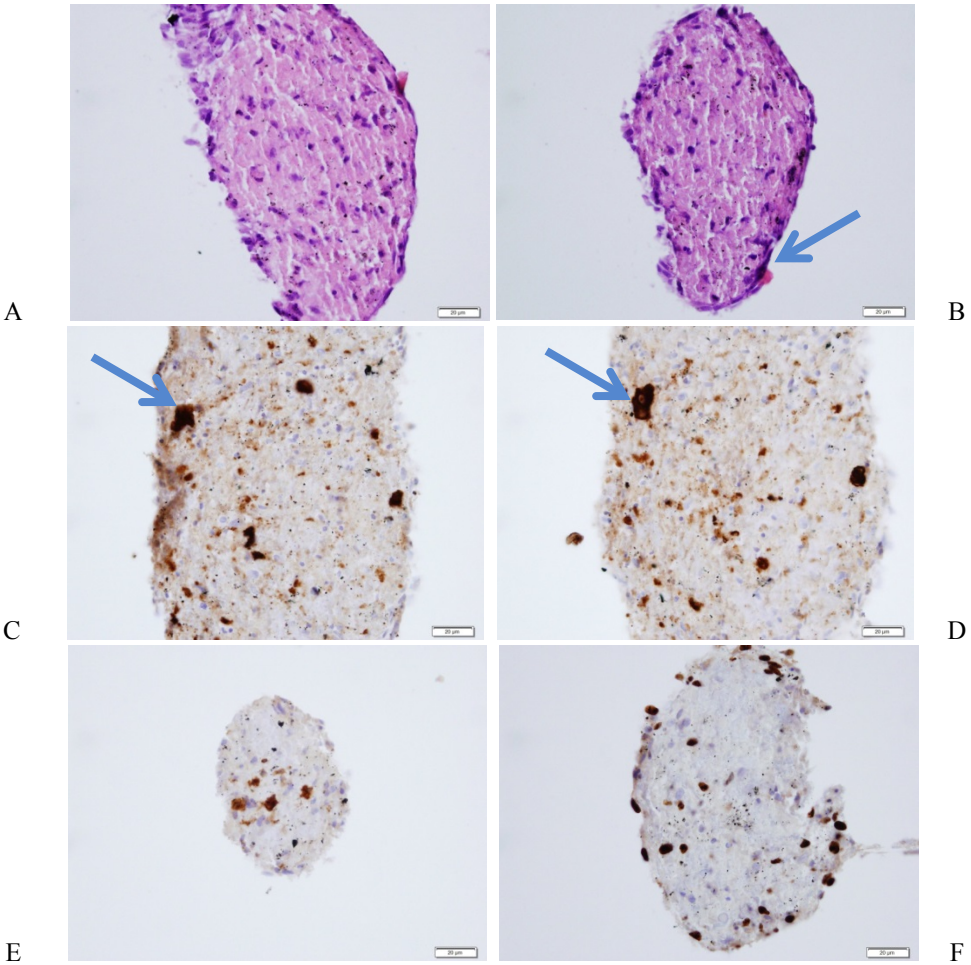

Figure 2: Lung adenocarcinoma organoids immunohistochemistry analysis: the cells are disposed on an eosinophilic fibrin-like background (HE, x40), the organoid is limited by some spindle cells (**A, B, arrow**). Some epithelial tumor cells with large cytoplasm (**C, D, arrow**) were stained by cytokeratin, mixed with some inflammatory elements (**E**). The proliferation index with Ki67 is moderate (**F**).

We have also performed lung organoids from healthy tissue collected reasonably far from the tumor site. The samples from healthy tissue formed also organoids, but they were more spherical structures and were rather homogeneous. The size of these organoids was about 200µm (Figure 3).

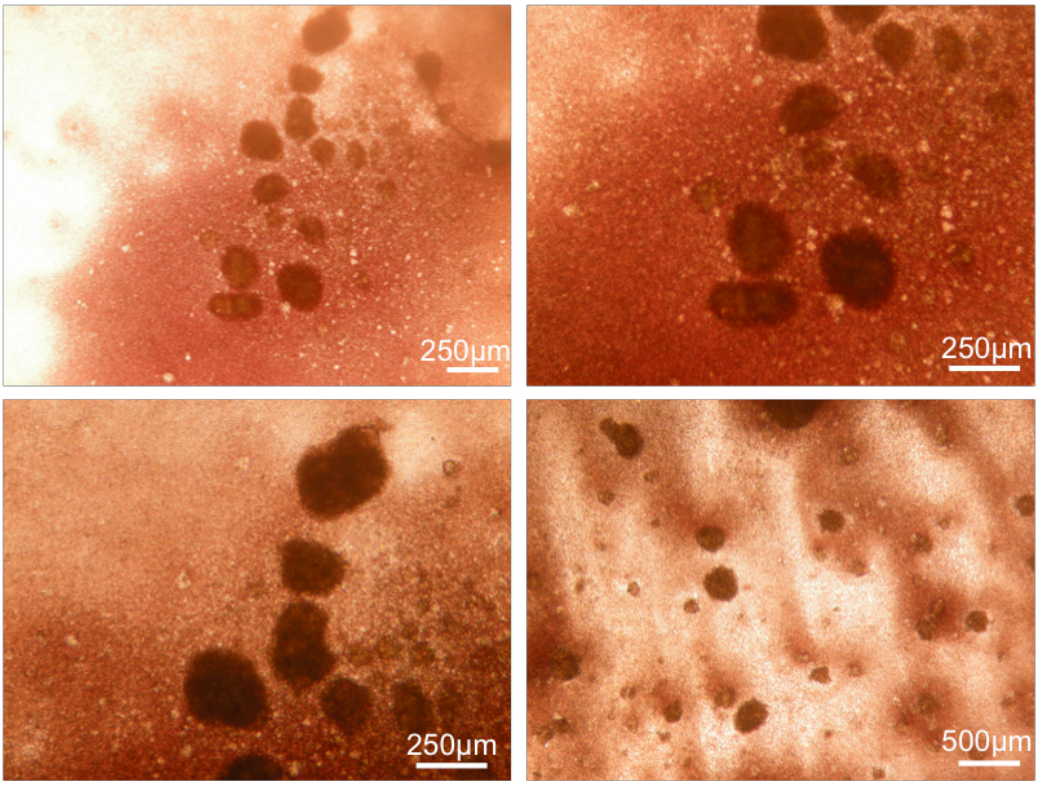

Figure 3: Optic microscopy observation of organoids derived from normal tissue of patient after 7 days of culture in ULA plate.

The main objective of this study was not only to perform the lung tumor and healthy organoids, but also to vascularize them. Recently, we reported the vascularization of osteosarcoma organoids by using cell lines (9). Here, we performed vascular network as we previously did. In this purpose, we settled them in fibrin gel with Human Umbilical Vein Endothelial Cells (HUVECs). To increase the speed of this vascular network formation we combined the HUVEC and Mesenchymal Stem Cells (MSCs). We compared the lung tumor and healthy organoids in order to see the effect of tumor tissue on endothelial cells in the presence of MSCs (Figure 4).

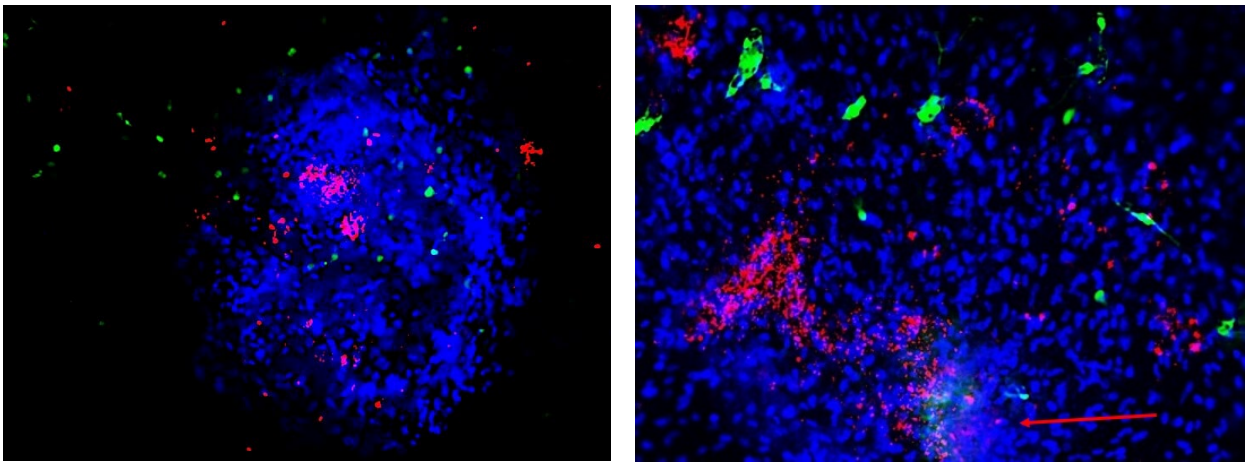

A B

Figure 4: Fluorescence microscopy observation of vascular network after 7 days of co-culture (PDO, HUVECs, MSCs) in fibrin gel insert. PDO from healthy tissue (**A**). PDO from tumor tissue (**B**). DAPI: blue, HUVEC-GFP: green, Ki67: red.

In Figure 4, we have shown that in PDO from healthy tissue (A), cells are still in spherical structure and do not spread through the fibrin gel (DAPI: blue), HUVECs cells seem quiescent (HUVEC-GFP: green), and proliferation marker Ki67 is poorly expressed (Ki67: red).

We have also shown that in PDO from tumor tissue (B), cells are spreading through the fibrin gel and invade the extracellular matrix; however, we can see that they come from PDO (DAPI, arrow). HUVECs cells do not form a vascular network but they seek to connect, forming fibrillar structures that intertwine. Proliferation marker Ki67 is co-expressed with DAPI of the PDO, and at the cellular invasion front, it is higher than in healthy tissue.

Even if these images show the beginning of a vascular network, with in particular the interconnection of endothelial cells near the organoid, it is necessary to further improve our culture technique.

As proof of concept of vascular network, we used under the same conditions organoids from osteosarcoma cell lines (line MG-63), and after 7 days we obtained a much more accomplished vascular network in the presence of HUVEC and MSCs (Figure 5). In this Figure, we have shown not only vascular network formation around organoids (A, B), but also vascular network infiltrating organoids (C, D). As a control, we have also shown a vascular network formation in the absence of organoids (E, F).

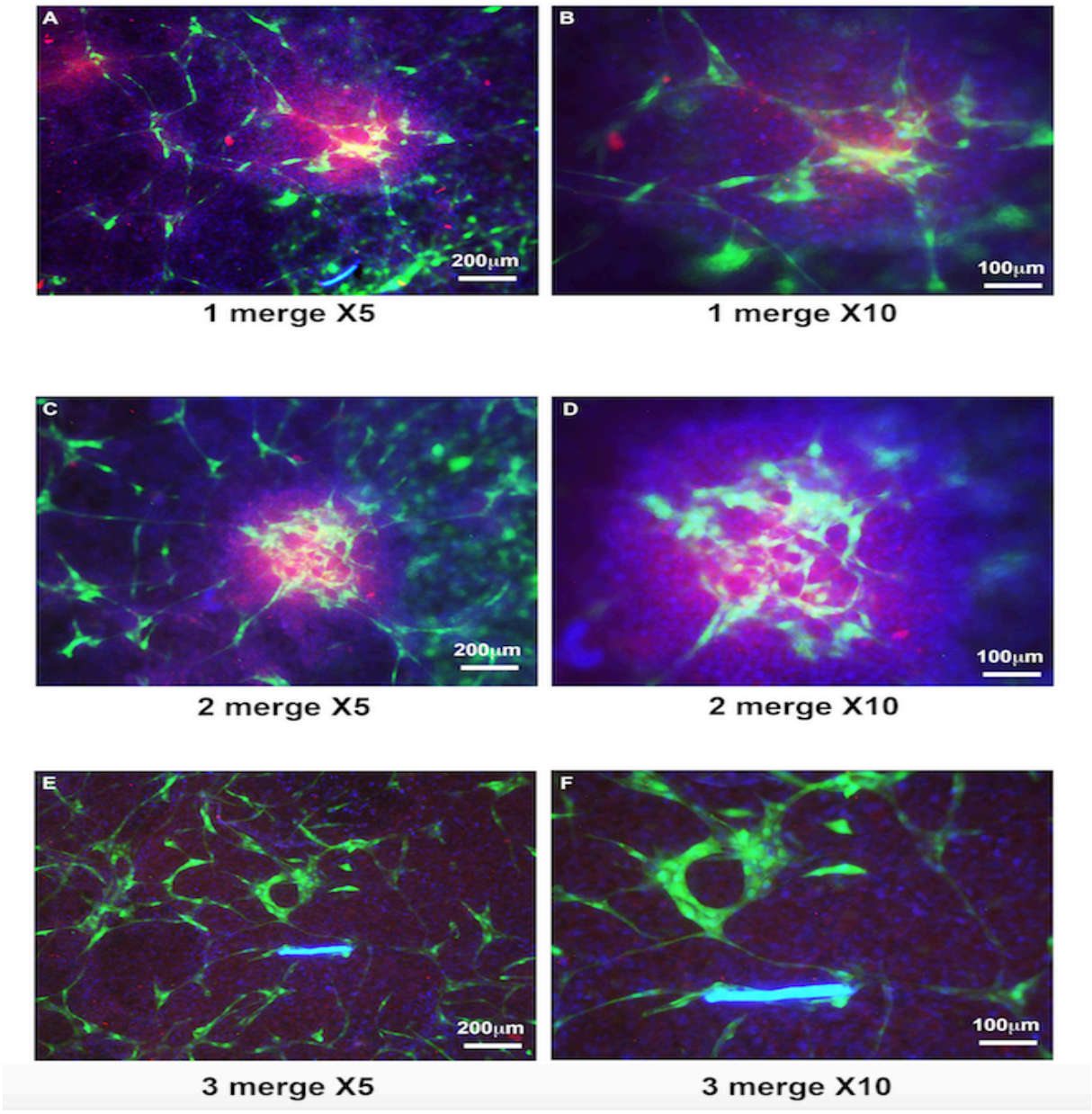

Figure 5: Fluorescence microscopy observation of vascular network after 7 days of co-culture (organoids from osteosarcoma cell line, HUVECs, MSCs) in fibrin gel insert. Organoids and vascular network (**A, B**): organoid is red (Phalloidin) and blue (DAPI), HUVECs form a vascular network (HUVEC-GFP: green). Vascular network in organoids (**C, D**): vascular network penetrates the organoid and form an anarchic vascular network. HUVECs cells (**E, F**). HUVECs cells are connected but do not form a vascular network in absence of organoids.

Discussion

With the advent of new therapeutic classes in multiple indications, the lack of solid *in vitro* test model is becoming increasingly important. Indeed, we cannot imagine using the PDX model to test immunotherapy molecules. More, in the era of personalized medicine, we need to obtain data about efficacy and toxicity on the patient cells. This evaluation is possible through our model because we produce tumor and healthy PDO.

However, we should say that we are still evaluating the best way to form quickly some homogeneous and more spherical organoids. In this purpose, we are trying several methods: the ULA plate that we used for these results, the hanging drop plate, and normal plate with agarose in the bottom. In the same way, we are trying to optimize our digestion method that remains in the association of 4 enzymes, in order to not kill tumor cells and preserve the viability of each cell. During the 7 days of culture, tumor PDO cells spread pretty fast in the fibrin gel and could hinder the evaluation of anti-tumor efficacy. Proliferation marker KI-67 is co-expressed with DAPI of PDO and at the cellular invasion front, and it is higher than in healthy tissue (figure 4). In healthy tissue, PDO cells seems to stay in spherical structure and do not spread through the fibrin gel.

Our ultimate aim is to design a model to test every new therapeutic including targeted therapies and immunotherapy. These tests can be relevant in presence of autologous immune cells and tumor cells (10). We are working with pathologist and immunologist to characterize the presence of immune cells in our organoids. More, we plan to test our organoids in presence of specific cytotoxic immune cells.

With the final objective to test drugs on our vascularized patient derived organoids, the first step is to establish the well-organized vascular network infiltrating the organoids in order to obtain a perfusable vasculature. The second step is to connect our *in vitro* model to a microfluidic device, allowing us to inject the different drugs.

Finally, as soon as possible, we will begin to test the different drug that we dispose, in order to study our *in vitro* model feasibility. As we focused on the complexity and the need of immune cells, we should not forget to assess the screening capacity of our device with conventional chemotherapy.

Materials

Digestion of biopsies

Both normal and tumor tissues were sent to the laboratory (in ice-cold culture medium, DMEM without Fetal Calf Serum, containing 100 units/mL of penicillin, 0.1mg/mL of streptomycin and 205 U/mL of fungizone). It is then cut into millimeter pieces using sterile scissors in a petri dish. These millimeter pieces are then digested in a 20mL solution containing type 1 collagenase at 0.5mg/mL, elastase at 25µg/mL, DNAse at 25µg/mL, and hyaluronidase at 100µg/mL, in a 50mL Falcon. Then comes a first digestion step of 60min, a vigorous 5-minute pipetting using a 5mL pipette, a second digestion step of 30 min, and a last vigorous 5-minute pipetting. The solution is then filtered through a 70µm Falcon Cell Filter ™. After centrifugation at 240 G for 3min, and counting the cells, they are settled in 10 wells of a 24-well ULA plate. We modified the protocol from a previous publication for colorectal cancer spheroids (11).

Cell culture

Human umbilical vein endothelial cells (HUVEC-GFP, IncuCyte® CytoLight Green Cells, Essen Bioscience, United Kingdom) were grown in a specific endothelial cell growth medium (PromoCell, Germany) with supplement mix. Mesenchymal stem cells (MSC, PromoCell) were grown in a specific mesenchymal stem cell growth medium (PromoCell, Germany) with supplement mix. Osteosarcoma cell line (MG-63, Sigma-Aldrich) and cells from patient biopsies were grown in DMEM medium (Lonza, France) with 10 U mL–1 penicillin, 100 µg mL−1 streptomycin, 250 U mL–1 fungizone, 1 mM Na-pyruvate, 2mM glutamine and 10% FBS. All cells were incubated at 37 °C in a humidified atmosphere of 5% CO2. When cells reached sub-confluence, they were harvested with trypsin and sub-cultured.

Organoids

The cells are cultured in a ULA plate after cell counting, with a number of about 1-2 million cells per well, depending on the number of cells obtained after digestion. They are grown in DMEM, 0.2 to 0.5 ml in each well. From the middle was added the next day, then every 48 hours. A passage is made after 10-14 days of cultivation. Organoids are formed from the 2nd or 3rd day of cultivation.

For the passage, the organoids are collected, centrifuged, washed with PBS, then centrifuged again and trypsins, they are put back into culture for 10-14 days, trying to obtain 1-1.5 million per well

Fibrin Gel

The 3 elements necessary for the formation of fibrin gel are fibrinogen (F3879-1G, Sigma-Aldrich™), thrombin (T6884-1KU, Sigma-Aldrich™) and culture medium, usually containing the cells to be sown. Fibrin gel is deposited at the bottom of culture inserts (Sarstedt™, 12 wells, membrane porosity 8µm). For a final volume of 300µL, 150 µL of fibrinogen at 5mg/ml are mixed with 138 µL of medium containing the cells (HUVEC cells, mesenchymal stem cells and the different PDO). At the bottom of each insert are deposited 6µL of 100 IU/ml thrombin. Finally, the fibrinogen/medium solution is added and mixed by pipetting with the thrombin drop. The critical point in the formation of the gel is to keep all the elements, except the medium, in the ice until the last moment before to use. Otherwise, fibrinogen may gel partially with the media or upon injection on the thrombin. Once the mixing is done, the gelation takes place very quickly in the incubator, in 10 to 20 minutes. Once gelation is complete, culture medium is added around the insert (about 1mL for a 12-well plate). The environment is changed the day after handling, then every 48 hours.

Organoids

The cells are cultured in a ULA plate after cell counting, with a number of about 1-2 million cells per well, depending on the number of cells obtained after digestion. They are grown in DMEM, 0.2 to 0.5 ml in each well. From the middle was added the next day, then every 48 hours. A passage is made after 10-14 days of cultivation. Organoids are formed from the 2nd or 3rd day of cultivation.

For the passage, the organoids are collected, centrifuged, washed with PBS, then centrifuged again and trypsins, they are put back into culture for 10-14 days, trying to obtain 1-1.5 million per well

Inserts

The inserts (Corning™) have a porous membrane of 3µm. This is an insert for 12-well plates. Once the cells have been sown in a gel, 1mL of medium is placed around the insert, which is changed on the 1st day and then every 48 hours. The medium in question is a DMEM- Endothelial cell media-MSC media mix at a ratio of 1/3-1/3-1-1/3.

Anatomopathologic analyze

The pathologist analyze was performed by the Department of Pathology, after fixation and paraffin inclusion in the laboratory. It consisted in Haematoxylin and Eosin staining and immunochemistry (cytokeratin AE1-AE3 (C and D)) for epithelial cells, CD 45 for immune cells and proliferative marker Ki67.

Immunofluorescence

We used the fluorescence microscope, available in the laboratory, to examine the organization of cells/microtissues in gels. The cells and organoids in the gel were previously fixed with 4% paraformaldehyde (PFA) for 10 min at 4°C. After three rinses with PBS, the fibrin gels were permeabilized and saturated with Triton 0.1% and 1% BSA for 1 hour, then rinsed again with PBS. Indirect immunofluorescence was performed after fixation. Primary antibodies were incubated overnight at 4°C at 1/200e, Ki67 (sc-15402, Santa Cruz Biotechnology). After 3 washes with PBS, the samples were incubated for 1 hour with an anti-rabbit Ac conjugated to Alexa Fluor 594, and 5 min with 200nM 4',6-diamino-2-phenylindole (DAPI, Sigma Aldrich). The samples were observed under an epifluorescence microscope (Leica DM4000 B).

Acknowledgements

This publication was made possible with the help of « Centre de Ressources Biologiques des Hôpitaux Universitaires de Strasbourg ». This research was carried out in the framework of a partnership with Groupe Pasteur Mutualité. Project carried out with a scholarship or research grant from the SFCTCV Marc Laskar endowment fund.

References

1. Jemal A, Bray F, Center MM, Ferlay J, Ward E, Forman D. Global cancer statistics. CA Cancer J Clin. 2011 Apr;61(2):69–90.
2. Hanahan D, Weinberg RA. Hallmarks of cancer: the next generation. Cell. 2011 Mar 4;144(5):646–74.
3. Couzin-Frankel J. Breakthrough of the year 2013. Cancer immunotherapy. Science. 2013 Dec 20;342(6165):1432–3.
4. Borghaei H, Paz-Ares L, Horn L, Spigel DR, Steins M, Ready NE, et al. Nivolumab versus Docetaxel in Advanced Nonsquamous Non-Small-Cell Lung Cancer. N Engl J Med. 2015 Oct 22;373(17):1627–39.
5. Reck M, Rodríguez-Abreu D, Robinson AG, Hui R, Csőszi T, Fülöp A, et al. Pembrolizumab versus Chemotherapy for PD-L1-Positive Non-Small-Cell Lung Cancer. N Engl J Med. 2016 10;375(19):1823–33.
6. Keller L, Wagner Q, Schwinté P, Benkirane-Jessel N. Double compartmented and hybrid implant outfitted with well-organized 3D stem cells for osteochondral regenerative nanomedicine. Nanomed. 2015;10(18):2833–45.
7. Keller L, Idoux-Gillet Y, Wagner Q, Eap S, Brasse D, Schwinté P, et al. Nanoengineered implant as a new platform for regenerative nanomedicine using 3D well-organized human cell spheroids. Int J Nanomedicine. 2017;12:447–57.
8. Keller L, Schwinté P, Gomez-Barrena E, Arruebo M, Benkirane-Jessel N. Smart Implants as a Novel Strategy to Regenerate Well-Founded Cartilage. Trends Biotechnol. 2017;35(1):8–11.
9. Chaddad H, Kuchler-Bopp S, Fuhrmann G, Gegout H, Ubeaud-Sequier G, Schwinté P, et al. Combining 2D angiogenesis and 3D osteosarcoma microtissues to improve vascularization. Exp Cell Res. 2017 15;360(2):138–45.
10. Sherman H, Gitschier HJ, Rossi AE. A Novel Three-Dimensional Immune Oncology Model for High-Throughput Testing of Tumoricidal Activity. Front Immunol [Internet]. 2018 [cited 2018 Aug 27];9. Available from: https://www.frontiersin.org/articles/10.3389/fimmu.2018.00857/full
11. Miyoshi H, Maekawa H, Kakizaki F, Yamaura T, Kawada K, Sakai Y, et al. An improved method for culturing patient-derived colorectal cancer spheroids. Oncotarget. 2018 Apr 24;9(31):21950–64.

Hassan Chaddad

Development of vascularized tumor spheroids mimicking the tumor environment: Angiogenesis and Hypoxia

Résumé

Le microenvironnement tumoral, l'angiogenèse tumorale et l'hypoxie jouent un rôle crucial dans la progression tumorale et le développement de thérapies de nombreux cancers. Les limites de pénétration des médicaments, les phénomènes de résistance aux anti-cancéreux, la vascularisation de la tumeur et l'hypoxie sont tous des paramètres influençant les effets du médicament. La culture cellulaire 3D permet de créer un microenvironnement qui imite l'architecture et la fonction des tissus *in vivo*. L'expression de gènes et de protéines modifiée par l'environnement 3D est une autre caractéristique qui impacte l'effet d'une molécule thérapeutique.

Dans notre première étude, afin de développer un modèle 3D vascularisé imitant celle des tumeurs *in vivo*, nous avons mis en culture des cellules endothéliales en 2D avec des cellules tumorales en 3D. Après 2 semaines de culture, un réseau vasculaire s'est organisé avec des structures de type tubulaire présentant une lumière et exprimant différents marqueurs angiogéniques tels que VEGF, CD31 et Collagène IV. Dans notre deuxième étude, nous avons développé un modèle d'hypoxie *in vitro* intégrant l'environnement 3D et un agent mimétique de l'hypoxie (CoCl2). Le but de ce modèle est de créer un modèle d'hypoxie imitant les tumeurs *in vivo* et de montrer l'importance de l'hypoxie dans la réponse et la résistance aux médicaments. Ces résultats ont révélé que la meilleure condition était la combinaison 3D+$CoCl_2$, conduisant à la surexpression des gènes relatifs à l'hypoxie (GLUT1/3, VEGF) et à la résistance aux médicaments (ABCG2, MRP1).

L'angiogenèse et l'hypoxie sont des facteurs clés pour le microenvironnement tumoral *in vivo* et ils doivent être adoptés dans la conception de modèles tumoraux *in vitro* pour mieux sélectionner et cribler les médicaments anticancéreux.

Mots clés : Microenvironnement tumoral, sphéroïdes tumoraux 3D, angiogenèse, hypoxie, criblage de médicaments

Abstract

The tumor microenvironment, tumor angiogenesis, and hypoxia play a critical role in the tumor progression and therapy development of many cancers. Limitations in drug penetration, multidrug resistance phenomena, tumor vascularization, and oxygen deficiency are all parameters influencing drug effects. 3D cell culture allows to create a microenvironment that more closely mimics *in vivo* tissue architecture and function, thus, gene and protein expression modified by the 3D environment are further features that affect treatment outcome.

In our first study, in order to develop a vascularized 3D model like *in vivo* tumors, we co-cultured 2D endothelial cells with 3D tumor cells. After 2 weeks of this combination, a vascular network was formed and organized with tubule-like structures presenting a lumen and expressing different angiogenic markers such as VEGF, CD31 and Collagen IV. In our second study, we developed an *in vitro* hypoxia model integrating the 3D environment and a hypoxia mimetic agent ($CoCl_2$) to mimic the *in vivo* tumors and to show the importance of hypoxia in drug response and resistance. Results revealed that the best condition was the combination 3D+$CoCl_2$ model, leading to overexpression oh hypoxia (GLUT1/3, VEGF) and drug resistance (ABCG2, MRP1) related genes.

Taken together, angiogenesis and hypoxia are key factors for *in vivo* tumor microenvironment and they should be adopted in *in vitro* model design to better select and screen anticancer drugs.

Keywords: Tumor microenvironment, 3D tumor spheroids, angiogenesis, hypoxia, drug screening.